

Cellulose based aerogel microfibers for biomedical applications

Citation for published version (APA):

Rostamitabar, M. (2022). *Cellulose based aerogel microfibers for biomedical applications*. [Doctoral Thesis, Maastricht University, RWTH Aachen University]. Maastricht University.
<https://doi.org/10.26481/dis.20221214mr>

Document status and date:

Published: 01/01/2022

DOI:

[10.26481/dis.20221214mr](https://doi.org/10.26481/dis.20221214mr)

Document Version:

Publisher's PDF, also known as Version of record

Please check the document version of this publication:

- A submitted manuscript is the version of the article upon submission and before peer-review. There can be important differences between the submitted version and the official published version of record. People interested in the research are advised to contact the author for the final version of the publication, or visit the DOI to the publisher's website.
- The final author version and the galley proof are versions of the publication after peer review.
- The final published version features the final layout of the paper including the volume, issue and page numbers.

[Link to publication](#)

General rights

Copyright and moral rights for the publications made accessible in the public portal are retained by the authors and/or other copyright owners and it is a condition of accessing publications that users recognise and abide by the legal requirements associated with these rights.

- Users may download and print one copy of any publication from the public portal for the purpose of private study or research.
- You may not further distribute the material or use it for any profit-making activity or commercial gain
- You may freely distribute the URL identifying the publication in the public portal.

If the publication is distributed under the terms of Article 25fa of the Dutch Copyright Act, indicated by the "Taverne" license above, please follow below link for the End User Agreement:

www.umlib.nl/taverne-license

Take down policy

If you believe that this document breaches copyright please contact us at:

repository@maastrichtuniversity.nl

providing details and we will investigate your claim.

Cellulose Based Aerogel Microfibers for Biomedical Applications

MATIN ROSTAMITABAR

Cellulose Based Aerogel Microfibers for Biomedical Applications

© M. Rostamitabar | Maastricht University, 2022

All rights reserved

ISBN: 978-94-6469-128-3

Printed by Proefschriftspecialist

Layout and design by Cassandra Moonen

Cellulose Based Aerogel Microfibers for Biomedical Applications

DISSERTATION

To obtain the degree of Doctor at the Maastricht University and
Dr. rerum medicinalium (Dr. rer. medic.) at the RWTH Aachen,
on the authority of the Rector Magnifici, Prof.dr. Pamela Habibović
and Univ.-Prof. Dr. rer. nat. Dr. h.c. mult. Ulrich Rüdiger
in accordance with the decision of the Board of Deans,
to be defended in public on Wednesday 14th of December 2022 at 10:00 hours

by

Matin Rostamitabar

SUPERVISOR

Prof. Dr. med. Stefan Jockenhoevel

CO-SUPERVISORS

Prof. Dr. Gunnar Seide

Dr. Samaneh Ghazanfari

ASSESSMENT COMMITTEE

Prof. Dr. Lorenzo Moroni (Chair)

Prof. Dr. Pasi Kallio, Tampere University

Prof. Dr. Andrij Pich

Prof. Dr. Aart Willem Van Vuure, KU Leuven

This project, as a part of the FibreNet consortium, has received funding from the European Union's Horizon 2020 - Research and Innovation Framework Programme under the H2020 Marie Skłodowska-Curie Actions grant agreement No. 764713.



FibreNet 

TO ALL YOUNG RESEARCHERS,

who left their homeland, graced into the great
unknown and believed in the beauty of their dreams.

TO MY PARENTS,

who gave little they had to ensure
I would have the opportunity of education.

TABLE OF CONTENTS

Chapter 1.

Introduction into wound dressing, aerogels and drug-eluting medical textiles: from fiber production and textile fabrication to drug loading and delivery	1
1.1 Wound and wound dressing	2
1.2 Aerogels	3
1.3 Importance of transforming aerogels into fibers and textiles	9
1.4 Drug-eluting medical textiles: from fiber production and textile fabrication to drug loading and delivery	10
1.5 Aim and scope	62
1.6 outline	63
References	66

Chapter 2.

Effect of cellulose characteristics on the properties of the wet-spun aerogel fibers	91
2.1 Introduction	92
2.2 Materials and methods	94
2.3 Results	97
2.4 Discussion	106
2.5 Conclusions	109
References	112

Chapter 3.

Cellulose aerogel microfibers for drug delivery applications	117
3.1 Introduction	118
3.2 Material and methods	120
3.3 Results and discussion	130
3.4 Conclusion	147
References	148

Chapter 4.	
Drug loaded cellulose-chitosan aerogel microfibers for wound dressing applications	153
4.1 Introduction	154
4.2 Materials and methods	155
4.3 Results and discussions	163
4.4 Conclusion	178
References	180
Chapter 5.	
Thymol loaded cellulose aerogel nonwoven for wound dressing application	185
5.1 Introduction	186
5.2 Materials and methods	188
5.3 Results and discussion	194
5.4 Conclusion	205
References	206
Chapter 6.	
General discussion	211
References	216
Chapter 7.	
Impact chapter	219
References	222
Appendix	224
Summary	226
Acknowledgments	230
About the author	234
List of Publications	236



Chapter 1.

INTRODUCTION INTO WOUND DRESSING, AEROGELS AND DRUG-ELUTING MEDICAL TEXTILES: FROM FIBER PRODUCTION AND TEXTILE FABRICATION TO DRUG LOADING AND DELIVERY

This chapter is mainly based on the following publication:

Rostamitabar, M.; Abdelgawad, A.M.; Jockenhoewel, S.; Ghazanfari, S. Drug-Eluting Medical Textiles: From Fiber Production and Textile Fabrication to Drug Loading and Delivery. *Macromolecular bioscience* 2021, 2100021.

1.1 Wound and wound dressing

An injury or disruption of anatomical structure and function of the skin is defined as a wound [1]. A wound can be formed by external stimuli including heat, freezing, electricity, chemicals, radiation, and friction, or through surgical interventions. Other types of wounds can happen due to human body malfunction or illness such as diabetic foot ulcers, pressure ulcers, and venous and arterial leg ulcers [2].

The wound healing process occurs in highly ordered phases of hemostasis and coagulation, in which bleeding is stopped, inflammation, when essential cells are recruited into the wound area, proliferation, when the new tissue is being formed, and finally maturation, in which remodeling of the initially formed tissue towards a more mature tissue occurs [1,3]. Based on the nature of the healing process, wounds are categorized as acute and chronic. Acute wounds are typically referred to those that are fully healed within one to twelve weeks with minimal scars left. On the other hand, chronic wounds generally require a longer time to heal with the possibility of reoccurrence [4]. Chronic wounds have a higher potential to be infectious, are significantly more difficult to heal, and can also lead to serious issues such as limb amputation or death.

There are high health issues and cost burdens concerning wound care and management. In both types of wounds, accelerated wound healing is favorable for recovery, overall health, and cost issues. Wound dressings are fabricated to assist, facilitate, and accelerate the wound healing process and protect the wound site from the factors that may delay or obstruct healing procedures such as infection, contamination, and moisture loss [4,5]. An ideal wound dressing is biocompatible, non-adherent, bactericide, and has the potential to be loaded with bioactive agents to have sustained-release on the wound site. Also, it should provide a suitable barrier against the penetration of microorganisms, provide a moist environment around the wound, and have the capability to absorb wound exudates [6,7].

Wound dressing materials are produced from natural, synthetic polymers, and hybrid polymers in various forms of films, sponges, textiles, hydrogels, and aerogels. Biopolymers are favorable for wound dressing applications because of their high biocompatibility and environmentally friendly characteristics. They could also resemble the structure of the extracellular matrix (ECM) and have good biological recognition which is often lacking when using synthetic polymers [4,8]. Although so many wound dressing products have been already introduced into the market, there has been no single treatment in order to fulfill all requirements of the wound healing process yet.

Thus, designing a novel wound dressing using bio-based materials holds considerable promise to cover this gap and get closer to a multi-functional wound dressing.

Recently, a category of materials so-called “cellulose aerogels” have shown promising results for being used in wound dressing application and drug delivery [9]. The most abundant organic polymer on earth, cellulose, is a linear and semi-crystalline carbohydrate polymer made of repeated D-glucose bounded by $\beta(1-4)$ glycosidic bonds $((C_6(H_{10}O)_5)_n)$ [10]. Cellulose biocompatibility, renewability, high moisture uptake, and biodegradability make it an interesting candidate for wound dressing application [11,12]. Furthermore, cellulose can be transformed into aerogel fibers as novel functional materials with low density, high porosity, and a large specific surface area [13,14], all of which are important when it comes to the fabrication of an ideal wound dressing.

In the following sections, terminologies and the current state of the art in the fabrication of drug loaded cellulose based aerogel fibers for biomedical applications are described. First, aerogel and its fabrication techniques with an emphasis on bioaerogels have been explained. Later, the importance of transforming aerogels into fibers and textiles as well as common techniques to fabricate drug-eluting fibrous materials for drug delivery, wound dressing, and tissue engineering applications have been reviewed.

1.2 Aerogels

In 1931, Kistler introduced the term “aerogel” to describe a gel whose liquid phase is exchanged by a gas without collapsing the structure of the solid network [15]. Aerogels are a class of novel materials with high porosity (80-99%), low density (0.003–0.5 g/cm³), and large specific surface area (100–1200 m²/g) [11,16]. These fascinating characteristics accompanied by flexibility in the synthesis and variety of initial precursors have made the aerogels very promising candidates for multiple applications such as thermal and sound insulation [17,18], pollution absorption [19,20], energy damping, storage, conversion [21-23], and biomedical applications [11,14].

Aerogels are typically fabricated in three main steps: dissolving or dispersion of the precursors, gel or network formation, and removing the solvent via different drying techniques such as ambient drying, freeze-drying, or supercritical CO₂ (scCO₂) drying in order to preserve the three-dimensional (3D) porous structure. In the past few years, some other methods have been proposed for the fabrication of nonwoven aerogels including electrospinning [24] and solution blowing [25]. Among the aforementioned techniques, gel formation followed by freeze-drying or scCO₂ drying method is the most reported and popular technique for aerogel fabrication. It should be noted that in

contrast to scCO_2 drying, freeze-drying can not lead to nanoporous materials since the growth of the ice crystals causes pore size enlargement.

Inorganic materials such as silica, metal oxides, mixed metal oxides, modern metal-based aerogels, and organic materials including a wide variety of polymers and biopolymers have been used as aerogel precursors [26,27]. Silica aerogels, as the first generation of aerogels, have been extensively studied and are even commercially available; however, due to their brittle nature and high production cost, their usage is limited [28]. Bioaerogels are a new generation of aerogels that has obtained more attention during the 21st century, thanks to their renewability, biodegradability, and low or non-toxic nature. Bioaerogels are made of natural polymers such as polysaccharides and proteins. Moreover, in comparison to silica aerogels, bioaerogels, especially polysaccharide aerogels, showed more ductile mechanical behavior [29,30]. Due to their different chemical functional group, such as hydroxyl-, carboxyl-, and amino groups, bioaerogels allow for targeted functionalization. Furthermore, their biocompatibility and biodegradability have made them suitable for a variety of biomedical applications such as tissue engineering, drug delivery, and wound dressing [12,29,31]. An overview of the progress of aerogel science from its invention to modern-day aerogels including examples of important precursors used in their fabrication process is represented in **Figure 1.1**.

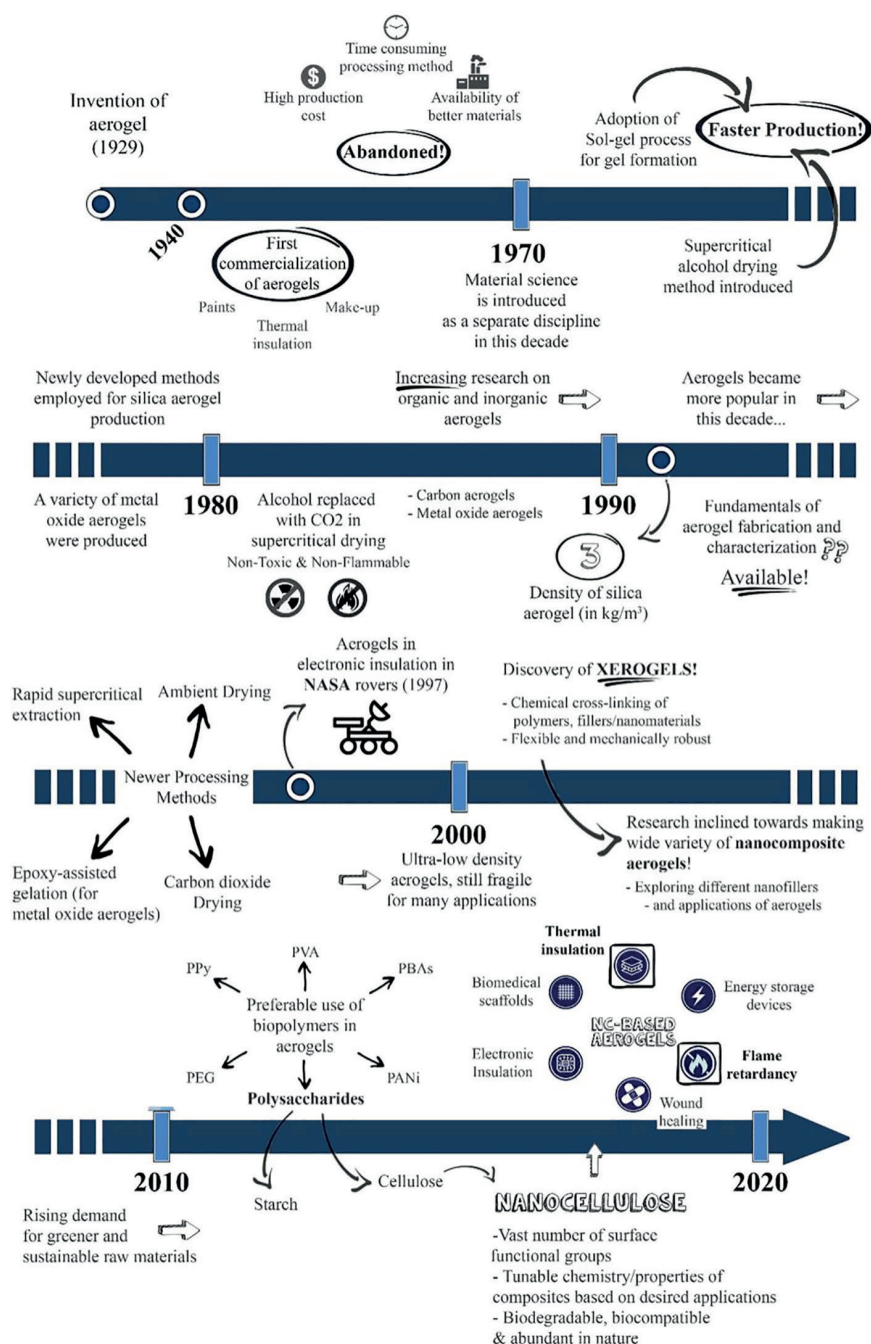


FIGURE 1.1.

Timeline of aerogel science and technology progress from its invention to modern-day aerogels with examples of important precursors used in their fabrication. The timeline is not drawn to any particular scale. Abbreviations: PEG, polyethylene glycol; PPy, polypyrrole; PVA, poly(vinyl alcohol); PBAs, polyhydroxybutyrates; and PANi, polyaniline. Reproduced with permission [18], Copyright © 2021 American Chemical Society.

1.2.1 Synthesis of bioaerogels

Bio-aerogels can be fabricated from fully dissolved polymer solutions or suspension/dispersion of biomacromolecules. The focus of this thesis is only on the usage of polysaccharides in solution to produce aerogel fibers due to the limitation of suspensions for fiber spinning techniques. Bioaerogel synthesis route mainly consists of biomacromolecule dissolution, gelation, or network formation followed by solvent exchange from a solvent to anti-solvent and drying with scCO_2 (**Figure 1.2A**) [32].

The network formation is a critical step of aerogel fabrication and it can occur by polymer gelation or by direct coagulation of the polymer solution. It is important to notice that the gelation of biomacromolecules is rather different from the small molecules and sol-gel route and it does not necessarily include a polymerization step. Therefore, physical and chemical gelation has been proposed for biopolymers network formation. In the first route, physical interactions by chain entanglements or weak forces (e.g. hydrogen bonds, ionic bonds, and hydrophobic interactions) between chains are the dominant causes of gelation. However, chemical crosslinking between chains by cross-linkers is the main force of gelation in the second route. The polymer characteristics such as molecular weight, chemical structure, functionalization, and the synthesis conditions including polymer concentration, pH, temperature, and crosslinker concentration affect the gelation and the final properties of the aerogel [33,34].

The aforementioned gelation routes have been challenged in some studies for cellulose [35,36], pectin [37], and alginate [38]. It has been discussed that for some polysaccharides, there might be no gelation, but rather another phenomenon occurs; this is known as non-solvent induced phase separation or immersion precipitation. It has been suggested that phase separation through reducing the solubility of the polysaccharide by the gradual increase of non-solvent during the solvent exchange is causing the polymer coagulation and contraction. In the case of polysaccharides above the overlap concentration, where the conformations of individual chains start to overlap each other, the coagulated polymers will not precipitate even if no gelation happens in the solutions. This is arising due to the chain rigidity of polysaccharides, leading to a 3D structure from the coagulated polymer and finally shaping the network of the aerogel precursor [32,39].

1.2.2 General aspects of the aerogels drying methods

A schematic of the capillary forces applied during evaporative drying is displayed in **Figure 1.2B**. The liquid phase between the pores of the gel matrix typically forms a concave meniscus since cohesive intermolecular forces are lower among liquid-liquid

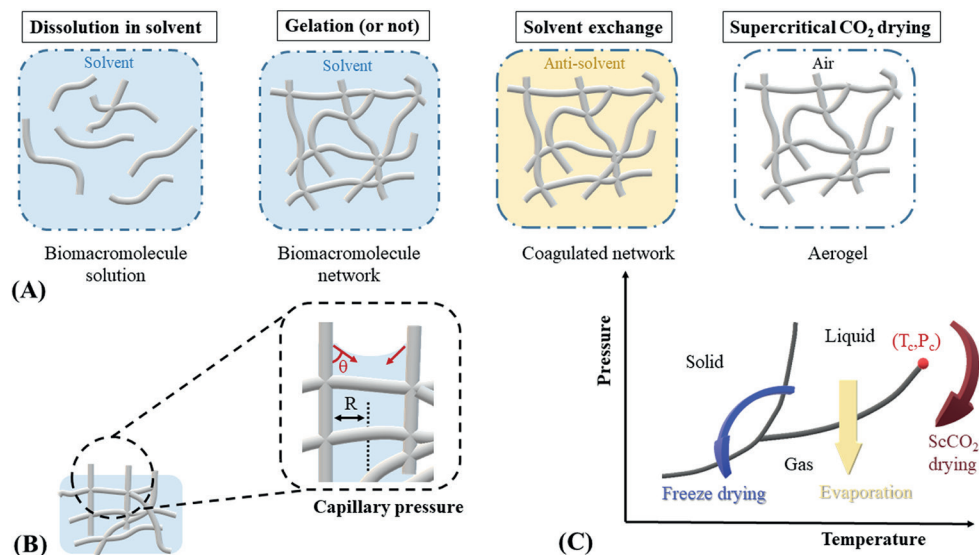
molecules in comparison to liquid-solid ones (pore walls). During evaporation of the liquid, the meniscus curvature enhances, causing stress applied to the pore's walls termed as "capillary forces". The young-Laplace equation defines the capillary pressure by:

$$P_c = \frac{2 \gamma \cos \theta}{R} \quad \text{Equation (1.1)}$$

P_c is the capillary pressure within the pores (Pa), γ is the surface tension between the liquid and the gas phase (N/m), θ is the meniscus angle formed between the solid (pore walls) and the liquid phase (in °), and R is the pore radius (m).

By evaporation of the liquid, the capillary pressure increases and the porous structure starts to deform and shrink. Such capillary pressure is higher for pores with a lower diameter and can lead to cracks, densification, and significant damage to the gel network structure. In order to prevent such a destructive process, it is vital to remove the liquid-gas surface tension or make the meniscus angle as high as possible (close to 90°) utilizing chemical treatment. The gels without chemical modification which are dried by conventional evaporation typically lead to dense, highly shrank, and low-porosity materials so-called xerogels. Cryogels are fabricated from the freeze-drying technique (also known as lyophilization) in which the liquid phase is frozen and then sublimated by lowering the pressure. In cryogels, pore wall densification and micro size pore formation occur due to the growth of ice crystals within the material.

Aerogels, on the other hand, are produced by supercritical CO_2 drying in which above the critical temperature and pressure of CO_2 ($T_{\text{critical}} \sim 31^\circ\text{C}$ and $P_{\text{critical}} \sim 75$ bars), densities of the liquid and vapor phases become equal leading to the formation of a single-phase supercritical fluid within the network. This will omit the capillary forces and prevents the network from collapsing, volume shrinkage, and gel cracking. After extracting the solvent by supercritical phase, slow and isothermal depressurization of the supercritical phase continues till the gaseous state at ambient pressure is reached. CO_2 benefits from low critical coordination, and it is commonly used due to its low cost and inert nature [32]. ScCO_2 is also used as a medium to load drugs into an aerogel; this technique is thoroughly explained in section 1.4.3.6. **Figure 1.2C** illustrates the above-mentioned drying processes of freeze-drying, evaporative drying, and supercritical drying in terms of phase changes. Moreover, biobased aerogels fabricated from natural polymers such as cellulose and chitosan are attractive as they confine their intrinsic chemical characteristics and the physical features of their nanostructure.

**FIGURE 1.2.**

Schematic illustration of general process route of aerogel preparation from biomacromolecules (A), capillary pressure in liquid-gas interphases in the pore structure of the network (B), and various drying procedures of freeze-drying, evaporation, and supercritical CO₂ drying (the critical temperature (T_c) and pressure (P_c)).

1.2.3 Aerogels based on cellulose and chitosan

The most studied bioaerogels are cellulose II [39,40]. Cellulose II aerogels are fabricated by dissolving cellulose in solvents such as N-Methylmorpholine N-oxide (NMMO) monohydrate, NaOH-water, salt melt hydrates such as zinc chloride ($\text{ZnCl}_2 \cdot 6\text{H}_2\text{O}$) and calcium thiocyanate ($\text{Ca}(\text{SCN})_2 \cdot 6\text{H}_2\text{O}$), and ionic liquids. Various ionic liquids can be used for the fabrication of cellulose aerogels including 1-Ethyl-3-methylimidazolium acetate (EmimAc), 1-Allyl-3-methylimidazolium chloride (AMIMCl), and 1-Butyl-3-methylimidazolium chloride (BMIMCl). The dissolved cellulose can be coagulated in different anti-solvents such as water, alcohols, acids, and acetone and subsequently solvent-exchanged and dried. It should be noted that the final structural and mechanical properties of the obtained cellulose II aerogel are highly dependent on the type of solvent and anti-solvent [39]. Cellulose-based aerogels can be used in drug delivery and wound dressing applications due to their high drug loading capacity, biocompatibility, degradability, oxygen permeability, and high moisture and exudate uptake [11,12]. Depending on the shape and structural arrangement of cellulose aerogels, both fast and slow sustained drug release rates are achievable [31]. Furthermore, other bioaerogels from natural polymers with an anionic or cationic moiety such as chitosan have been studied to overcome the limitations of cellulose such as lack of antibacterial properties. Chitin is typically extracted from the exoskeleton of arthropods, such as sea

crustaceans, and upon deacetylation reaction, it will turn into chitosan. Chitosan is a linear polysaccharide composed of β -(1 \rightarrow 4) linked D-glucosamine (deacetylated unit) and N-acetyl-D-glucosamine (acetylated unit) [41]. The chitosan degree of deacetylation is typically varying from 60 to 95% and can significantly impact the final properties of the chitosan aerogel. In acidic conditions, at pH below pKa (\sim 6.5), chitosan transforms into a cationic polyelectrolyte, while total charge density relies on the degree of deacetylation and pH conditions. Therefore, chitosan can react with negatively charged materials and is soluble in an aqueous acidic medium. Gelation of chitosan can occur by hydrogen bonding at pH > pKa or through chemical crosslinking. Chitosan is usually used to fabricate composite aerogels with cellulose, alginate, or pectin [42,43]. Chitosan aerogel can be utilized in drug delivery applications for instance to achieve fast dissolution of poorly water-soluble drugs in gastric acid media. It is also appealing material for wound healing, thanks to its hemostatic and antibacterial properties and the possibility to establish polyelectrolyte complexes with other bio-based polyanions including alginate, pectin, carrageenan, xanthan gum, carboxymethyl cellulose, chondroitin sulfate, and hyaluronic acid [32,43,44].

1.3 Importance of transforming aerogels into fibers and textiles

Some types of inorganic aerogels have already reached the market in construction materials and aerospace engineering, but the full potential of aerogels is still to be assessed for other sectors such as the biomedical field. Despite the recent enhancement of polysaccharide aerogels' research in the academic field, their transformation to pilot and industrial scales is still pending. This is mainly due to the fact that even though the aerogels from biopolymers possess excellent textural characteristics, they suffer from poor processability, weak mechanical stability, high production cost, and time-consuming fabrication process which are severe challenges for large-scale production of these materials [19].

Textile fabrication technologies could be the key to overcoming this issue via offering multiple processing techniques such as electrospinning, wet spinning, and solution blowing. Moreover, the fibers can be fabricated in different sizes and have the potential to be transformed into various fibrous structures such as woven, knitted, braided, and nonwoven [20]. It can also reduce the time and cost of fabrications by reducing the drying time and utilizing available techniques in textile engineering, respectively [11,45]. In the current doctorate thesis, the aim was to transform bioaerogels from cellulose and chitosan into the fibers and textiles by using two principal techniques of wet spinning and solution blowing followed by scCO_2 processes. The products have been analyzed by different material characterization and *in vitro* assessment methods to check their

properties for biomedical applications of drug delivery and wound dressing.

In the next section, advances in fabrication and analysis of drug-eluting medical textiles for biomedical applications such as wound care, tissue engineering, and transdermal drug delivery are reviewed. From this, the technical requirements for the current study were derived and further developed into the overall concept.

1.4 Drug-Eluting Medical Textiles: From Fiber Production and Textile Fabrication to Drug Loading and Delivery

The market of medical textiles has great potential as it was worth USD 13.94 billion in 2014, which constituted 10% of the technical textile market in Europe and was predicted to increase its share to about 12% in the near future [46,47]. Various textile features such as their flexibility, light-weight, wide range of dimensions, surface, physical, and structural properties made these constructs favorable to be used in different medical applications [48,49]. Textile fabrics have been extensively used as drug delivery systems in wound dressings, synthetic skin graft substitutes, scaffolds for tissue repair and regeneration, and other topical applications [49,50].

Textile fibers are categorized into natural and man-made groups based on their origin or the way they have been produced. Natural fibers refer to naturally occurring fibers found in animals, vegetables, and minerals in which their properties depend on the source, the region where they have been produced or stored [51,52]. On the other hand, man-made textile fibers do not occur in nature although they might be made from natural materials in which the physical and chemical properties of the initial mater have been altered notably during processing. Man-made fibers can be made from synthetic and natural materials [52,53]. These fibers can be manufactured using different fiber production methods, such as melt spinning [54], wet spinning [55], and electrospinning [56] depending on the material used and the properties required for the final fibrous construct.

The cross-sectional shape of the fibers has a significant influence on their physical and mechanical properties, such as flexural rigidity, crispness, and stiffness [57]. Various shapes have been observed in natural fibers. For example, silk fibers have a triangular shape with rounded edges, while wool fibers have oval to round cross-sectional shapes [58,59]. Man-made fibers resulting from different production methods can also have different cross-sectional forms such as round, trilobal, and crenulated, and various morphologies, such as hollow and porous [50,60,61]. In addition, different types of polymers can be combined to produce fibers with the properties required for different

medical applications. For example, synthetic and natural polymers can be combined as the natural polymer can provide biological recognition and the synthetic polymer can be used for tuning the mechanical properties [62]. This combination can also appear in various morphologies, including core-shell structures,[63,64] micro/nanotubes, interpenetrating phase morphologies,[65] and nanoscale geometries, such as spheres, rods, micelles, lamellae, vesicle tubules, and cylinders.[66] Finally, produced fibers can be assembled into a 3D construct as woven, knitted, braided, or non-woven.

In woven textiles, the fibers are intermeshed together through a pattern called “warp” and “weft”, which typically results in a more robust and dimensionally stable structure than non-woven structures [67]. However, in non-woven textiles, no interwoven strands exist and fibers are bound by applying heat, chemicals, pressure, or a combination of these methods. The mechanical and thermal properties can be tuned by orienting fibers randomly or favorably in specific directions [50,68,69]; therefore, suitable constructs for various biomedical applications, such as wound care [70] and skin grafts [71], can be obtained. Finally, both woven and non-woven constructs can be functionalized with different bioactive agents using different drug loading methods [72].

Fibers can be loaded with bioactive agents or drugs using suitable physical or chemical processes. Examples of physical drug loading methods are absorption or adsorption, coating, and encapsulation, and examples of chemical loading methods are covalent conjugation and grafting [49,73-76]. Fibrous textiles used for drug delivery can also be categorized based on the mechanism by which the drug is released [77]. Some major types of releasing mechanisms are drug or solvent diffusion-controlled systems [78,79], chemically controlled systems, such as enzymatic or hydrolytic degradation [80], and externally regulated systems in which the application of an external stimulus, such as ultrasound or electrical field, triggers the release of the drug [81,82]. The release mechanism of the drug-containing fibers as a drug delivery system can be engineered based on the final application to avoid unwanted results, such as burst effect.

To investigate the kinetics of drug release, various statistical methods, such as repeated measures design [83,84], and model-dependent approaches, such as zero-order model [85,86], have been developed based on the different phenomena which control the drug release profiles [87]. Among various kinetic models, the zero-order is commonly used as it provides a consistent delivery pace of the drug independent of the concentration [85]. Another simple and frequently used model of drug release kinetic is the Korsmeyer-Peppas Model, the so-called power law, which describes the fractional amount of the drug released over time based on the assumption that the drug diffuses through the

polymer or the solvent diffuses inside [86]. Other models take more parameters, such as the effect of desorption, degradation, concentration gradient, and porosity, into account and thus provide more accurate outcomes [56,88,89].

Developing pioneering biomaterials with tunable physical and chemical properties that are qualified to provide controlled delivery of different biomolecules has great importance in the field of biomedical engineering. Hereby, the materials, production, and fabrication of drug eluting fibers, mechanisms of drug loading and delivery systems, and ultimately different biomedical applications of drug eluting textiles are discussed. Finally, the benefits and drawbacks of different types of drug eluting textiles and mechanisms of drug loading and release kinetics are summarized and potential future directions are provided.

1.4.1 Classification of fibers and materials

The main structural elements in textile products are made from natural and manufactured fibers. Natural fibers are sorted depending on their resource, originating from plants, animals, or minerals [49]. The most frequently used natural fibers in medical products are cotton, silk, and flax [90,91]. In addition, manufactured or man-made fibers can be divided into organic and inorganic fibers. Organic fibers can be further categorized into two large groups based on their sources which can be either natural or synthetic polymers [50,59,92]. Textile fibers classification, including some examples from each group, is shown in **Figure 1.3**.

1.4.1.1 Materials

By considering the difference in intrinsic functionality and physio-chemical properties of various materials, the selection of the right material or polymer plays a crucial role in designing and developing eluting drug textile. Natural, synthetic polymers, and inorganic compounds can be spun into fibers and form drug eluting textiles for versatile biomedical applications with varying properties, including macromolecule-drug interaction, drug loading efficiency, and release profiles [93].

1.4.1.1.1 Natural polymers

Natural polymers are widely present and produced in living organisms and are used in numerous fields such as tissue engineering [94,95], the food industry [96,97], and the pharmaceutical industry [98,99]. Natural polymers are biodegradable, biocompatible, low/non-toxic, relatively inexpensive, and readily available in many parts of the world [100,101]. However, they have some drawbacks, such as batch-to-batch variations, an uncontrolled hydration rate, and a slow production rate [101,102]. Natural polymers are

obtained directly from living organisms, such as carbohydrates and proteins, and those made from renewable resources that need to be polymerized, such as lactic acid and triglycerides [103,104].

Carbohydrate polymers or polysaccharides are polymerized out of monosaccharides. Polysaccharides have a high molecular weight and can possess different charges or pH values. Various 3D structure of these macromolecules is governed by the linkage configuration of monomers [105,106]. The most well-known carbohydrate polymer is cellulose which is typically obtained from processed cotton, wood pulp, or bacterial sources [107]. Cellulose and its derivatives are utilized for applications such as wound dressings due to their high tendency to form blood clots [8,108]. Furthermore, fibers obtained from modified polysaccharides such as alginates from algae, chitosan from crustacean shells, hyaluronan from the extracellular matrix (ECM), dextran and reticulated cellulose from bacterial fermentation are used for biomedical applications. Examples of polysaccharide-based products are wound dressings from alginate or bacterial cellulose [109,110], surgical sutures made out of cellulose, alginate or chitosan [111,112], scaffold materials or implants from chitosan, cellulose or hyaluronan [113,114].

Protein based fibers have been commercially produced since the 1950s [115]. Protein based fibers are widely used in medical textiles to possess biological recognition for cells to adhere to and promote cell infiltration and proliferation compared to carbohydrates and synthetic polymers [50,116]. Protein based fibers are obtained from living organisms using two main methods. In the first method, proteins are dissolved by solvents or enzymes before being precipitated and reconstituted into fibrils. In the second approach, other elements of living organisms are removed by solvent or enzymes [117]. Natural proteins such as collagen, and gelatin from thermal denaturation or acid/alkali degradation of collagen, fibrinogen, glycoprotein, and elastin have been extensively used to produce medical textiles [100,103,118,119].

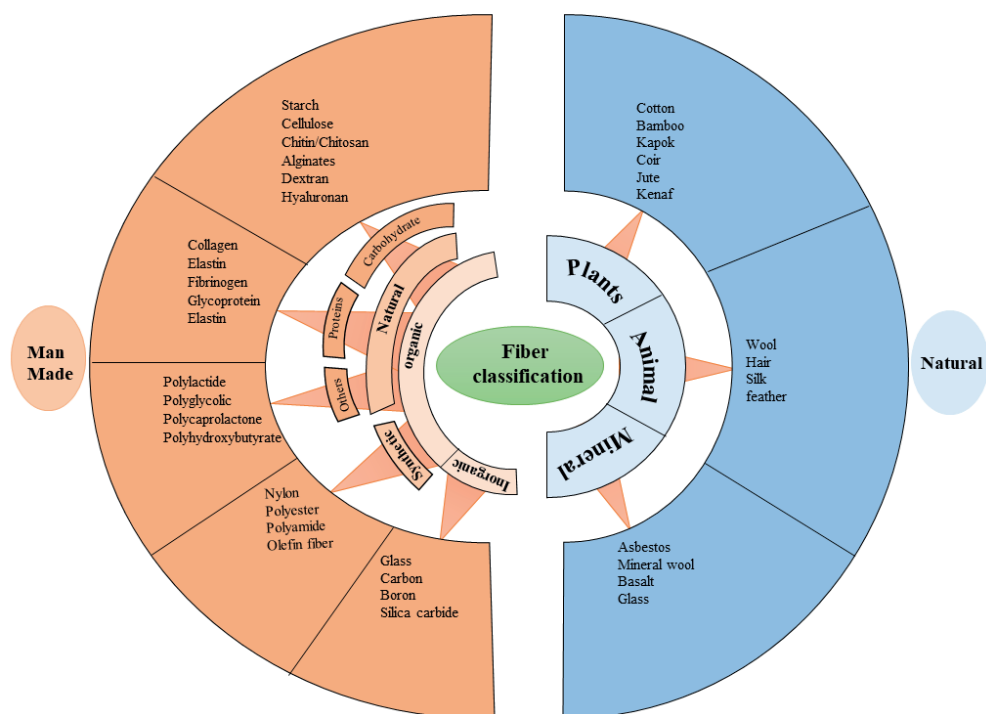
Natural polymers can be modified via their functional groups, such as amino carboxylic and hydroxyl groups, to improve their functionality, such as solubility, using chemical [96] or enzymatic modifications [97]. For example, chitosan, the deacetylated form of chitin, is a water-soluble polymer at a low pH, while chitin is insoluble in typical regular solvents such as water, organic solvents, mild acidic or basic solution [43]. Fibers spun from some natural polymers lose their mechanical properties in the human body typically faster than required. Thus, hybrid materials are preferred when using natural-based polymers, especially proteins, to reach the desired physical properties and improve the processability [50,120-123].

1.4.1.1.2 Synthetic polymers

Synthetic fibers are typically produced from chemicals or petrochemicals based materials. Through various polymerization processes, long molecular chains can be formed with different molecular weights and functional groups [124]. Therefore, engineering the structural characteristics of the material, such as melting point, crystallinity, and glass transition temperature, can lead to medical textiles' advancement and innovation. Three classes of widely used synthetic fibers which dominate the market are nylon, polyester, and acrylic [125]. Other popular synthetic polymers such as poly lactic-co-glycolic acid (PLGA), polycaprolactone (PCL) [126], polyethylene oxide (PEO) [127], and water-soluble polymers, such as polyvinyl alcohol (PVA) [128], poly(N-vinylpyrrolidone) (PVP) [129], are used to fabricate drug-eluting textiles for versatile biomedical applications. There are some challenges with the biocompatibility and biodegradability of synthetic fibers, however, they are more preferred than inorganic materials due to their carbon element based nature, which is more similar to the structure of biological tissue [130].

1.4.1.1.3 Inorganic materials

The inorganic fibers are composed mainly of inorganic chemicals, such as alumina, aluminum, carbon, silicon, and boron, which can be shaped into fibers after processing at elevated temperatures [131]. Inorganic fibers usually have high thermal and mechanical resistance. Many inorganic fibers, such as carbon nanotube, hydroxyapatite, and glass, have been successfully used in biomedical applications such as artificial hips [132], and vascular stents [131,133]. **Figure 1.3** shows a summarized schematic of fiber classification.

**FIGURE 1.3.**

Classification of textile fibers and materials. Fibers are divided into two main categories of natural and man-made fibers, each of which has several subgroups as shown in the figure.

1.4.2 Classification of drug-eluting textiles

Drug eluting medical textiles can be divided into three leading categories of filament fibers, woven, and nonwoven fabrics. Such textiles can be degradable or non-degradable based on the nature of the base polymer from which they are made. Among these three categories, nanofiber nonwovens have attracted more attention in recent years and have been extensively developed for various biomedical applications using different polymers. Additionally, individual fibers produced in the form of continuous filaments have been of great interest too. Such fibers may contain the active bio-agents inside or chemically bond to their surface. Braided surgical suture for wound closure is an example of mono and multifilament fibers. Such continuous filaments are usually manufactured using two main techniques of melt spinning and wet spinning based on whether the polymer is spun in melt or solution state [56,134-136].

Typically, natural fibers have diameters ranging from 10 to 100 μm , and manufactured fibers, using melt or wet spinning, could reach a similar diameter range. However, by using the electrospinning method, the size of produced fibers could decrease to

the nanometer scale [50]. Nevertheless, electrospinning is considered as a textile manufacturing technique rather than a fiber production method since nonwoven mats are the output products and not single fibers. Ultimately, multicomponent spinning is an approach to combining two or several polymers in the spinning head using the aforementioned techniques which enables us to obtain fibers with a wide range of biological and mechanical properties [137]. Different classes of drug eluting textiles including various fabrication technologies are discussed in the following section.

1.4.2.1 Fiber production methods

1.4.2.1.1 Melt spinning

During melt spinning, the polymer granules or resin are heated within an extrusion to reach the melting point. The molten polymer is then extruded through the spinning head, and based on the number of spinneret holes, either mono- or multi-filament is obtained (**Figure 1.4A**) [134]. The geometry of the spinneret defines the cross-sectional appearance of the fibers which can be, for instance, round, trilobal or hollow [50,134]. Fibers are then cooled and solidified in the air and further post fabrication processes such as drawing, lubricating, twisting or entangling prior to being wound on a bobbin can be applied on them [49].

Melt spinning is typically performed using thermoplastic polymers with high degradation temperatures and low melt viscosities. Therefore, it is not possible to use this technique for some natural polymers, such as chitin or chitosan, due to the strong interchain forces that raise the melting point above the thermal degradation or the thermal sensitivity of the backbone [42]. However, polymers from renewable sources like poly(L-lactic acid) (PLA) [138], poly(ϵ -caprolactone) (PCL) [139], and cellulose derivatives, such as cellulose acetate butyrate [140], can be spun using this technique. Finally, due to the high processing temperature, melt spinning is typically not suitable for fabricating drug loaded fibers, especially when the drug is impregnated into the fibers during the spinning process [141].

1.4.2.1.2 Wet/gel spinning

In wet spinning, the polymer solution is extruded through a spinneret into an anti-solvent in a regeneration bath where the fluid coagulates and regenerates into continuous solid filaments. Afterward, solvent and anti-solvent are washed, and fibers are drawn and dried before winding (**Figure 1.4B**). Dry-jet wet spinning is similar in principle to wet spinning; however, the only difference is that the polymer solution will be spun through an air gap before reaching the anti-solvent regeneration bath, causing higher molecular chain orientation compared to wet spinning [142,143]. Due

to the diffusion of the solvent into the anti-solvent, the cross-sectional shape of the fibers is often crenulated with multiple grooves [50,69,144]. Cellulose (viscose rayon) [64], chitosan [69], alginate [145], PCL [146] are some examples of natural polymers that have been spun using this method.

The spinneret diameter, air pressure, injection rate, concentration of the polymer, and the type of solvent and anti-solvent have a noteworthy impact on the characteristics of the final fibers [69,147]. For example, wet spun alginate hydrogel wound dressings with different fiber sizes (~ 55 – $170\ \mu\text{m}$), Young's modulus (0.026 – $0.148\ \text{MPa}$), swelling ratio, release efficacy, water vapor transmission rate, and antibacterial activity were manufactured only by changing the spinning parameters such as air pressure (3 – $6\ \text{bar}$), the concentration of alginate and calcium (1.5 to $3\ \text{w v}^{-1}\%$ alginate; 0.5 to $5\ \text{w v}^{-1}\%$ calcium), and nozzle diameter (150 – $200\ \mu\text{m}$). The control sample ($\sim 60\ \mu\text{m}$ diameter) was spun with the air pressure of $6\ \text{bar}$, needle size of $150\ \mu\text{m}$, and calcium and alginate concentration of $5\ \text{w v}^{-1}\%$, $1.5\ \text{w v}^{-1}\%$, respectively. In this study, the lower pressure or lower injection rate and longer manufacturing time formed loosely bound large-diameter fibers ($\sim 160\ \mu\text{m}$, $E=0.04\ \text{MPa}$), as it allowed more time for calcium to crosslink the fiber. The ten-time decrease in the calcium concentration ($0.5\ \text{w v}^{-1}\%$) led to the fabrication of thicker fibers ($80\ \mu\text{m}$) since the alginate molecules had more time to expand before complete crosslinking occurred [148].

Furthermore, co-axial wet-spinning fabrication can be utilized to create core-shell fibers as a method to impregnate both hydrophilic and hydrophobic drugs in one structure. For instance, Wade *et al.* produced co-axial alginate-PCL microfibers which were loaded with gemcitabine and nab-paclitaxel in the alginate core and PCL shell, respectively in order to treat unresectable pancreatic ductal adenocarcinoma. More than $94\ \%$ of the gemcitabine was released in the first $10\ \text{h}$ in the simulated body fluid (SBF) and phospholipase D, while nab-paclitaxel exhibited a sustained release profile over three weeks with less than 39% of the drug released in PBS [149].

1.4.2.1.3 Electrospinning

The first usage of electrospinning to fabricate microfibers and nanofibers goes back to 1934, when Formhals released his work on artificial threads using the electrostatic procedure [150]. In this method, fibers with diameters ranging from micrometer to nanometer from a polymer solution or melt subjected to an electric field can be fabricated. The electrospinning system is composed of a syringe pump that controls the flow rate of the solution and a high voltage power supply connecting an electrode with a needle-like nozzle to a collector electrode (**Figure 1.4C**) [56,151–153].

The final properties of the fibers are influenced by different processing variables such as voltage, nozzle to collector distance, needle diameter, flow rate, spinning ambient, and solution parameters, such as concentration, viscosity, conductivity, surface tension, and solvent volatility. Fiber orientation can be controlled by selecting the proper collector for a specific end application. Rotating drums or parallel plates can be used to produce fiber mats with aligned and unoriented fibers, respectively [154]. For example, for the fabrication of the scaffolds for vascular grafts, it is essential to produce tubular constructs with the fibers predominantly aligned in the circumferential direction mimicking the preferential alignment of the ECM fibers in native blood vessels [8,155].

The possibility of incorporating hydrophobic and hydrophilic drugs/proteins and metallic nanoparticles within the bulk phase of fibers makes electrospinning an efficient and highly flexible process to produce drug eluting fibers [56,156]. We reported the loading and controlled release of tetracycline hydrochloride (TC.HCl) from Curdlan nanofibers over a period of 6 hours [157]. Curdlan, an extracellular polysaccharide produced by *Alcaligenes faecalis* bacterium, was blended with polyethylene oxide in different ratios. Antimicrobial activity was acquired by loading TC.HCl to the fibrous system. The cross-linked nanofibers showed an initial burst release behavior in the first two hours due to the release of TC.HCl which is attached to the surface of poly(ethylene oxide) (PEO) nanofibers. Afterward, a sustained release profile over 6 hours was observed. Several other polymers, such as PLA [158], gelatin [159], PCL [160], and polymers from bacterial sources, such as polyhydroxyalkanoate [161], poly(3-hydroxybutyrate-co-3-hydroxyvalerate) [162], can be used to produce ultrafine fibers using electrospinning.

Moreover, a summary of spinning feed type and parameters as well as the resultant cross-sectional shape of the fibers using three spinning methods of melt spinning, wet spinning, and electrospinning are provided in **Table 1.1**.

TABLE 1.1.

An overview of spinning methods, processing parameters and the resultant fiber shape [58,154,163].

SPINNING METHODS	FEED TYPE	PROCESS PARAMETERS		CROSS-SECTIONAL SHAPE
Melt spinning	Granules	- Viscosity	- Geometry of the spinneret	- Round
	Resin	- Mw and Đ ^{a)}		- Squares
	Thermoplastic-polymers		- Drawing ratio	- Trilobal
			- Take up speed	- Ellipse
			- Temperature	- Hollow
			- Humidity	
Wet spinning	Solution	- Concentration	- Geometry of the spinneret	- Round
		- Viscosity		- Regular serrated
		- Mw and Đ	- Air pressure	- Trilobal
			- Injection rate	- Hollow
			- Anti-solvent	
			- Washing	
			- Drying	
			- Drawing ratio	
			- Take up speed	
			- Temperature	
			- Humidity	
Electrospinning	Solution	- Concentration	- Flow rate	- Round
	Polymer melt	- Viscosity	- Needle diameter	
		- Conductivity	- Applied voltage	
		- Surface tension	- Tip to collector distance	
		- Solvent volatility	- Collector types	
		- Mw and Đ	- Temperature	
			- Humidity	
Multicomponent spinning	Solution	- Concentration	- Similar to melt	- Segmented Pie
	Polymer melt	- Viscosity	- or wet spinning	- Islands in Sea
		- Ratio of components		
		- Components miscibility		
		- Mw and Đ		

^{a)} Mw (weight average molecular weight), Đ (dispersity, $\bar{D}_M = Mw/Mn$).

1.4.2.1.4 Multicomponent spinning

Multicomponent spinning technology can provide the opportunity to tune the mechanical and the biological properties of the fibers by, for example, combining a material with desired mechanical properties for the final use with another material possessing proper biological properties. Multicomponent spinning requires combining two or more polymers at the spinning head while the resulted fibers contain all the polymer components in isolated pieces of the cross-section [137,164]. Melt-spinning, wet spinning, and electrospinning can be utilized to form multicomponent fibers [56,165,166]. Moreover, it is possible to fabricate ultrafine fibers by multicomponent fiber spinning, using thermal treatments or dissolutions to remove the polymer matrix of some of the components of the fibers [50,164,167].

Bicomponent spinning is used to produce nanofibers via two essential techniques: (i) spinning islands-in-the sea (INS), which contains a large number of islands surrounded by the sea (matrix) polymer, and (ii) splittable bicomponent fibers, known as segmented pie fibers, which is another approach to produce nanofibers with noncircular cross-section [164,166,168]. Furthermore, bicomponent fiber spinning can be used to spin a resorbable polymer sheath around a non-degradable polymer; drugs and bioactive agents can be loaded into the outer resorbable sheath and released at controlled rates based on the polymer thickness, molecular weight, and morphology [169,170].

Multicomponent fibers containing bioactive agents or function-regulating biomolecules, such as DNA and growth factors, are widely used in biomedical textiles [50,165,171]. They offer various fiber morphologies, such as core-sheath [63], side-by-side fibers [172], micro/nanotubes, and interpenetrating phase morphologies [65] as shown in **(Figure 1.4D)**. In addition, a large group of nanoscale morphologies [66] such as spheres, rods, micelles, lamellae, vesicle tubules, and cylinders are fabricated by self-assembly of block copolymers [165,173]. Therefore, multicomponent spun fibers have great potential to be designed and fabricated as drug eluting fibers.

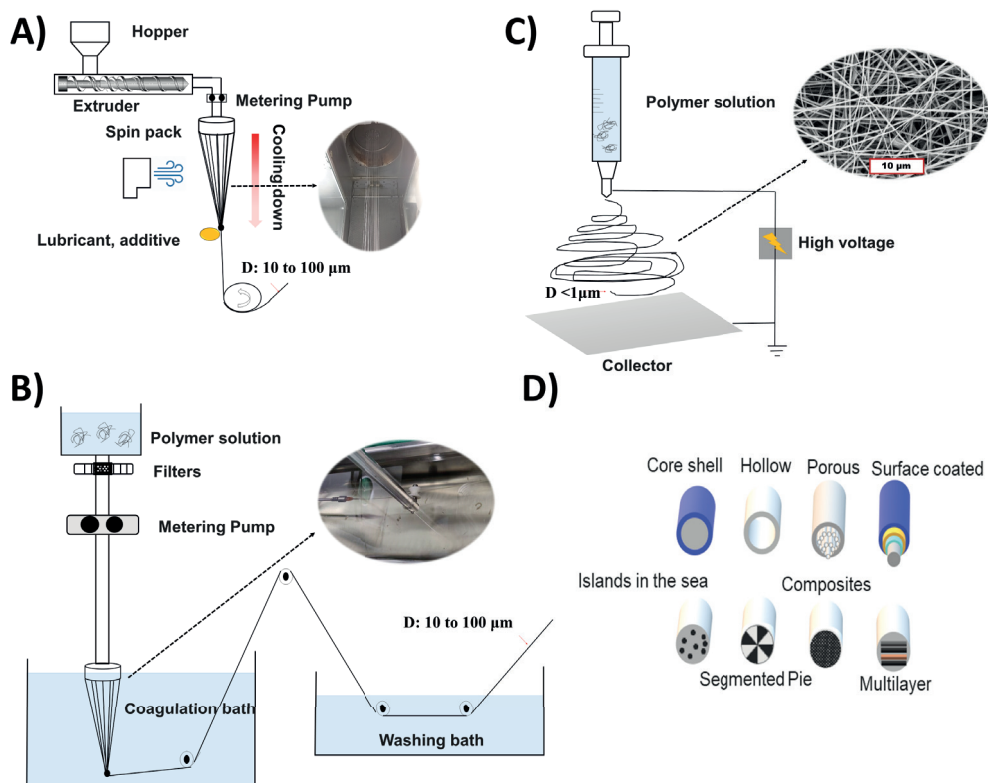


FIGURE 1.4.

The schematic of fiber production techniques and their representative morphologies. A) Melt-spinning method in which the molten polymer is extruded through the spinning head. B) Wet-spinning process showing that the polymer solution is extruded through a spinneret into an anti-solvent to form a solidified fiber. C) Electrospinning in which polymer solution or melt is subjected to an electric field to fabricate micro or nanofibers, and D) some examples of various morphologies of multicomponent fibers.

Each aforementioned fiber spinning methods have advantages and disadvantages for producing drug eluting textiles. For instance, melt and wet spinning methods typically lead to fibers with larger diameters compared to electrospinning; however, an additional fabrication process is usually required to turn fibers into textiles. In addition, melt spinning is considered as a fast solvent-free technique, but the degradation of polymers and incorporated drugs are likely to happen due to the harsh processing conditions such as high temperature and shear rates. Also, extended exposure to organic solvents during the spinning and regeneration might in wet spinning negatively impact the fiber biocompatibility, but it is applicable to many natural based polymers and benefit from mild temperature processing conditions. Although electrospinning is a simple, inexpensive technique resulting in submicron fibers, the toxicity of the solvents and the instability of the jets, and the processing issues with conductive polymers can be highly challenging [141,174].

1.4.2.2 Textile fabrication techniques

Textiles as the final processed products of the fibers are typically categorized to woven or nonwoven fabrics which are reviewed in this section.

1.4.2.2.1 Knitted fabrics

The knitting process creates forming loop stitches in rows (longitudinal direction of fabrics). These stitches intermesh with the next and previous rows and form either flat or tubular fabrics. Unlike weaving, where yarns are always running straight both in the transverse (weft) or the longitudinal (warp) directions, the yarn in knitted fabrics follows the forming sequence of symmetric loops above below the mean path of the yarn. These knitted loops are extensible in the course and wales (X and Y , respectively) directions, giving the knit fabrics much more elasticity than woven fabrics. Therefore, it is commonly used in medicated bandages and adhesive tapes [175]. Depending on the loops' formation direction, the knitting process is categorized into two main classes of warp and weft knitting (**Figure 1.5A-I, II**) [176].

More fibers are involved in the knitting process than any other textile technology to allow the fabrication of complex 2D and 3D structures [177]. Li *et al.* developed a weft-knitted stent for colorectal cancer treatment from 5-fluorouracil (5-FU)-loaded polydioxanone membrane [178]. 5-FU was incorporated into the nanofibres and coated onto the surface of the knitted stent. The half-maximal inhibitory concentration (IC50) and the median lethal dose (LD50) validated that the membranes outperformed the pure 5-FU and exhibited higher antitumor activity due to the sustainable drug-releasing profile of the coated stent (**Figure 1.5A-III**).

Shanmugasundaram *et al.* developed wound-healing flat-knitted cellulosic fabrics coated with chitosan and alginates [179]. Chloramphenicol and tetracycline hydrochloride drugs were loaded into the coating polymers to improve the antibacterial and wound healing properties. A gel-like with chunky-complexed granules was formed; consequently, heterogeneous films were created upon mixing chitosan and alginates due to the electrostatic interactions between the amino groups in chitosan and the carboxyl groups in alginate. The study concluded that when the drug on the fabric's surface is exhausted, the polymer coating on the surface provides a succeeding shield against bacteria.

In another study, an anti-inflammatory dressing was developed via eluting hydrocortisone (HCr) on activated cotton knitted fabrics for skin-friendly treatment of coetaneous [180]. Drug elution was attained either via covalent grafting of cotton

with monochloro triazinyl-beta-cyclodextrin (MCT- β -CD), or through the inclusion of sodium sulfate in an ionic crosslinked chitosan-based hydrogel. The developed systems were deposited on the knitted fabrics and are meant for a temporary generation of HCr inclusion. Although the drug-loading method is different, the drug-release mechanism is relatively identical. In the case of MCT- β -CD, the wet conditions, due to perspiration, triggers the substitution of HCr from the internal hydrophobic cavity and promote its transfer to the dermis. For the hydrogel, the medium swells the chitosan-based hydrogel to form a mesh, and then the drug is diffused toward the dermis.

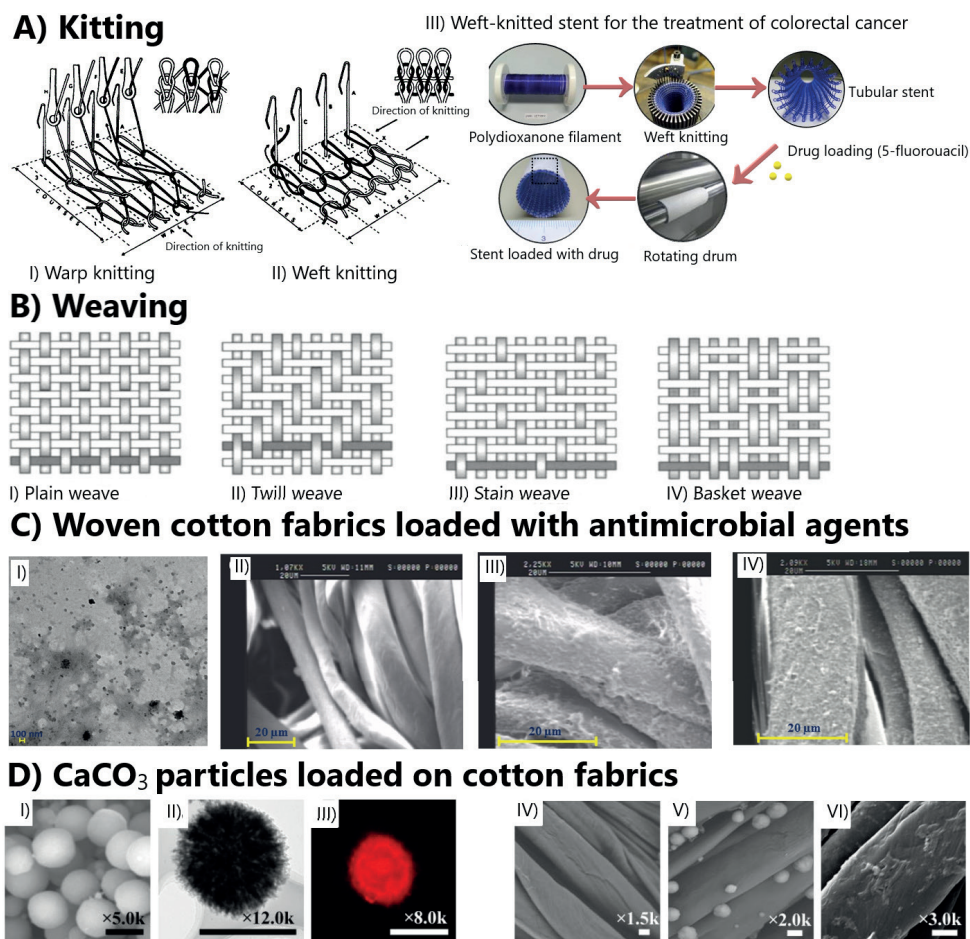
1.4.2.2.2 Woven fabrics

The woven fabric is made by linking two orthogonal arrays of yarns, the first is the warp at 0 degrees and the second is weft at 90 degrees [181]. The yarns are seized in place due to the inter-yarn friction. The weaving loom technology is well established and provides low manufacturing costs through high productivity rates. The yarns' interlacement acquires stability to the structure and enables complex shapes with no gaps. Different woven structures such as plain, twill, stain, and basket weaving are shown in **Figure 1.5B**. In some medical applications, woven systems involve the assembly of fabrics that are encapsulated with drugs or active ingredients. Besides woven fabrics can be decorated with bioactive agents via physical absorption and coating or with the aid of modifiers to bond them covalently [136]. Apart from drug releasing properties, medicated woven fabrics offer defined geometry, pore structure, as well as the strength that are suitable for various medical applications such as wound dressing, artificial skin grafts, and scaffolds for tissue engineering [182,183].

Ayikut *et al.* investigated the weaving of polyvinyl alcohol yarn and cotton to produce a high strength drug delivery system. The woven fabrics were treated with different concentrations of aqueous crosslinkers, namely borax and glutaraldehyde solutions [184]. In another study, woven cotton and viscose-micromodal fabrics were loaded with caffeine nanoparticles for transdermal antioxidant patches. Once worn next to the skin, the system can deliver caffeine for several hours without any further action from the patient [185]. The self-assembled coating on woven cotton fabrics utilizing the layer-by-layer (L-B-L) technique to acquire antimicrobial properties was explored by Gadkari *et. al* [186]. In this study, chitosan loaded with silver nanoparticles (**Figure 1.5C-I**) was used to coat the surface of the fabrics (**Figure 1.5C-II, III, IV**). The sustained release of silver ions (Ag^+) from cotton fabrics was confirmed by atomic absorption spectroscopy over 48 hours.

Bioactive woven cotton gauze is suitable for antimicrobial wound dressings; for instance, medical gauze was decorated with silver nanoparticles and medicated via acacia gum. The woven fabric was found active against the infectious bacterial strains *Staphylococcus aureus* and *Pseudomonas aeruginosa* [187]. Synthetic polyester fabric has been investigated as a carrier for skin lubrication via polytherapeutic substances. The loaded materials increased the durability and abrasion resistance of the textile fabric in addition to its medical effect [136].

In another study, the microgel particles from poly(N-vinylcaprolactam) and chitosan were prepared in calcium carbonate templates (CaCO_3) (**Figure 1.5C-I, II, III**) to be on woven cotton fabrics for the treatment of sunburn (**Figure 1.5C-IV, V, VI**) [188]. The *in vitro* drug release behavior, in response to temperature, was evaluated at pH 7.4 in phosphate buffer saline. The drug-release profile exhibited extended-release above the lower critical solution temperature due to the shrinkage of the microgels. Mihailiasa *et al.* reported the mobilization of hyperbranched polymers on the surface of woven cotton fabrics. Nanosponges from hyperbranched β -CD were loaded with melatonin in water/ethanol suspension and mobilized on the surface of the fabrics [189]. A zero-order kinetic behavior was observed for the functionalized fabrics as an indication of a typical reservoir diffusion-controlled system.

**FIGURE 1.5.**

Knitted and woven fabrics in drug delivery applications. A) Schematic drawings of different knitting patterns, (I) warp knitted, (II) weft knitted. Reproduced with permission [176]. Copyright 2000, Elsevier, and (III) weft knitted stent for treatment of colorectal cancer are presented. Reproduced with permission [178]. Copyright 2013, Elsevier. B) Schematic drawings of different woven patterns, plain (I), twill (II), stain (III), basket (IV). Reproduced with permission [190]. Copyright 2000, Elsevier. C) SEM images of chitosan-silver nanoparticles (I), untreated woven cotton (II), and loaded woven cotton fabrics with nanoparticles (III, IV). Reproduced with permission [186]. Copyright 2020, Elsevier. D) SEM images of microgel particles from poly(N-vinylcaprolactam) and chitosan were prepared in calcium carbonate templates (CaCO_3) (I), TEM image of porous CaCO_3 (II), CLSM images of microgel after core removal (III), pure cotton fibers (IV), microparticle-loaded cotton (V), and microgel-loaded cotton (VI). Reproduced with permission [188]. Copyright 2017, Elsevier.

1.4.2.2.3 Nonwoven Fabrics

In general, nonwovens are widely used as medical textiles and are usually considered disposable products. Surgical gowns, masks, surgical drapes, pads, medical filters, and wound dressings can be made from nonwoven fabrics. Its high flexibility, short

production cycles, and low-cost production are popular reasons for using nonwovens in medical applications. During the past several years, melt-blowing (**Figure 1.6A**), solution blowing (**Figure 1.6B**), needle-punching (**Figure 1.6C**), air laying, wet laying, chemical bonding, thermal bonding, hydro-entangling, spunbonding, and carding have been essential technologies for the formation of nonwovens for medical applications [191,192].

Most nonwoven fabrics are anisotropic, meaning having more fibers oriented in longitudinal (machine direction) than in the cross direction. The fibers entanglement in a web has a profound effect on the final web properties. Also, fiber configuration impacts fiber packing pore size, capillary dimensions, and capillary orientation. Although nonwovens possess several advantages when used as medicated wound dressing, such as optimal fluid absorbency, breathability, excellent barrier properties, lightweight, and comfortable contact with skin, they inherit weak mechanical stability when compared with woven and knitted fabrics. This is mostly attributed to the lack of fiber interlacing and yarn locking [193].

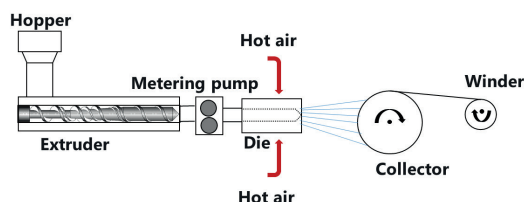
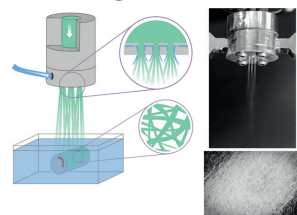
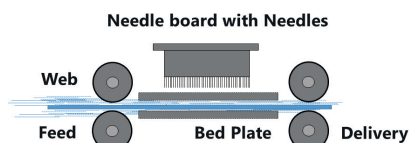
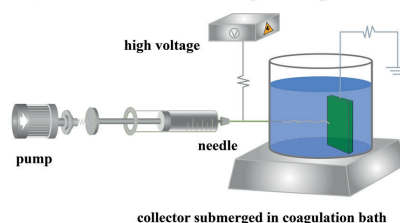
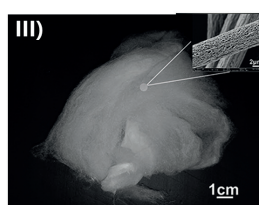
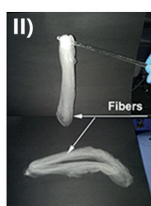
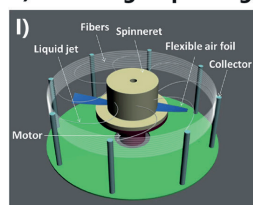
The most recent nonwoven innovation is the fabrication of 2D and 3D nanofiber mats for implantable scaffolds, biological filters, and drug eluting systems. Recent advances in material science enabled the materials and devices to be fabricated on the nanoscale. The primary reason for minimizing the object size compartments to nano scales is to provide superior mechanical properties and a high surface-to-volume ratio [194]. Electrospinning has been widely investigated to produce nanoscale fibrous structures in various conditions such as immersion electron spinning in which the fiber collectors can be immersed in coagulant solutions (**Figure 1.6D**), and the fibers can be collected in the wet state. Different active materials such as drugs can be dispersed in the coagulation bath and loaded into the nanofibers upon their precipitation [195].

Different techniques are being used for nanofiber formation, among which biocomponent extrusion is widely used. In this technique, two different polymers with various blending ratios are spun together in the same fiber from the same spinneret. Usually, one fiber component can be removed by heat, solvent, or mechanical device, leaving the core fiber alone [196]. Another fiber formation process is the phase separation technique. It is a five-stage procedure in which the polymer is dissolved in a proper solvent followed by gelation, solvent extraction, freezing, and freeze-drying. This system relies on phase separation due to physical inconsistency between solvents and polymer. The dissolving agent is extracted and leaves the residual fibers dry [197]. On the other hand, nanofibers from polymer melts can be produced through the melt-blowing technology.

Nanofibers can be created by extruding molten polymer into pressurized gas/air streams. Furthermore, self-bonded webs can be collected on a rotating drum or belt. The air jet creates a drag force that attunes the fibers rapidly and dramatically reduces its diameter below the nozzle diameter.

Nagy *et al.* investigated the production of a melt-blown nanofiber system based on a hydrophilic vinylpyrrolidone-vinyl acetate copolymer and PEO plasticizer for drug delivery applications [198]. In addition, the blowing of polymer solutions through concentric nozzles can lead to the formation of nanofibers. Solution blow spinning was first developed in 2009 by Medeiros *et al.* [199] to fabricate submicron fibers at a high production rate. Nonwovens from PLA as well as PLA/poly(vinyl pyrrolidone) blend containing 20% (wt/wt) antimicrobial Copaibla oil [200]. A recent emerging method for nanofiber formation is centrifugal spinning (**Figure 1.6E**) [201]. This spinning method relies on centrifugal forces to achieve the high production rate of nanofibers. Both polymer solution and melt can be used to fabricate nanofibers [202]. Stojanovska *et al.* were the first to report the formation of lignin-based nanofibers via an industrially scalable centrifugal spinning system [203]. The research aimed at the large-scale production of lignin/thermoplastic-polyurethane (TPU) nanofibers for bioactive materials. In another recent study by Rampichova *et al.*, a 3D PCL scaffold was loaded with a combination of TGF- β , IGF, and bFGF growth factors and was used as a delivery system in the treatment of skeletal disorders [204].

In general, non-woven and woven drug-loaded fibrous constructs are selected based on the final requirements of the biomedical application. However, drug eluting woven and knitted fabrics provide more precise geometry, pore structure, and strength than nonwoven fabrics. On the other hand, nonwoven fabrics such as electrospun fibers with smaller pore sizes are more feasible to reach nanostructures with sophisticated morphologies. Nevertheless, considerable challenges must be solved to scale up the fabrication procedure and transform electrospinning into a commercial and operational process [141,174]. For instance, the poor reproducibility, high dependency of processing conditions on polymer-solution nature, and limitation of the obtainable mesh thickness are the main challenges in the aspect of the mass production of nanofiber fabrics [205].

A) Melt blowing**B) Solution blowing****C) Needle punching****D) Immersion electrospinning****E) Centrifugal spinning****FIGURE 1.6.**

Schematic representation of some nonwoven manufacturing technologies from bulk fibers as well as nanofiber. A) Melt-blowing. B) Solution blowing. Reproduced with permission [192]. Open access, copyright "Creative Commons CC BY license", Wiley. C) needle-punching. D) Immersion electrospinning. Reproduced with permission [195]. Copyright 2020, Elsevier. E) Centrifugal spinning (I). Reproduced with permission [206]. Open access, copyright "Creative Commons Attribution-NonCommercial 3.0 Unported Licence", 2017, the Royal Society of Chemistry, (II) an image of ethyl cellulose/polyvinyl pyrrolidone fibers fabricated from centrifugal spinning, (III) SEM images indicating micro- and nano-porous structures produced by centrifugal spinning. Reproduced with permission [207]. Copyright 2017, Elsevier.

1.4.3 Drug loading of fiber-based constructs

Drug eluting systems provide sustained delivery of drugs and other bioactive agents over a period of time from hours to months. Drug eluting fibers are recently used for delivering different kinds of drugs, such as antibiotics, anti-inflammatory drugs, growth factors, anti-cancer drugs, proteins, DNA, gens, and vaccines [208,209]. A variety of loading mechanisms are used to produce drug eluting fibers depending on the parameters such as the type of drug, fiber production method, and the expected drug release profile. For instance, the drug can be incorporated at the pre-spinning stage by mixing with a polymer solution or after spinning using methods such as coating and supercritical loading [75,210,211]. Coating [212,213], encapsulation [214,215], hollow fiber filling [216], ion exchange [217-219], inclusion complex [220,221], direct conjugation [222,223], hot-melt extrusion [224], and supercritical impregnation

[75,78] are some important methods that have been used to load fibers with drugs through physical adsorption, entrapment, and covalent attachment of the drugs to the fibers [49].

1.4.3.1 Coating

Using this loading method, the drug is incorporated on the surface of the fiber by immersing it in a drug solution [213] or by coating it with drug encapsulated micro- or nanoparticles [225] (**Figure 1.7A**). Several coating methods, such as electrochemical deposition [226,227], immersion [212], dispersion, and curtain coating [174] are used for drug incorporation onto the fibers. Coating parameters such as pH, solids content, and coating thickness can be tuned to reach the desired coating [174]. In addition, the bioactive components can be grafted to the coating material. Therefore, the coating efficiency is depended on the type of the material, the affinity of the drug to the fiber, coating thickness, and the coating formula [228].

One of the main issues in the controlled drug delivery systems is the initial burst release. There are some strategies applied to the coating procedure which can help to achieve sustained release over time, such as using microcapsules and adhesives drugs that can adhere to biological tissues for an extended period of time [225,229], repeated layers of drug coating on fibers using L-B-L deposition [230], or taking advantage of processes, such as ultrasound, ion-beam, and irradiation [49,73,231]. For instance, Ma *et al.* [225] coated cotton fabrics with a solution comprised of tamoxifen drug microencapsulated in gelatin B and acacia gum as an anti-cancer drug for the treatment of breast cancer. Microcapsules remained on fabrics even after 5 and 10 cycles of washing. The coating was stable, and the compound was released over 10 hours after an initial burst release. The initial burst effect (30-60%, 1 hour incubation time) was attributed to the fact that a significant amount of tamoxifen was loaded in the vicinity of the microcapsule surface.

In addition, different structures of fibers can be formed using coating methods. For example, in a study by Zilberman [232], core-shell structures were created by coating the core polymers of poly(L-lactic acid) (PLLA) for eluting hydrophilic horseradish peroxidase and nylon for eluting hydrophobic paclitaxel. The shell was made out of drug/protein-containing poly (DL-lactic-co-glycolic acid) to form a porous shell structure. The fibers were dip-coated in fresh emulsions of the shell material and subsequently freeze-dried. The structure and pore size of the shell was tuned by organic:aqueous phase ratio, polymer concentration in the organic phase, and the amount of drug. Both types of drug loaded fibers had an initial burst effect followed by a reduction in the

release rate over time, normal for diffusion-controlled systems. In most of the samples, the horseradish peroxidase and loaded PLLA fibers released 90% of the active agent over 90 days. Paclitaxel exhibited a very low initial burst effect (less than 3%), and over 30% of the drug was released within the first 30 days. It was shown that a suitable formulation of the emulsion could lead to a variety of new core-shell structures with favorable drug release profiles.

Coating can also be used to protect the drug layer or as an option for selective contact surface of the fibers with the target area [174]. For instance, dispersion coating in which polymer dispersions are applied and dried on the surface to make a uniform and non-porous film, can provide a protective layer for drugs against possibly toxic substances by utilizing separate converting machines or printing press. Also, the desired drug-coated surface area can be obtained by sealing the unwanted sides [141,174].

1.4.3.2 Encapsulation

In this method, incorporation of bioactive agents or drugs can be done either before the fiber production (**Figure 1.7B-I**), by homogeneously mixing the polymer and the drug solution [233], or during the post-fabrication process (**Figure 1.7B-II**), for example, by soaking swellable fabrics in a drug solution [122,234]. Encapsulation of drugs in the fibers is better performed in the preparation stage as a higher dosage of drugs can be loaded [215]. Loading the fibers through the pre-fabrication process depends on the solubility of the drug and the polymer. However, it depends on the swelling of the fiber and diffusion of the drug in the polymer matrix in post-fabrication [49,56]. In case of the low solubility of the drug or the polymer in the solution, drug-polymer suspensions can be prepared by dispersing fine drug particles followed by agitation or exposing the drug-polymer solution to ultrasonic waves [73].

Furthermore, the drug eluting fiber can be made out of suspension by electrospinning [235], wet spinning [236], or microfluidic spinning [237-239]. In wet spinning and microfluidic spinning, encapsulation efficiency dramatically depends on the type of anti-solvent used to regenerate and solidify the fibers as it might lead to partial dissolution of the drug [148,236,237]. Wu *et al.* [240] fabricated microfibers made of polyacrylonitrile (PAN) encapsulated with curcumin and vitamin E acetate. The encapsulation at the solution preparation stage was successful and both drugs were loaded; however, the actual drug loading content was lower than the theoretical drug loading content due to the diffusion of the drugs into the coagulation bath. The drug-loaded filaments showed a microvoid structure caused by entrapment of solvent and non-solvent molecules and subsequent drying of the fibers. The pores could enhance the specific surface area, air

permeability, and the drug release rate. Woven textiles from PAN filaments showed good cytocompatibility with a prolonged drug release profile over more than 600 hours.

1.4.3.3 Bioconjugation

In this approach, to couple the bioactive agents to the surface of the fiber, the presence of functional groups, such as carboxyl [241], amine [242], and sulfonic groups [243], on fibers are required. Surface functionalization can be performed using plasma treatment, wet chemical method, grafting, and co-spinning. When the surface is functionalized, drugs can be coupled to the surface of the fiber by, for instance, chemical conjugation, such as covalent, or physical conjugation, such as adsorption [222,223,243,244].

1.4.3.3.1 Plasma treatment

In this method, surface adhesion and hydrophobic or hydrophilic properties can be tuned by altering the surface chemical structure. Furthermore, various functional groups, such as carboxyl and amine, depending on the gas used to create plasma, can be added to the surface (**Figure 1.7C-I**). Fiber surfaces with activated functional groups created by plasma treatment have been used to couple with protein-based materials, such as gelatin, collagen, laminin, and fibronectin, to enhance cellular adhesion and proliferation [234,245,246].

1.4.3.3.2 Wet chemical method

Plasma treatment is limited to the surface area, whereas wet chemical methods, such as partial surface hydrolysis, can be a solution to increase the conjugation sites [247,248]. This means that the surficial ester linkages in the polymer chain backbones of biodegradable aliphatic polyesters under acidic or basic conditions will be chemically cleaved; therefore, carboxylic and hydroxyl groups will be generated while the polymer remains water-insoluble [222]. Sun *et al.* [249] investigated simple alkali hydrolysis as an efficient way to modify polyesters, such as PCL, to couple a cell-recognizing peptide to a carboxylated surface.

1.4.3.3.3 Graft copolymerization

Another approach to conjugate bioactive molecules on the fiber surface is via graft copolymerization. In this technique, particular monomers are covalently linked to the backbone of the macromolecule via free or controlled radical polymerization. The polymerization is often initiated with plasma or UV radiation treatment to create free radicals for the polymerization. (**Figure 1.7C-II**) [222,250]. Using this method, multi-functional macromolecules with hydrophobic or hydrophilic groups can be tailored [222]. In a research done by Park *et al.* [251], poly(glycolic acid) (PGA), PLLA, and poly

(lactic-co-glycolic acid) (PLGA) electrospun fibers were functionalized using oxygen plasma treatment, and *in situ* grafting of hydrophilic acrylic acid (AA) to incorporate hydrophilic functional groups resulted in better fibroblast proliferation.

1.4.3.3.4 Co-spinning

In this approach, it is essential to achieve a homogenous polymer blend solution of nanofibers, nanoparticles, and functional polymer segments prior to spinning [49,222]. Functional groups can be located on the fiber surface via co-spinning of different polymers containing various functionalities (**Figure 1.7C-III**). For example, Sun *et al.* [252] fabricated antibacterial surface biofunctionalized electrospun PEO fibers as a host polymer and an oligopeptide conjugate. This was a single-step method to obtain surface biofunctionalized fibers which possess three repeated units of a triad serine, glutamic acid, and glutamic acid (Ser-Glu-Glu)₃ using the co-spinning method.

1.4.3.4 Inclusion complex

An inclusion complex is a compound in which a small molecule (the guest) can be accommodated in its cavity (the host) (**Figure 1.7D**). Usually, inclusion complexes are referred to as textile slow-release systems due to their ability to release the guest compound in a slow and continuous manner [49,174,253]. Several large molecules such as CD, fullerene, azacrown ether, and their derivatives can be used to produce inclusion complexes [254,255]. The most well-known inclusion compound used in drug releasing textiles is CD, cyclic alpha-1,4 linked oligosaccharides consisting of numerous D-glucose units, alpha-, beta- and gamma. The hydrophilic interior and hydrophobic exterior of CDs make them favorable substances in the complexation of drugs [255-257].

The first step in loading fibers is to introduce cyclodextrin on the surface of fibers which can be achieved by using one of the bioconjugations explained in section 1.4.3.3. [220,221] Then, the surface of the fibers is ready to form inclusion complexes with bioactive agents for drug delivery purposes (**Figure 1.7D**) [253]. As an example of using CD, wool fibers grafted with β -CD using low-temperature oxygen plasma treatment and dyed with antibacterial natural colorant berberine [220] or polyamide fibers coated with a CD-ciprofloxacin [221] proved to have significant antibacterial activity.

Furthermore, CDs can be introduced into the fiber during fiber fabrication. For example, CDs entrapment within the fibers was achieved by melt spinning using materials such as polyesters and polyamides. It was shown that instant cooling of the fiber exiting from the spinneret forced CDs to migrate to the surface of the fiber and thus made them accessible to form complexes with drugs. This migration occurred

due to hydrophilic external surface of the CD which blocked complete perforation into the fiber [258,259]. In another research, Yildiz *et al.* [260] studied the potential of co-spinning conjugated polymer and drug solution to fabricate self-standing and quick-dissolving fibrous textiles from carvacrol/CD inclusion complexes. The result enhanced the hydrosolubility, thermal stability, and antioxidant activity of the fibrous web, which can have the potential to be used for food and oral care applications.

1.4.3.5 Ion complexes

Drugs can bind to the surface of the fibers by using opposite charges in order to build ion complexes. Drug release is then relying on the external solution or the ability of the fiber surface to preferentially exchange counter-ions that are influenced by the type and the concentration of the surface ion-exchange groups (**Figure 1.7E**) [49,72,141,174]. Ion complexes undergo a stoichiometric exchange reaction and can have extensive exchange potential, making them a suitable candidate as multiple drug carriers [80,218,219]. In a study by Liao *et al.* [217], fibers from a blend of chitosan-alginate with charged surfaces were produced. Drug complexation was created with several bioactive charges including dexamethasone, BSA, growth factor (PDGF-bb), and avidin mixed with either chitosan or alginate solution. Electrostatic interaction among the charged fiber and the charged drugs controlled their release mechanism and profile from the fibers; therefore, the elution time of the components from these fibers ranged from hours to weeks.

In another study, Gao *et al.* [261] investigated the drug release from the poly(propylene-glycol-styrene sulphonic acid) fibers loaded with tramadol hydrochloride as a model drug. The tramadol was consistently delivered from the drug-loaded fiber when iontophoretic, a non-invasive technique to increase transdermal penetration using a voltage gradient, was applied since combining ion-exchange fiber with iontophoresis will decrease the fluctuation of the drug release [262]. Some commercially available ion-exchange fibers are the Smopex® fibers, which contain polyethylene backbone grafted with other polymers such as polystyrene sulphonic acid (Smopex®-101), polyacrylic acid (Smopex®-102) [263], or polyamide (Smopex®-108) [218]. In short, ion-exchange fibers have demonstrated great abilities to release various ionic drugs loaded into ion-exchange groups. These functional fibers can be ultimately used to produce woven or nonwoven fabrics.

1.4.3.6 Supercritical CO₂ impregnation

Supercritical impregnation is a mild temperature process to load fibers with bioactive agents, providing a drug-loaded textile free of any solvent residue. CO₂ above its critical

temperature and pressure, 31.1 °C and 73.8 bar, respectively, is in the supercritical state. The critical temperature of CO₂ is relatively low and easily achievable, making it a mild solvent for temperature-sensitive materials. Supercritical CO₂ (scCO₂) is a 'tunable solvent' as its properties, such as viscosity, density, and diffusivity, can be controlled by varying pressure or temperature [45,60,75,264]. Furthermore, scCO₂ has an intermediate behavior between gas and liquid, possessing a density similar to that of the liquid, 0.2-1.5 g cm⁻³, and transport properties close to those of the gas. In addition, scCO₂ is a dissolvable medium for nonpolar low molecular weight compounds; however, in case of poor solubility, a co-solvent like ethanol is used to increase the solubility of the polar molecules [75,265].

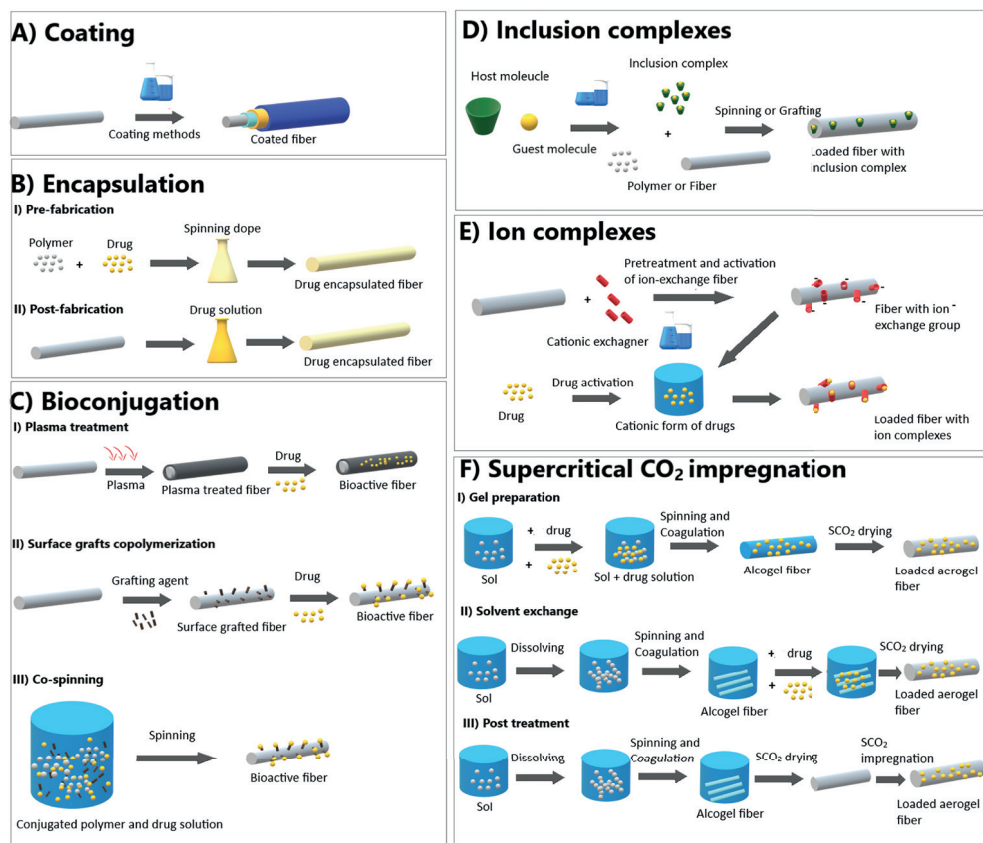
In biomedical applications, temperature and pressure ranges between 35-55 °C and 90-200 bar have been investigated for drug loading [75,266]. This method has been mainly used in producing and loading aerogel. However, due to the low mechanical properties of aerogels in fibers, they have not been extensively investigated [39,45]. Drug loading in the aerogel fibers can be done either during gel preparation (**Figure 1.7F-I**), during the conventional sol-gel process, so-called solvent exchange (**Figure 1.7F-II**) [267], or during the post-treatment of the synthesized gel (**Figure 1.7F-III**) [27]. Post-treatment loading has been extensively utilized for non-aerogel materials too [27,266].

The post-treatment loading process consists of three main steps. At first, the solute is dissolved in the scCO₂ and then the polymer is exposed to the solution of scCO₂, where the bioactive agents and the solution diffuses into the polymer bulk. Finally, the last step is depressurization, in which CO₂ and non-impregnated drugs are removed from the loading chamber [268,269]. The drug loading efficiency in this method depends on the solubility of the drug in CO₂, CO₂ sorption, polymer swelling, the affinity of the drugs to the polymer, and the processing factors, such as pressure, temperature, loading time, diffusion process, and depressurization conditions [75,269-271]. Some examples of loaded textiles are cellulose acetate (CA) fibers impregnated with menthol and vanillin [264], chitosan with dexamethasone as a scaffold for bone tissue engineering [272], and collagen and cellulose as a commercial wound dressing (Promogran®) impregnated with anti-inflammatory jucá (*Libidibia ferrea*).[273]

Using the supercritical impregnation method, fibers with different geometries can be loaded with hydrophilic or hydrophobic drugs. For instance, a dual-drug solvent exchange impregnation into core-shell electrospun nanofibers was achieved by scCO₂ method [274]. The scCO₂ was able to load the model BODIPY 493/503, as a hydrophobic model drug, into the hydrophobic PCL core and impregnation of the Rhodamine B, as

a hydrophilic model drug, into the hydrophilic shell. Hydrophobic or hydrophilic drug-polymer interactions improved the drug loading and caused a steady linear release. Since scCO_2 localized the drugs throughout the entire fiber matrix, scCO_2 drug-loaded fibers demonstrated a controlled and extended bimodal release compared to immersed fibers in a solution containing the two drugs. Therefore, scCO_2 can be used as a tunable medium for loading various drugs into a fibrous structure.

Selecting a suitable drug impregnation method is crucial in the final properties of the fibrous delivery system. Therefore, several factors should be considered in the selection process including material or production cost, biostability, biodegradability, toxicity, *ex vivo* or *in vivo* drug delivery, and their compatibility with the fiber/textile production. For instance, in the case of inclusion complexes, known for creating slow-release systems, modified cyclodextrins costs are high; also their final fixation on the textile surface is required since high dosage release of cyclodextrins can be toxic [77,93]. The fiber spinning condition, final morphology, and drug loading capacity are other factors that can limit the choice of impregnation method. Nevertheless, conventional fiber and drug loading production techniques such as coating and incorporating the drugs into the polymer or melt solution are yet favorable due to their simplicity.

**FIGURE 1.7.**

Schematic representation of drug loading methods onto the fiber-based constructs. A) Coating; incorporation of the drug on the surface of the fiber. B) Encapsulation; incorporation of bioactive agents in the fiber matrix. C) Bioconjugation; coupling the bioactive agents to the surface of the fiber in the presence of the functional groups. D) Inclusion complexes; accommodation of a small molecule (the guest, drug) in the cavity (the host, drug carrier), where the complexes can be loaded on the surface of the fiber. E) Ion complexes; binding drugs to the surface of the fibers by using opposite charges to build ion complexes. F) Supercritical CO₂ impregnation; the mild temperature process to obtain solvent residue-free drug-loaded fibers using CO₂ above its critical coordination (31.1 °C, 73.8 bar).

1.4.4 Characterization of drug-eluting textiles

Several methods are used to characterize drug releasing textiles; however, the most common methods are those that determine the chemical functionality, biological activity, surface morphology, mechanical properties, durability and degradation, and drug-loading and release kinetics. Infrared (IR) spectroscopy is widely used in identifying the chemical functionalities of fiber surfaces. Most chemical functionalities absorb infrared frequencies that correspond to their molecular vibrational frequencies. IR can detect the majority of the mobilized compounds on the textile surfaces. In addition, any changes to the surface morphology of the textiles can be detected by scanning electron microscopy (SEM) [275]. The surface analysis can also give an idea about the durability

and surface degradation, which indirectly refers to the release behavior of the drug eluting textiles [276]. For the degradation studies, simulated body fluids at physiological temperature are used. Enzymes can be added to the testing medium to accelerate the degradation of the base textiles [277].

Determining the biological activities of the medical textiles, especially, antibacterial properties is essential when antibiotics are incorporated. Test methods such as AATCC 100 and 147 are widely used in the antimicrobial assessment of textile fabrics. In addition, evaluation of the physical and mechanical properties of the drug eluting systems is essential in order to determine their suitability for different applications [278]. Finally, understanding the release behavior of the drugs is crucial to satisfy the requirement of the final application. Different mechanisms of drug release from fiber-based constructs are thoroughly discussed in the following sections.

1.4.4.1 Drug release mechanisms

Textile-based drug release systems should be able to deliver the drugs efficiently, accurately, and for a defined timeframe. The term ‘release mechanism’ illustrates the procedure in which drugs are transported or released [174]. In textile-based systems, regulation of the drug release rate is dependent on parameters such as geometry (size and shape), morphology, and material properties, such as swelling and degradation, of the carriers or host-molecules [72,141,174].

The most addressed drug release mechanisms are immediate, extended, and triggered or delayed release [72,174,279]. As shown in **Figure 1.8A-I**, in the immediate release, there is a rapid release of the drugs in a short time. However, in extended release (**Figure 1.8A-II**), the drug is delivered at a lower rate constantly or variably over an extended period of time. Finally, in triggered release (**Figure 1.8A-III**), different stimuli, such as pH or temperature, initiate the release procedure, which can be immediate or extended [72,174].

1.4.4.1.1 Immediate release

In some circumstances, where an instant reaction is necessary, immediate drug release is preferred. For example, a rapid release rate of antibiotics in the first hours following the biomaterial implantation is vital to avoid implant-related infection [280,281]. He *et al.* [282] spun a fibrous structure blend using electrospinning to incorporate a model drug TC.HCl into PLLA fibers. The nanofibers from the TC.HCl /PLLA blend showed an immediate release and prevented bacterial infection. Johnson *et al.* investigated the release of a hydrophobic model drug, Nile Red, from the emulsion electrospun fibers

containing PCL (oil) and non-ionic surfactant, Span 80. The samples with and without surfactant exhibited an initial burst release continued by a slower continuous drug release over one hour. However, the burst release of the model drug from nanofibers with surfactant was lower, due to the interaction of the model drug at the interface of emulsion and the fiber body and the lower surface area of samples with the surfactant [283].

1.4.4.1.2 Extended release

In extended release systems, the drug is released at a constant or variable slow rate over an extended time [141,174]. In this systems, different phenomena such as diffusion [78], decomplexation [220], ion exchange [219], dissolution, erosion, swelling, and degradation [284] can control the release rate [285]. In systems such as fibers loaded with encapsulated drugs [215] or hollow fibers [135], the main mechanism of the release is based on the diffusion; therefore, the concentration gradient and diffusion coefficient govern the release rate. The release rate of inclusion complexes is controlled by k_c and k_d , the complexation and decomplexation constants, respectively [256], and is usually dependent on the interactiveness of the drug as the guest molecule and host molecule.

In some cases, the release rate is regulated by the dissolution rate of the macromolecular structure in which the drug is loaded. Examples of such systems are fibers loaded with encapsulated drugs in which the matrix is soluble in the surrounding media. Some drugs can bind to ion-exchange materials as explained in section 1.4.3.5. In ion-exchange textile systems, the eluting rate of the bioactive compounds attached to ion-exchange fibers is controlled by the ability of the textile surface to preferentially exchange counter-ions, the concentration of the surface ion-exchange groups, the ionic characteristics or the pH of the local medium, and the type of the ion-exchange material. In addition, erosion and degradation governed structures benefit from a biodegradable macromolecule that is gradually eroded or degraded and as a result, drugs are eluted.

The fiber erosion or degradation rate regulates the release rate of the drugs [285]. However, dissolution, ion-exchange, erosion, and degradation can be the mechanism behind triggered or delayed release too [72,174]. Volokhova *et al.* irradiated electron beam on paracetamol-loaded PCL electrospun meshes covered with pure PCL nanofibers. The combination of e-beam irradiation and the fibrous layer resulted in an extended release profile with no burst effect and enhanced drug release quantities over time since e-beam reduced the PCL molecular weight and the multilayers created a diffusion barrier and declined swelling [126].

1.4.4.1.3 Triggered or delayed release

A trigger/stimulus or time can determine the release of the drug in these systems. Therefore, the type of release can be immediate or extended based on the material and design. The release can be triggered by stimuli such as light, pH, temperature, ionic strength, sonification, erosion, degradation, and dissolution. Therefore, consecutive release profiles over a longer period can be achieved [72,174]. Zhao *et al.* [286] fabricated a smart and tumor pH-triggered PLLA electrospun fabric for inhibiting cancer relapse. Mesoporous silica nanoparticles (MSNs) were loaded to the fibrous structure to extend the anticancer drug doxorubicin (DOX) release, which was physically adsorbed onto MSNs. CaCO_3 inorganic caps were incorporated to temporarily block the pores of MSN loaded nanofibers until the pH change triggered the drug release. CaCO_3 caps were stable at physiological pH of 7.4; however, in an acidic media where protons were released from the tumor cells ($\text{pH} < 6.8$), CaCO_3 gates dissolved into biocompatible Ca^{2+} (cations) and released CO_2 gas. This phenomenon led to increased water penetration into the PLLA nanofibers and accelerated DOX release. This pH-dependent drug-loaded fibrous system can inhibit long-term exposure of drugs to healthy cells by preventing drug release at non-acidic conditions.

In this study, three main groups of PLLA fibers co-electrospun with DOX (**Figure 1.8B-x,w,x'**), MSN-DOX (**Figure 1.8B-y,v,y'**), and MSN-DOX- CaCO_3 (**Figure 1.8B-z,u,z'**) were fabricated, and SEM, transmission electron microscopy (TEM), and energy dispersive X-Ray (EDX) were used to analyze the morphology of fibrous structures and the effect of drug loading on the fiber structure. Comparing the release profiles of DOX loaded fibers (**Figure 1.8C-I**) with the electrospun CaCO_3 capped fibers (**Figure 1.8C-II**) at various pHs demonstrated significant pH-dependent drug eluting behavior. Moreover, sustained drug release over a period of 40 days from MSN-DOX- CaCO_3 fibers was observed only when the environment became acidic (**Figure 1.8C-III**). Finally, this example showed the importance of the triggered release in providing a sustained drug release while minimizing the damage to untargeted tissues.

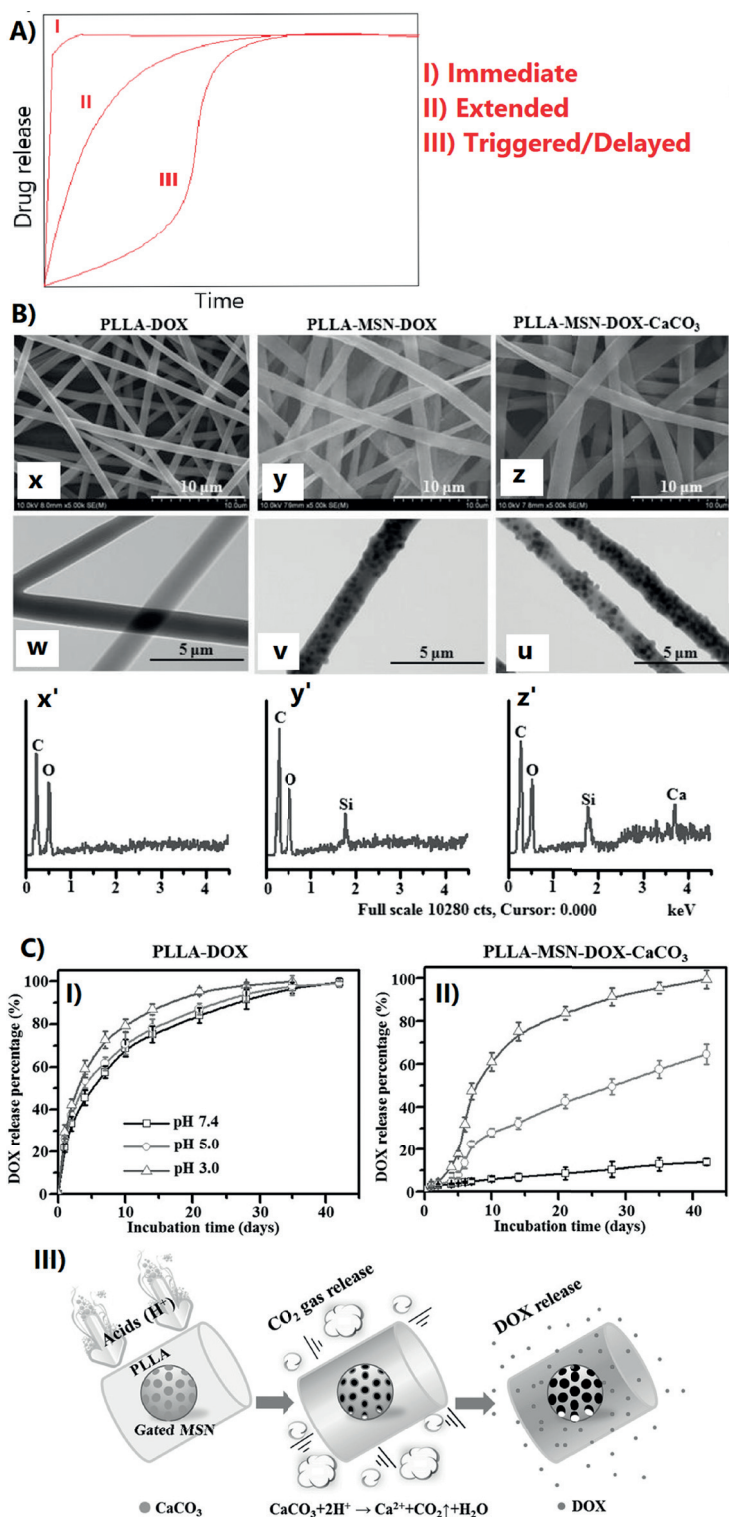


FIGURE 1.8.

Drug release mechanisms. A) Most common examples of drug release mechanisms, immediate, extended, and triggered or delayed-release. B) SEM (x,y,z) and TEM (w,v,u) images of PLLA fibers co-electrospun with (x,w) DOX, (y,v) MSN-DOX, and (z, u) MSN-DOX-CaCO₃. EDX spectra of x') PLLA-DOX, y') PLLA-MSN-DOX, and z') PLLA-MSN-DOX-CaCO₃. C) Drug release profiles of I) PLLA and II) PLLA-MSN-DOX-CaCO₃ at various pH conditions. III) Schematic explanation of drug release mechanism of electrospun fibers. The interaction of protons (H⁺) from the acidic media diffusion into the nanofibers; protons react with the CaCO₃ channel gates of MSN to release the encapsulated DOX inside the mesoporous structure and produce CO₂ gas, causing water penetration into the PLLA fibers and accelerating the DOX release. B and C reproduced with permission [286]. Copyright 2015, Elsevier.

1.4.4.2 Kinetics of drug release

The drug release kinetics from fiber-based structures is influenced by various mechanisms, vigorously relying on polymer-drug system properties and interactions, such as physico-chemical characteristics of the drug, fiber spinning and loading methods, the solubility of the drug in the release medium, and the interactions between the loaded material and the target tissue [49]. Various mass transport mechanisms, including diffusion, swelling, dissolution, erosion, or a combination of them governs the drug extraction from a polymer matrix. Generally, hydrophilic drugs release occurs through simple diffusion, whereas water-insoluble drugs release happens by swelling or erosion of the macromolecule matrix [287]. Mathematical models have been proposed to describe, quantify, and predict the kinetics of drug release. Therefore, fitting experimental data on drug release with various mathematical models is a key to understanding how the polymer-drug systems affect the transport mechanisms to tune therapeutic parameters, such as the drug dose, release rate, and the release time.

The drug dissolution rate in a medium can be explained by:

$$\frac{dC}{dt} = D.Ah(C_s - C_{(t)}) \quad \text{Equation (1.2)}$$

As dC/dt is the dissolving rate, D the diffusion coefficient of the drug, h the width of the diffusion path, A the surface area of the subjected polymer to medium, C_s the saturated amount of dissolvable drug, and $C_{(t)}$ the drug concentration in the release medium at time t .

The drug release profile can be obtained by plotting the drug release fraction versus time:

$$Q_{(t)} = \frac{M_t}{M_{tot}} \quad \text{Equation (1.3)}$$

$Q_{(t)}$ is the cumulative fraction, M_t is the amount of drug at time t , and M_{tot} is the total amount of loaded drug.

The release profiles of each polymer-drug system can be assessed and explained by a mathematical model. The statistical coefficients, namely the higher coefficient of determination (R^2) and the lower AIC (Akaike Information Criterion), are used to check the accuracy of the model to justify the experimental data. Therefore, the mechanisms with the highest potential to control the drug release can be recognized from the best fit model (**Figure 1.9A**). Several common mathematical models applicable for macromolecule systems, zero-order, first-order, Higuchi, Korsmeyer-Peppas, Hixson-Crowell, and Peppas-Sahlin, are reviewed in the following sections with an emphasis on drug eluting fibers.

1.4.4.2.1 Zero-order model

Zero-order kinetics is an “ideal” linear drug release profile. The eluting rate is independent of the drug concentration in the system and remains constant over time [288,289]. This model can be explained by:

$$Q_{(t)} = k_0 t^n \quad \text{Equation (1.4)}$$

Where $Q_{(t)}$ is the cumulative fraction of the drug released at the time t , k_0 is the constant rate or apparent dissolution rate, and n is geometrically dependent, 1.0 for a thin film, 0.89 for a cylinder, and 0.85 for a sphere. In some studies, the researchers have considered electrospun meshes as thin films, while for single micro-fibers, the cylinder geometry seems to be more accurate.

A graphical representation of the model is shown in **Figure 1.9B-I**. Zero-order release typically happens in transdermal or osmotic systems and for prolonged-release from a system that doesn't break down when loaded with a very low soluble drug. Ahadi and coworkers [290] fabricated electrospun vancomycin hydrochloride (Vanco HCL) loaded PLLA fibers. The electrospun fibers were added to a silk fibroin/oxidized pectin hydrogel as a secondary structure where drug-loaded hydrogel/fiber complexes were fabricated. During the first day (24h), the release amount of vanco HCL from drug-loaded hydrogel was 35.97% while from hydrogel/fiber composite was 13.83%. The drug release mechanism in such a gel-fiber system can be complicated and affected by parameters such as polymer degradation, hydrogel swelling, and hydrophobicity or hydrophilicity of the fibers. In order to evaluate the kinetics model, maximum linearity was considered to check the accuracy of the model. The drug-loaded hydrogel/fiber proved to have zero-order release with $K_0=3.307$ and $R^2=0.98$.

1.4.4.2.2 First-order model

First-order release kinetics is corresponding to the amount of the loaded drug in the matrix. This model results in constant release overtime, and the rate is only dependent on the initial drug concentration [291]. The cumulative released fraction can be described by:

$$Q_{(t)} = 1 - \exp(-k_1 t) \text{ or } \log(1 - Q_{(t)}) = k_1 \cdot \frac{t}{2.303} \quad \text{Equation (1.5)}$$

where $(1 - Q_{(t)})$ indicates the residual fraction of drug at the time t in the system, and k_1 is the first-order constant (**Figure 1.9B-II**).

The first-order kinetics is favorable for the sustained release of the drug delivery systems. For example, it can be observed in systems consisting of water-soluble drugs loaded in a porous matrix, where the release rate is only controlled by diffusion or dissolution.

Painely *et al.* [214] studied a drug delivery system based on gelatin nanofibers for two contraceptive drugs comprising levonorgestrel (LNG) and ethinylestradiol (EE). In the case of individual loading of the drugs, it was observed that the release of EE was altered by the initial content of the loaded drug, whereas no significant difference was seen for the LNG with a sustained release of 30–35 $\mu\text{g day}^{-1}$. This could be attributed to the hydrophobic nature of LNG as no significant difference in morphology of the loaded fibers with increasing the LNG dosage was observed. On the other hand, fibers loaded with both LNG and EE showed a minor burst release on the first day, followed by a sustained release of both drugs up to 7 days.

In addition, LNG release was ~ 4 –5 fold increased in dual drug-loaded samples compared to single LNG loaded fibers due to the combination of drugs. *In vitro* LNG release kinetics could be fitted by zero-order and first-order models with $R^2 \geq 0.99$ for both models. EE/gelatin nanofibers were described convincingly by zero- and first-order models with R^2 in the range of 0.93–0.97. In the case of dual drug loading, the release of LNG and EE were described by zero-order and first-order models for LNG ($R^2 \geq 0.99$), whereas Higuchi and Korsmeyer-Peppas model, explained in the following section, could better describe the EE release ($n=0.49$, $R^2 \geq 0.97$).

1.4.4.2.3 Higuchi model

There was no mathematical model to explain drug dissolution from matrix systems until the 1960s. One of the earliest models has been described by Higuchi [292] which

was initially effective only for a planar matrix but later was adjusted to be applied to different geometries and matrices [293]. Higuchi model is based on Fick law and describes the release kinetics of a hydrosoluble drug dispersed in a homogeneous solid matrix. Drug release happens by Fickian diffusion of the release medium and the drug within the pores macromolecule structure. The model is justifiable if the diffusion coefficient or matrix geometrical dimensions of the matrix are persistent over time [292], meaning that it does not apply to cases such as swellable or soluble delivery systems.

The cumulative released fraction in this model is:

$$Q_{(t)} = \frac{\sqrt{D\varepsilon}}{\tau} \times (2m_d - \varepsilon S_d)t \quad \text{Equation (1.6)}$$

where ε is the polymer porosity, τ is the capillary tortuosity factor, m_d is the initial amount of the drug, and S_d is the solubility of the drug. Tortuosity is used to describe diffusion and fluid flow in porous media and it is the proportion of radius and branching of the pores and canals in the matrix.

This model is simplified as:

$$Q_{(t)} = k_H \sqrt{t} \quad \text{Equation (1.7)}$$

where K_H is the release constant of the Higuchi model. As expected from Fick's law, the amount of released drug is proportional to the square root of time. A graphical representation of the model is shown in **Figure 1.9B-III**.

In a study by Pisani *et al.* [294], gentamicin sulfate (GS) was encapsulated into polylactide-co-polycaprolactone (PLA-PCL) electrospun nanofibers. Due to the antibacterial activity of the GS-loaded fibrous meshes, they were used for topical controlled drug delivery for treating infected skin and gum or for preventing infection in bone surgery. The kinetic release of the drug-loaded fibers could be predicted and explained by the Higuchi kinetic model, both in dynamic and static conditions ($R^2 \geq 0.9$).

1.4.4.2.4 Hixson-Crowell model

The Hixson-Crowell model is based on two assumptions; drug release is limited only by drug dissolution rate, and the matrix erosion happens by decreasing the dimension of the matrix while keeping the initial shape constant [295].

$$\sqrt[3]{M_0} - \sqrt[3]{M_t} = k_{HC}t \quad \text{Equation (1.8)}$$

where M_0 is the initial amount of the drug in the system. The remaining drug in the system at time t is M_t , and k_{HC} is the constant of incorporation, which connects the surface and the volume of the drug.

The Equation (1.8) could be simplified by dividing it by $\sqrt[3]{M_0}$:

$$(\sqrt[3]{1-Q_{(t)}}) = 1 - k_{\beta} \cdot t \quad \text{Equation (1.9)}$$

where $(1-Q_{(t)})$ is the remaining fraction of drug within the polymer matrix, and k_{β} is a release constant (**Figure 1.9B-IV**).

Hixson-Crowell model could satisfactorily represent the release kinetics of curcumin (CUR) loaded in zein (zein-CUR) electrospun fibers, where the morphology and the size of fibers were strongly dependent on CUR loading dosage. This was mainly due to the hydrogen bonding between CUR and the fibers and a slight increase in the Tg of the zein matrix. In the case of 20% w/w CUR loading, around 70% of the drug was released in 180 minutes. Furthermore, a higher dosage loading caused a faster release rate due to the diffusion-controlled release behavior of the system which was derived from CUR dosage change.

By investigating several models for three different CUR loading dosages, the first-order model exhibited the highest value of R^2 (0.9940-0.9969), indicating that the CUR diffusion in fibers might be a rate-limiting step. Furthermore, the release profile was explained by Hixson-Crowell model with a relatively high R^2 (0.9638-0.9896), which additionally clarified that the CUR release from the fibers was mainly based on diffusion rather than the matrix erosion mechanism. Finally, the system was evaluated for antibacterial activities using *Escherichia coli* and *Staphylococcus aureus* bacteria. The outcomes showed good antibacterial activity towards the targeted bacteria where the bacterial inhibition capability improved with the increased CUR contents [296].

1.4.4.2.5 Korsmeyer-Peppas model

The Korsmeyer-Peppas, as a semi-empirical model, explains the exponential relationship between the release and the time. It is mainly used to inspect the release of the drug from a hydrophilic polymer-based system [297,298]. The model is expressed by:

$$Q_{(t)} = \frac{M_t}{M_{\infty}} = K_{KP} t^n \quad \text{Equation (1.10)}$$

Where K_{kp} is the constant accounting for the dimensional properties of the system, also assessed as the release rate constant, and n is the exponent of release related to the drug release mechanism as shown in **Figure 1.9B-V**. This model can be used when the release mechanism is unknown or when more than a known mechanism is involved. The dominant physical mechanism of drug release is recognized by obtaining the value of the exponent n based on the optimal fit with experimental data (for $(t) < 60\%$) and the system dimension.

Fickian diffusion or non-Fickian mechanisms alter with the rate of solvent diffusion. In the case of $n = 0.45$ or Fickian diffusion, the typical molecular diffusion of the drug occurs due to a chemical potential gradient. In other words, the rate of solvent diffusion is much slower than polymer relaxation (swelling or/and erosion of matrix) time. This case is similar to the model described by Higuchi for Fickian diffusion. However, in non-Fickian mechanisms, when $0.45 < n < 0.89$, the release is controlled by both diffusion and macromolecule relaxation (swelling or erosion) since solvent diffusion and polymer relaxation occur at comparable time rates. When $n = 0.89$, the mechanism is governed by polymer relaxation, which is similar to zero-order kinetics. Finally, in the case of $n > 0.89$, an extreme form of transport, called non-Fickian diffusion, driven by the acceleration of solvent penetration occurs.

Generally, these models have been used to study drug delivery from sources such as tablets, hydrogels, membranes, and fibers. The water molecules in the majority of the studied systems are the initiators of the drug release process through swelling of the loaded polymer matrix [299,300]. Furthermore, the rate-restricting phenomena for a hydrophilic drug loaded in water-insoluble and non-erodible fibrous structure, such as CA nanofibers, is diffusion through typically a hydrophobic hindrance [301].

For instance, gallic acid (GA) was microencapsulated in PCL by solvent vaporization, and the homogenous PCL-microspheres were applied onto textile substrates of cotton and polyamide. GA has shown biological activities, including antioxidant, antityrosinase, antimicrobial, anti-inflammatory, and anticancer properties [300]. The apparent diffusivity, D , was obtained using the Fick's second law, Higuchi model (Equation 1.7). The kinetic studies done using Korsmeyer-Peppas equation proved that the hydrophobicity and affinity of the textiles and GA affected the eluting mechanism. The apparent diffusion coefficients were predicated on plane surfaces. For cotton, an explicit Fickian diffusion was obtained ($n \approx 0.46$, $n \leq 0.5$); however, for polyamide, the diffusion was anomalous ($n \approx 0.63$, $0.5 < n < 1$).

Moreover, no differences were found in the K_{kp} (Equation 1.10), which is the constant comprising the dimensional properties of the system.

1.4.4.2.6 Peppas-Sahlin

Peppas-Sahlin is a power-law model originated from Korsenmeyer-Peppas (Equation 1.10) which take into account the role of two physical mechanisms: diffusion and macromolecule relaxation [302]. This model is expressed by:

$$Q_{(t)} = \frac{M_t}{M_\infty} = K_F t^m + K_R t^{2m} = F + R \quad \text{Equation (1.11)}$$

where K_F is the diffusion constant, K_R is the relaxation constant, and m is the Fickian diffusion exponent of a matrix of any dimensional shape (cylinders, tablets, and films).

The model assumes that drug is eluted from any matrix, disregarding of its dimensional structure shape, consisting of a Fickian and a relaxation term. If the Fickian character can be stated as a function of t^m , the polymer relaxation role can be indicated as a function of t^{2m} . The Fickian diffusional exponent, m , differs with the ratio between the width and height of the matrix in which Peppas and Sahlin defined it as $2a/l$, where $2a$ is the width (diameter) and l is the height (thickness) (**Figure 1.9B-VI**). The drug release by the Fickian mechanism, F , is obtained by:

$$F = \frac{1}{1 + K_R / K_F t^m} \quad \text{Equation (1.12)}$$

And the ratio of relaxation over Fickian is:

$$\frac{R}{F} = \frac{K_R}{K_F} t^m \quad \text{Equation (1.13)}$$

PLA/polyvinyl alcohol (PVA) core-shell nanofiber scaffolds loaded with BMP-2 proteins to enhance the recovery of alveolar bone tissue were used in a study. Albumin was utilized as a model drug to optimize fiber production and loading parameters. Fabricated core-shell nanofibers released 30% of the loaded albumin while PVA monolithic fibers released 92% of the encapsulated albumin in 1 h. Peppas-Sahlin could sufficiently explain the release of albumin ($R^2 > 0.98$, $m=0.45$), suggesting that the albumin release occurred through the Fickian diffusion process. Based on the *in vitro* results, cell viability, adhesion, and proliferation were observed [303].

Other models such as Hopfenberg [304], Gallagher–Corrigan [305], Weibull [306], have been also utilized in different research studies to predict the drug release from various drug-loaded materials. In summary, these models are valuable tools to discover the exact mass transport and quantitative estimation of drug release. Using these models, scientists are able to design a controlled and tunable release from drug-eluting systems in various applications. Examples of the applications that have used the drug-eluting systems are reviewed in the next section.

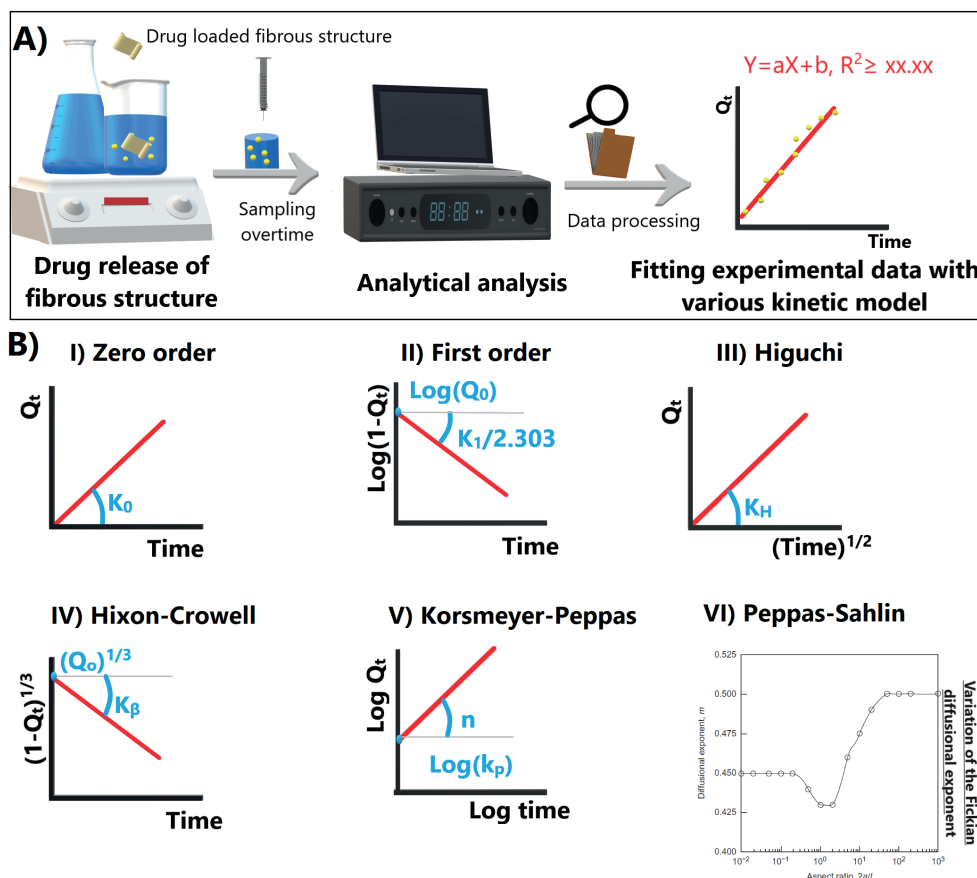


FIGURE 1.9.

Representation of the release kinetics models. A) Evaluation process of experimental drug release data with empirical models. B) linearized plots of most common release model drugs, I) Zero-order model, II) First-order model, III) Higuchi simplified model, IV) Hixon-Crowell model, V) Korsmeyer-Peppas (power-law model), and VI) Peppas-Sahlin, variation of the Fickian diffusional exponent, m , with the aspect ratio, $2a/l$, where $2a$ is the diameter (width) and l is the thickness (height) of the matrix. Reproduced with permission [87]. Copyright, 2015, Elsevier; originally from [302] copyright 1989, Elsevier.

1.4.5 Applications

A wide spectrum of drug-loaded textiles has been designed to deliver various bioactive agents in various manners. Numerous manufacturing processes alongside the loading methods of various pharmaceutical agents have made the drug eluting fibrous system an interesting candidate for three main application areas of wound care, tissue engineering, and transdermal drug delivery system (**Figure 1.10A**).

1.4.5.1 Wound care

An ideal wound dressing has characteristics such as oxygen and water vapor permeability, resistance to the penetration of microorganisms, and antimicrobial activity to prevent infection. Furthermore, it should be easy and comfortable to apply to the wound, minimize the pain, and inhibit bleeding [44,174]. The delivery of bioactive agents has a significant role in the wound-healing process. This includes a wide range of compounds and measures including antimicrobials to avoid or heal infection, growth factors to help cellular proliferation, cleansing or debriding agents for eliminating necrotic tissue [49]. The biomaterials used for wound dressing should also be biocompatible and assist the growth of skin cells. Woven and nonwoven textiles that have small pore sizes to permit controlled fluid transport and resist the infiltration of infectious microorganisms can be sued for this application. Moreover, both degradable and non-degradable materials have been used for the production of wound dressings [49,174].

Degradable polymers are suitable candidates to be used as skin scaffolds, whereas non-degradable polymers can be employed as temporary wound dressings [307]. As an example, polyurethane (PU), as a non-degradable polymer, has been used for wound dressing applications due to its elastic properties [308]. However, it is also possible to synthesize PU in a degradable form, such as poly(ester-urethane) urea (PEUU), which could be used as a scaffold for skin tissue engineering [309]. If an individual material cannot satisfy the requirements of the application, a combination of various materials, such as degradable and non-degradable, can enhance the firmness, spinnability, strength, wettability and bioactivity of the fibrous system.

Medical device-related infections and antibiotic-resistant issues require anti-infective materials to preserve wounds and medical devices [310]. In this direction, the utilization of chitosan as a base material for antimicrobial wound dressings was explored. A tri-component antimicrobial nanofiber composite from chitosan/polyvinyl alcohol/silver nanoparticles was developed via electrospinning [311], where green chemistry principles were applied. Chitosan was employed as a capping agent and glucose as a reducing agent for silver nanoparticles (25 nm diameter). Nanofibers with 150 nm

average diameter of regular cylindrical shape morphology were obtained upon blending chitosan/silver nanoparticles with PVA and cross-linking with glutaraldehyde. The release profile of silver ions from nanofiber mats was assessed by atomic absorption. The nanofiber mats attained sustainable release behavior over 7 days and exhibited high antibacterial activity against *E. coli* at low silver nanoparticle loads. In another study, the chemical modification of chitosan using iodoacetic acid was evaluated, where 1-ethyl-3(3-dimethylamminopropyl) carbodiimide hydrochloride with hydrochloric acid (EDAC-HCl) and N-hydroxysuccinimide (NHS) coupling was employed [312]. The chitosan iodoacetamide derivative exhibited bactericidal properties when tested against *E. coli*. It is thought that the incorporation of iodine active terminal into a chitosan backbone resulted in an increase in the antibacterial effectiveness by disulfide bond development with the proteins of the bacterial outer membrane.

Electrospun mats were made out of gelatin and incorporated with polyhydroxy antibiotics. These antibacterial drugs have a various number of hydroxyl groups in order to make strong interfacial bonds to gelatin with the aid of *in-situ* crosslinking with polydopamine (pDA). Vancomycin (Van) loaded fibers showed to have high mechanical properties and modulate cytokine production essential in stopping sepsis after burn injury [313]. The direct electrospinning of Van-loaded gelatin on cotton gauze bandages eliminated structural irregularity and provided an easy to wrap wound dressing. The mesh was crosslinked, and its efficacy was investigated in white pig models with similar pathophysiology of burn wounds to humans. The result was compared to untreated wound, non-loaded mats of Gel_pDA, and silver-based wound dressings called Aquacel Ag. It was observed that encapsulation of Van enhanced the wound closure and led to faster re-epithelialization, decreased inflammation, and higher keratinization (**Figure 1.10B-I, II, III**). Moreover, pDA crosslinking did not influence the wound healing process. Van_Gel_pDA (**Figure 1.10B-IV-z**) showed less number of inflammatory cells compared to the untreated (**Figure 1.10B-IV-x**) and non-loaded mat (**Figure 1.10B-IV-y**), and exhibited signs of connective tissue remodeling. However, silver loaded dressing proved to have fewer inflammatory cells and a confluent epithelial layer compared to untreated, non-loaded and loaded wound dressings (**Figure 1.10B-IV-w**) [314].

Microfibers have also been utilized to fabricate wound care products. Melt spun fibers from acrylonitrile-co-1-vinylimidazole (AN/VIM) copolymer to release nitric oxide (NO) were fabricated to enhance the wound healing process. NO plays an important role in the stimulation of collagen deposition and angiogenesis during the wound healing process. A 12-24 h delay in the NO release showed to be ideal in the wound healing process as

this factor could accelerate the transition of the inflammatory phase to the proliferative phase. To produce the NO donating group, the diazeniumdiolate (NONOate), melt-spun AN/VIM fibers were reacted with NO at a constant pressure of 4 atm for 1 hour. As a result, the NONOate formed on acrylonitrile segments of fibers, where each NONOate released two molar equivalents of NO upon reaction with a proton source. In addition, to extend the release time of NO-loaded AN/VIM fibers, they were dip-coated in a solution of PCL and chloroform (2 w w⁻¹%). The coating created an evenly distributed porous layer along the entire surface of the fibers. After 3 days, the PCL coated melt-spun AN/VIM copolymer fibers released a total of 84 $\mu\text{mol NO g}^{-1}$, while uncoated fibers released 91 $\mu\text{mol NO g}^{-1}$ in 3 h [315].

Eventually, modification of the experimental set-up in terms of the fiber production methods, the type of materials and drugs, and the employed release mechanisms leads to well-structured nano- or micro- fibrous textiles with a high surface-to-volume ratio and interconnected pore structures to support tissue regeneration and remodeling, and to assist gas exchange and bioactive agents supply. A review of studies in which drug-eluting constructs are used for wound care application is summarized in **Table 1.2**.

1.4.5.2 Tissue engineering

Tissue engineering requires the generation of biological alternatives to restore and regenerate damaged tissues [316,317]. Tissue engineering involves the utilization of a biodegradable matrix, so-called scaffold, sometimes loaded with pharmaceutical agents and/or cells in order to assist the three-dimensional tissue development [318-321]. Drug eluting scaffolds have been fabricated based on non-woven and woven structures. Electrospun non-wovens have been well studied for regenerative medicine and tissue engineering applications since an ultrafine fibrous network with a high surface-to-volume ratio resembles the natural extracellular matrix [174,322-324]. Nonwoven fabrics with the capability to deliver bioactive components, such as antibiotics, growth factors, and chemotherapeutic agents, have proven to accelerate or inhibit certain activities during tissue regeneration and remodeling [49].

Release of encapsulated bone morphogenetic proteins growth factor from electrospun composite scaffolds made of silk fibroin/PEO or poly(D,L-lactide-co-glycolide)/hydroxylapatite (PLGA/HAp) accelerated osteogenesis and nerve regeneration processes [325,326]. In another study conducted by Bide and coworkers, endothelialization was promoted to reduce thrombus formation by immobilizing vascular endothelial growth factor and an anticoagulant agent on the surface of the knitted polyester grafts [327]. Although electrospun constructs have been vastly used for

tissue engineering applications, cell infiltration through the nanofiber is still the major limitation of this method due to their small pore sizes. Particle leaching and sacrificial nanofibers are the two proposed solutions to overcome this issue [328]. Removing long molecular polymer chains of sacrificial fibers might be more difficult compared to the leaching particles but leads to better inter-connected pores between the fibers [329].

Nonwoven wet-spun fibers from natural-based polymers, such as chitosan [330,331], starch-based [332], and PLLA [333], have also been used for the fabrication of scaffolds. In a study, wet-spinning and electrospinning were used for preparing fibrous bioactive scaffolds to stimulate bone regeneration. The fibrous scaffold was made of a solution of biodegradable three-arm branched-star PCL, hydroxyapatite nanoparticles (HNPs), and clodronate (CDE), a bisphosphonate anti-inflammatory drug that has revealed effectiveness in the healing of different bone diseases, including osteoporosis and hyperparathyroidism. To introduce physical binding between CDE and HNP, CDE-HNP complex particles were developed to obtain better control over drug release and enhance osteoconductivity due to the presence of the inorganic phase.

In both wet-spun and electrospun nonwoven structures, the addition of HNPs, CDE, or CDE-HNPs changed the morphology and caused aggregation of the particles that were not loaded into the fibers. In addition, in contrast to the unloaded fibers, the surface porosity of wet-spun CDE-HNP loaded fibers was decreased, and the fibers did not exhibit binding at the bonding points. The formation of the defects induced by loading was minimized by optimizing the spinning conditions, mainly increasing the solution feed rate. Finally, it was suggested to study a system composed of a combination of the electrospun and wet-spun fibers in a modulated ratio into a multi-scale fibrous structure to keep a balance between the material binding sites to the cell membrane receptors and the release kinetics [334].

Melt spinning can be a helpful method to produce scaffolds in a scalable, rapid, and solvent-free process. For instance, melt-spun aligned PLLA fibers glued by 5% PLLA tetrahydrofuran solution were fabricated to obtain fiber-aligned scaffolds to imitate the morphology of collagen fibrils. The fibers were coated with collagen and chitosan to achieve the biochemical and surface-aligned topography cues. In the case of coated fibers, viability, adherence, length, and migration functioning of osteoblasts were enhanced *in vitro*. The aligned fibrous scaffold coated with collagen had the most significant cell length and migration rate, and the osteoblasts favorably relocated and adhered across the parallel fiber direction (**Figure 1.10C-II**).

However, the cell directional growth angles on the PLLA and coated fibrous scaffolds showed no significant difference (**Figure 1.10C-IV**). The cell viability on the coated fibers was higher than pure PLLA fibers after the first and seven days of measurement (**Figure 1.10C-V**). Confocal laser scanning microscopy proved that osteoblasts cells were adhered and grew on the fibers, while the untreated fibers had weaker interaction with the cells due to the presence of a random and irregular distribution of actin fibers. Coated fibers displayed more robust cell-substrate interaction, and stressed actin fibers were established in the cells, specifically in the fibers coated with collagen (**Figure 1.10C-VI**). This indicates the potential of the coated fibrous constructs as a suitable biomimetic microenvironment for osteoblast growth and bone regeneration [335].

As a result, surface topography and morphology of the fiber scaffolds, such as diameter, pattern, and pore size, have an essential role in regulating cell behaviors [319,336,337]. In general, the larger specific surface area of the fibers will make a higher ratio of the functional groups of the polymer chains exposed to the tissue. Consequently, more accessible binding sites to cell membrane receptors are present to enhance cell adhesion and growth [338]. The aforementioned features also influence the solute transport mechanism, which will facilitate drug release and the rate of material degradation [339].

Although the electrospun meshes mimic the ECM structure and stimulate tissue growth and remodeling, the pore sizes are usually in the nanometer scale and can hinder cell infiltration through the fibrous system, which leads to an undesired tissue growth besides the burst effect of the drugs due to the high surface-to-volume ratio [123]. This emphasizes the necessity of micro-fabrication processes, including wet- or melt- spinning. Ultimately, combining the advantages of micro and nanofiber production helps to obtain a fibrous construct with better properties required for tissue engineering applications. **Table 1.2** provides examples of drug-loaded fibrous systems for tissue engineering applications.

1.4.5.3 Transdermal drug delivery

Transdermal fibrous systems can deliver bioactive materials across the skin in a sustained manner [340]. However, not many commercial transdermal drug eluting systems have been introduced. The reason is mainly due to the impermeability of the stratum corneum, the external layer of skin. Therefore, drug molecule size cannot exceed more than 400–500 Da, and should have a balance of lipophilicity, log octanol-water partition coefficient around 2 to 3 ideally, to be incorporated into the bloodstream [340,341]. In the case of larger molecules, microneedles are mounted into transdermal systems so that the drugs can bypass the skin layers mechanically [342,343].

To treat various diseases, including superficial nociceptive pains, such as myalgia and muscular pain, transdermal drug delivery methods have been developed based on fibrous structures. These fibrous drug delivery systems take advantage of the minimum required drug dosage and avoid nonspecific site toxicity. A wide range of release profiles for this application can be governed by varying different parameters such as bioactive agent/polymer ratio, fiber shape, diameter, morphology, and combination of micro and nanofibers [49,344].

Nonwoven electrospun fibers have been loaded with bioactive agents using various loading procedures, such as encapsulation [345,346], coaxial electrospinning [347], and chemical or physical surface modifications [348]. Transdermal electrospun mats have been fabricated from natural-based polymers, such as CA, PLA, and PCL. The fibrous constructs for treatment of local muscular pain and inflammation were loaded with various bioactive agents including nonsteroidal anti-inflammatory drugs (NSAID), such as naproxen, indomethacin, ibuprofen, and sulindac [349], vitamins, such as vitamin A and E [348], topical disinfectants, such as chlorhexidine [350], and antibiotics and antimicrobial agents, such as amoxicillin [351], tetracycline hydrochloride [352], ornidazole [210,353] and N-halamin [354].

Cellulose micro-/nano-fiber meshes with 2 and 3 w v⁻¹% were fabricated by electrospinning of the pulp in an ionic liquid, 1-butyl-3-methylimidazolium chloride, and subsequently washed in water for 72 hours. Ibuprofen (IBU), with an efficiency of 6%, was deposited on the fiber surface or trapped in the web porous areas by immersing the meshes in the IBU solution. During the fabrication process of the low concentration mesh (2 w v⁻¹%), the ionic liquid could not be washed off rapidly, and the fibers collected on the water surface were adhered together and created fusing areas. However, in the meshes with higher concentration of cellulose (3 w v⁻¹%), most fusing areas were disappeared. Furthermore, the higher concentration led to nano-scale fibers with a diameter of 1 μm or less, and the micro-scale fibers with a diameter of around 20 μm .

The IBU loading process did not influence the morphology of the cellulose fibers significantly. The frictional roughness, as an indication of skin irritation, was not significantly different between loaded and non-loaded nonwovens. Cell cytotoxicity assay performed on the nonwoven textiles showed that the normalized cells viability was more than 80%. The *in vitro* release studies revealed that 80% of IBU was released within 250 min from both 2% and 3% cellulose concentration meshes. In both meshes, the initial fast release within 100 mins was attributed to the adsorbed surface of

the fiber and fused fiber areas. The release kinetics based on Korsmeyer-Peppas was performed, and loaded nonwovens of the 2% and 3% showed typical Fickian diffusion mechanism ($Q_{2\%} = 8.35t^{0.42}$ ($R^2 = 0.9388$) and $Q_{3\%} = 18.53t^{0.26}$ ($R^2 = 0.9908$)) [355].

Adepu *et al.* produced a mesh for transdermal drug release to prevent undesirable toxic burst release of diclofenac sodium from encapsulated micropatterned CA electrospun nanofibers. The micropatterning via nylon meshes with 50 and 100 μm size openings produced a hydrophobic surface which assisted in controlling the initial burst release of the hydrophilic NSAID drug. The zero-order release profile changed from 30 min for the non-patterned mat to 12 hours for the micropatterned mat [301]. This study suggests that the fabrication of multi-layered hydrophobic mats using different spinning methods would provide the opportunity to obtain a zero-order profile for an extended period.

In another example for the treatment of obesity, PVA fibers were fabricated and impregnated with curcumin encapsulated gelatin/albumin nanoparticles. The curcumin-loaded fibers form a fibrous transdermal drug delivery system for reducing the volume of subcutaneous adipose tissue. The fibers were optimized in terms of fiber dimension and porosity to achieve minimal drug diffusion time from the nanofiber matrix to the surface and to reach the maximum uniformity of the structure to increase the reproducibility of the drug release (**Figure 1.10D-I**).

Curcumin release profile was investigated in phosphate-buffered saline (PBS) and NaCl solution to simulate skin sweating in the existence of a transdermal mesh, where a burst release profile was observed in both solutions. NaCl solution reached a higher maximum release percent, more than 80% in less than 150 minutes, due to higher solubility of PVA and gelatin in water (**Figure 1.10D-II**). Whereas *ex vivo* transdermal test in a diffusion cell system using rat abdomen skin sample displayed a different profile with a delay in release rate in which the drug release reached 50% after 20 hours.

The fast drug release was explained by the fact that the targeted tissue was below the skin and that the hydrophobic nature of the drug avoided quick evacuation of adipose tissue into the bloodstream. *In vivo* animal tests were conducted on the rats with high-calorie diets, and the results were analyzed by magnetic resonance imaging scans (MRI) and blood tests of leptin, triglyceride, and cholesterol. The results indicated that the volume percentage of adipose tissue in the treated group decreased significantly (4-7%), compared to the obese animals (**Figure 1.10D-III**) [356].

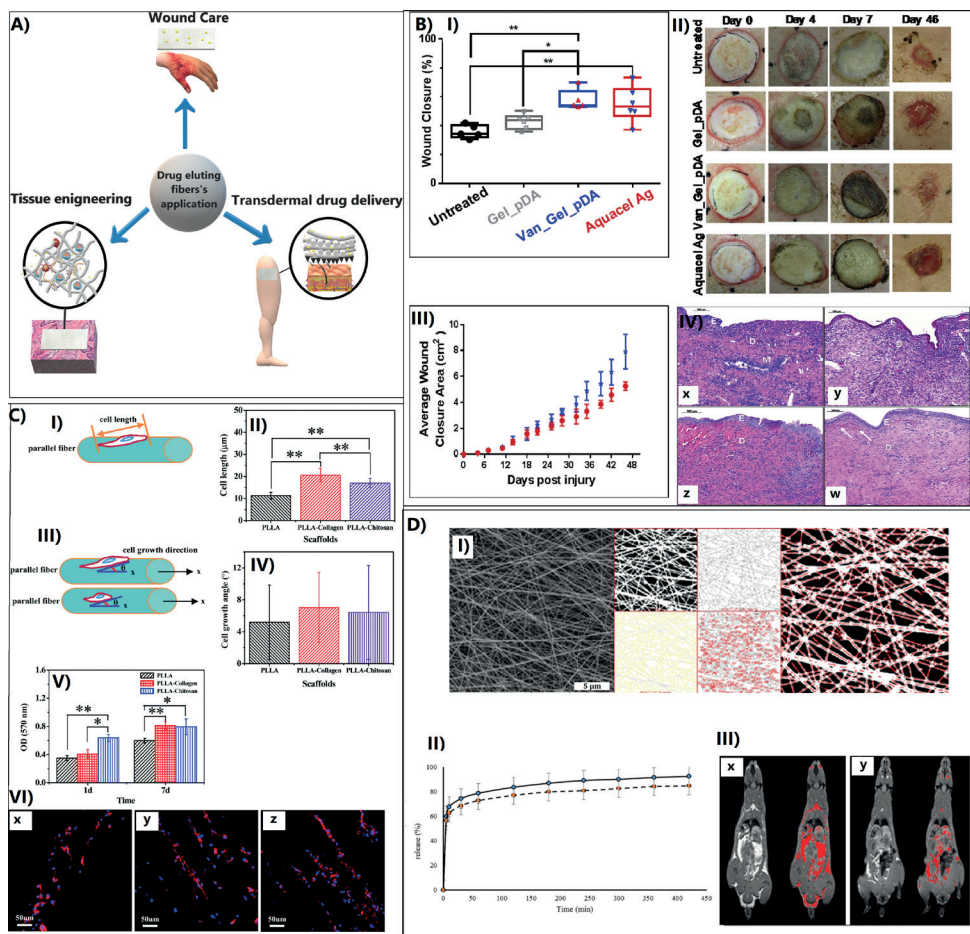


FIGURE 1.10.

Applications of drug-loaded fibrous structures. A) Wound care, tissue engineering, and transdermal drug delivery applications using drug-loaded fibers. B) *In vivo* wound healing efficacy of antibacterial wound dressing made of Van_Gel_pDA in a pig model, (I) Relative wound closure of different groups at 46 days post-injury. The obvious impact of Vanco_Gel_pDA on wound closure rate in comparison with nonloaded nanofibers of Gel_pDA and untreated wounds. (II) Images indicating the condition of the wounds before the debridement at different days (0, 4, 7, 46). The wound surface showed moderately dry and decreased pus creation in Van_Gel_pDA mats and Aquacel Ag cured wounds, (III) Average wound closing (cm²) for Gel_pDA (red bars) and Van_Gel_pDA (blue bars) medicated wounds proved that loading the antibiotics enhanced the wound healing and re-epithelialization, (IV) Histological changes during wound healing after burn injury, (x) Untreated control; Injuries treated with (y) Gel_pDA, (z) Van_Gel_pDA, and (w) Aquacel Ag. Epidermis (E), dermis (D), inflammatory cells (M), and the blood vessels (arrows) are indicated in the figure. Scale bar = 100 Qm. Reproduced with permission [314]. Copyright 2017, Elsevier. C) (I) Schematic representation of the cell size, (II) cell size on various categories of scaffolds (N = 10), (III) schematic illustration of the cell promotion angle between the cell growth direction and the fiber parallel direction (x axis), (IV) cell proliferation angle on various scaffolds (N = 10), and V) Cell viability (N = 3). * and ** exhibited remarkable difference at $p < 0.05$ and $p < 0.01$, respectively, (VI) CLSM images of osteoblasts on (a) PLLA, (b) PLLA-collagen, and (c) PLLA-chitosan aligned scaffolds, respectively. Cell nuclei are shown in blue and actin fibers in red. Reproduced with permission [335]. Copyright 2013, the royal society of chemistry. D) (I) PVA nanofibers fabricated utilizing optimum point parameters and processed SEM in similar conditions, (II)

Curcumin loaded release into PBS buffer (dashed curve) and NaCl solution (solid curve), (III) Adipose tissue imaging using MRI in (x) untreated rats versus (y) treated rats by the transdermal patch. Reproduced with permission [356]. Copyright 2018, Elsevier.

Among all the techniques used for fabrication of the drug-eluting transdermal textiles, electrospinning is the most studied one since it is a simple and cost-effective method. Moreover, unique characteristics including a large surface area to volume ratio, ultrafine fibrous structure, and high porosity with pore sizes ranging from sub-micron to nanometer make the electrospun nonwoven a suitable carrier for delivering various bioactive agents. An overview of drug eluting medical textiles with their corresponding fiber spinning methods, drug impregnation techniques, release profiles, and kinetics are provided in **Table 1.2**.

TABLE. 1.2.
Drug eluting fibrous systems used in wound care applications.

APPLICATION	MATERIAL	DRUG	SPINNING METHOD	LOADING METHOD	TYPE OF RELEASE	TRANSPORT MECHANISM	RELEASE KINETICS	REMARKS AND OUTCOME
WOUND CARE	Poly(lactide-co-polyε-caprolactone)	Gentamicin sulfate	Electrospinning	Encapsulation	Extended	Fickian diffusion and polymer swelling	Higuchi ($R^2=0.97$)	Effective against <i>S.aureus</i> and <i>E.coli</i> bacteria [294].
	Poly(vinyl alcohol/chitosan	Antibacterial peptide OH-CATH30	Electrospinning	Encapsulation of carboxymethyl chitosan nanoparticles loaded with antibacterial peptide OH-CATH30	Extended	-	-	Dual antibacterial activity due to the presence of chitosan and peptide OH-CATH30 against <i>E.coli</i> and <i>S.aureus</i> , with promoted wound healing functionality [128].
	Nylon 6,6 DuPont type 200 woven fabric (PA)	Gallie acid microencapsulated in poly-ε-caprolactone	-	Coating (Pad-Drying process)	Extended	Fickian diffusion and retention of the microspheres on the surface	Korsmeyer-Peppas ($n=0.46$, $R^2=0.88$)	Drug-delivery (GA-PCL) system for medical and cosmetic textiles [300].
	Zein	Curcumin	Electrospinning	Encapsulation	Extended	Diffusion (concentration depended)	First-order R^2 (0.9940- 0.9969)	The antimicrobial applications of zein-CUR nanofibers showed to prevent bacterial growth [296].
	Chitin	-	Wet-spinning	-	-	-	-	Nonwoven chitin fabrics maintained the intrinsic structure of α-chitin and enhanced wound closure rate [357].
	Acrylonitrile-co-1-vinylimidazole (copolymer)	Nitric oxide	Melt-spinning	Release of NO was controlled with PCL coating	Triggered	-	-	By PCL coating, the release of nitric oxide was extended [315].

TABLE. 1.2.
Drug eluting fibrous systems used in tissue engineering.

APPLICATION	MATERIAL	DRUG	SPINNING METHOD	LOADING METHOD	TYPE OF RELEASE	TRANSPORT MECHANISM	RELEASE KINETICS	REMARKS AND OUTCOME
TISSUE ENGINEERING	Poly (l-lactide) fiber and silk fibroin/oxidized pectin hydrogel	Vancomycin Hydrochloride	Electrospinning	Encapsulation	Extended (sustained)	Degradation, swelling, and diffusion	Zero order ($R^2=0.98$)	Loading of aminolyzed PLLA-drug fibers in hydrogel reduced the swelling ratio, enhanced the mechanical properties, and led to a more sustainable release of vanco HCl [290].
	Poly(lactide)/polyvinyl alcohol	Albumin BMP-2	Coaxial electrospinning	Encapsulation	Extended	Diffusion and polymer chain relaxation	Peppas-Sahlin ($R^2 > 0.98$, $m=0.45$)	BMP-2 loaded coaxial electrospun PLA/PVA scaffolds guided regeneration of bone [303].
	Three-arm branched-star PCL	Hydroxyapatite nanoparticles (HNPs) and clodronate (CD)	Wet spinning and electrospinning	Encapsulation	-	-	-	Formation of defects induced by loading were minimized by optimizing the spinning conditions [334].
	Poly-L-lactide	Collagen, chitosan	Melt-spinning	Coating	-	-	-	Collagen coated melt-spun fibers enhanced the viability, adhesion, alignment, and migration of osteoblasts <i>in vitro</i> [335].
	Polyacrylonitrile	Acyclovir	Electrospinning	Bioconjugation	Extended	Fickian diffusion	Korsmeyer-Peppas ($n=0.26$, $R^2=0.96$)	Oxidized chitosan modified polyacrylonitrile loaded with acyclovir showed a controllable sustained-release profile of acyclovir with improved cell adhesion and proliferation of adipose-derived stem cells [358].
	Poly-L-lactide	DNA plasmid	Electrospinning	Encapsulation	Extended	-	-	PLA electrospun meshes impregnated with DNA plasmid and pBMP-2 genes and incorporated into gelatin methacryloyl and thiolated chitosan hydrogel system promoted bone repair and regeneration [359].

TABLE.1.2.
Drug eluting fibrous systems used in transdermal drug delivery.

APPLICATION	MATERIAL	DRUG	SPINNING METHOD	LOADING METHOD	TYPE OF RELEASE	TRANSPORT MECHANISM	RELEASE KINETICS	REMARKS AND OUTCOME
TRANSDERMAL DRUG DELIVERY	Gelatin	Levonorgestrel (LNG), ethinylestradiol (EE)	Electrospinning	Encapsulation	Extended (with first day burst effect)	Fickian diffusion	Both individual and dual loading of LNG zero-order and first-order model ($R^2=0.99$), individual loading of EE first-order model ($R^2=0.93$ - 0.97), dual loading of EE Higuchi model ($R^2 \geq 0.97$)	A high encapsulation efficiency (~90–100%) and drug loading (>90%) were obtained. The fibrous construct showed to be biocompatible and both drugs were permeable through the filter membrane [214].
	Cellulose	Ibuprofen	Electrospinning	Coating (immersing)	Immediate	Fickian diffusion	Korsmeyer-Peppas ($2\% w/v$, $n = 0.42$ and $R^2=0.93$; $3\% w/v$, $n=0.26$ and $R^2=0.99$)	A micro-/nano-fibrous nonwoven made out non-derivative cellulose showed the potential to be used for transdermal applications as a biocompatible construct [355].
	Polycaprolactone	Vitamin B12	Electrospinning	Encapsulation and plasma treatment	Extended	Polymer swelling	Higuchi	The drug release rate of hydrophobic nanofiber impregnated with the hydrophilic drug was controllable by plasma treatment time which increased the hydrophilicity of the surface [360].
	Poly (lactic-co-glycolic acid)	Daidzein	Electrospinning	Encapsulation	Extended	Non-Fickian diffusion	Korsmeyer-Peppas ($n=0.52$, $R^2=0.99$)	Core shell nanofibers of poly(lactic-co-glycolic acid) were loaded with daidzein nanostructured lipid carriers azone proved to have a sustained drug delivery. In vivo tests showed an increase in skin permeation of daidzein efficiently without skin irritation [361].
	psyllium husk mucilage	Paclitaxel	Electrospinning	Encapsulation	Extended	-	-	Paclitaxel loaded poly (bis (carboxyphenoxy) phosphazene)-cholic acid micelles were loaded in the psyllium husk mucilage to form the novel stimuli-responsive core-shell nanofibers. The meshes can actively inhibit the growth of MCF-7 cancer cells and provide a safe cancer therapy [362].

1.4.6 Discussion

In the previous sections, fiber fabrication processes, drug loading methods, release mechanisms, and kinetics were reviewed. Drug eluting fibers obtained from various raw materials vary extensively in terms of their chemistry and therefore performance characteristics. Moreover, various fabrication methods, such as melt- or wet-spinning, can be used both in the laboratory or industrial scales. The fabrication method depends on not only the raw material and the final application, but also the dimension and shape of the fibers, the biocompatibility of the solvent, and the processing parameters [363,364]. Woven and nonwoven structures from a broad range of natural to synthetic polymers or a combination of them have been used in various biomedical applications, such as wound care, tissue engineering, and regenerative medicine, due to features such as a high surface area to volume ratio, porous structure, and surface modification and functionalization.

Bioactive agents could also be loaded into fibers both in pre-and post-fabrication stages. However, loading methods should be selected based on the parameters such as bioactive agent chemistry, optimal release profile, the technical complexity of the spinning process, and the final application to avoid undesired results including low drug efficiency, degradation of the bioactive agents, poor mechanical properties, drug burst effect, and toxicity [141]. Mathematical models proposed to describe, quantify, and predict the kinetics of drug release can help to portray a better picture of the drug release profiles; however, it should be realized that most models have been investigated based on laboratory-driven data with limitations compared to real conditions. Therefore, there is a demand to overcome the simplifications of these models by verifying and improving them with drug release data obtained from fibrous constructs in real applications [87].

Recently, scientists have produced functional fibrous structures with the possibility of sensing the physiological data of the tissue and the ability to control drug delivery profiles [365,366]. Nanoscale sensors can be embedded into medical textiles to enable a programmable responsive drug delivery system to tune the release profile of the bioactive agent [174]. The drug release can be triggered by environmental stimuli, such as pH [367,368], temperature [369], and chemical reactions or external stimuli, such as the magnetic field [370], electric field [371], and light [372]. For example, various metals including gold, silver, magnesium, and zinc can be patterned with low-temperature radiofrequency sputtering on the nanofibrous meshes to apply thermal stimulation to elute antibiotics when needed.

The stimulation can be manipulated via wires or wireless devices, such as smartphones. The use of smart textiles has been mainly investigated for wound dressing applications where integrated sensors could provide information on the healing status and the wound environment concerning its pH, bacterial level, tissue oxygenation, and inflammation [373]. The need for devices that can provide diagnostic information on the wound status and combat the infection is growing. However, improving sensor incorporation onto the fibrous network, stable sensors, and reliable networks for data management are required [373].

The majority of studies reviewed in this article involve *in vitro* investigations of the drug-loaded fibers using different kinds of kinetic models. However, drug release and kinetics studies *in vivo* and in a 'physiologically relevant' environment are very essential to move forward toward clinical studies and commercialization of the fibrous drug delivery systems.

Designing proper methods to fabricate drug-eluting textiles requires not only a sound understanding of the fabrication and loading techniques but also the theoretical perception of human physiological systems and their biological mechanisms. Engineering databases and the mathematical stimulations could be evolved for advanced computer-aided textile design by considering different physiological processes and the physico-chemical functions of the textiles [374]. This can lead to achieving technical solutions with timely and cost effective designs.

Finally, it should be noted that despite all the progress in the field of drug eluting fibrous systems, there are still some limitations that should be addressed. For example, initial burst release of the drugs from fibers or aggregation of drug molecules on the surface of fibers can lead to undesired results. Using smart medical textiles and triggered drug-release systems could be applied to overcome some of the shortcomings of the current fibrous drug delivery systems. Lastly, due to the interdisciplinary nature of this field, fabrication of a functional drug eluting fibrous system with the desired release profile requires the joint efforts of experts from different disciplines such as chemistry, biology, and engineering.

1.5 Aim and scope

The design and fabrication of novel wound dressing materials with enhanced performance is a continuous clinical demand. Cellulose aerogels are promising candidates for the biomedical applications of drug delivery and wound dressing, thanks to their outstanding characteristics including high porosity, low density, large specific

surface area, high water and moisture uptake, biocompatibility, biodegradability, and the possibility to load and locally release drug and bioactive agents at the wound site.

The portfolio of aerogel processing possibilities is poor and few methods allow the production of various bioaerogels mainly in the form of films, monoliths, cylinders, and micro- and nanoparticle systems. Furthermore, despite the significance of cellulose aerogel, very little is known about the impact of cellulose type and the fiber processing and fabrication parameters on the properties of cellulose aerogels. Current production of cellulose aerogels is typically time consuming and expensive and their potential for scaling up is unclear. The possibility of cellulose aerogel fibers for blending with other natural polymers such as chitosan has not been studied. Moreover, the physico-chemical properties and *in vitro* characteristics of cellulose aerogel fibers such as drug loading capacity, drug release behavior, and cytotoxicity are not thoroughly studied. Therefore, the following objectives were investigated in this thesis:

- I. Evaluating the effect of the cellulose properties and the preparation conditions on the internal structure of the aerogel and its physicochemical properties.
- II. Optimizing and designing the fiber processing conditions and textile fabrication techniques for cellulose aerogel microfibers (CAFs) production.
- III. Investigating the feasibility of using cellulose aerogels as advanced biomaterials for the two different applications of drug delivery and wound dressing.

To address these goals, the current thesis covers the novel technologies for the synthesis and processing of drug loaded cellulose-based aerogels in the form of fibers and textiles for wound treatment and drug delivery applications. Cellulose was also blended with other natural polymers such as chitosan to obtain added value functionality such as antibacterial properties. Moreover, in this work, drug-loaded cellulose based aerogel microfibers having different dimensions and textile structures, including knitted, braided, and nonwoven, were fabricated, and their potential applications as drug delivery and wound dressing systems were explored. Finally, the manuscript is divided into 5 chapters and the outline has been described in the next section.

1.6 Outline

It is well known that the internal structure and physical properties of aerogels govern their final application features. Despite the significance of designing aerogels' morphology for the specific applications, few studies provide the correlations between

the type of polysaccharide, processing conditions, the bio-aerogel structure, and the final application properties. In **chapter 2**, the impact of cellulose intrinsic characteristics, such as crystallinity and molecular weight and distribution, on the fabricated aerogel microfibers as well as their potential for biomedical applications have been evaluated. It was demonstrated that by selecting the right source of cellulose, it is possible to tune the structure and properties of the cellulose aerogel fibers. The fibers produced in this study showed promising potential for biomedical applications.

Cellulose-based aerogels are favorable drug delivery systems due to their low cytotoxicity profile, biodegradability, open porosity, and high inner surface area. In **chapter 3**, scCO_2 impregnation of drug models within two different diameters of aerogel fibers and their possibility to form different textile structures were investigated. It was proven that the solvent exchange scCO_2 impregnation was an effective single-step technique for drug loading and aerogel formation. Humidity and water uptake assessments indicated that the fibrous structures were highly moisture absorbable and non-toxic with immediate drug release profiles due to the highly open interconnected porous structure of the fibers. Although the results of this study showed that these fibers are suitable candidates for wound dressing applications, it is important to note that cellulose by itself does not possess antibacterial properties to prevent wound infection. Therefore, it was decided to overcome this issue by fabricating a hybrid cellulose-chitosan aerogel in the following study.

Chitosan has a potential to be blended with other polysaccharides such as cellulose and it displays a broad antibacterial spectrum against the growth of bacteria, yeast, and fungi and promotes wound healing by accelerating the infiltration of inflammatory cells. **Chapter 4** explores the potential of ibuprofen loaded chitosan-cellulose hybrid aerogel microfibers which are fabricated through wet spinning and scCO_2 processes for wound dressing application. Highly porous hybrid fibers proved to have a higher specific surface area and pore volume than cellulose aerogel fibers. Chitosan-cellulose aerogel fibers were bactericide against *E. coli* and *S. aureus* (in $\text{pH} < 6.5$) and showed a more sustained drug release profile in comparison to cellulose aerogel fibers. These novel aerogel fibers are demonstrated to have a great potential to be used for wound dressing applications. However, an additional fabrication step is required to produce the wound dressing from the wet spun fibers.

In contrast to the previous chapters which wet spinning was used to fabricate microfibers, solution blowing spinning was investigated for fabrication of nonwoven aerogels in **chapter 5**. Solution blowing spinning as an innovative technique for spinning micro-/

nano-fibers from polymer solution has been combined with scCO_2 drying to develop highly porous cellulose aerogel nonwovens. In order to tune the hydrophobicity and drug release profile of the cellulose aerogel nonwovens, the meshes were surface treated through gas-phase esterification with palmitoyl chloride. The treated and untreated nonwovens were loaded by thymol as a natural antibacterial, antioxidant, and anti-inflammatory drug through the post-treatment scCO_2 technique. The palmitoyl chloride gas-phase reaction enhanced the contact angle drastically (from 0 to $\sim 130^\circ$) for the surface modified samples and resulted in a more sustained thymol release profile in comparison to the non-modified samples. The cellulose aerogel nonwovens exhibited cell viability, and the thymol loaded samples were bactericides against *E. coli* and *S. aureus*, indicating their potential as suitable material for wound dressing applications.

References

1. Velnar, T.; Bailey, T.; Smrkolj, V. The wound healing process: an overview of the cellular and molecular mechanisms. *Journal of International Medical Research* **2009**, *37*, 1528-1542.
2. Girard, D.; Laverdet, B.; Buhé, V.; Trouillas, M.; Ghazi, K.; Alexaline, M.M.; Egles, C.; Misery, L.; Coulomb, B.; Lataillade, J.-J. Biotechnological management of skin burn injuries: challenges and perspectives in wound healing and sensory recovery. *Tissue Engineering Part B: Reviews* **2017**, *23*, 59-82.
3. Parani, M.; Lokhande, G.; Singh, A.; Gaharwar, A.K. Engineered Nanomaterials for Infection Control and Healing Acute and Chronic Wounds. *ACS Applied Materials & Interfaces* **2016**, *8*, 10049-10069, doi:10.1021/acsami.6b00291.
4. Naseri-Nosar, M.; Ziora, Z.M. Wound dressings from naturally-occurring polymers: A review on homopolysaccharide-based composites. *Carbohydrate Polymers* **2018**, *189*, 379-398, doi:https://doi.org/10.1016/j.carbpol.2018.02.003.
5. Saghazadeh, S.; Rinaldi, C.; Schot, M.; Kashaf, S.S.; Sharifi, F.; Jalilian, E.; Nuutila, K.; Giatsidis, G.; Mostafalu, P.; Derakhshandeh, H., et al. Drug delivery systems and materials for wound healing applications. *Advanced drug delivery reviews* **2018**, *127*, 138-166, doi:10.1016/j.addr.2018.04.008.
6. Boateng, J.S.; Matthews, K.H.; Stevens, H.N.; Eccleston, G.M. Wound healing dressings and drug delivery systems: a review. *Journal of pharmaceutical sciences* **2008**, *97*, 2892-2923, doi:https://doi.org/10.1002/jps.21210.
7. Ganesan, P. Natural and bio polymer curative films for wound dressing medical applications. *Wound Medicine* **2017**, *18*, 33-40, doi:https://doi.org/10.1016/j.wndm.2017.07.002.
8. Hakkarainen, T.; Koivuniemi, R.; Kosonen, M.; Escobedo-Lucea, C.; Sanz-Garcia, A.; Vuola, J.; Valtonen, J.; Tammela, P.; Mäkitie, A.; Luukko, K., et al. Nanofibrillar cellulose wound dressing in skin graft donor site treatment. *Journal of Controlled Release* **2016**, *244*, 292-301, doi:https://doi.org/10.1016/j.jconrel.2016.07.053.
9. Bernardes, B.G.; Del Gaudio, P.; Alves, P.; Costa, R.; García-González, C.A.; Oliveira, A.L. Bioaerogels: Promising Nanostructured Materials in Fluid Management, Healing and Regeneration of Wounds. *Molecules* **2021**, *26*, 3834.
10. Sahana, T.G.; Rekha, P.D. Biopolymers: Applications in wound healing and skin tissue engineering. *Molecular Biology Reports* **2018**, *45*, 2857-2867, doi:10.1007/s11033-018-4296-3.
11. Rostamitabar, M.; Subrahmanyam, R.; Gurikov, P.; Seide, G.; Jockenhoevel, S.; Ghazanfari, S. Cellulose aerogel micro fibers for drug delivery applications. *Materials Science and Engineering: C* **2021**, *127*, 112196, doi:https://doi.org/10.1016/j.msec.2021.112196.
12. Darpentigny, C.; Nonglaton, G.; Bras, J.; Jean, B. Highly absorbent cellulose nanofibrils aerogels prepared by supercritical drying. *Carbohydrate Polymers* **2020**, *229*, 115560, doi:https://doi.org/10.1016/j.carbpol.2019.115560.
13. Abdul Khalil, H.P.S.; Adnan, A.S.; Yahya, E.B.; Olaiya, N.G.; Safrida, S.; Hossain, M.S.; Balakrishnan, V.; Gopakumar, D.A.; Abdullah, C.K.; Oyekanmi, A.A., et al. A Review on Plant Cellulose Nanofibre-Based Aerogels for Biomedical Applications. *Polymers* **2020**, *12*, 1759.
14. Maleki, H.; Durães, L.; García-González, C.A.; del Gaudio, P.; Portugal, A.; Mahmoudi, M. Synthesis and biomedical applications of aerogels: Possibilities and challenges. *Advances in Colloid and Interface Science* **2016**, *236*, 1-27, doi:https://doi.org/10.1016/j.cis.2016.05.011.
15. Kistler, S.S. Coherent Expanded Aerogels and Jellies. *Nature* **1931**, *127*, 741-741, doi:10.1038/127741a0.

16. Smirnova, I.; Suttiruangwong, S.; Arlt, W. Aerogels: Tailor-made Carriers for Immediate and Prolonged Drug Release. *KONA Powder and Particle Journal* **2005**, *23*, 86-97, doi:10.14356/kona.2005012.
17. Cao, L.; Fu, Q.; Si, Y.; Ding, B.; Yu, J. Porous materials for sound absorption. *Composites Communications* **2018**, *10*, 25-35, doi:https://doi.org/10.1016/j.coco.2018.05.001.
18. Ahankari, S.; Paliwal, P.; Subhedar, A.; Kargarzadeh, H. Recent Developments in Nanocellulose-Based Aerogels in Thermal Applications: A Review. *ACS Nano* **2021**, *15*, 3849-3874, doi:10.1021/acsnano.0c09678.
19. Dilamian, M.; Noroozi, B. Rice straw agri-waste for water pollutant adsorption: Relevant mesoporous super hydrophobic cellulose aerogel. *Carbohydrate Polymers* **2021**, *251*, 117016, doi:https://doi.org/10.1016/j.carbpol.2020.117016.
20. Maleki, H. Recent advances in aerogels for environmental remediation applications: A review. *Chemical Engineering Journal* **2016**, *300*, 98-118, doi:https://doi.org/10.1016/j.cej.2016.04.098.
21. Mao, J.; Iocozzia, J.; Huang, J.; Meng, K.; Lai, Y.; Lin, Z. Graphene aerogels for efficient energy storage and conversion. *Energy & Environmental Science* **2018**, *11*, 772-799.
22. Huang, Y.; Lai, F.; Zhang, L.; Lu, H.; Miao, Y.-E.; Liu, T. Elastic carbon aerogels reconstructed from electrospun nanofibers and graphene as three-dimensional networked matrix for efficient energy storage/conversion. *Scientific reports* **2016**, *6*, 1-11.
23. Yang, J.; Tang, L.-S.; Bai, L.; Bao, R.-Y.; Liu, Z.-Y.; Xie, B.-H.; Yang, M.-B.; Yang, W. High-performance composite phase change materials for energy conversion based on macroscopically three-dimensional structural materials. *Materials Horizons* **2019**, *6*, 250-273.
24. Dilamian, M.; Joghataei, M.; Ashrafi, Z.; Bohr, C.; Mathur, S.; Maleki, H. From 1D electrospun nanofibers to advanced multifunctional fibrous 3D aerogels. *Applied Materials Today* **2021**, *22*, 100964, doi:https://doi.org/10.1016/j.apmt.2021.100964.
25. Wang, H.; Zhang, X.; Wang, N.; Li, Y.; Feng, X.; Huang, Y.; Zhao, C.; Liu, Z.; Fang, M.; Ou, G., et al. Ultralight, scalable, and high-temperature-resilient ceramic nanofiber sponges. *Science Advances* **2017**, *3*, e1603170, doi:10.1126/sciadv.1603170.
26. Montes, S.; Maleki, H. 12 - Aerogels and their applications. In *Colloidal Metal Oxide Nanoparticles*, Thomas, S., Tresa Sunny, A., Velayudhan, P., Eds. Elsevier: 2020; https://doi.org/10.1016/B978-0-12-813357-6.00015-2pp. 337-399.
27. Corrias, A.; Casula, M.; Aegerter, M.; N Leventis, M.K. Aerogel handbook. Aerogels containing metal, alloy and oxide nanoparticles in dielectric matrices. Springer, New York **2010**.
28. Lamy-Mendes, A.; Silva, R.F.; Durães, L. Advances in carbon nanostructure-silica aerogel composites: a review. *Journal of Materials Chemistry A* **2018**, *6*, 1340-1369.
29. García-González, C.A.; Alnaief, M.; Smirnova, I. Polysaccharide-based aerogels—Promising biodegradable carriers for drug delivery systems. *Carbohydrate Polymers* **2011**, *86*, 1425-1438, doi:https://doi.org/10.1016/j.carbpol.2011.06.066.
30. Mehling, T.; Smirnova, I.; Guenther, U.; Neubert, R. Polysaccharide-based aerogels as drug carriers. *Journal of Non-Crystalline Solids* **2009**, *355*, 2472-2479, doi:https://doi.org/10.1016/j.jnoncrysol.2009.08.038.
31. Liu, Z.; Zhang, S.; He, B.; Wang, S.; Kong, F. Synthesis of cellulose aerogels as promising carriers for drug delivery: a review. *Cellulose* **2021**, *28*, 2697-2714, doi:10.1007/s10570-021-03734-9.
32. GROULT, S. Pectin-based aerogels: Advanced materials for thermal insulation and drug delivery applications. PSL Research University, France, 2019.
33. Subrahmanyam, R.; Gurikov, P.; Meissner, I.; Smirnova, I. Preparation of Biopolymer Aerogels Using Green

- Solvents. *JoVE* **2016**, doi:10.3791/54116, e54116, doi:doi:10.3791/54116.
34. Smirnova, I.; Gurikov, P. Aerogels in Chemical Engineering: Strategies Toward Tailor-Made Aerogels. *Annual Review of Chemical and Biomolecular Engineering* **2017**, *8*, 307-334, doi:10.1146/annurev-chembioeng-060816-101458.
35. Buchtová, N.; Budtova, T. Cellulose aero-, cryo- and xerogels: towards understanding of morphology control. *Cellulose* **2016**, *23*, 2585-2595, doi:10.1007/s10570-016-0960-8.
36. Innerlohinger, J.; Weber, H.K.; Kraft, G. Aerocellulose: Aerogels and Aerogel-like Materials made from Cellulose. *Macromolecular Symposia* **2006**, *244*, 126-135, doi:https://doi.org/10.1002/masy.200651212.
37. Horvat, G.; Khanari, K.; Finšgar, M.; Gradišnik, L.; Maver, U.; Knez, Ž.; Novak, Z. Novel ethanol-induced pectin-xanthan aerogel coatings for orthopedic applications. *Carbohydr Polym* **2017**, *166*, 365-376, doi:10.1016/j.carbpol.2017.03.008.
38. Gurikov, P.; Smirnova, I. Non-Conventional Methods for Gelation of Alginate. *Gels* **2018**, *4*, 14, doi:10.3390/gels4010014.
39. Budtova, T. Cellulose II aerogels: a review. *Cellulose* **2019**, *26*, 81-121, doi:10.1007/s10570-018-2189-1.
40. Long, L.-Y.; Weng, Y.-X.; Wang, Y.-Z. Cellulose Aerogels: Synthesis, Applications, and Prospects. *Polymers* **2018**, *10*, 623.
41. Yilmaz Atay, H. Antibacterial Activity of Chitosan-Based Systems. In *Functional Chitosan: Drug Delivery and Biomedical Applications*, Jana, S., Jana, S., Eds. Springer Singapore: Singapore, 2019; 10.1007/978-981-15-0263-7_15pp. 457-489.
42. Agboh, O.C.; Qin, Y. Chitin and Chitosan Fibers. *Polymers for Advanced Technologies* **1997**, *8*, 355-365, doi:doi:10.1002/(SICI)1099-1581(199706)8:6<355::AID-PAT651>3.0.CO;2-T.
43. Ramya, R.; Venkatesan, J.; Kim, S.K.; Sudha, P.N. Biomedical Applications of Chitosan: An Overview. *Journal of Biomaterials and Tissue Engineering* **2012**, *2*, 100-111, doi:10.1166/jbt.2012.1030.
44. Bano, I.; Arshad, M.; Yasin, T.; Ghauri, M.A.; Younus, M. Chitosan: A potential biopolymer for wound management. *International journal of biological macromolecules* **2017**, *102*, 380-383, doi:https://doi.org/10.1016/j.ijbiomac.2017.04.047.
45. Rostamitabar, M.; Seide, G.; Jockenhoevel, S.; Ghazanfari, S. Effect of Cellulose Characteristics on the Properties of the Wet-Spun Aerogel Fibers. *Applied Sciences* **2021**, *11*, 1525, doi:https://doi.org/10.3390/app11041525.
46. Medical Textiles Market Analysis By Raw Material (Non-woven, Knitted, Woven), By Application (Implantable Goods, Non-implantable Goods, Healthcare & Hygiene Products) And Segment Forecasts To 2022; Reportlinker: April 2019; p 124.
47. Rajendran, S.; Anand, S. High Performance Textiles and Their Applications. Wood head publishing: UK, 2014; p. 190.
48. Dijcker, R.; Wijk, M.V.D. Geotextile enabled smart monitoring solutions for safe and effective management of tailings and waste sites: Two case studies: Volgermeerpolder (The Netherlands) and Suncor (Canada). In *Proceedings of Proceedings Tailings and Mine Waste*, Vancouver.
49. V.T.Bartels. *Handbook of medical textiles*; Woodhead publishing: 2011.
50. Ratner, B.D.; Hoffman, A.S.; Schoen, F.J.; Lemons, J.E. *Biomaterials Science: An Introduction to Materials in Medicine*; Academic Press: London, 1996.
51. Rowell, R.M.; Han, J.S.; Rowell, J.S. Characterization and factors effecting fiber properties.

- In *Natural polymers and agrofibers based composites: preparation, properties and applications*. , E. Frollini, A.L.L.a.L.H.C.M., Ed. L.H.C., Embrapa: San Carlos, Brazil, 2000; pp. 115–134.
52. Denton, M.; Daniels, P. *Textile Terms and Definitions*; Manchester, 2002.
 53. Preston, J. Man-made fibre. In *Encyclopædia Britannica*, Encyclopædia Britannica, inc., 2016.
 54. Hooshmand, S.; Aitomäki, Y.; Skrifvars, M. All-cellulose nanocomposite fibers produced by melt spinning cellulose acetate butyrate and cellulose nanocrystals. *Cellulose* **2014**, *21*, 2665–2678.
 55. Meyer, M.; Baltzer, H.; Schwikal, K. Collagen fibres by thermoplastic and wet spinning. *Materials Science and Engineering: C* **2010**, *30*, 1266-1271, doi:<https://doi.org/10.1016/j.msec.2010.07.005>.
 56. NATU, M.V.; SOUSA, H.C.d.; GIL, M.H. Electrospun Drug-Eluting Fibers for Biomedical Applications. In *Active Implants and Scaffolds for Tissue Regeneration*. , Springer: Berlin, 2011; pp. 57-85.
 57. Wang, X.; Liu, X.; Deakin, C.H. 4 - Physical and mechanical testing of textiles. In *Fabric Testing*, Hu, J., Ed. Woodhead Publishing: 2008; <https://doi.org/10.1533/9781845695064.90pp>. 90-124.
 58. Bueno, M.A.; Aneja, A.P.; Renner, M. Influence of the shape of fiber cross section on fabric surface characteristics. *Journal of Materials Science* **2004**, *39*, 557-564, doi:[10.1023/B:JMSE.0000011511.66614.48](https://doi.org/10.1023/B:JMSE.0000011511.66614.48).
 59. Wulforst, B.; Gries, T.; Veit, D. Raw Materials. In *Textile Technology*, Wulforst, B., Gries, T., Veit, D., Eds. Hanser: 2006; <https://doi.org/10.3139/9783446433472.002pp>. 13-73.
 60. Karadagli, I.; Schulz, B.; Schestakow, M.; Milow, B.; Gries, T.; Ratke, L. Production of porous cellulose aerogel fibers by an extrusion process. *The Journal of Supercritical Fluids* **2015**, *106*, 105-114, doi:<https://doi.org/10.1016/j.supflu.2015.06.011>.
 61. Sasaki, M.; Morita, H.; Sakakibara, H.; Saruhashi, M.; Matsumoto, Y. Hollow cellulose fibers, method for making, and fluid processing apparatus using same. 1988.
 62. McClure, M.J.; Sell, S.A.; Ayres, C.E.; Simpson, D.G.; Bowlin, G.L. Electrospinning-aligned and random polydioxanone-polycaprolactone-silk fibroin-blended scaffolds: geometry for a vascular matrix. *Biomedical materials (Bristol, England)* **2009**, *4*, 055010, doi:[10.1088/1748-6041/4/5/055010](https://doi.org/10.1088/1748-6041/4/5/055010).
 63. Wei, M.; Kang, B.; Sung, C.; Mead, J. Core-Sheath Structure in Electrospun Nanofibers from Polymer Blends. *Macromolecular Materials and Engineering* **2006**, *291*, 1307-1314, doi:[10.1002/mame.200600284](https://doi.org/10.1002/mame.200600284).
 64. Lundahl, M.J.; Klar, V.; Adjary, R.; Norberg, N.; Ago, M.; Cunha, A.G.; Rojas, O.J. Absorbent Filaments from Cellulose Nanofibril Hydrogels through Continuous Coaxial Wet Spinning. *ACS applied materials & interfaces* **2018**, *10*, 27287-27296, doi:[10.1021/acsami.8b08153](https://doi.org/10.1021/acsami.8b08153).
 65. Bognitzki, M.; Frese, T.; Steinhart, M.; Greiner, A.; Wendorff, J.H.; Schaper, A.; Hellwig, M. Preparation of fibers with nanoscaled morphologies: Electrospinning of polymer blends. *Polymer Engineering & Science* **2004**, *41*, 982-989, doi:[10.1002/pen.10799](https://doi.org/10.1002/pen.10799).
 66. Kalra, V.; Kakad, P.A.; Mendez, S.; Ivannikov, T.; Kamperman, M.; Joo, Y.L. Self-Assembled Structures in Electrospun Poly(styrene-block-isoprene) Fibers. *Macromolecules* **2006**, *39*, 5453-5457, doi:[10.1021/ma052643a](https://doi.org/10.1021/ma052643a).
 67. Wilson, J. 6 - Woven structures and their characteristics. In *Woven Textiles*, Gandhi, K.L., Ed. Woodhead Publishing: 2012; <https://doi.org/10.1533/9780857095589.2.163pp>. 163-204.
 68. Whyte, W.; Hodgson, R.; Bailey, P.; Graham, J. The reduction of bacteria in the operation room through the use of non-woven clothing. *Br J Surg* **1978**, *65*, 469-474.
 69. Tuzlakoglu, K.; Alves, C.M.; Mano, J.F.; Reis, R.L. Production and characterization of chitosan fibers and 3-D fiber mesh scaffolds for tissue engineering applications. *Macromolecular bioscience* **2004**, *4*, 811-819,

- doi:10.1002/mabi.200300100.
70. Fahmy, H.M.; Aly, A.A.; Abou-Okeil, A. A non-woven fabric wound dressing containing layer - by - layer deposited hyaluronic acid and chitosan. *International journal of biological macromolecules* **2018**, *114*, 929-934, doi:10.1016/j.ijbiomac.2018.03.149.
71. Augustine, R.; Kalarikkal, N.; Thomas, S. Advancement of wound care from grafts to bioengineered smart skin substitutes. *Progress in biomaterials* **2014**, *3*, 103-113, doi:10.1007/s40204-014-0030-y.
72. Nierstrasz, V.A. 3 - Textile-based drug release systems. In *Smart Textiles for Medicine and Healthcare*, Van Langenhove, L., Ed. Woodhead Publishing: 2007; <https://doi.org/10.1533/9781845692933.1.50pp>. 50-73.
73. Perelshtein, I.; Applerot, G.; Perkash, N.; Guibert, G.; Mikhailov, S.; Gedanken, A. Sonochemical coating of silver nanoparticles on textile fabrics (nylon, polyester and cotton) and their antibacterial activity. *Nanotechnology* **2008**, *19*, 1-6.
74. Kumbar, S.; Bhattacharyya, S.; Sethuraman, S.; Laurencin, C. A preliminary report on a novel electrospray technique for nanoparticle based biomedical implants coating: precision electrospraying. *J Biomed Mater Res B Appl Biomater* **2007**, *81*, 91-103.
75. Champeau, M.; Thomassin, J.M.; Tassaing, T.; Jérôme, C. Drug loading of polymer implants by supercritical CO₂ assisted impregnation: A review. *Journal of Controlled Release* **2015**, *209*, 248-259, doi:<https://doi.org/10.1016/j.jconrel.2015.05.002>.
76. Soni, B. Chemically modified Cotton fibers for antimicrobial applications; 2015; pp. 36.
77. Breteler, M.R.t.; Nierstrasz, V.; Warmoeskerken, M. Textile slow-release systems with medical applications. *AUTEX Research Journal* **2002**, *2*.
78. Haimer, E.; Wendland, M.; Schlufner, K.; Frankenfeld, K.; Miethe, P.; Potthast, A.; Rosenau, T.; Liebner, F. Loading of Bacterial Cellulose Aerogels with Bioactive Compounds by Antisolvent Precipitation with Supercritical Carbon Dioxide. *Macromolecular Symposia* **2010**, *294*, 64-74, doi:10.1002/masy.201000008.
79. Sikareepaisan, P.; Suksamrarn, A.; Supaphol, P. Electrospun gelatin fiber mats containing a herbal-Centella asiatica-extract and release characteristic of asiaticoside. *Nanotechnology* **2008**, *19*, 015102, doi:10.1088/0957-4484/19/01/015102.
80. Jaskari, T.; Vuorio, M.; Kontturi, K.; Urtti, A.; Manzanares, J.A. Controlled transdermal iontophoresis by ion-exchange fibre. *J. Controlled release* **2000**, *67*, 179-190.
81. Bagherifard, S.; Tamayol, A.; Mostafalu, P.; Akbari, M.; Comotto, M.; Annabi, N.; Ghaderi, M.; Sonkusale, S.; Dokmeci, M.R.; Khademhosseini, A. Dermal Patch with Integrated Flexible Heater for on Demand Drug Delivery. *Advanced healthcare materials* **2016**, *5*, 175-184, doi:10.1002/adhm.201500357.
82. Song, B.; Wu, C.; Chang, J. Ultrasound-triggered dual-drug release from poly(lactic-co-glycolic acid)/mesoporous silica nanoparticles electrospun composite fibers. *Regenerative biomaterials* **2015**, *2*, 229-237, doi:10.1093/rb/rbv019.
83. Mauger, J.W.; Chilko, D.; Howard, S. On the Analysis of Dissolution Data. *Drug Development and Industrial Pharmacy* **1986**, *12*, 969-992, doi:10.3109/03639048609048052.
84. Polli, J.E.; Rekhi, G.S.; Augsburger, L.L.; Shah, V.P. Methods to compare dissolution profiles and a rationale for wide dissolution specifications for metoprolol tartrate tablets. *J Pharm Sci* **1997**, *86*, 690-700, doi:10.1021/js960473x.
85. Dash, S.; Murthy, P.N.; Nath, L.; Chowdhury, P. Kinetic modeling on drug release from controlled drug delivery systems. *Acta Pol Pharm* **2010**, *67*, 217-223.

86. Costa, P.; Sousa Lobo, J.M. Modeling and comparison of dissolution profiles. *European journal of pharmaceutical sciences : official journal of the European Federation for Pharmaceutical Sciences* **2001**, *13*, 123-133.
87. 5 - Mathematical models of drug release. In *Strategies to Modify the Drug Release from Pharmaceutical Systems*, Bruschi, M.L., Ed. Woodhead Publishing: 2015; <https://doi.org/10.1016/B978-0-08-100092-2.00005-9>pp. 63-86.
88. Peppas, N.A.; Brannon-Peppas, L. Water diffusion and sorption in amorphous macromolecular systems and foods. *Journal of Food Engineering* **1994**, *22*, 189-210, doi:[https://doi.org/10.1016/0260-8774\(94\)90030-2](https://doi.org/10.1016/0260-8774(94)90030-2).
89. Peppas, N.A.; Narasimhan, B. Mathematical models in drug delivery: How modeling has shaped the way we design new drug delivery systems. *Journal of Controlled Release* **2014**, *190*, 75-81, doi:<https://doi.org/10.1016/j.jconrel.2014.06.041>.
90. DeFrates, K.G.; Moore, R.; Borges, J.; Lin, G.; Mulderig, T.; Beachley, V.; Hu, X. Protein-Based Fiber Materials in Medicine: A Review. *Nanomaterials (Basel, Switzerland)* **2018**, *8*, doi:10.3390/nano8070457.
91. Sanjay, M.; Arpitha, G.; Naik, L.L.; Gopalakrishna, K.; Yogesha, B. Applications of natural fibers and its composites: An overview. *Natural Resources* **2016**, *7*, 108.
92. Qin, Y. 3 - A brief description of textile fibers. In *Medical Textile Materials*, Qin, Y., Ed. Woodhead Publishing: 2016; <https://doi.org/10.1016/B978-0-08-100618-4.00003-0>pp. 23-42.
93. Zhu, L.M.; Yu, D.G. 9 - Drug delivery systems using biotextiles. In *Biotextiles as Medical Implants*, King, M.W., Gupta, B.S., Guidoin, R., Eds. Woodhead Publishing: 2013; <https://doi.org/10.1533/9780857095602.2.213pp>. 213-231.
94. Gomes, M.; Azevedo, H.; Malafaya, P.; Silva, S.; Oliveira, J.; Silva, G.; Sousa, R.; Mano, J.; Reis, R. Chapter 6 - Natural Polymers in tissue engineering applications. In *Tissue Engineering*, Blitterswijk, C.v., Thomsen, P., Lindahl, A., Hubbell, J., Williams, D.F., Cancedda, R., Bruijn, J.D.d., Sohier, J., Eds. Academic Press: Burlington, 2008; <https://doi.org/10.1016/B978-0-12-370869-4.00006-9>pp. 145-192.
95. Malafaya, P.B.; Silva, G.A.; Reis, R.L. Natural-origin polymers as carriers and scaffolds for biomolecules and cell delivery in tissue engineering applications. *Advanced drug delivery reviews* **2007**, *59*, 207-233, doi:<https://doi.org/10.1016/j.addr.2007.03.012>.
96. Rayner, M.; Östbring, K.; Purhagen, J. Application of Natural Polymers in Food. In *Natural Polymers: Industry Techniques and Applications*, Olatunji, O., Ed. Springer International Publishing: Cham, 2016; [10.1007/978-3-319-26414-1_5pp](https://doi.org/10.1007/978-3-319-26414-1_5pp). 115-161.
97. Aider, M. Chitosan application for active bio-based films production and potential in the food industry: Review. *LWT - Food Science and Technology* **2010**, *43*, 837-842, doi:<https://doi.org/10.1016/j.lwt.2010.01.021>.
98. Nayak, A.; Olatunji, O.; Bhusan Das, D.; Vladislavljević, G. Pharmaceutical Applications of Natural Polymers. In *Natural Polymers: Industry Techniques and Applications*, Olatunji, O., Ed. Springer International Publishing: Cham, 2016; [10.1007/978-3-319-26414-1_9pp](https://doi.org/10.1007/978-3-319-26414-1_9pp). 263-313.
99. Ahmadi, F.; Oveis, Z.; Samani, S.M.; Amoozgar, Z. Chitosan based hydrogels: characteristics and pharmaceutical applications. *Res Pharm Sci* **2015**, *10*, 1-16.
100. Kennedy, J.F. *Carbohydrate Chemistry*; Oxford University Press: Oxford, 1988.
101. Jania, G.K.; Shahb, D.P.; Prajapatia, V.D.; Jainb, V.C. Gums and mucilages: versatile excipients for pharmaceutical formulations. *Asian Journal of Pharmaceutical Sciences* **2009**, *4*, 308-322.
102. Shirwaikar, A.; Shirwaikar, A.; Prabu, S.L.; Kumar, G.A. Herbal excipients in novel drug delivery systems. *Indian journal of pharmaceutical sciences* **2008**, *70*, 415-422, doi:10.4103/0250-474X.44587.

103. Kennedy, J.F.; White, C.A. *Bioactive Carbohydrates in Chemistry*; Ellis Horwood: Chichester, 1983.
104. Jacob John, M.; Thomas, S. CHAPTER 1 Natural Polymers: An Overview. In *Natural Polymers: Volume 1: Composites*, The Royal Society of Chemistry: 2012; Vol. 1, pp. 1-7.
105. Thakur, V.K.; Thakur, M.K. Processing and characterization of natural cellulose fibers/thermoset polymer composites. *Carbohydrate Polymers* **2014**, *109*, 102-117, doi:https://doi.org/10.1016/j.carbpol.2014.03.039.
106. Poletto, M.; Pistor, V.; Zattera, A.J. Structural characteristics and thermal properties of native cellulose. *Cellulose-fundamental aspects* **2013**, *2*, 45-68.
107. Maneerung, T.; Tokura, S.; Rujiravanit, R. Impregnation of silver nanoparticles into bacterial cellulose for antimicrobial wound dressing. *Carbohydrate Polymers* **2008**, *72*, 43-51, doi:https://doi.org/10.1016/j.carbpol.2007.07.025.
108. Kollar, P.; Suchy, P.; Muselik, J.; Bajerova, M.; Havelka, P.; Sopuch, T. Hemostatic effects of oxidized cellulose. *Ceska a Slovenska farmacie : casopis Ceske farmaceuticke spolcnosti a Slovenske farmaceuticke spolcnosti* **2008**, *57*, 11-16.
109. Marian, F.; Mårten, S.; Petter, S.; Eleonor, P.; Christopher, A.; Andreas, S.; Grzegorz, G.; Hazem, K.; Torbjörn, B.; Daniel, A. Functionalization of bacterial cellulose wound dressings with the antimicrobial peptide ϵ -poly-L-Lysine. *Biomed. Mater.* **2018**, *13*, 025014.
110. Lee, K.Y.; Mooney, D.J. Alginate: properties and biomedical applications. *Progress in polymer science* **2012**, *37*, 106-126, doi:10.1016/j.progpolymsci.2011.06.003.
111. Altinel, Y.; Chung, S.S.; Okay, G.; Ugras, N.; Isik, A.F.; Ozturk, E.; Ozturk, H. Effect of chitosan coating on surgical sutures to strengthen the colonic anastomosis. *Ulusal travma ve acil cerrahi dergisi = Turkish journal of trauma & emergency surgery : TJTES* **2018**, *24*, 405-411, doi:10.5505/tjtes.2018.59280.
112. Laurén, P.; Somersalo, P.; Pitkänen, I.; Lou, Y.-R.; Urtti, A.; Partanen, J.; Seppälä, J.; Madetoja, M.; Laaksonen, T.; Mäkitie, A., et al. Nanofibrillar cellulose-alginate hydrogel coated surgical sutures as cell-carrier systems. *PLOS ONE* **2017**, *12*, e0183487, doi:10.1371/journal.pone.0183487.
113. Xing, Q.; Zhao, F.; Chen, S.; McNamara, J.; DeCoster, M.A.; Lvov, Y.M. Porous biocompatible three-dimensional scaffolds of cellulose microfiber/gelatin composites for cell culture. *Acta biomaterialia* **2010**, *6*, 2132-2139, doi:https://doi.org/10.1016/j.actbio.2009.12.036.
114. Tan, H.; Wu, J.; Lao, L.; Gao, C. Gelatin/chitosan/hyaluronan scaffold integrated with PLGA microspheres for cartilage tissue engineering. *Acta biomaterialia* **2009**, *5*, 328-337, doi:https://doi.org/10.1016/j.actbio.2008.07.030.
115. Sturken, O. Protein plastic. 1939.
116. Li, Y.V. Proteins and Protein-Based Fibers. In *Lightweight Materials from Biopolymers and Biofibers*, American Chemical Society: 2014; Vol. 1175, pp. 21-36.
117. Le Bao Ha, T.; Minh, T.; Nguyen, D.; Minh, D. Naturally Derived Biomaterials: Preparation and Application. 2013; 10.5772/55668.
118. Bloomfield, M.M.; Stephens, L.J. *Chemistry and the Living Organism*; John Wiley & Sons: New York, 1996.
119. McManus, M.C.; Boland, E.D.; Simpson, D.G.; Barnes, C.P.; Bowlin, G.L. Electrospun fibrinogen: feasibility as a tissue engineering scaffold in a rat cell culture model. *Journal of biomedical materials research. Part A* **2007**, *81*, 299-309, doi:10.1002/jbm.a.30989.
120. Stitzel, J.; Liu, J.; Lee, S.J.; Komura, M.; Berry, J.; Soker, S.; Lim, G.; Van Dyke, M.; Czerw, R.; Yoo, J.J., et al. Controlled fabrication of a biological vascular substitute. *Biomaterials* **2006**, *27*, 1088-1094,

- doi:<https://doi.org/10.1016/j.biomaterials.2005.07.048>.
121. Huang, L.; Nagapudi, K.; PApkarian, R.; Chaikof, E.L. Engineered collagen-PEO nanofibers and fabrics. *Journal of Biomaterials Science, Polymer Edition* **2001**, *12*, 979-993, doi:10.1163/156856201753252516.
 122. Meng, W.; Kim, S.-Y.; Yuan, J.; Kim, J.C.; Kwon, O.H.; Kawazoe, N.; Chen, G.; Ito, Y.; Kang, I.-K. Electrospun PHBV/collagen composite nanofibrous scaffolds for tissue engineering. *Journal of Biomaterials Science, Polymer Edition* **2007**, *18*, 81-94, doi:10.1163/156856207779146114.
 123. Sill, T.J.; von Recum, H.A. Electrospinning: Applications in drug delivery and tissue engineering. *Biomaterials* **2008**, *29*, 1989-2006, doi:<https://doi.org/10.1016/j.biomaterials.2008.01.011>.
 124. McIntyre, J.E. 1 - Historical background. In *Synthetic Fibres*, McIntyre, J.E., Ed. Woodhead Publishing: 2005; <https://doi.org/10.1533/9781845690427.1pp>. 1-19.
 125. Jamir, M.R.M.; Majid, M.S.A.; Khasri, A. 8 - Natural lightweight hybrid composites for aircraft structural applications. In *Sustainable Composites for Aerospace Applications*, Jawaid, M., Thariq, M., Eds. Woodhead Publishing: 2018; <https://doi.org/10.1016/B978-0-08-102131-6.00008-6pp>. 155-170.
 126. Volokhova, A.A.; Kudryavtseva, V.L.; Spiridonova, T.I.; Kolesnik, I.; Goreninskii, S.I.; Sazonov, R.V.; Remnev, G.E.; Tverdokhlebov, S.I. Controlled drug release from electrospun PCL non-woven scaffolds via multi-layering and e-beam treatment. *Materials Today Communications* **2021**, *26*, 102134, doi:<https://doi.org/10.1016/j.mtcomm.2021.102134>.
 127. Xing, G.; Shao, L.; Du, Y.; Tao, H.; Qi, C. Citric acid crosslinked chitosan/poly(ethylene oxide) composite nanofibers fabricated by electrospinning and thermal treatment for controlled drug release. *Cellulose* **2021**, *28*, 961-971, doi:10.1007/s10570-020-03562-3.
 128. Zou, P.; Lee, W.-H.; Gao, Z.; Qin, D.; Wang, Y.; Liu, J.; Sun, T.; Gao, Y. Wound dressing from polyvinyl alcohol/chitosan electrospun fiber membrane loaded with OH-CATH30 nanoparticles. *Carbohydrate Polymers* **2020**, *232*, 115786, doi:<https://doi.org/10.1016/j.carbpol.2019.115786>.
 129. Franco, P.; De Marco, I. The Use of Poly(N-vinyl pyrrolidone) in the Delivery of Drugs: A Review. *Polymers* **2020**, *12*, 1114.
 130. Maitz, M.F. Applications of synthetic polymers in clinical medicine. *Biosurface and Biotribology* **2015**, *1*, 161-176, doi:<https://doi.org/10.1016/j.bsbt.2015.08.002>.
 131. Liu, W.; Ma, J.; Yao, X.; Fang, R. Chapter 1 - Inorganic fibers for biomedical engineering applications. In *Materials for Biomedical Engineering*, Grumezescu, V., Grumezescu, A.M., Eds. Elsevier: 2019; <https://doi.org/10.1016/B978-0-12-818431-8.00001-5pp>. 1-32.
 132. Dimitrievska, S.; Whitfield, J.; Hacking, S.; Bureau, M. Novel carbon fiber composite for hip replacement with improved in vitro and in vivo osseointegration. *Journal of biomedical materials research. Part A* **2009**, *91*, 37-51, doi:10.1002/jbm.a.32175.
 133. Rajtar, A.; Kaluza, G.; Yang, Q.; Hakimi, D.; Liu, D. Hydroxyapatite-coated cardiovascular stents. *EuroIntervention* **2006**, *2*, 113-115.
 134. Tuzlakoglu, K.; Reis, R.L. Biodegradable Polymeric Fiber Structures in Tissue Engineering. *Tissue Engineering Part B: Reviews* **2008**, *15*, 17-27, doi:10.1089/ten.teb.2008.0016.
 135. Ellis, M.J.; Chaudhuri, J.B. Poly(lactic-co-glycolic acid) hollow fibre membranes for use as a tissue engineering scaffold. *Biotechnology and bioengineering* **2007**, *96*, 177-187, doi:10.1002/bit.21093.
 136. Gerhardt, L.-C.; Lottenbach, R.; Rossi, R.; Derler, S. Tribological investigation of a functional medical textile with lubricating drug-delivery finishing. *Colloids and Surfaces B: Biointerfaces* **2013**, *108*, 103-109.
 137. Zhou, F.-L.; Gong, R.-H. Manufacturing technologies of polymeric nanofibres and nanofibre yarns.

- Polymer International* **2007**, 57, 837-845, doi:10.1002/pi.2395.
138. Fambri, L.; Pegoretti, A.; Fenner, R.; Incardona, S.; Migliaresi, C. Biodegradable fibres of poly (L-lactic acid) produced by melt spinning. *Polymer* **1997**, 38, 79-85.
139. Mochizuki, M.; Hirano, M.; Kanmuri, Y.; Kudo, K.; Tokiwa, Y. Hydrolysis of polycaprolactone fibers by lipase: Effects of draw ratio on enzymatic degradation. *Journal of Applied Polymer Science* **1995**, 55, 289-296, doi:10.1002/app.1995.070550212.
140. Wang, X.; Wang, Y.; Xia, Y.; Huang, S.; Wang, Y.; Qiu, Y. Preparation, structure, and properties of melt spun cellulose acetate butyrate fibers. *Textile Research Journal* **2017**, 88, 1491-1504, doi:10.1177/0040517517703599.
141. Qin, Y. 13 - Medical textile materials with drug-releasing properties. In *Medical Textile Materials*, Qin, Y., Ed. Woodhead Publishing: 2016; <https://doi.org/10.1016/B978-0-08-100618-4.00013-3>. 175-189.
142. Plaza, G.R.; Corsini, P.; Marsano, E.; Pérez-Rigueiro, J.; Elices, M.; Riekel, C.; Vendrely, C.; Guinea, G.V. Correlation between processing conditions, microstructure and mechanical behavior in regenerated silk worm silk fibers. *Journal of Polymer Science Part B: Polymer Physics* **2012**, 50, 455-465, doi:10.1002/polb.23025.
143. Um, I.C.; Ki, C.S.; Kweon, H.; Lee, K.G.; Ihm, D.W.; Park, Y.H. Wet spinning of silk polymer: II. Effect of drawing on the structural characteristics and properties of filament. *International journal of biological macromolecules* **2004**, 34, 107-119, doi:<https://doi.org/10.1016/j.ijbiomac.2004.03.011>.
144. Adanur, S. *Wellington Sears Handbook of Industrial Textiles*.; Technomic Publishing Company.: Lancaster, 1995.
145. Xu, G.K.; Liu, L.; Yao, J.M. Fabrication and Characterization of Alginate Fibers by Wet-Spinning. *Advanced Materials Research* **2013**, 796, 87-91, doi:10.4028/www.scientific.net/AMR.796.87.
146. Williamson, M.R.; Coombes, A.G.A. Gravity spinning of polycaprolactone fibres for applications in tissue engineering. *Biomaterials* **2004**, 25, 459-465, doi:[https://doi.org/10.1016/S0142-9612\(03\)00536-2](https://doi.org/10.1016/S0142-9612(03)00536-2).
147. MirafTAB, M.; Qiao, Q.; Kennedy, J.F.; Anand, S.C.; Grocock, M.R. Fibres for wound dressings based on mixed carbohydrate polymer fibres. *Carbohydrate Polymers* **2003**, 53, 225-231, doi:[https://doi.org/10.1016/S0144-8617\(03\)00108-5](https://doi.org/10.1016/S0144-8617(03)00108-5).
148. Lin, H.-Y.; Wang, H.-W. The influence of operating parameters on the drug release and antibacterial performances of alginate fibrous dressings prepared by wet spinning. *Biomatter* **2012**, 2, 321-328, doi:10.4161/biom.22817.
149. Wade, S.J.; Sahin, Z.; Piper, A.-K.; Talebian, S.; Aghmesheh, M.; Foroughi, J.; Wallace, G.G.; Moulton, S.E.; Vine, K.L. Dual Delivery of Gemcitabine and Paclitaxel by Wet-Spun Coaxial Fibers Induces Pancreatic Ductal Adenocarcinoma Cell Death, Reduces Tumor Volume, and Sensitizes Cells to Radiation. *Advanced healthcare materials* **2020**, 9, 2001115, doi:<https://doi.org/10.1002/adhm.202001115>.
150. Formhals, A. Process and apparatus for preparing artificial threads. 1934.
151. Doshi, J.; Reneker, D.H. Electrospinning process and applications of electrospun fibers. *Journal of Electrostatics* **1995**, 35, 151-160, doi:[https://doi.org/10.1016/0304-3886\(95\)00041-8](https://doi.org/10.1016/0304-3886(95)00041-8).
152. Huang, Z.-M.; Zhang, Y.; Kotaki, M.; Ramakrishna, S. A Review on Polymer Nanofibers by Electrospinning and Their Applications in Nanocomposites; 2003; Vol. 63, pp. 2223-2253.
153. Fridrikh, S.; H Yu, J.; P Brenner, M.; C Rutledge, G. *Controlling the Fiber Diameter During Electrospinning*; 2003; Vol. 90, pp. 144502.
154. Brown, T.D.; Dalton, P.D.; Hutmacher, D.W. Melt electrospinning today: An opportune time for an emerging polymer process. *Progress in Polymer Science* **2016**, 56, 116-166, doi:<https://doi.org/10.1016/j.progpolymsci.2016.01.001>.

155. McClure, M.J.; Sell, S.A.; Ayres, C.E.; Simpson, D.G.; Bowlin, G.L. Electrospinning-aligned and random polydioxanone-polycaprolactone-silk fibroin-blended scaffolds: geometry for a vascular matrix. *Biomed. Mater.* **2009**, *4*, 13, doi:10.1088/1748-6041/4/5/055010.
156. Pornsopone, V.; Supaphol, P.; Rangkupan, R.; Tantayanon, S. Electrospun Methacrylate-Based Copolymer/Indomethacin Fibers and Their Release Characteristics of Indomethacin. *Journal of Polymer Research* **2007**, *14*, 53-59, doi:10.1007/s10965-006-9080-8.
157. El-Naggar, M.E.; Abdelgawad, A.M.; Salas, C.; Rojas, O.J. Curdlan in fibers as carriers of tetracycline hydrochloride: Controlled release and antibacterial activity. *Carbohydrate polymers* **2016**, *154*, 194-203.
158. Li, S.; Lv, R.; Liu, H.; Na, B.; Zhou, H.; Ge, L. Uniform high-molecular-weight polylactide nanofibers electrospun from a solution below its entanglement concentration. *Journal of Applied Polymer Science* **2017**, *134*, doi:10.1002/app.44853.
159. Okutan, N.; Terzi, P.; Altay, F. Affecting parameters on electrospinning process and characterization of electrospun gelatin nanofibers. *Food Hydrocolloids* **2014**, *39*, 19-26, doi:https://doi.org/10.1016/j.foodhyd.2013.12.022.
160. Ginestra, P.; Ceretti, E.; Fiorentino, A. Electrospinning of Poly-caprolactone for Scaffold Manufacturing: Experimental Investigation on the Process Parameters Influence. *Procedia CIRP* **2016**, *49*, 8-13, doi:https://doi.org/10.1016/j.procir.2015.07.020.
161. Volova, T.; Goncharov, D.; Sukovaty, A.; Shabanov, A.; Nikolaeva, E.; Shishatskaya, E. Electrospinning of polyhydroxyalkanoate fibrous scaffolds: effects on electrospinning parameters on structure and properties. *Journal of biomaterials science. Polymer edition* **2014**, *25*, 370-393, doi:10.1080/09205063.2013.862400.
162. Tong, H.-W.; Wang, M. Electrospinning of Poly(Hydroxybutyrate-co-hydroxyvalerate) Fibrous Scaffolds for Tissue Engineering Applications: Effects of Electrospinning Parameters and Solution Properties. *Journal of Macromolecular Science, Part B* **2011**, *50*, 1535-1558, doi:10.1080/00222348.2010.541008.
163. Wulfhorst, B.; Gries, T.; Veit, D. *Textile Technology*. In *Textile Technology*, Wulfhorst, B., Gries, T., Veit, D., Eds. Hanser: 2006; https://doi.org/10.3139/9783446433472.fmpp. I-VIII.
164. Durany, A.; Anantharamaiah, N.; Pourdeyhi, B. High surface area nonwovens via fibrillating spunbonded nonwovens comprising Islands-in-the-Sea bicomponent filaments: structure–process–property relationships. *Journal of Materials Science* **2009**, *44*, 5926-5934, doi:10.1007/s10853-009-3841-9.
165. Clark, D.F.; Duellman, J.M.; Haynes, B.D.; Lake, M.B.; McManus, J.L.; Smith, K.E. Fine multicomponent fiber webs and laminates thereof. 1999.
166. Fedorova, N.; Pourdeyhi, B. High strength nylon micro- and nanofiber based nonwovens via spunbonding. *Journal of Applied Polymer Science* **2007**, *104*, 3434-3442, doi:10.1002/app.25939.
167. Gong, R.H.; Nikoukhesal, A. Hydro-entangled bi-component microfiber nonwovens. *Polymer Engineering & Science* **2009**, *49*, 1703-1707, doi:10.1002/pen.21400.
168. Srinivasan, J.; Kathirvelu, S. An introduction to spunbond and meltblown nonwovens. *Synthetic Fibres* **2006**, *35*, 27.
169. Martin, D.H.; Southern, J.H. Implantable fibers and medical articles. 1996.
170. King, M.W. Designing fabrics for blood vessel replacement. *Canadian Textile Journal* **1991**, *108*, 24–30.
171. Casper, C.L.; Yamaguchi, N.; Kiick, K.L.; Rabolt, J.F. Functionalizing Electrospun Fibers with Biologically Relevant Macromolecules. *Biomacromolecules* **2005**, *6*, 1998-2007, doi:10.1021/bm050007e.
172. Gupta, P.; Wilkes, G.L. Some investigations on the fiber formation by utilizing a side-by-side bicomponent electrospinning approach. *Polymer* **2003**, *44*, 6353-6359,

doi:[https://doi.org/10.1016/S0032-3861\(03\)00616-5](https://doi.org/10.1016/S0032-3861(03)00616-5).

173. Gupta, B.S. 1 - Textile fiber morphology, structure and properties in relation to friction. In *Friction in Textile Materials*, Gupta, B.S., Ed. Woodhead Publishing: 2008; <https://doi.org/10.1533/9781845694722.1.3pp.3-36>.
174. Shah, T.; Halacheva, S. 6 - Drug-releasing textiles. In *Advances in Smart Medical Textiles*, van Langenhove, L., Ed. Woodhead Publishing: Oxford, 2016; <https://doi.org/10.1016/B978-1-78242-379-9.00006-2pp.119-154>.
175. Spencer, D.J. Knitting technology: a comprehensive handbook and practical guide; Woodhead Publishing: 2001.
176. Leong, K.H.; Ramakrishna, S.; Huang, Z.M.; Bibo, G.A. The potential of knitting for engineering composites—a review. *Composites Part A: Applied Science and Manufacturing* **2000**, *31*, 197-220, doi:[https://doi.org/10.1016/S1359-835X\(99\)00067-6](https://doi.org/10.1016/S1359-835X(99)00067-6).
177. Akbari, M.; Tamayol, A.; Bagherifard, S.; Serex, L.; Mostafalu, P.; Faramarzi, N.; Mohammadi, M.H.; Khademhosseini, A. Textile technologies and tissue engineering: a path toward organ weaving. *Advanced healthcare materials* **2016**, *5*, 751-766.
178. Li, G.; Chen, Y.; Hu, J.; Wu, X.; Hu, J.; He, X.; Li, J.; Zhao, Z.; Chen, Z.; Li, Y. A 5-fluorouracil-loaded polydioxanone weft-knitted stent for the treatment of colorectal cancer. *Biomaterials* **2013**, *34*, 9451-9461.
179. Shanmugasundaram, O.; Mahendra Gowda, R. Development and characterization of cotton, organic cotton flat knit fabrics coated with chitosan, sodium alginate, calcium alginate polymers, and antibiotic drugs for wound healing. *Journal of Industrial Textiles* **2012**, *42*, 156-175.
180. Radu, C.; Parteni, O.; Popa, M.; Muresan, I.; Ochiuz, L.; Bulgariu, L.; Munteanu, C.; Istrate, B.; Ule, E. Comparative study of a drug release from a textile to skin. *J Pharm Drug Deliv Res* **2015**, *4*, 2.
181. Behera, B.K.; Hari, P. Woven textile structure: Theory and applications; Elsevier: 2010.
182. Perelshtein, I.; Applerot, G.; Perkash, N.; Guibert, G.; Mikhailov, S.; Gedanken, A. Sonochemical coating of silver nanoparticles on textile fabrics (nylon, polyester and cotton) and their antibacterial activity. *Nanotechnology* **2008**, *19*, 245705.
183. Wollina, U.; Heide, M.; Müller-Litz, W.; Obenauf, D.; Ash, J. Functional textiles in prevention of chronic wounds, wound healing and tissue engineering. *Curr Probl Dermatol* **2003**, *31*, 82-97.
184. Koc, U.; Aykut, Y.; Eren, R. One-step preparation of woven fabric-reinforced hydrogel composite. *Journal of Industrial Textiles* **2019**, 1528083719850832.
185. Massella, D.; Ancona, A.; Garino, N.; Cauda, V.; Guan, J.; Salaun, F.; Barresi, A.; Ferri, A. Preparation of bio-functional textiles by surface functionalization of cellulose fabrics with caffeine loaded nanoparticles. In Proceedings of IOP Conference Series: Materials Science and Engineering; p. 012044.
186. Gadkari, R.R.; Ali, S.W.; Joshi, M.; Rajendran, S.; Das, A.; Alagirusamy, R. Leveraging antibacterial efficacy of silver loaded chitosan nanoparticles on layer-by-layer self-assembled coated cotton fabric. *International journal of biological macromolecules* **2020**, *162*, 548-560, doi:<https://doi.org/10.1016/j.ijbiomac.2020.06.137>.
187. El-Naggar, M.E.; Abdelgawad, A.M.; Elsherbiny, D.A.; El-shazly, W.A.; Ghazanfari, S.; Abdel-Aziz, M.S.; Abd-Elmoneam, Y.K. Bioactive Wound Dressing Gauze Loaded with Silver Nanoparticles Mediated by Acacia Gum. *Journal of Cluster Science* **2019**, 1-14.
188. Sun, X.-Z.; Wang, X.; Wu, J.-Z. Development of thermosensitive microgel-loaded cotton fabric for controlled drug release. *Applied Surface Science* **2017**, *403*, 509-518.
189. Mihailiasa, M.; Caldera, F.; Li, J.; Peila, R.; Ferri, A.; Trotta, F. Preparation of functionalized cotton fabrics by means of melatonin loaded β -cyclodextrin nanosponges. *Carbohydrate polymers* **2016**, *142*, 24-30.
190. Campbell, F.C. Chapter 2 - Fibers and Reinforcements: The String That Provides the Strength. In *Manufacturing*

- Processes for Advanced Composites*, Campbell, F.C., Ed. Elsevier Science: Amsterdam, 2004; <https://doi.org/10.1016/B978-185617415-2/50003-4>pp. 39-62.
191. Kocak, D.; Akalin, M.; Usta, I.; Merdan, N. New approach to produce absorbent pads for new end uses. In *Medical Textiles and Biomaterials for Healthcare*, Elsevier: 2006; pp. 320-326.
 192. Jedvert, K.; Idström, A.; Köhnke, T.; Alkhagen, M. Cellulosic nonwovens produced via efficient solution blowing technique. *Journal of Applied Polymer Science* **2020**, *137*, 48339, doi:10.1002/app.48339.
 193. Ajmeri, J.; Ajmeri, C.J. Nonwoven materials and technologies for medical applications. In *Handbook of Medical Textiles*, Elsevier: 2011; pp. 106-131.
 194. Tan, E.; Lim, C. Mechanical characterization of nanofibers—a review. *Composites Science and Technology* **2006**, *66*, 1102-1111.
 195. Wang, X.; Nakane, K. Preparation of polymeric nanofibers via immersion electrospinning. *European Polymer Journal* **2020**, *134*, 109837, doi:<https://doi.org/10.1016/j.eurpolymj.2020.109837>.
 196. Fitzgerald, W.; Knudsen, J. Mixed-stream spinning of bicomponent fibers1. *Textile Research Journal* **1967**, *37*, 447-453.
 197. Ma, P.X.; Zhang, R. Synthetic nano-scale fibrous extracellular matrix. *Journal of Biomedical Materials Research: An Official Journal of The Society for Biomaterials, The Japanese Society for Biomaterials, and The Australian Society for Biomaterials* **1999**, *46*, 60-72.
 198. Balogh, A.; Farkas, B.; Faragó, K.; Farkas, A.; Wagner, I.; Verreck, G.; Nagy, Z.K.; Marosi, G. Melt-blown and electrospun drug-loaded polymer fiber mats for dissolution enhancement: a comparative study. *Journal of Pharmaceutical Sciences* **2015**, *104*, 1767-1776.
 199. Medeiros, E.S.; Glenn, G.M.; Klamczynski, A.P.; Orts, W.J.; Mattoso, L.H. Solution blow spinning: A new method to produce micro- and nanofibers from polymer solutions. *Journal of applied polymer science* **2009**, *113*, 2322-2330.
 200. Bonan, R.F.; Bonan, P.R.; Batista, A.U.; Sampaio, F.C.; Albuquerque, A.J.; Moraes, M.C.; Mattoso, L.H.; Glenn, G.M.; Medeiros, E.S.; Oliveira, J.E. In vitro antimicrobial activity of solution blow spun poly (lactic acid)/polyvinylpyrrolidone nanofibers loaded with Copaiba (*Copaifera* sp.) oil. *Materials Science and Engineering: C* **2015**, *48*, 372-377.
 201. Ren, L.; Ozisik, R.; Kotha, S.P. Rapid and efficient fabrication of multilevel structured silica micro-/nanofibers by centrifugal jet spinning. *Journal of colloid and interface science* **2014**, *425*, 136-142.
 202. Zhang, X.; Lu, Y. Centrifugal spinning: an alternative approach to fabricate nanofibers at high speed and low cost. *Polymer Reviews* **2014**, *54*, 677-701.
 203. Stojanovska, E.; Kurtulus, M.; Abdelgawad, A.; Candan, Z.; Kilic, A. Developing lignin-based bio-nanofibers by centrifugal spinning technique. *International journal of biological macromolecules* **2018**, *113*, 98-105.
 204. Rampichová, M.; Lukášová, V.; Buzgo, M.; Vocetková, K.; Sovková, V.; Blahnová, V.; Amler, E.; Filová, E. Coaxial Nanofibrous Scaffold Prepared Using Centrifugal Spinning as a Drug Delivery System for Skeletal Tissue Engineering. In *Proceedings of Key Engineering Materials*; pp. 162-168.
 205. Persano, L.; Camposo, A.; Tekmen, C.; Pisignano, D. Industrial Upscaling of Electrospinning and Applications of Polymer Nanofibers: A Review. *Macromolecular Materials and Engineering* **2013**, *298*, 504-520, doi:<https://doi.org/10.1002/mame.201200290>.
 206. Li, Y.; Zou, C.; Shao, J.; Zhang, X.; Li, Y.n. Preparation of SiO₂/PS superhydrophobic fibers with bionic controllable micro–nano structure via centrifugal spinning. *RSC Advances* **2017**, *7*, 11041-11048, doi:10.1039/C6RA25813A.

207. Hou, T.; Li, X.; Lu, Y.; Yang, B. Highly porous fibers prepared by centrifugal spinning. *Materials & Design* **2017**, *114*, 303-311, doi:<https://doi.org/10.1016/j.matdes.2016.11.019>.
208. Tiwari, G.; Tiwari, R.; Sriwastawa, B.; Bhati, L.; Pandey, S.; Pandey, P.; Bannerjee, S.K. Drug delivery systems: An updated review. *International journal of pharmaceutical investigation* **2012**, *2*, 2-11, doi:10.4103/2230-973X.96920.
209. Banik, B.L.; Brown, J.L. Chapter 23 - Polymeric Biomaterials in Nanomedicine. In *Natural and Synthetic Biomedical Polymers*, Kumbar, S.G., Laurencin, C.T., Deng, M., Eds. Elsevier: Oxford, 2014; <https://doi.org/10.1016/B978-0-12-396983-5.00024-7>pp. 387-395.
210. Bolgen, N.; Vargel, I.; Korkusuz, P.; Menciloglu, Y.Z.; Piskin, E. In vivo performance of antibiotic embedded electrospun PCL membranes for prevention of abdominal adhesions. *J Biomed Mater Res B Appl Biomater* **2007**, *81*, 530-543, doi:10.1002/jbm.b.30694.
211. Kim, T.G.; Lee, D.S.; Park, T.G. Controlled protein release from electrospun biodegradable fiber mesh composed of poly(epsilon-caprolactone) and poly(ethylene oxide). *International journal of pharmaceutics* **2007**, *338*, 276-283, doi:10.1016/j.ijpharm.2007.01.040.
212. Yao, Y.; Wang, J.; Cui, Y.; Xu, R.; Wang, Z.; Zhang, J.; Wang, K.; Li, Y.; Zhao, Q.; Kong, D. Effect of sustained heparin release from PCL/chitosan hybrid small-diameter vascular grafts on anti-thrombogenic property and endothelialization. *Acta biomaterialia* **2014**, *10*, 2739-2749, doi:10.1016/j.actbio.2014.02.042.
213. Gao, C.; Gao, Q.; Li, Y.; Rahaman, M.N.; Teramoto, A.; Abe, K. Preparation and in vitro characterization of electrospun PVA scaffolds coated with bioactive glass for bone regeneration. *J. Biomed. Mater. Res., Part A* **2012**, *100A*, 1324-1334, doi:10.1002/jbm.a.34072.
214. Painuly, D.; Nisha, U.; Arya, S.; Sangeeth Krishnan, J.B. Effect on in-vitro release of individual and dual contraceptive drug loading from gelatin electrospun fibers. *Journal of Drug Delivery Science and Technology* **2019**, *51*, 454-463, doi:<https://doi.org/10.1016/j.jddst.2019.03.026>.
215. Nelson, G. Application of microencapsulation in textiles. *International journal of pharmaceutics* **2002**, *242*, 55-62.
216. Cheung, T.W.; Luo, X.; Li, L. Functional design of traditional hollow fibers: opening up a second life of being a medical drug delivery carrier. *Textile Research Journal* **2018**, *88*, 2425-2434, doi:10.1177/0040517517723023.
217. Liao, I.C.; Wan, A.C.A.; Yim, E.K.F.; Leong, K.W. Controlled release from fibers of polyelectrolyte complexes. *Journal of Controlled Release* **2005**, *104*, 347-358, doi:<https://doi.org/10.1016/j.jconrel.2005.02.013>.
218. Jaskari, T.; Vuorio, M.; Kontturi, K.; Manzanares, J.A.; Hirvonen, J. Ion-exchange fibers and drugs: an equilibrium study. *Journal of controlled release : official journal of the Controlled Release Society* **2001**, *70*, 219-229.
219. Yuan, J.; Gao, Y.; Liu, T.; Wang, X.; Liu, H.; Li, S. Dual drug load and release behavior on ion-exchange fiber: influencing factors and prediction method for precise control of the loading amount. *Pharmaceutical Development and Technology* **2015**, *20*, 755-761, doi:10.3109/10837450.2014.920356.
220. Haji, A.; Khajeh Mehrizi, M.; Akbarpour, R. Optimization of β -cyclodextrin grafting on wool fibers improved by plasma treatment and assessment of antibacterial activity of berberine finished fabric. *Journal of Inclusion Phenomena and Macrocyclic Chemistry* **2015**, *81*, 121-133, doi:10.1007/s10847-014-0440-4.
221. El Ghoul, Y.; Blanchemain, N.; Laurent, T.; Campagne, C.; El Achari, A.; Roudesli, S.; Morcellet, M.; Martel, B.; Hildebrand, H.F. Chemical, biological and microbiological evaluation of cyclodextrin finished polyamide inguinal meshes. *Acta biomaterialia* **2008**, *4*, 1392-1400, doi:10.1016/j.actbio.2008.02.019.
222. Yoo, H.S.; Kim, T.G.; Park, T.G. Surface-functionalized electrospun nanofibers for tissue engineering and drug

- delivery. *Advanced drug delivery reviews* **2009**, *61*, 1033-1042, doi:10.1016/j.addr.2009.07.007.
223. Zhu, X.; Chian, K.S.; Chan-Park, M.B.; Lee, S.T. Effect of argon-plasma treatment on proliferation of human-skin-derived fibroblast on chitosan membrane in vitro. *Journal of biomedical materials research. Part A* **2005**, *73*, 264-274, doi:10.1002/jbm.a.30211.
 224. van Laarhoven, J.A.H.; Kruft, M.A.B.; Vromans, H. Effect of supersaturation and crystallization phenomena on the release properties of a controlled release device based on EVA copolymer. *J. Controlled Release* **2002**, *82*, 309-317, doi:10.1016/S0168-3659(02)00139-6.
 225. Ma, Z.H.; Yu, D.G.; Branford-White, C.J.; Nie, H.L.; Fan, Z.X.; Zhu, L.M. Microencapsulation of tamoxifen: application to cotton fabric. *Colloids and surfaces. B, Biointerfaces* **2009**, *69*, 85-90, doi:10.1016/j.colsurfb.2008.11.005.
 226. Abidian, M.R.; Kim, D.-H.; Martin, D.C. Conducting-Polymer Nanotubes for Controlled Drug Release. *Advanced Materials* **2006**, *18*, 405-409, doi:10.1002/adma.200501726.
 227. Wang, Y.; Gao, Y.; Xu, G.; Liu, H.; Xiang, Y.; Cui, W. Accelerated fabrication of antibacterial and osteoinductive electrospun fibrous scaffolds via electrochemical deposition. *RSC Advances* **2018**, *8*, 9546-9554, doi:10.1039/C8RA01011K.
 228. Zafar, M.; Shah, T.; Rawal, A.; Siores, E. Preparation and characterisation of thermoresponsive nanogels for smart antibacterial fabrics. *Materials science & engineering. C, Materials for biological applications* **2014**, *40*, 135-141, doi:10.1016/j.msec.2014.03.033.
 229. Chen, D.; Singh, D.; Sirkar, K.K.; Pfeffer, R. Continuous Polymer Coating/Encapsulation of Submicrometer Particles Using a Solid Hollow Fiber Cooling Crystallization Method. *Industrial & Engineering Chemistry Research* **2014**, *53*, 6388-6400, doi:10.1021/ie403993c.
 230. Dubas, S.T.; Kumlangdudsana, P.; Potiyaraj, P. Layer-by-layer deposition of antimicrobial silver nanoparticles on textile fibers. *Colloids and Surfaces A: Physicochemical and Engineering Aspects* **2006**, *289*, 105-109, doi:https://doi.org/10.1016/j.colsurfa.2006.04.012.
 231. Klueh, U.; Wagner, V.; Kelly, S.; Johnson, A.; Bryers, J.D. Efficacy of silver-coated fabric to prevent bacterial colonization and subsequent device-based biofilm formation. *Journal of biomedical materials research* **2000**, *53*, 621-631.
 232. Zilberman, M. Novel composite fiber structures to provide drug/protein delivery for medical implants and tissue regeneration. *Acta biomaterialia* **2007**, *3*, 51-57, doi:10.1016/j.actbio.2006.06.008.
 233. Liu, L.; Jiang, L.; Xu, G.K.; Ma, C.; Yang, X.G.; Yao, J.M. Potential of alginate fibers incorporated with drug-loaded nanocapsules as drug delivery systems. *Journal of Materials Chemistry B* **2014**, *2*, 7596-7604, doi:10.1039/C4TB01392A.
 234. Hou, Q.; Walsh, M.C.; Freeman, R.; Barry, J.J.; Howdle, S.M.; Shakesheff, K.M. Incorporation of proteins within alginate fibre-based scaffolds using a post-fabrication entrapment method. *The Journal of pharmacy and pharmacology* **2006**, *58*, 895-902, doi:10.1211/jpp.58.7.0003.
 235. Yan, S.; Xiaoqiang, L.; Lianjiang, T.; Chen, H.; Xiumei, M. Poly (l-lactide-co-ε-caprolactone) electrospun nanofibers for encapsulating and sustained releasing proteins. *Polymer* **2009**, *50*, 4212-4219.
 236. Yu, D.; Shen, X.; Zhang, X.; Zhu, L.; Branford-White, C.; White, K. Applications of Polarization Microscope in Determining the Physical Status of API in the Wet-Spinning Drug-Loaded Fibers. In *Proceedings of 2009 Symposium on Photonics and Optoelectronics*, 14-16 Aug. 2009; pp. 1-4.
 237. Hwang, C.M.; Khademhosseini, A.; Park, Y.; Sun, K.; Lee, S.H. Microfluidic chip-based fabrication of PLGA microfiber scaffolds for tissue engineering. *Langmuir : the ACS journal of surfaces and colloids* **2008**, *24*,

- 6845-6851, doi:10.1021/la800253b.
238. Kumbar, S.G.; Nair, L.S.; Bhattacharyya, S.; Laurencin, C.T. Polymeric nanofibers as novel carriers for the delivery of therapeutic molecules. *Journal of nanoscience and nanotechnology* **2006**, *6*, 2591-2607.
239. Marimuthu, M.; Kim, S. Spontaneous extrusion of porous amphiphilic triblock copolymeric microfibers under microfluidic conditions. *Polymer Journal* **2010**, *42*, 100, doi:10.1038/pj.2009.301 <https://www.nature.com/articles/pj2009301#supplementary-information>.
240. Wu, H.-l.; Bremner, D.H.; Li, H.-y.; Shi, Q.-q.; Wu, J.-z.; Xiao, R.-q.; Zhu, L.-m. A novel multifunctional biomedical material based on polyacrylonitrile: Preparation and characterization. *Mater. Sci. Eng., C* **2016**, *62*, 702-709, doi:10.1016/j.msec.2016.02.026.
241. Zhu, X.; Chian, K.S.; Chan-Park, M.B.E.; Lee, S.T. Effect of argon-plasma treatment on proliferation of human-skin-derived fibroblast on chitosan membrane in vitro. *Journal of Biomedical Materials Research Part A: An Official Journal of The Society for Biomaterials, The Japanese Society for Biomaterials, and The Australian Society for Biomaterials and the Korean Society for Biomaterials* **2005**, *73*, 264-274.
242. Ma, Z.; He, W.; Yong, T.; Ramakrishna, S. Grafting of gelatin on electrospun poly (caprolactone) nanofibers to improve endothelial cell spreading and proliferation and to control cell orientation. *Tissue engineering* **2005**, *11*, 1149-1158.
243. Yao, C.; Li, X.; Neoh, K.G.; Shi, Z.; Kang, E.T. Surface modification and antibacterial activity of electrospun polyurethane fibrous membranes with quaternary ammonium moieties. *Journal of Membrane Science* **2008**, *320*, 259-267, doi:<https://doi.org/10.1016/j.memsci.2008.04.012>.
244. Perrotta, A.; Werzer, O.; Coclite, A.M. Strategies for Drug Encapsulation and Controlled Delivery Based on Vapor-Phase Deposited Thin Films. *Advanced Engineering Materials* **2017**, *20*, 1700639, doi:10.1002/adem.201700639.
245. Baek, H.S.; Park, Y.H.; Ki, C.S.; Park, J.-C.; Rah, D.K. Enhanced chondrogenic responses of articular chondrocytes onto porous silk fibroin scaffolds treated with microwave-induced argon plasma. *Surface and Coatings Technology* **2008**, *202*, 5794-5797, doi:<https://doi.org/10.1016/j.surfcoat.2008.06.154>.
246. Koh, H.S.; Yong, T.; Chan, C.K.; Ramakrishna, S. Enhancement of neurite outgrowth using nano-structured scaffolds coupled with laminin. *Biomaterials* **2008**, *29*, 3574-3582, doi:10.1016/j.biomaterials.2008.05.014.
247. Croll, T.I.; O'Connor, A.J.; Stevens, G.W.; Cooper-White, J.J. Controllable Surface Modification of Poly(lactic-co-glycolic acid) (PLGA) by Hydrolysis or Aminolysis I: Physical, Chemical, and Theoretical Aspects. *Biomacromolecules* **2004**, *5*, 463-473, doi:10.1021/bm0343040.
248. Zhu, Y.; Gao, C.; Liu, X.; Shen, J. Surface modification of polycaprolactone membrane via aminolysis and biomacromolecule immobilization for promoting cytocompatibility of human endothelial cells. *Biomacromolecules* **2002**, *3*, 1312-1319.
249. Sun, H.; Önnby, S. Facile polyester surface functionalization via hydrolysis and cell-recognizing peptide attachment. *Polymer International* **2006**, *55*, 1336-1340, doi:10.1002/pi.2090.
250. Kim, M.; Saito, K. Preparation of silver-ion-loaded nonwoven fabric by radiation-induced graft polymerization. *Reactive and Functional Polymers* **1999**, *40*, 275-279, doi:[https://doi.org/10.1016/S1381-5148\(98\)00050-9](https://doi.org/10.1016/S1381-5148(98)00050-9).
251. Park, K.; Ju, Y.M.; Son, J.S.; Ahn, K.D.; Han, D.K. Surface modification of biodegradable electrospun nanofiber scaffolds and their interaction with fibroblasts. *Journal of biomaterials science. Polymer edition* **2007**, *18*, 369-382, doi:10.1163/156856207780424997.
252. Sun, X.-Y.; Shankar, R.; Börner, H.G.; Ghosh, T.K.; Spontak, R.J. Field-Driven Biofunctionalization of Polymer Fiber Surfaces during Electrospinning. *Advanced Materials* **2007**, *19*, 87-91, doi:10.1002/adma.200601345.

253. Kurkov, S.V.; Loftsson, T.; Messner, M.; Madden, D. Parenteral delivery of HP β CD: effects on drug-HSA binding. *AAPS PharmSciTech* **2010**, *11*, 1152-1158, doi:10.1208/s12249-010-9482-0.
254. Denter, U.; Buschmann, H.-J.; Schollmeyer, E. Modifizierung von Faseroberflächen durch permanente Fixierung supramolekularer Komponenten, Teil 3: Azakronenether. *Die Angewandte Makromolekulare Chemie* **1998**, *258*, 75-81, doi:10.1002/(SICI)1522-9505(19980801)258:1<75::AID-APMC75>3.0.CO;2-1.
255. Murthy, C.N.; Geckeler, K.E. The water-soluble β -cyclodextrin-[60]fullerene complex. *Chemical Communications* **2001**, 10.1039/B102142G, 1194-1195, doi:10.1039/B102142G.
256. Davis, M.E.; Brewster, M.E. Cyclodextrin-based pharmaceuticals: past, present and future. *Nature reviews. Drug discovery* **2004**, *3*, 1023-1035, doi:10.1038/nrd1576.
257. Loftsson, T.; Brewster, M.E. Pharmaceutical applications of cyclodextrins. 1. Drug solubilization and stabilization. *Journal of Pharmaceutical Sciences* **1996**, *85*, 1017-1025, doi:doi:10.1021/js950534b.
258. Poukalis, K.; Buschmann, H.J.; Schollmeyer, E. 1992.
259. Buschmann, H.J.; Knittel, D.; Schollmeyer, E. New Textile Applications of Cyclodextrins. *Journal of inclusion phenomena and macrocyclic chemistry* **2001**, *40*, 169-172, doi:10.1023/A:1011892600388.
260. Yildiz, Z.I.; Celebioglu, A.; Kilic, M.E.; Durgun, E.; Uyar, T. Fast-dissolving carvacrol/cyclodextrin inclusion complex electrospun fibers with enhanced thermal stability, water solubility, and antioxidant activity. *Journal of Materials Science* **2018**, *53*, 15837-15849, doi:10.1007/s10853-018-2750-1.
261. Gao, Y.; Yuan, J.; Liu, H.; Yang, Y.; Hou, Y.; Li, S. Tramadol loading, release and iontophoretic characteristics of ion-exchange fiber. *Int. J. Pharm. (Amsterdam, Neth.)* **2014**, *465*, 102-111, doi:10.1016/j.ijpharm.2014.02.017.
262. Kankkunen, T.; Sulkava, R.; Vuorio, M.; Kontturi, K.; Hirvonen, J. Transdermal iontophoresis of tacrine in vivo. *Pharmaceutical research* **2002**, *19*, 704.
263. Kankkunen, T.; Huupponen, I.; Lahtinen, K.; Sundell, M.; Ekman, K.; Kontturi, K.; Hirvonen, J. Improved stability and release control of levodopa and metaraminol using ion-exchange fibers and transdermal iontophoresis. *European Journal of Pharmaceutical Sciences* **2002**, *16*, 273-280, doi:https://doi.org/10.1016/S0928-0987(02)00113-6.
264. Shen, Z.; Huvard, G.S.; Warriner, C.S.; Mc Hugh, M.; Banyasz, J.L.; Mishra, M.K. CO₂-assisted fiber impregnation. *Polymer* **2008**, *49*, 1579-1586, doi:https://doi.org/10.1016/j.polymer.2008.01.020.
265. Chimowitz, E.H.; Pennisi, K.J. Process synthesis concepts for supercritical gas extraction in the crossover region. *AIChE Journal* **1986**, *32*, 1665-1676, doi:10.1002/aic.690321010.
266. Kikic, I.; Vecchione, F. Supercritical impregnation of polymers. *Current Opinion in Solid State and Materials Science* **2003**, *7*, 399-405, doi:https://doi.org/10.1016/j.cossms.2003.09.001.
267. Ulker, Z.; Erkey, C. An advantageous technique to load drugs into aerogels: Gas antisolvent crystallization inside the pores. *The Journal of Supercritical Fluids* **2017**, *120*, 310-319, doi:https://doi.org/10.1016/j.supflu.2016.05.033.
268. Ma, S.-L.; Lu, Z.-W.; Wu, Y.-T.; Zhang, Z.-B. Partitioning of drug model compounds between poly(lactic acid)s and supercritical CO₂ using quartz crystal microbalance as an in situ detector. *The Journal of Supercritical Fluids* **2010**, *54*, 129-136, doi:https://doi.org/10.1016/j.supflu.2010.04.013.
269. Kazarian, S.G.; Vincent, M.F.; Bright, F.V.; Liotta, C.L.; Eckert, C.A. Specific Intermolecular Interaction of Carbon Dioxide with Polymers. *Journal of the American Chemical Society* **1996**, *118*, 1729-1736, doi:10.1021/ja950416q.
270. Tabernero, A.; Martín del Valle, E.M.; Galán, M.A. Supercritical fluids for pharmaceutical particle engineering:

- Methods, basic fundamentals and modelling. *Chemical Engineering and Processing: Process Intensification* **2012**, *60*, 9-25, doi:https://doi.org/10.1016/j.cep.2012.06.004.
271. Champeau, M.; Thomassin, J.M.; Jérôme, C.; Tassaing, T. In situ FTIR micro-spectroscopy to investigate polymeric fibers under supercritical carbon dioxide: CO₂ sorption and swelling measurements. *The Journal of Supercritical Fluids* **2014**, *90*, 44-52, doi:https://doi.org/10.1016/j.supflu.2014.03.006.
272. Duarte, A.R.C.; Mano, J.F.; Reis, R.L. Dexamethasone-loaded scaffolds prepared by supercritical-assisted phase inversion. *Acta biomaterialia* **2009**, *5*, 2054-2062, doi:https://doi.org/10.1016/j.actbio.2009.01.047.
273. Dias, A.M.A.; Rey-Rico, A.; Oliveira, R.A.; Marceneiro, S.; Alvarez-Lorenzo, C.; Concheiro, A.; Júnior, R.N.C.; Braga, M.E.M.; de Sousa, H.C. Wound dressings loaded with an anti-inflammatory jucá (*Libidibia ferrea*) extract using supercritical carbon dioxide technology. *The Journal of Supercritical Fluids* **2013**, *74*, 34-45, doi:https://doi.org/10.1016/j.supflu.2012.12.007.
274. Geiger, B.C.; Nelson, M.T.; Munj, H.R.; Tomasko, D.L.; Lannutti, J.J. Dual drug release from CO₂-infused nanofibers via hydrophobic and hydrophilic interactions. *Journal of Applied Polymer Science* **2015**, *132*, doi:10.1002/app.42571.
275. Tao, W.; Collier, B.J. The Environmental Scanning Electron Microscope: A New Tool for Textile Studies. *Textile Chemist & Colorist* **1994**, *26*.
276. Ueland, M.; Howes, J.M.; Forbes, S.L.; Stuart, B.H. Degradation patterns of natural and synthetic textiles on a soil surface during summer and winter seasons studied using ATR-FTIR spectroscopy. *Spectrochimica Acta Part A: Molecular and Biomolecular Spectroscopy* **2017**, *185*, 69-76.
277. Zambrano, M.C.; Pawlak, J.J.; Daystar, J.; Ankeny, M.; Venditti, R.A. Impact of dyes and finishes on the aquatic biodegradability of cotton textile fibers and microfibers released on laundering clothes: Correlations between enzyme adsorption and activity and biodegradation rates. *Marine Pollution Bulletin* **2021**, *165*, 112030, doi:https://doi.org/10.1016/j.marpolbul.2021.112030.
278. Kumbar, S.G.; Nukavarapu, S.P.; James, R.; Nair, L.S.; Laurencin, C.T. Electrospun poly (lactic acid-co-glycolic acid) scaffolds for skin tissue engineering. *Biomaterials* **2008**, *29*, 4100-4107.
279. Uekama, K.; Hirayama, E.; Irie, T. Cyclodextrin Drug Carrier Systems. *Chemical Reviews* **1998**, *98*, 2045-2076, doi:10.1021/cr970025p.
280. Puppi, D.; Piras, A.M.; Piroso, A.; Sandreschi, S.; Chiellini, F. Levofloxacin-loaded star poly(epsilon-caprolactone) scaffolds by additive manufacturing. *Journal of materials science. Materials in medicine* **2016**, *27*, 44, doi:10.1007/s10856-015-5658-1.
281. Puppi, D.; Dinucci, D.; Bartoli, C.; Mota, C.; Migone, C.; Dini, F.; Barsotti, G.; Carlucci, F.; Chiellini, F. Development of 3D wet-spun polymeric scaffolds loaded with antimicrobial agents for bone engineering. *Journal of Bioactive and Compatible Polymers* **2011**, *26*, 478-492, doi:10.1177/0883911511415918.
282. He, C.-L.; Huang, Z.-M.; Han, X.-J. Fabrication of drug-loaded electrospun aligned fibrous threads for suture applications. *Journal of Biomedical Materials Research Part A* **2009**, *89A*, 80-95, doi:10.1002/jbm.a.32004.
283. Johnson, P.M.; Knewton, K.E.; Hodge, J.G.; Lehtinen, J.M.; Trofimoff, A.S.; Fritz, D.J.; Robinson, J.L. Surfactant location and internal phase volume fraction dictate emulsion electrospun fiber morphology and modulate drug release and cell response. *Biomaterials Science* **2021**, *9*, 1397-1408, doi:10.1039/D0BM01751E.
284. Goddard III, W.A.; Brenner, D.; Lyshevski, S.E.; Iafrate, G.J. *Handbook of nanoscience, engineering, and technology*; CRC press: 2012.
285. Kumar, N.; Ravikumar, M.N.; Domb, A.J. Biodegradable block copolymers. *Advanced drug delivery reviews*

- 2001, 53, 23-44.
286. Zhao, X.; Yuan, Z.; Yildirimer, L.; Zhao, J.; Lin, Z.Y.; Cao, Z.; Pan, G.; Cui, W. Tumor-Triggered Controlled Drug Release from Electrospun Fibers Using Inorganic Caps for Inhibiting Cancer Relapse. *Small* **2015**, *11*, 4284-4291, doi:10.1002/smll.201500985.
 287. Agnes, E.; Ortega, G.G. Mathematical models and physicochemical of diffusion. *Pharmacy Book* **2003**, *19*, 9-19.
 288. Möckel, J.E.; Lippold, B.C. Zero-Order Drug Release from Hydrocolloid Matrices. *Pharmaceutical Research* **1993**, *10*, 1066-1070, doi:10.1023/A:1018931210396.
 289. Hsieh, D.S.T.; Rhine, W.D.; Langer, R. Zero-Order Controlled-Release Polymer Matrices for Micro- and Macromolecules. *Journal of Pharmaceutical Sciences* **1983**, *72*, 17-22, doi:https://doi.org/10.1002/jps.2600720105.
 290. Ahadi, F.; Khorshidi, S.; Karkhaneh, A. A hydrogel/fiber scaffold based on silk fibroin/oxidized pectin with sustainable release of vancomycin hydrochloride. *European Polymer Journal* **2019**, *118*, 265-274, doi:https://doi.org/10.1016/j.eurpolymj.2019.06.001.
 291. Mulye, N.V.; Turco, S.J. A Simple Model Based on First Order Kinetics to Explain Release of Highly Water Soluble Drugs from Porous Dicalcium Phosphate Dihydrate Matrices. *Drug Development and Industrial Pharmacy* **1995**, *21*, 943-953, doi:10.3109/03639049509026658.
 292. Higuchi, T. Rate of Release of Medicaments from Ointment Bases Containing Drugs in Suspension. *Journal of Pharmaceutical Sciences* **1961**, *50*, 874-875, doi:https://doi.org/10.1002/jps.2600501018.
 293. Abdekhodaie, M.J.; Cheng, Y.L. Diffusional release of a dispersed solute from planar and spherical matrices into finite external volume. *Journal of Controlled Release* **1997**, *43*, 175-182, doi:https://doi.org/10.1016/S0168-3659(96)01482-4.
 294. Pisani, S.; Dorati, R.; Chiesa, E.; Genta, I.; Modena, T.; Bruni, G.; Grisoli, P.; Conti, B. Release Profile of Gentamicin Sulfate from Polylactide-co-Polycaprolactone Electrospun Nanofiber Matrices. *Pharmaceutics* **2019**, *11*, 161, doi:10.3390/pharmaceutics11040161.
 295. Hixson, A.W.; Crowell, J.H. Dependence of Reaction Velocity upon surface and Agitation. *Industrial & Engineering Chemistry* **1931**, *23*, 923-931, doi:10.1021/ie50260a018.
 296. Wang, H.; Hao, L.; Wang, P.; Chen, M.; Jiang, S.; Jiang, S. Release kinetics and antibacterial activity of curcumin loaded zein fibers. *Food Hydrocolloids* **2017**, *63*, 437-446, doi:https://doi.org/10.1016/j.foodhyd.2016.09.028.
 297. Korsmeyer, R.W.; Gurny, R.; Doelker, E.; Buri, P.; Peppas, N.A. Mechanisms of solute release from porous hydrophilic polymers. *International journal of pharmaceutics* **1983**, *15*, 25-35, doi:https://doi.org/10.1016/0378-5173(83)90064-9.
 298. Ritger, P.L.; Peppas, N.A. A simple equation for description of solute release I. Fickian and non-fickian release from non-swelling devices in the form of slabs, spheres, cylinders or discs. *Journal of Controlled Release* **1987**, *5*, 23-36, doi:https://doi.org/10.1016/0168-3659(87)90034-4.
 299. Siepmann, J.; Peppas, N.A. Modeling of drug release from delivery systems based on hydroxypropyl methylcellulose (HPMC). *Advanced drug delivery reviews* **2001**, *48*, 139-157, doi:https://doi.org/10.1016/S0169-409X(01)00112-0.
 300. Martí, M.; Martínez, V.; Lis, M.J.; Coderch, L. Mathematical models for drug delivery from textile. *Journal of Industrial Textiles* **0**, 1528083719858769, doi:10.1177/1528083719858769.
 301. Adepu, S.; Gaydhane, M.K.; Kakunuri, M.; Sharma, C.S.; Khandelwal, M.; Eichhorn, S.J. Effect of

- micropatterning induced surface hydrophobicity on drug release from electrospun cellulose acetate nanofibers. *Applied Surface Science* **2017**, 426, 755-762, doi:<https://doi.org/10.1016/j.apsusc.2017.07.197>.
302. Peppas, N.A.; Sahlin, J.J. A simple equation for the description of solute release. III. Coupling of diffusion and relaxation. *International journal of pharmaceutics* **1989**, 57, 169-172, doi:[https://doi.org/10.1016/0378-5173\(89\)90306-2](https://doi.org/10.1016/0378-5173(89)90306-2).
 303. da Silva, T.N.; Gonçalves, R.P.; Rocha, C.L.; Archanjo, B.S.; Barboza, C.A.G.; Pierre, M.B.R.; Reynaud, F.; de Souza Picciani, P.H. Controlling burst effect with PLA/PVA coaxial electrospun scaffolds loaded with BMP-2 for bone guided regeneration. *Materials Science and Engineering: C* **2019**, 97, 602-612, doi:<https://doi.org/10.1016/j.msec.2018.12.020>.
 304. Hopfenberg, H.B. Controlled Release from Erodible Slabs, Cylinders, and Spheres. In *Controlled Release Polymeric Formulations*, AMERICAN CHEMICAL SOCIETY: 1976; Vol. 33, pp. 26-32.
 305. Gallagher, K.M.; Corrigan, O.I. Mechanistic aspects of the release of levamisole hydrochloride from biodegradable polymers. *Journal of Controlled Release* **2000**, 69, 261-272, doi:[https://doi.org/10.1016/S0168-3659\(00\)00305-9](https://doi.org/10.1016/S0168-3659(00)00305-9).
 306. Papadopoulou, V.; Kosmidis, K.; Vlachou, M.; Macheras, P. On the use of the Weibull function for the discernment of drug release mechanisms. *International journal of pharmaceutics* **2006**, 309, 44-50, doi:<https://doi.org/10.1016/j.ijpharm.2005.10.044>.
 307. Bacakova, L.; Zikmundova, M.; Pajorova, J.; Broz, A.; Filova, E.; Blanquer, A.; Matejka, R.; Stepanovska, J.; Mikes, P.; Jencova, V. Nanofibrous Scaffolds for Skin Tissue Engineering and Wound Healing Based on Synthetic Polymers. In *Applications of Nanobiotechnology*, IntechOpen: 2019.
 308. Kim, J.I.; Pant, H.R.; Sim, H.-J.; Lee, K.M.; Kim, C.S. Electrospun propolis/polyurethane composite nanofibers for biomedical applications. *Materials Science and Engineering: C* **2014**, 44, 52-57, doi:<https://doi.org/10.1016/j.msec.2014.07.062>.
 309. Yu, K.; Zhu, T.; Wu, Y.; Zhou, X.; Yang, X.; Wang, J.; Fang, J.; El-Hamshary, H.; Al-Deyab, S.S.; Mo, X. Incorporation of amoxicillin-loaded organic montmorillonite into poly(ester-urethane) urea nanofibers as a functional tissue engineering scaffold. *Colloids and Surfaces B: Biointerfaces* **2017**, 151, 314-323, doi:<https://doi.org/10.1016/j.colsurfb.2016.12.034>.
 310. America, I.D.S.o. Combating antimicrobial resistance: policy recommendations to save lives. *Clinical Infectious Diseases* **2011**, 52, S397-S428.
 311. Abdelgawad, A.M.; Hudson, S.M.; Rojas, O.J. Antimicrobial wound dressing nanofiber mats from multicomponent (chitosan/silver-NPs/polyvinyl alcohol) systems. *Carbohydrate polymers* **2014**, 100, 166-178.
 312. Abdelgawad, A.M.; El-Naggar, M.E.; Hudson, S.M.; Rojas, O.J. Fabrication and characterization of bactericidal thiol-chitosan and chitosan iodoacetamide nanofibres. *International journal of biological macromolecules* **2017**, 94, 96-105.
 313. Bode, C.; Muenster, S.; Diedrich, B.; Jahnert, S.; Weisheit, C.; Steinhagen, F.; Boehm, O.; Hoeft, A.; Meyer, R.; Baumgarten, G. Linezolid, vancomycin and daptomycin modulate cytokine production, Toll-like receptors and phagocytosis in a human in vitro model of sepsis. *The Journal of antibiotics* **2015**, 68, 485-490.
 314. Dhand, C.; Venkatesh, M.; Barathi, V.A.; Harini, S.; Bairagi, S.; Goh Tze Leng, E.; Muruganandham, N.; Low, K.Z.W.; Fazil, M.H.U.T.; Loh, X.J., et al. Bio-inspired crosslinking and matrix-drug interactions for advanced wound dressings with long-term antimicrobial activity. *Biomaterials* **2017**, 138, 153-168, doi:<https://doi.org/10.1016/j.biomaterials.2017.05.043>.
 315. Lowe, A.; Deng, W.; Smith, D.W.; Balkus, K.J. Acrylonitrile-Based Nitric Oxide Releasing Melt-Spun Fibers for

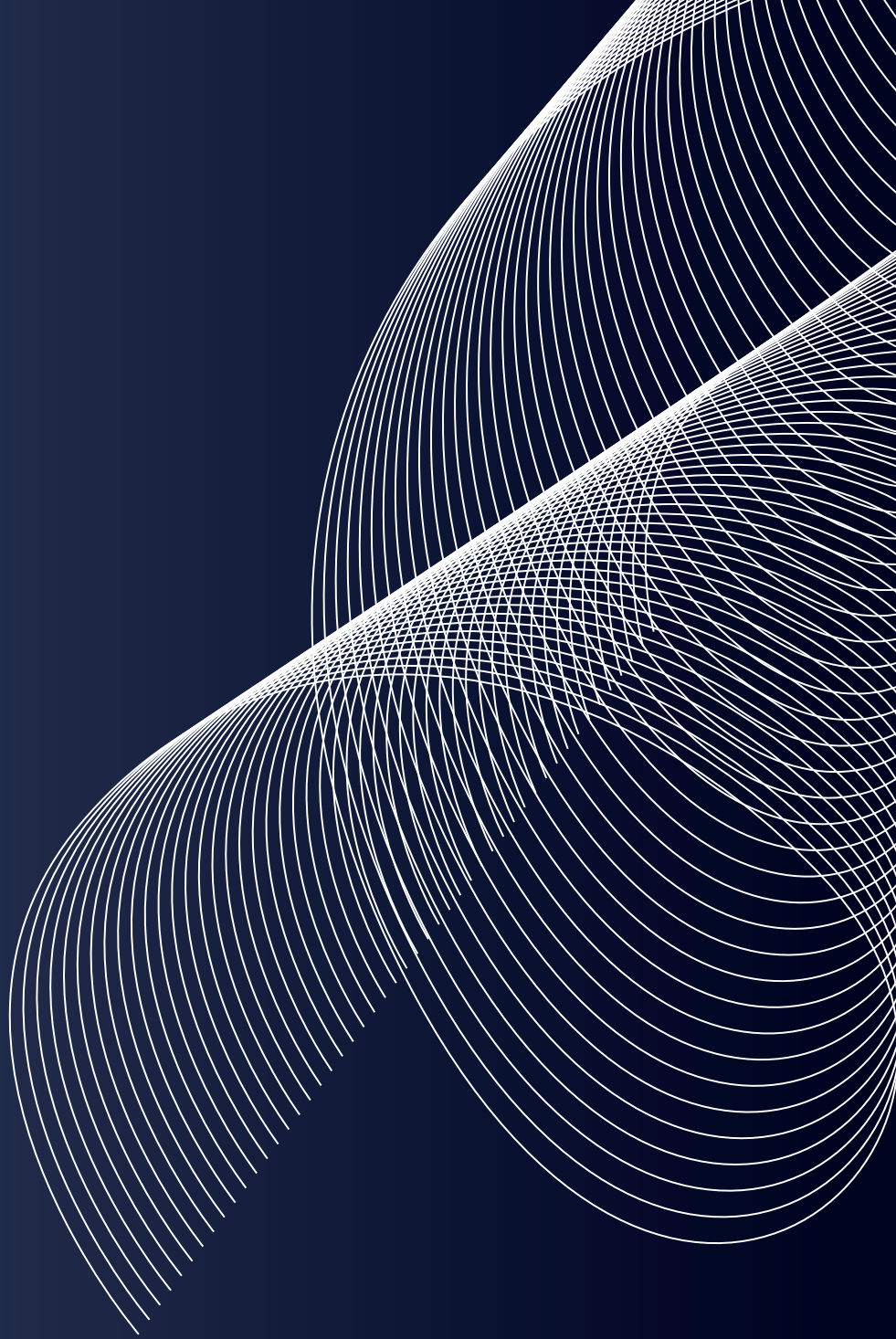
- Enhanced Wound Healing. *Macromolecules* **2012**, *45*, 5894-5900, doi:10.1021/ma300913w.
316. Coenen, A.M.J.; Bernaerts, K.V.; Harings, J.A.W.; Jockenhoevel, S.; Ghazanfari, S. Elastic materials for tissue engineering applications: Natural, synthetic, and hybrid polymers. *Acta biomaterialia* **2018**, *79*, 60-82, doi:https://doi.org/10.1016/j.actbio.2018.08.027.
 317. Ghazanfari, S.; Alberti, K.A.; Xu, Q.; Khademhosseini, A. Evaluation of an elastic decellularized tendon-derived scaffold for the vascular tissue engineering application. *Journal of Biomedical Materials Research Part A* **2019**, *107*, 1225-1234, doi:10.1002/jbm.a.36622.
 318. Puppi, D.; Zhang, X.; Yang, L.; Chiellini, F.; Sun, X.; Chiellini, E. Nano/microfibrous polymeric constructs loaded with bioactive agents and designed for tissue engineering applications: A review. *Journal of Biomedical Materials Research Part B: Applied Biomaterials* **2014**, *102*, 1562-1579, doi:10.1002/jbm.b.33144.
 319. Porter, J.R.; Ruckh, T.T.; Popat, K.C. Bone tissue engineering: A review in bone biomimetics and drug delivery strategies. *Biotechnology Progress* **2009**, *25*, 1539-1560, doi:10.1002/btpr.246.
 320. In Vivo Collagen Remodeling in the Vascular Wall of Decellularized Stented Tissue-Engineered Heart Valves. *Tissue Engineering Part A* **2015**, *21*, 2206-2215, doi:10.1089/ten.tea.2014.0417.
 321. Ghazanfari, S.; Driessen-Mol, A.; Hoerstrup, S.P.; Baaijens, F.P.T.; Bouten, C.V.C. Collagen Matrix Remodeling in Stented Pulmonary Arteries after Transapical Heart Valve Replacement. *Cells Tissues Organs* **2016**, *201*, 159-169, doi:10.1159/000442521.
 322. Kumbar, S.G.; Nukavarapu, S.P.; James, R.; Nair, L.S.; Laurencin, C.T. Electrospun poly(lactic acid-co-glycolic acid) scaffolds for skin tissue engineering. *Biomaterials* **2008**, *29*, 4100-4107, doi:https://doi.org/10.1016/j.biomaterials.2008.06.028.
 323. Ghazanfari, S.; Driessen-Mol, A.; Strijkers, G.J.; Baaijens, F.P.T.; Bouten, C.V.C. The Evolution of Collagen Fiber Orientation in Engineered Cardiovascular Tissues Visualized by Diffusion Tensor Imaging. *PLOS ONE* **2015**, *10*, e0127847, doi:10.1371/journal.pone.0127847.
 324. Ghazanfari, S.; Khademhosseini, A.; Smit, T.H. Mechanisms of lamellar collagen formation in connective tissues. *Biomaterials* **2016**, *97*, 74-84, doi:https://doi.org/10.1016/j.biomaterials.2016.04.028.
 325. Nie, H.; Soh, B.W.; Fu, Y.C.; Wang, C.H. Three-dimensional fibrous PLGA/HAp composite scaffold for BMP-2 delivery. *Biotechnology and bioengineering* **2008**, *99*, 223-234, doi:10.1002/bit.21517.
 326. Li, C.; Vepari, C.; Jin, H.J.; Kim, H.J.; Kaplan, D.L. Electrospun silk-BMP-2 scaffolds for bone tissue engineering. *Biomaterials* **2006**, *27*, 3115-3124, doi:10.1016/j.biomaterials.2006.01.022.
 327. Bide, M.; Phaneuf, M.; Logerfo, F.; Quist, W.; Szycher, M. Arterial Grafts as Biomedical Textiles. 2001; Vol. 792, pp. 125-154.
 328. Nam, J.; Huang, Y.; Agarwal, S.; Lannutti, J. Improved cellular infiltration in electrospun fiber via engineered porosity. *Tissue engineering* **2007**, *13*, 2249-2257, doi:10.1089/ten.2006.0306.
 329. Ifkovits, J.L.; Wu, K.; Mauck, R.L.; Burdick, J.A. The influence of fibrous elastomer structure and porosity on matrix organization. *PLoS One* **2010**, *5*, e15717, doi:10.1371/journal.pone.0015717.
 330. Ucar, S.; Yilgor, P.; Hasirci, V.; Hasirci, N. Chitosan-based wet-spun scaffolds for bioactive agent delivery. *Journal of Applied Polymer Science* **2013**, *130*, 3759-3769, doi:10.1002/app.39629.
 331. Yilgor, P.; Tuzlakoglu, K.; Reis, R.L.; Hasirci, N.; Hasirci, V. Incorporation of a sequential BMP-2/BMP-7 delivery system into chitosan-based scaffolds for bone tissue engineering. *Biomaterials* **2009**, *30*, 3551-3559, doi:https://doi.org/10.1016/j.biomaterials.2009.03.024.
 332. Tuzlakoglu, K.; Pashkuleva, I.; Rodrigues, M.T.; Gomes, M.E.; van Lenthe, G.H.; Müller, R.; Reis, R.L. A new route to produce starch-based fiber mesh scaffolds by wet spinning and subsequent surface modification

- as a way to improve cell attachment and proliferation. *Journal of Biomedical Materials Research Part A* **2010**, 92A, 369-377, doi:10.1002/jbm.a.32358.
333. Gao, H.; Gu, Y.; Ping, Q. The implantable 5-fluorouracil-loaded poly(l-lactic acid) fibers prepared by wet-spinning from suspension. *Journal of Controlled Release* **2007**, 118, 325-332, doi:https://doi.org/10.1016/j.jconrel.2006.12.028.
334. Puppi, D.; Piras, A.M.; Chiellini, F.; Chiellini, E.; Martins, A.; Leonor, I.B.; Neves, N.; Reis, R. Optimized electro- and wet-spinning techniques for the production of polymeric fibrous scaffolds loaded with bisphosphonate and hydroxyapatite. *Journal of Tissue Engineering and Regenerative Medicine* **2011**, 5, 253-263, doi:10.1002/term.310.
335. Feng, J.; Zhang, D.; Zhu, M.; Gao, C. Poly(l-lactide) melt spun fiber-aligned scaffolds coated with collagen or chitosan for guiding the directional migration of osteoblasts in vitro. *Journal of Materials Chemistry B* **2017**, 5, 5176-5188, doi:10.1039/C7TB00601B.
336. He, L.; Liao, S.; Quan, D.; Ma, K.; Chan, C.; Ramakrishna, S.; Lu, J. Synergistic effects of electrospun PLLA fiber dimension and pattern on neonatal mouse cerebellum C17.2 stem cells. *Acta biomaterialia* **2010**, 6, 2960-2969, doi:10.1016/j.actbio.2010.02.039.
337. Ingavle, G.C.; Leach, J.K. Advancements in electrospinning of polymeric nanofibrous scaffolds for tissue engineering. *Tissue engineering. Part B, Reviews* **2014**, 20, 277-293, doi:10.1089/ten.TEB.2013.0276.
338. Detta, N.; Puppi, D.; Errico, C.; Federica, C.; Piras, A.; Chiellini, E. Polymeric Nanofibre Constructs in Drug Delivery and Tissue Engineering. 2010; pp. 271-291.
339. Zhang, Y.; Lim, C.T.; Ramakrishna, S.; Huang, Z.M. Recent development of polymer nanofibers for biomedical and biotechnological applications. *Journal of materials science. Materials in medicine* **2005**, 16, 933-946, doi:10.1007/s10856-005-4428-x.
340. Prausnitz, M.R.; Langer, R. Transdermal drug delivery. *Nature biotechnology* **2008**, 26, 1261-1268, doi:10.1038/nbt.1504.
341. Wiedersberg, S.; Guy, R.H. Transdermal drug delivery: 30+ years of war and still fighting! *Journal of Controlled Release* **2014**, 190, 150-156, doi:https://doi.org/10.1016/j.jconrel.2014.05.022.
342. Lee, H.; Song, C.; Baik, S.; Kim, D.; Hyeon, T.; Kim, D.H. Device-assisted transdermal drug delivery. *Advanced drug delivery reviews* **2018**, 127, 35-45, doi:10.1016/j.addr.2017.08.009.
343. Schoellhammer, C.M.; Blankschtein, D.; Langer, R. Skin permeabilization for transdermal drug delivery: recent advances and future prospects. *Expert Opin Drug Deliv* **2014**, 11, 393-407, doi:10.1517/17425247.2014.875528.
344. Rahmani, M.; Arbabi Bidgoli, S.; Rezayat, S.M. Electrospun polymeric nanofibers for transdermal drug delivery. *Nanomedicine Journal* **2017**, 4, 61-70, doi:10.22038/nmj.2017.8407.
345. Sawicka, K.M.; Fu, A.; Simon, S.R. Composite nanofibrous membrane of immunoreactive H5-hemagglutinin as a transdermal bird flu vaccine. 2009/04/01; pp. 1-2.
346. Mofidfar, M.; Prausnitz, M.R. Electrospun Transdermal Patch for Contraceptive Hormone Delivery. *Current Drug Delivery* **2019**, 16, 577-583, doi:10.2174/1567201816666190308112010.
347. Liao, I.C.; Leong, K.W. Efficacy of engineered FVIII-producing skeletal muscle enhanced by growth factor-releasing co-axial electrospun fibers. *Biomaterials* **2011**, 32, 1669-1677, doi:https://doi.org/10.1016/j.biomaterials.2010.10.049.
348. Taepaiboon, P.; Rungsardthong, U.; Supaphol, P. Vitamin-loaded electrospun cellulose acetate nanofiber mats as transdermal and dermal therapeutic agents of vitamin A acid and vitamin E. *European journal of*

pharmaceutics and biopharmaceutics : official journal of Arbeitsgemeinschaft fur Pharmazeutische Verfahrenstechnik e.V **2007**, 67, 387-397, doi:10.1016/j.ejpb.2007.03.018.

349. Tungprapa, S.; Jangchud, I.; Supaphol, P. Release characteristics of four model drugs from drug-loaded electrospun cellulose acetate fiber mats. *Polymer* **2007**, 48, 5030-5041, doi:https://doi.org/10.1016/j.polymer.2007.06.061.
350. Chen, L.; Bromberg, L.; Hatton, T.A.; Rutledge, G.C. Electrospun cellulose acetate fibers containing chlorhexidine as a bactericide. *Polymer* **2008**, 49, 1266-1275, doi:https://doi.org/10.1016/j.polymer.2008.01.003.
351. Castillo-Ortega, M.M.; Nájera-Luna, A.; Rodríguez-Félix, D.E.; Encinas, J.C.; Rodríguez-Félix, F.; Romero, J.; Herrera-Franco, R.J. Preparation, characterization and release of amoxicillin from cellulose acetate and poly(vinyl pyrrolidone) coaxial electrospun fibrous membranes. *Materials Science and Engineering: C* **2011**, 31, 1772-1778, doi:https://doi.org/10.1016/j.msec.2011.08.009.
352. Kenawy el, R.; Bowlin, G.L.; Mansfield, K.; Layman, J.; Simpson, D.G.; Sanders, E.H.; Wnek, G.E. Release of tetracycline hydrochloride from electrospun poly(ethylene-co-vinylacetate), poly(lactic acid), and a blend. *Journal of controlled release : official journal of the Controlled Release Society* **2002**, 81, 57-64, doi:10.1016/s0168-3659(02)00041-x.
353. Meinel, A.J.; Germershaus, O.; Luhmann, T.; Merkle, H.P.; Meinel, L. Electrospun matrices for localized drug delivery: Current technologies and selected biomedical applications. *European Journal of Pharmaceutics and Biopharmaceutics* **2012**, 81, 1-13, doi:https://doi.org/10.1016/j.ejpb.2012.01.016.
354. Sun, X.; Zhang, L.; Cao, Z.; Deng, Y.; Liu, L.; Fong, H.; Sun, Y. Electrospun composite nanofiber fabrics containing uniformly dispersed antimicrobial agents as an innovative type of polymeric materials with superior antimicrobial efficacy. *ACS Appl Mater Interfaces* **2010**, 2, 952-956, doi:10.1021/am100018k.
355. Liu, Y.; Nguyen, A.; Allen, A.; Zoldan, J.; Huang, Y.; Chen, J.Y. Regenerated cellulose micro-nano fiber matrices for transdermal drug release. *Materials Science and Engineering: C* **2017**, 74, 485-492, doi:https://doi.org/10.1016/j.msec.2016.12.048.
356. Ariamoghaddam, A.R.; Ebrahimi-Hosseinizadeh, B.; Hatamian-Zarmi, A.; Sahraeian, R. In vivo anti-obesity efficacy of curcumin loaded nanofibers transdermal patches in high-fat diet induced obese rats. *Materials Science and Engineering: C* **2018**, 92, 161-171, doi:https://doi.org/10.1016/j.msec.2018.06.030.
357. Huang, Y.; Zhong, Z.; Duan, B.; Zhang, L.; Yang, Z.; Wang, Y.; Ye, Q. Novel fibers fabricated directly from chitin solution and their application as wound dressing. *Journal of Materials Chemistry B* **2014**, 2, 3427-3432, doi:10.1039/C4TB00098F.
358. Shekh, M.I.; Amirian, J.; Stadler, E.J.; Du, B.; Zhu, Y. Oxidized chitosan modified electrospun scaffolds for controllable release of acyclovir. *International journal of biological macromolecules* **2020**, 151, 787-796, doi:https://doi.org/10.1016/j.ijbiomac.2020.02.230.
359. Huang, L.; Zhang, Z.; Guo, M.; Pan, C.; Huang, Z.; Jin, J.; Li, Y.; Hou, X.; Li, W. Biomimetic Hydrogels Loaded with Nanofibers Mediate Sustained Release of pDNA and Promote In Situ Bone Regeneration. *Macromolecular bioscience n/a*, 2000393, doi:https://doi.org/10.1002/mabi.202000393.
360. Madhaiyan, K.; Sridhar, R.; Sundarajan, S.; Venugopal, J.R.; Ramakrishna, S. Vitamin B12 loaded polycaprolactone nanofibers: A novel transdermal route for the water soluble energy supplement delivery. *International journal of pharmaceutics* **2013**, 444, 70-76, doi:https://doi.org/10.1016/j.ijpharm.2013.01.040.
361. Song, J.; Fan, X.; Shen, Q. Daidzein-loaded nanostructured lipid carriers-PLGA nanofibers for transdermal delivery. *International journal of pharmaceutics* **2016**, 501, 245-252, doi:https://doi.org/10.1016/j.

- ijpharm.2016.02.003.
362. Mehnath, S.; Chitra, K.; Karthikeyan, K.; Jeyaraj, M. Localized delivery of active targeting micelles from nanofibers patch for effective breast cancer therapy. *International journal of pharmaceutics* **2020**, *584*, 119412, doi:<https://doi.org/10.1016/j.ijpharm.2020.119412>.
363. Gupta, B.S. 1 - Manufacture, types and properties of biotextiles for medical applications. In *Biotextiles as Medical Implants*, King, M.W., Gupta, B.S., Guidoin, R., Eds. Woodhead Publishing: 2013; <https://doi.org/10.1533/9780857095602.1.3pp>. 3-47.
364. Sharifi, F.; Sooriyarachchi, A.C.; Altural, H.; Montazami, R.; Rylander, M.N.; Hashemi, N. Fiber Based Approaches as Medicine Delivery Systems. *ACS Biomaterials Science & Engineering* **2016**, *2*, 1411-1431, doi:10.1021/acsbiomaterials.6b00281.
365. Mostafalu, P.; Kiaee, G.; Giatsidis, G.; Khalilpour, A.; Nabavinia, M.; Dokmeci, M.R.; Sonkusale, S.; Orgill, D.P.; Tamayol, A.; Khademhosseini, A. A Textile Dressing for Temporal and Dosage Controlled Drug Delivery. *Advanced Functional Materials* **2017**, *27*, 1702399, doi:10.1002/adfm.201702399.
366. Mostafalu, P.; Akbari, M.; Alberti, K.A.; Xu, Q.; Khademhosseini, A.; Sonkusale, S.R. A toolkit of thread-based microfluidics, sensors, and electronics for 3D tissue embedding for medical diagnostics. *Microsystems & Nanoengineering* **2016**, *2*, 16039.
367. Huang, C.; Soenen, S.J.; van Gulck, E.; Vanham, G.; Rejman, J.; Van Calenbergh, S.; Vervae, C.; Coenye, T.; Verstraelen, H.; Temmerman, M., et al. Electrospun cellulose acetate phthalate fibers for semen induced anti-HIV vaginal drug delivery. *Biomaterials* **2012**, *33*, 962-969, doi:<https://doi.org/10.1016/j.biomaterials.2011.10.004>.
368. Tamayol, A.; Akbari, M.; Zilberman, Y.; Comotto, M.; Lesha, E.; Serex, L.; Bagherifard, S.; Chen, Y.; Fu, G.; Ameri, S.K. Flexible pH-sensing hydrogel fibers for epidermal applications. *Advanced healthcare materials* **2016**, *5*, 711-719.
369. Song, F.; Wang, X.-L.; Wang, Y.-Z. Poly (N-isopropylacrylamide)/poly (ethylene oxide) blend nanofibrous scaffolds: Thermo-responsive carrier for controlled drug release. *Colloids and Surfaces B: Biointerfaces* **2011**, *88*, 749-754, doi:<https://doi.org/10.1016/j.colsurfb.2011.08.015>.
370. Najafabadi, A.H.; Tamayol, A.; Annabi, N.; Ochoa, M.; Mostafalu, P.; Akbari, M.; Nikkiah, M.; Rahimi, R.; Dokmeci, M.R.; Sonkusale, S., et al. Biodegradable Nanofibrous Polymeric Substrates for Generating Elastic and Flexible Electronics. *Advanced Materials* **2014**, *26*, 5823-5830, doi:10.1002/adma.201401537.
371. Tamayol, A.; Hassani Najafabadi, A.; Mostafalu, P.; Yetisen, A.K.; Commotto, M.; Aldhahri, M.; Abdel-wahab, M.S.; Najafabadi, Z.I.; Latifi, S.; Akbari, M., et al. Biodegradable elastic nanofibrous platforms with integrated flexible heaters for on-demand drug delivery. *Scientific Reports* **2017**, *7*, 9220, doi:10.1038/s41598-017-04749-8.
372. Abdalkarim, S.Y.H.; Yu, H.; Wang, C.; Chen, Y.; Zou, Z.; Han, L.; Yao, J.; Tam, K.C. Thermo and light-responsive phase change nanofibers with high energy storage efficiency for energy storage and thermally regulated on-off drug release devices. *Chemical Engineering Journal* **2019**, *375*, 121979, doi:<https://doi.org/10.1016/j.cej.2019.121979>.
373. Derakhshandeh, H.; Kashaf, S.S.; Aghabaglou, F.; Ghanavati, I.O.; Tamayol, A. Smart Bandages: The Future of Wound Care. *Trends in Biotechnology* **2018**, *36*, 1259-1274, doi:<https://doi.org/10.1016/j.tibtech.2018.07.007>.
374. Li, Y. Computational Textile Bioengineering. In *Computational Textile*, Zeng, X., Li, Y., Ruan, D., Koehl, L., Eds. Springer Berlin Heidelberg: Berlin, Heidelberg, 2007; 10.1007/978-3-540-70658-8_12pp. 203-221.



Chapter 2.

EFFECT OF CELLULOSE CHARACTERISTICS ON THE PROPERTIES OF THE WET-SPUN AEROGEL FIBERS

This chapter is based on the following publication:

Rostamitabar, M.; Seide, G.; Jockenhoevel, S.; Ghazanfari, S. Effect of Cellulose Characteristics on the Properties of the Wet-Spun Aerogel Fibers. *Applied Sciences* 2021, 11, 1525.

Abstract: Cellulose aerogels (CAs) from plant or bacterial-derived cellulose have advantages such as low density, high porosity, and high specific surface area and have been used in various applications including biomedical fields. One limiting factor in developing CAs is their demanding shaping process since it involves several steps of dissolution/dispersion of cellulose, geometry configurations using molds or nozzles, coagulation and washing of the gel body, and drying techniques. CA fibers can be converted into textiles and enhance the design ability, stiffness, and flexibility of the CAs. This study aims to understand the correlations between the initial cellulose characteristics, aerogel's internal structure, and its prospective biomedical application. Wet-spun CA fibers were obtained by supercritical CO₂ drying from low and high molecular weight microcrystalline cellulose in calcium thiocyanate tetrahydrate solution. Fiber spinning, thermal behavior, textural properties, and biological assessments of the CA fibers were inspected. The CA microfibers from high molecular weight cellulose proved to have a higher surface area ($\sim 197 \text{ m}^2/\text{g}$), denser structure, and finer nanofibrils ($\sim 20 \text{ nm}$) with better thermal stability in comparison with the fibers produced from low molecular weight cellulose. The fibers were nontoxic, and cell proliferation was observed over time. CA fibers showed promising results to be used for biomedical applications such as tissue engineering and wound care.

2.1 Introduction

Aerogels are open pores nanostructured solid networks with high porosity, high specific surface area, and low density [1]. In particular, aerogels are versatile porous materials with tunable textural and morphological characteristics for various fields such as adsorption and separation of materials, thermal insulation, and biomedical application [2-4]. Aerogels' morphological characteristics are controllable with various processing parameters such as gelation, shaping, drying, and functionalization [3,5]. Typically, inorganic silica aerogels with very high surface areas (400–1000 m²/g) are the most well studied and commercially prosperous ones; however, there is an increasing attentiveness to produce aerogels from natural polymers such as cellulose as a sustainable, biodegradable and often biocompatible resource [6,7].

The drying process of precursor gel aims plays an important role in aerogel fabrication in order to retain 3D porous structure with minimal shrinkage and deformation. Freeze drying and supercritical CO₂ (scCO₂) drying have been widely used in cellulose aerogels (CAs) production; recently ambient pressure drying methods that require physical and chemical modification of the gels have been also studied [8,9]. However, typically scCO₂ dried CAs show better textural and minimal shrinkage in contrast to other drying methods. Furthermore, scCO₂ processes are mild temperature techniques and favorable for sterilization and bioactive agent loading in biomedical fields [10,11].

Drying in supercritical conditions goes back to 1932 [12]. In the past, supercritical drying was mainly performed in the direct route, which utilized high temperature and pressure supercritical drying of the solvent in the wet matrix. However, these solvents are typically flammable and enhance safety risks. In another method, liquid CO₂ was replaced by the solvent, so-called solvent exchange, and then drying at low supercritical temperature was performed [13].

Since 1994, Bommel *et al.*'s novel study became a turning point in the scCO₂ drying process [14]. In order to fabricate crack-free silica aerogels, they used this theory that in the case of certain binary mixtures such as ethanol-CO₂, for each temperature, there is a pressure (critical pressure) above which the system is always in a single phase regardless of the composition. Therefore, it provided the chance to use scCO₂ drying to produce aerogels in milder operation conditions and reduced drying time. Then, the next generation of biomass- and polysaccharide-based aerogels, emerged at the beginning of the twenty-first century which contrary to silica aerogels were less fragile under compression forces [3]. Benefiting from scCO₂ drying, the morphology of the bio gel remains reasonably intact or with minimal shrinkage after drying [3,15].

Cellulose, an amphiphilic polysaccharide consisting of linear polymer chains of β -1,4-linked d-glucopyranose molecules, is one of the most abundant natural polymers from renewable resources. Cellulose and its derivatives have widely been used in areas such as conductive materials, energy storage, paper industry, textiles, and pharmaceuticals [16-20]. Furthermore, it is one of the most aged materials that has been used to produce fibers and yarns [21]. Several processes have been described in the literature for the fabrication of cellulose aerogels (CAs) in various geometries of monoliths [22,23], cylinders [24], and beads [25,26] based on different types of cellulose and their derivatives. Fiber and textile production can overcome this designability limitation and enhance the flexibility and mechanical properties of aerogels by fabricating woven or nonwoven textiles from CA fibers and filaments. Furthermore, the fine structure of fibers can decrease the scCO_2 drying processing time from few hours to a couple of minutes since the drying procedure is dependent on the thickness and geometries of the samples.

Various inorganic salt hydrates such as $\text{LiClO}_4 \cdot 3\text{H}_2\text{O}$, $\text{NaSCN/KSCN/LiSCN} \cdot 2\text{H}_2\text{O}$, $\text{Ca(SCN)}_2 \cdot 6\text{H}_2\text{O}$ and $\text{LiCl/ZnCl}_2/\text{H}_2\text{O}$ have been used as efficient agents for dissolving cellulose in a wide range of degrees of polymerization [27]. For the first time, Jin *et al.* investigated producing CAs monoliths from salt melt hydrate of cellulose and $\text{Ca(SCN)}_2 \cdot 6\text{H}_2\text{O}$ by freeze drying [28]. Hoepfner *et al.* [21] produced CA fibers based on Jin *et al.*'s work by spinning a similar solution using a thermally insulated injection device where the fibers were regenerated in an ethanol bath and later dried in scCO_2 as the first fabricated open porous aerogel microfibers using cellulose. Karadagli *et al.* investigated the spinning dope preparation, extrusion, and characteristics of porous cellulose aerogels fibers from a similar solution and regeneration bath using a micro-extruder and scCO_2 drying [29]. CA fibers have been also fabricated from ZnCl_2 salt melt hydrate in similar processing methods in order to investigate their insulation properties in aerospace [30] and automobile applications [31].

Although CAs in other geometrical shapes have been used in multiple biomedical applications such as drug delivery [32,33], tissue engineering scaffolds [34,35], antibacterial and wound dressing [36,37], the potential of CA microfibers for biomedical application has not been determined. Therefore, the processing, cytotoxicity, and biological assessment of these nano-biomaterials produced by assisting inorganic salts remain essential. This study aims to understand the correlations between initial polysaccharide characteristics, dissolution, and processing of the cellulose using $\text{Ca(SCN)}_2 \cdot 6\text{H}_2\text{O}$ on the final aerogel's internal structure and biological properties. In particular, this research inspects the effect of two different molecular weights of microcrystalline cellulose on

the physicochemical and cytotoxicity of the wet spun microfiber CAs that originated from them.

The microcrystalline cellulose and CA fiber are characterized in terms of crystallinity, morphology, physical and textural properties, thermal stability, and cytotoxicity. The CA microfibers produced from high molecular weight powder proved to have a higher surface area and lower crystallinity with a smaller average fibrillar diameter compared to the fibers with lower molecular weight. In comparison to powders, both CA fibers went through cellulose I to cellulose II transformation and were mainly in an amorphous form with lower thermal stability. Fibers were nontoxic and showed cell viability and proliferation as promising indications for using these fibers in biomedical applications where porous fibers are required.

2.2 Materials and Methods

2.2.1 Materials

Two different types of microcrystalline cellulose powder with product number C6288 (referred to as C_c) and S6790 (highly purified, referred to as C_s) and calcium thiocyanate tetrahydrate ($\text{Ca}(\text{SCN})_2 \cdot 4\text{H}_2\text{O}$) salt with a purity of 95%, all from Sigma–Aldrich (Darmstadt, Germany), were used in this study. The cellulose powders were dried at 100 °C in a vacuumed oven to remove the moisture. For regeneration and washing of the spun fibers, the absolute isopropanol (iPrOH) ($\geq 99,8\%$, 2-Propanol CP) from Biosolve was used. Carbon-dioxide (CO_2) cylinders (2.7 grade, 50 liters) with a purity of 99.7 % from Linde Gas Benelux were consumed in the scCO_2 drying process. Cell proliferation kit II (XTT) was purchased from Sigma–Aldrich. Finally, all materials were used without further purification.

2.2.2 Solution preparation, wet spinning, and washing

The salt melt hydrate system of $\text{Ca}(\text{SCN})_2 \cdot x\text{H}_2\text{O}$ ($x \leq 4$) + $y\text{H}_2\text{O}$ ($y \leq 6$) [38] was used to dissolve C_c and C_s . The addition of 2 mol of water to the salt ($\text{Ca}(\text{SCN})_2 \cdot 4\text{H}_2\text{O}$) is necessary to dissolve the cellulose. Homogenous clear solutions were obtained by dissolving C_c and C_s (6% wt.) at 110 °C using a mechanical stirrer (200 rpm) after approximately 25 and 35 min, respectively.

Fiber spinning was done by a customized wet-spinning “LabLineCompact” unit (DIENES Apparatebau GmbH, Germany). The solution needed to be wet spun at temperatures above 80 °C which is the gelation temperature of the solution. Therefore, three heaters with a controller were added to the tank, the pump, and the nozzle pipe. The algogel

fibers (wet alcohol gel bodies) with a diameter of 330 μm were produced using a Dispenstec metal dispensing needle (23AWG, internal diameter 330 μm , 12,7 mm length). Temperature ranges between (110–115 $^{\circ}\text{C}$), air pressure (2-3 bar), pump rate (1.5 mL/min), winding rate (25-30 rpm) and the iPrOH bath was used to achieve a continuous process for fiber production. The solution solidification in an alcohol bath happened when the temperature of the spun gel decreased from the melting point of the salt to room temperature. Finally, to remove the residual salt from fibers, they were solvent exchanged in 1 liter of fresh absolute iPrOH for 5 times. The presence of salt leftover was checked by a conductivity meter and spot test. The spot test was performed with iron (III) nitrate (1% wt/v) since thiocyanate ions react with iron (III) ions in the solution and form an intense red-colored complex ion.

2.2.3 Supercritical CO_2 drying

The drying procedure was performed using supercritical CO_2 dryer HPE 300 (EUROTECHNICA, Bargteheide, Germany). The fabricated alcogel fibers were wrapped in the filter papers and placed in the vessel ($V=400$ ml) with a defined excess amount of iPrOH. Samples were dried at 120 bar and 50 $^{\circ}\text{C}$ over 60 min. During the drying process, the extraction valve of the vessel was manually opened to vent the alcohol-rich mixture of CO_2 into a plastic flask while the pressure and temperature of the vessel remained constant. The extraction cycle of the alcohol rich stream was repeated 5 times for a duration of 3 min. In the end, the vessel was depressurized by a backpressure regulator over 30 min, and the vessel was opened when it cooled down to room temperature. The fibers were instantly placed in a tightly sealed sample holder under a dry N_2 purge to prevent the samples from absorbing the moisture.

2.2.4 Size exclusion chromatography (SEC)

Size Exclusion Chromatography (SEC) was carried out on cellulose powders with an Agilent 1200 Series LC Equipment (SEC pump G1310A, RI detector G1362A, columns: PSS Gram30 and PSS Gram1000 in series, flow rate: 1 mL min^{-1} ; eluent for cellulose samples: DMAc/LiCl). The calibration was done with pullulan standards. Cellulose dissolution in DMAc/LiCl is reported to remain stable over a long time and avoids the degradation of cellulose during the dissolution process; therefore, it is a reasonable solvent for SEC measurement [39].

2.2.5 Fourier transform infrared spectroscopy (FTIR)

The Fourier transform infrared spectroscopy technique is one of the useful methods to study the structure of cellulose and regenerated fibers. Fourier Transform Infrared (FTIR) spectroscopy was performed on the powders and fibers with an FT-IR/NIR unit

(Perkin Elmer, Waltham, MA, USA). The spectrum was averaged over 32 spectra with a resolution of 2 cm^{-1} from a range of $4000\text{ till }500\text{ cm}^{-1}$ in the reflectance mode.

2.2.6 X-ray diffraction (XRD)

Two-dimensional (2D) wide-angle X-ray diffraction (WAXD) analysis was performed on the samples using a SAXSLAB Ganesha diffractometer (SAXSLAB, Denmark), with a sample-to-detector distance of 116.536 mm using Cu K α radiation ($\lambda = 1.5406\text{ \AA}$) and silver behenate ($d_{001} = 58.380\text{ \AA}$), and calibration standard measured for 600 s .

The crystallinity index percentage (CrI (%)) was calculated for all samples by the empirical approximation method of Segal *et. al* [40] as expressed by the following equation:

$$\text{CrI}(\%) = \frac{I_{002} - I_{\text{amorphous}}}{I_{002}} \quad \text{Equation (2.1)}$$

where for cellulose I, I_{002} is the maximum intensity of the (002) lattice diffraction at $2\theta \approx 22.6^\circ$, representing the crystalline aspect of the cellulose and $I_{\text{amorphous}}$ is the intensity at $2\theta \approx 18.7^\circ$ representing the amorphous part in the cellulose fibers. For cellulose II, $I_{\text{crystallinity}}$ and $I_{\text{amorphous}}$ the intensity is at $2\theta \approx 20^\circ$ and 13° , respectively.

2.2.7 Thermal stability test

The thermal behavior of cellulose powders and produced fibers was investigated by a thermo-gravimetric instrument TA Q500 (TA Instruments, New Castle, DE, USA). Samples were heated from $20\text{ }^\circ\text{C}$ to $500\text{ }^\circ\text{C}$ with a rate of $10\text{ }^\circ\text{C}/\text{min}$ under a nitrogen purge.

2.2.8 Imaging, scanning electron microscope and X-ray microtomography

To observe the morphology and microstructure of the cross-section of CA fibers, the aerogel fibers were broken in liquid nitrogen and coated with a 3 nm thick layer of iridium. Micrograph images of the fibers' cross-sections were acquired by Teneo scanning electron (FEI, Thermo Fisher Scientific, Waltham, MA, USA). All images were obtained using 5 kV voltage at a working distance of 10 mm . The pore size distribution and the average diameter of microfibrils and internal nanofibrils were measured by analyzing SEM images using Image J (version 1.8.0_172, NIH, Bethesda, MD, USA). In particular, the cross-section images were binarized using a similar thresholding procedure for all samples after calibrating the precise scale of the pixels in the software. The pore size distribution was calculated in the particle analyses tool with a minimum size of 1 nm and circularity of 25% .

X-ray microtomography (μ -CT) images were obtained using Skyscann 127211MP (Bruker, Billerica, MA, USA) at the source voltage and current of 40 kV and 200 μ A with an exposure time of 1.5 s and image pixel size of 0.8 μ m. A CTAn analyzer (version 1.18.8.0+, Bruker) was utilized to calculate the parameters from 2D aerogel structures within three different regions of interest for each sample. In order to visualize 3D images of the samples, CTvox software (version 3.3.0 r1403, Bruker) was used.

2.2.9 N_2 adsorption-desorption

Surface area and porosimetry measurements of aerogel fibers were performed by ASAP[™] 2020 (micrometrics, Norcross (Atlanta), GA, USA). The samples were degassed at 80 °C over 24 h and the Brunauer–Emmet–Teller (BET) method was utilized to determine the surface area. The pore size distribution and average pore size were obtained by Barrett-Joyner-Halenda (BJH).

2.2.10 Cytotoxicity test

XTT cell proliferation assay was performed on C_c and C_s powders and two CA fibers produced from them [26]. The negative control was a piece of polyethylene tube, and the positive control was dimethyl sulfoxide (DMSO). The skin fibroblast cell viability was measured on the first and third day of culture using absorbance reading. The absorbance was measured in a multimode microplate reader M200 (Tecan, Männedorf, Switzerland). The assessment was performed in three replicates.

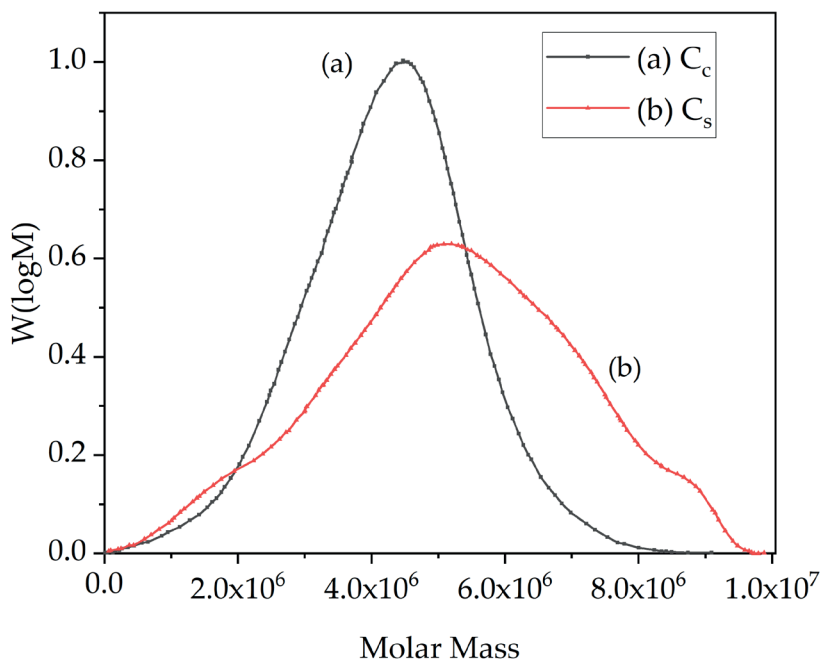
2.2.11 Statistical analysis

Experimental data are expressed as means \pm standard errors (SD). The statistical analysis was done by Originlab (2019 b) using a significance level of $p < 0.05$. Student t-test was performed to determine the differences between different time points.

2.3 Results

2.3.1 Properties of microcrystalline cellulose powder and fabricated fibers

The molecular weight of microcrystalline powders was obtained by SEC. The number average molecular weight (M_n), weight average molecular weight (M_w), z-average molecular weight, and dispersity (\bar{D}) results from cellulose powder samples are shown in **Figure 2.1** and **Table 2.1**. As shown in **Figure 2.1**, cellulose type S (C_s) has a higher number and weight average molecular weight and a broader range of molecular weight distribution. The higher molecular weight of C_s led to a 10 min longer dissolution time in the salt melt hydrate compared to the C_c .

**FIGURE 2.1.**

The weight distribution ($W(\log M)$) versus molar mass graphs of microcrystalline cellulose powders were obtained from SEC; cellulose type C (C_c , (a), black) has a narrow distribution of molecular weight while cellulose type S (C_s , (b), red)) has a broader distribution of molecular weight.

TABLE 2.1.

The result of size exclusion chromatography of cellulose powders C_c and C_s . C_s has a higher molecular weight and dispersity (\bar{D}).

SAMPLE	Mn (g.mol ⁻¹)	Mw (g.mol ⁻¹)	Mz (g.mol ⁻¹)	\bar{D}
C_c	61,760	163,500	404,220	2.647
C_s	78,700	565,630	1,942,200	7.187

The alcogel fibers (6% wt.) were spun, regenerated, and winded in the regeneration bath around a porous stainless steel bobbin. No salt leftover was observed because the conductivity for all samples was less than 1 $\mu\text{S}/\text{cm}$ and spot tests from all samples were negative and did not show any precipitation of salt. Yellowish-white opaque aerogel fibers were obtained after scCO_2 drying. The fibers obtained from cellulose type C and S are called F_c and F_s , respectively, in the following sections.

2.3.2 Fourier transform infrared spectroscopy (FTIR)

Figure 2.2 shows the FTIR spectra characteristic of the cellulose powders and fabricated CA fibers in the region of $4000\text{--}500\text{ cm}^{-1}$. The cellulose spectra show peaks at $3650\text{--}3000\text{ cm}^{-1}$ (O-H hydroxyl group stretching vibration), $2900\text{--}2800\text{ cm}^{-1}$ ($-\text{CH}_2-$ alkyl stretching vibration), 1645 cm^{-1} (C=O stretching), and 1020 cm^{-1} (C-O stretching). Furthermore, the crystalline structural alteration of cellulose from cellulose I to cellulose II were studied with the investigation of the peaks of 897 , 1107 , 1161 , and 1430 cm^{-1} absorption bands, which were assigned to group C_1 frequency, ring asymmetric stretching, C-O-C asymmetric stretching, and CH_2 symmetric bending vibration mainly in cellulose I, respectively [41].

Moreover, the 893 cm^{-1} absorption band (β -glucosidic linkages between the sugar units) also confirms that the crystalline cellulose I can be almost negligible in the regenerated cellulose fibers since the 893 cm^{-1} is assigned to group C_1 frequency in cellulose II [42,43]. Besides, the typical vibrations in amorphous cellulose at 1260 and 1460 cm^{-1} are similar to those in cellulose in the hydrated melts.

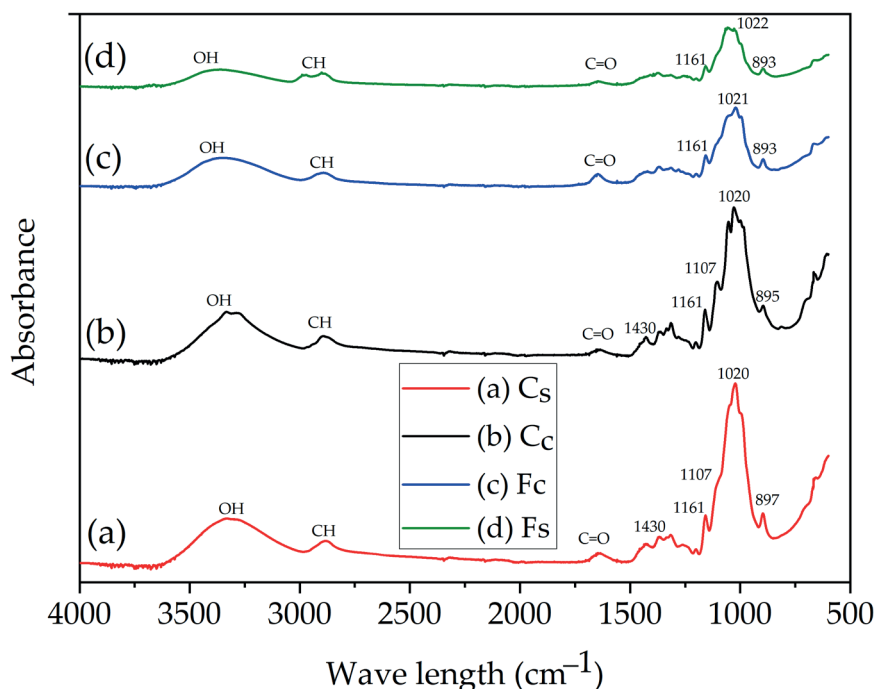
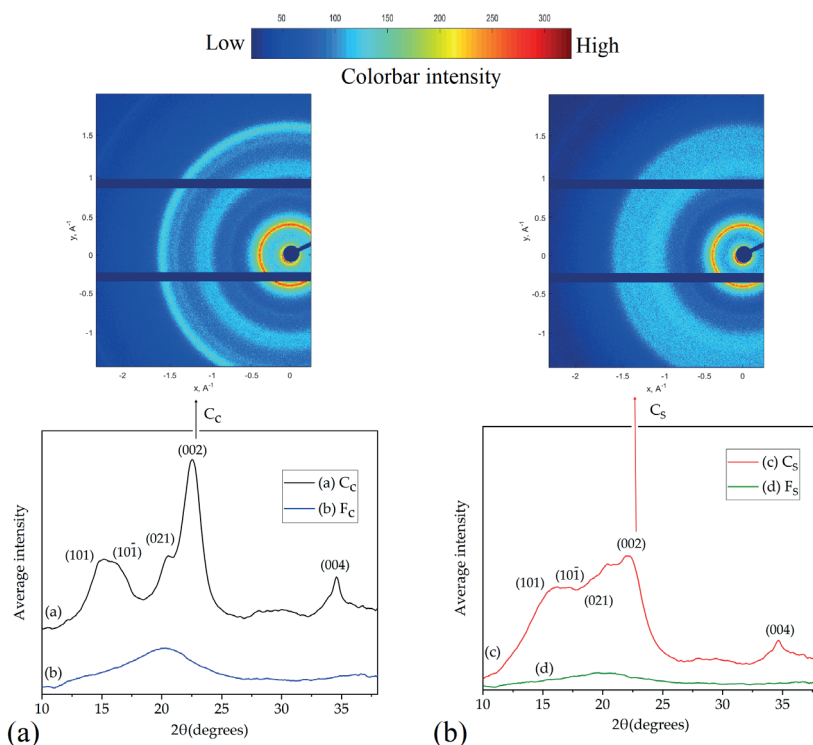


FIGURE 2.2.

The Fourier transform infrared spectra of cellulose powders (C_S , (a), red and C_C , (b), black) and wet-spun CA fibers (F_C , (c), blue and F_S , (d) green).

2.3.3 Wide-angle X-ray diffraction (WAXD)

The XRD diffractogram of C_c and C_s with CA fibers generated from them, along with the detector image of the relative microcrystalline cellulose are displayed in **Figure 2.3**. Five major diffraction peaks at $2\theta = 14.9^\circ$ (101), 15.9° ($10\bar{1}$), 21° (021), 22.4° (002) and 34.5° (004) are observed for the microcrystalline cellulose which is in line with values known in the literature for cellulose [41]. However, the CA fibers show a diffractogram with the absence or significant reduction of all peaks corresponding to planes (101), and (002), the values of the Bragg angle characteristic of cellulose I, specifying an amorphous structure. Furthermore, the aerocellulose patterns display peaks at $2\theta = 13^\circ$ and 20° which is the corresponding characteristic of cellulose II [27,44]. It is also explicit that C_c had sharper peaks at (002) as well as more intense regions of radiation absorbance in the detector image and therefore higher crystallinity (**Figure 2.3a**) in contrast to C_s (**Figure 2.3b**) [45]. The crystallite index for the C_c , F_c , C_s and F_s was 81.15, 27.58, 42.13 and 12.78 (%), respectively. Therefore, it demonstrates that the degree of crystallinity of the F_c and F_s was extremely lower than the original cellulose powder, but F_c had higher crystallinity than F_s .

**FIGURE 2.3.**

(a) The XRD spectra of microcrystalline type C (C_c , (a), black) and originated fiber (F_c , (b), blue) with the detector image of the C_c . (b) The XRD pattern of microcrystalline type s (C_s , (c), red) and fabricated fiber (F_s , (d), green) with the detector image of the C_s . C_c had a higher crystallinity index than C_s and fibers regenerated from both cellulose went through cellulose I to cellulose II transformation and formed an amorphous structure.

2.3.4 Thermal stability

The thermal behavior and initial decomposition temperature of the cellulose powders and fibers are shown in **Figure 2.4a**. The weight loss between 40–110 °C was due to the evaporation of the water molecules. Water molecules could have been absorbed on the hydroxyl group of the powder and CA fibers; besides, it is clear that a higher number of water molecules in CA fibers was absorbed in the porous framework [46,47]. From 120 °C to 260 °C, the weight loss was almost unaltered. The weight rapidly decreased from 255 °C to 360 °C because of dehydration and decomposition of the cellulose chains. In derivative thermogravimetry curves (DTG), as shown in **Figure 2.4b**, it was indicated that the starting decomposing temperature shifts toward a lower temperature and the maximal weight loss peak was broadened in CA fibers comparing to their initial powder.

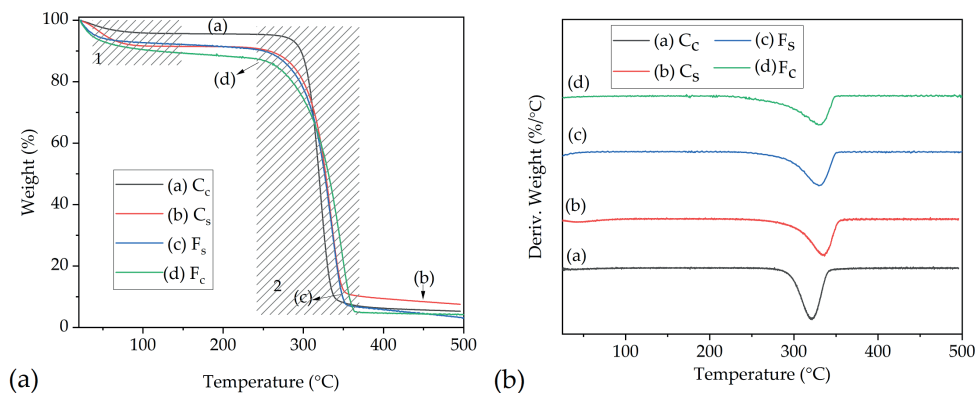


FIGURE 2.4.

(a) TGA graphs of the cellulose powder C (C_c , (a), black), cellulose powders type S (C_s , (b), red) and aerogel fibers type S (F_s , (c), blue) and type C (F_c , (d), green). The first step from 40 to 110 °C in the mass loss was due to the evaporation of water molecules and the second step at elevated temperatures (from 255 to 360 °C) happened due to the relatively fast decomposition of cellulose chains. (b) DTG curves show that the decomposing temperature of CA fibers compared to powders shifted toward a lower temperature and the maximal weight peak was broadened.

2.3.5 Morphology and textural properties of the aerogel fibers

2.3.5.1 Imaging by scanning electron microscope

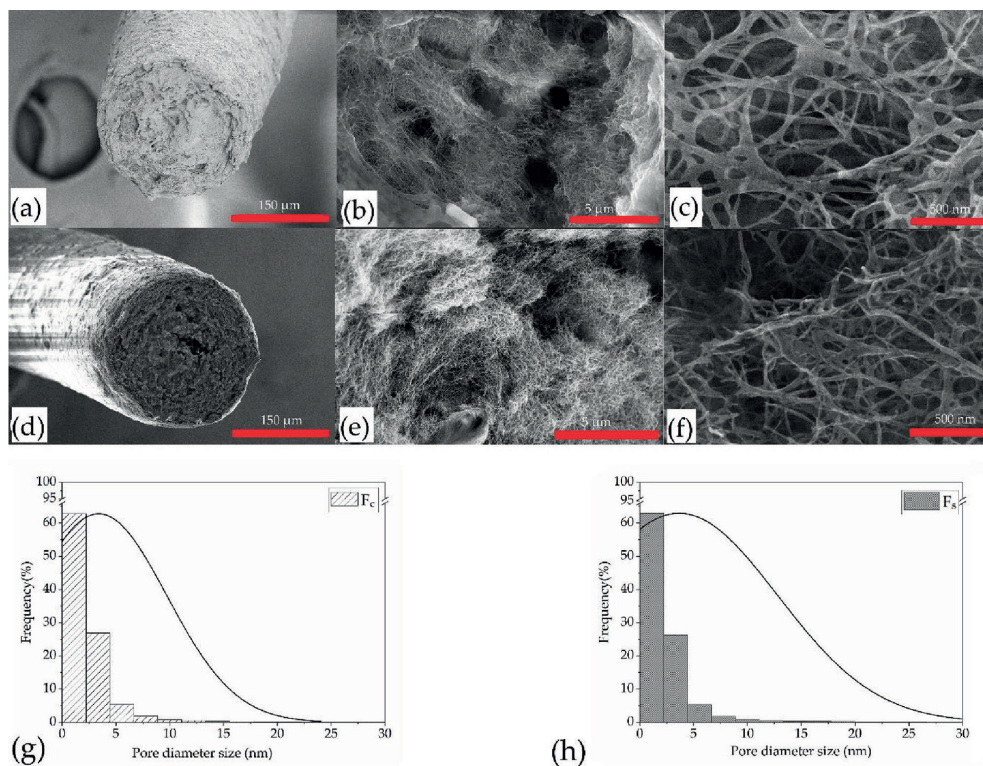
SEM images of the aerogel fibers showed porous meshes of randomly oriented cellulose nano-fibrils (**Figure 2.5a,f**); the morphology of the fibers is similar to the typical fibrillar cellulose aerogels reported in the literature [21,29]. The image analysis showed more than 60% of the pore sizes are under 5 nm for both fibers (**Figure 2.5 g&h**) however, few macropores (> 50 nm) existed for both fibers. **Table 2.2** provides detailed information on the average pore size, minimum pore size of the CA fibers obtained from SEM image processing.

Furthermore, by measuring the diameter of the microfibers, it was proven that F_c diameter was $275.66 \pm 1.24 \mu\text{m}$ while F_s diameter was $281 \pm 2.16 \mu\text{m}$. Based on the measured diameters the calculated volume shrinkage of CA fibers after regeneration, washing, and scCO_2 drying was 16.47% and 14.85%, respectively. The diameter of nanofibers in F_s was $22.28 \pm 7.61 \text{ nm}$ while F_c had thicker nanofibrils with a diameter of $38.11 \pm 7.26 \text{ nm}$.

TABLE 2.2.

The pore size diameter analysis of F_c and F_s obtained from SEM image processing using Image J software

SAMPLE	AVERAGE PORE SIZE (nm)	MINIMUM SIZE (nm)
F_c	3.398 ± 6.346	2.142
F_s	3.657 ± 9.165	2.139

**FIGURE 2.5.**

Scanning electron micrographs of the cross-section of cellulose aerogel fibers after regeneration in isopropanol and scCO_2 drying (6 wt. % cellulose content). (a) cross-section of F_c (scale bar 150 μm), (b) randomly oriented nanofibrils in F_c (scale bar 5 μm), (c) cellulose fibrils of F_c (scale bar 500 nm), (d) cross-section of F_s (scale bar 150 μm), (e) dense and randomly arranged nanofibril in F_s (scale bar 5 μm), (f) cellulose fibrils of F_s (scale bar 500 nm). The pore size distribution of F_c (g) and F_s (h) was acquired by image analysis using Image J software; the analyses showed that more than 60% of the pore sizes were under 5 nm for both fibers.

2.3.5.2 X-ray microtomography

μ -CT images showed that fibers from both cellulose types were highly porous and consisted of inter-connected open pores structure (**Figure 2.6**). The color bar shows the intensity of the X-ray absorbed by the fiber matrix. It was shown by the high

intensity (blue-white color) regions that F_s had more condensed regions of nanofibrils. The computed amount of open and closed pores calculated from the image stacks are shown in (Table 2.3). The F_c has a slightly higher total amount of porosity and open pores compared to the F_s . However, the number of closed pores in both fibers is negligible ($< 0.01\%$).

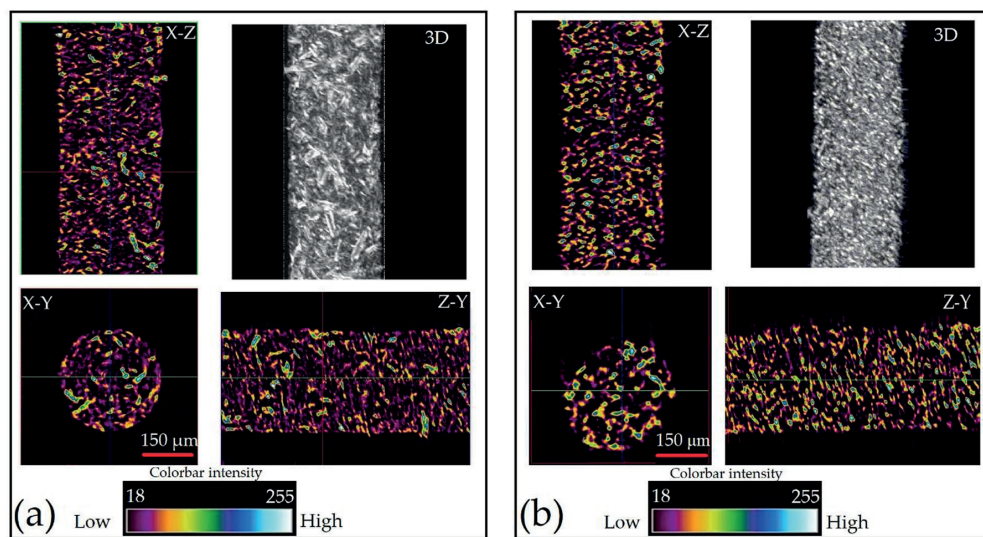


FIGURE 2.6.

μ -CT images of cellulose aerogel F_c (a) and F_s (b) in 3 different planes (X-Z, X-Y, Z-Y) with their 3D computed structure. The color bar shows the intensity of the X-ray absorbed by the fiber matrix (min: black and max: white). Scale bar length is 150 μ m in all images.

TABLE 2.3.

The porosity analysis of F_c and F_s obtained by μ -CT assessment using 3D analysis in CTAn software.

SAMPLE	TOTAL POROSITY (%)	CLOSED POROSITY (%)	OPEN POROSITY (%)
F_c	77.3 ± 2.33	<0.01	77.32
F_s	71.6 ± 3.12	<0.01	71.65

2.3.5.3 N_2 adsorption-desorption

The specific surface area, pore volume, and pore size distribution of the CA fibers was obtained by BET adsorption and BJH desorption. The fibers isotherm curves over relative pressure are shown in Figure 2.7a and b, and incremental pore volume versus pore size width are displayed in Figure 2.7c and d. The F_s has a higher N_2 quantity adsorbed. The isotherms curves are similar to IUPAC type IV with a hysteresis loop in

the range of 0.7–1.0, representing the presence of meso and macro-porous structure [48,49]. The multipoint BET specific surface area (SA_{BET}) results showed that F_s had a SA_{BET} of 197 m^2/g while low molecular weight F_c with the same concentration (6 wt.%) proved to have SA_{BET} of 85 m^2/g . The average nanofibril diameter ($D_{average}$) can be calculated from skeletal density ($\rho_{skeletal}$) and SA_{BET} by the formula $D_{average} = 4/(\rho_{skeletal} \times SA_{BET})$, where $\rho_{skeletal}$ is 1.501 g/cm^3 for cellulose [29,48].

The BJH method discovered that majority of pores are distributed under 50 nm in both samples. The dissimilarity was observed over the highest peak of pore size distribution as it was narrower in the F_s and located in the range of 20–30 nm, while the F_c had a broader distribution of pores with a shorter peak height in the range of 20–40 nm (Figure 2.7d). BJH method clarified that the pore volume of F_s and F_c was 1.03 cm^3/g and 0.36 cm^3/g , respectively; moreover, the BJH desorption average pore width was 19.34 and 17.47 nm for F_s and F_c , respectively.

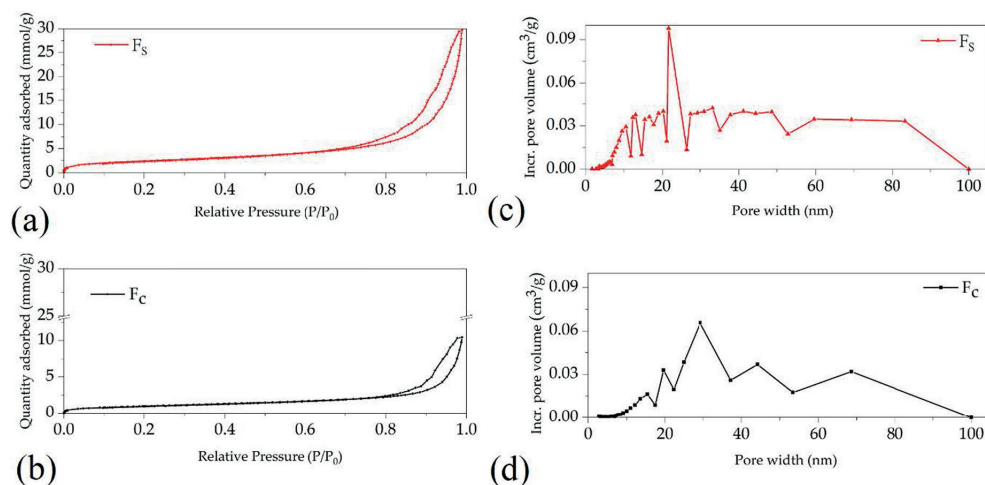


FIGURE 2.7.

Nitrogen adsorption-desorption isotherms curve and representation of pore size distribution by incremental pore volume versus pore size width of F_s (a and b) and F_c (c and d). In contrast to F_c , the F_s had a higher N_2 quantity adsorbed. The majority of pores were distributed under 50 nm in both samples and F_s had a higher pore volume. The specific surface area of F_s and F_c was 197 m^2/g and 85 m^2/g , respectively.

2.3.6 Cytotoxicity

The cell viability observed in all samples on the first and third days of cell culture proved that the samples were nontoxic. The proliferation of fibroblast cells from day 1 to day 3 was observed in all samples with the exemption of C_c powder (Figure 2.8). It was also noted that the viability of F_s is slightly lower than F_c .

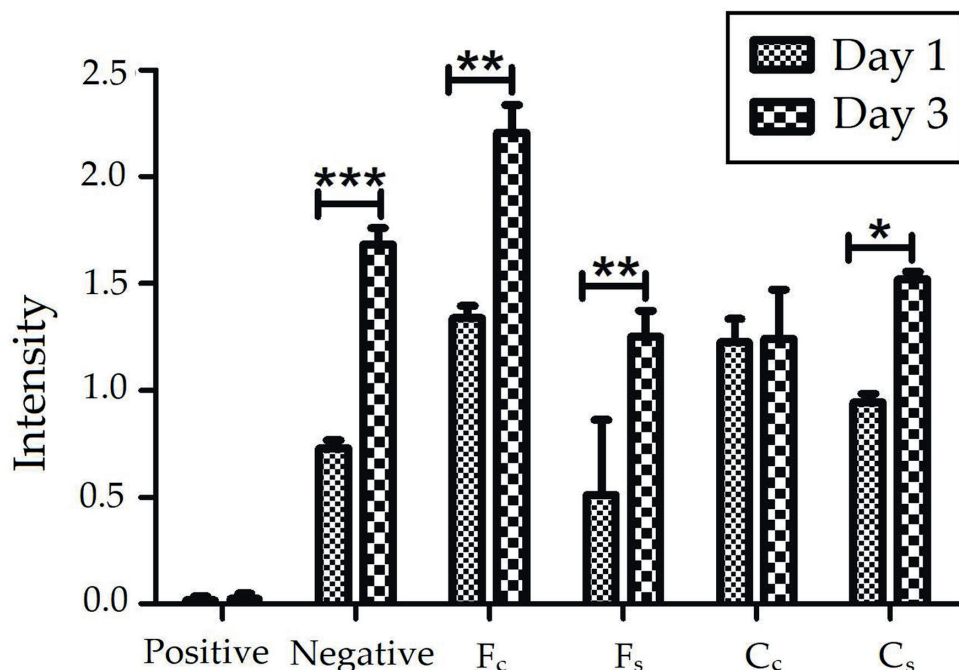


FIGURE 2.8.

XTT assay of cellulose powders (C_c and C_s) and fabricated alcogel fibers (F_c and F_s). The cell viability was observed in all samples; (***, $P < 0.001$; **, $P < 0.01$; *, $P < 0.05$). Negative samples were polyethylene and positive samples were DMSO. All test samples showed proliferation from day 1 to 3 except C_c .

2.4 Discussion

The aerogel fibers were fabricated using a semi-pilot scale wet spinning line and utilizing $scCO_2$ drying unit. $ScCO_2$ processes are gaining more attention in the biomedical field since they are being used as a mild temperature processing method to produce porous materials, such as aerogels, besides being used as a sterilization technique for biomedical products [10]. The significant difference in the type of polysaccharide used for fabricating the aerogels, especially in the structure and length of chains, might have an impact on the morphological properties of fibers because the properties of the cellulosic products rely on the biomacromolecule assembly and its degree of polymerization [50,51]. Two fabricated CA microfibers ($\phi \approx 270 \mu m$) from low and high molecular weight cellulose exhibited different physical and textural properties in the structural, morphological, thermal, and biological assessment.

The FTIR results proved that the dissolution of the initial biomacromolecule in salt melt hydrate altered the crystalline structure of the material from cellulose I to cellulose II, but no presence of salt leftover was observed. The NCS groups (N bonded) can appear around $2060\text{--}2100 \text{ cm}^{-1}$, and SCN groups (S bonded) can appear above 2100 cm^{-1} . As

there is no clear peak in the mentioned range of FTIR patterns (**Figure 2.2**), it implies that NCS groups are not present in the structure of the fiber after washing steps [52].

Furthermore, XRD showed that the regenerated CA fibers were in the amorphous state and mainly in the form of cellulose II, and F_c had higher crystallinity than F_s , as it was originated from high crystalline initial cellulose (C_c). From XRD and FTIR measurements, it can be concluded that the dissolution and the spinning of cellulose in $\text{Ca}(\text{SCN})_2$ molten salt hydrate did not change the cellulose chemical structure during the dissolution and regeneration but weakened or broke the inter- and intra-cellulose hydrogen bonding, and inevitably deranged the final CA fiber crystalline arrangement [27,44].

The thermogravimetric measurements disclosed that the CA fibers were slightly less thermally stable than their original cellulose powder due to the decrease of initial degradation temperature. This lower thermal stability was based on several elements such as the conversion of cellulose I to cellulose II, degradation of cellulose chains known for cellulose during dissolution in inorganic salts, and higher specific surface area of the CA fibers compared to the powders, which made the internal surface of fibers more prone to thermal degradation [27,38,53].

To reveal structural and textural properties of the CA fibers SEM, μ -CT, and BET/BJH results needed to be integrated as different compartment length scales from nanometer to micrometer existed in the fiber matrix [54]. The SEM and μ -CT outcomes showed that CA fibers consist of randomly ordered nanofibrils with interconnected pore structure. The BET calculated average nanofibril diameters were 13.5 and 31 nm for F_s and F_c , respectively, which were close to the diameter range of the results obtained via SEM image analysis (~ 20 –38 nm). The larger fibril diameter of F_c might trigger some small pores to get closer and agglomerate, leading to lower pore volume [34]. The SEM analysis showed that the average pore width quantities in both samples (~ 3 –4 nm) were lower than the obtained results in BJH desorption method (~ 17 –20 nm), but both methods proved that F_s had a higher pore size diameter than F_c . The low percentage of closed pores in both fibers achieved by μ -CT ($< 0.01\%$) was in line with the SEM and N_2 adsorption-desorption results. Alongside scCO_2 drying processes, the regeneration solvent is also essential in achieving a low amount of closed pores. Isopropanol was used as the main regeneration and washing solvents since its low surface tension (0.023 N/m), tends to decrease the number of closed pores during scCO_2 drying; besides, in previous studies, it has been proven the CAs regenerated in iProH have higher mechanical properties than other forms of alcohols (e.g., EtOH) [3,30].

BJH desorption results also showed that F_s had significantly higher pore volume ($1.03 \text{ cm}^3/\text{g}$) than F_c ($0.36 \text{ cm}^3/\text{g}$). The obtained value for F_c was lower compared to the porosity acquired by μ -CT because of the resolution limitation of the μ -CT technique which will be discussed further. Overall, both fibers have mainly mesoporous structure with few macro scale pores. Based on the results of the aforementioned methods, F_s originated from the high molecular weight with lower crystallinity cellulose (C_s) led to thinner nanofibrillar formation (SEM, BET/BJH), interconnected pore structure (μ -CT) and higher surface area and pore volume (BET/BJH).

The difference in the results needs to be explained by understanding the sample preparation and measurement basis of each technique. SEM image analysis is limited to 2D and is highly dependent on the settings used during binary image production. Inaccuracy might also arise from the fibers cross-section preparation since even cutting in liquid N_2 can deform the nanofibrillars. Additionally, fibrils are highly sensitive to the electron beam and throughout the imaging process, they can form clusters upon applying high voltages (2-5 kV) [55]. In addition, although the μ -CT analyses provide a more in-depth and accurate overview of 3D structures with insight into the closed pores, the resolution of this technique is limited (in this study, $0.8 \text{ }\mu\text{m}$); this can cause errors, such as neglecting nanofibrils, or considering the agglomeration in the fiber matrix, therefore it might fail to obtain a precise internal computed construction.

On the other hand, N_2 adsorption and desorption data based on BET and BJH theory report the pores which are accessible for gas; miscalculations might arise due to nanofibrillar structural changes in the N_2 pressure variation during the measurements causing some errors in pore diameter values [48,54]. In the case of microfiber shapes, this error can be even higher due to brittleness, high electrostatic charges, and the very lightweight nature of samples. After all, to add enough mass of the fibers in the bulb of the test tube, the aerogel fibers might have been compressed by transferring the samples into the bottom of the tube. It is challenging to control the applied compression when the ultralight aerogel microfibers samples were filled in the test tube. More advanced characterization methods, such as nano-CT as a super high-resolution imaging techniques, are required to obtain a better understanding of the textural properties of CA fibers [56].

The difference in the cell proliferation of the powders might arise from their purity. Regarding the CA fibers, the slower cell proliferation in the F_s can be due to minor trapped salt molecules, which can be thoroughly investigated by elemental analysis methods. The non-toxicity and cell proliferation of samples in addition to their open

and accessible interconnected porous network are in favor of tissue integration and vascularization and it shows the potential of CA fibers for scaffold or drug delivery applications [51,57]. The textile production from CA fibers will lead to unique constructs with a macro/micro-porous structure emerging from the space between microfibers and mesoporous structure originating from porosity of each aerogel fiber; this also enhances the surface to volume ratio of the end product which is favorable for transdermal, wound care and tissue engineering applications [2,58].

In the prospective studies, the processing route could be more optimized to decrease the destruction of initial polysaccharide chain length and crystallinity as it led to a reduction in the physical and mechanical properties of the end products; for instance, ionic liquids with lower melting temperatures can be used as a dissolving agent [3,59]. Furthermore, the development of greener isolation methods to obtain cellulose from plant resources can minimize the toxicity of the powders. Bacterial cellulose can be a promising candidate to replace plant-derived cellulose since it is produced by enzymes leading to a higher molecular weight and more crystalline assembly of cellulose [4].

In general, tunable macro and micro designability, biomimetic structure, non-toxicity and biodegradability introduce these CA fibers and possible outcome textile as promising candidates for several biomedical application including tissues engineering, wound care and drug delivery. However, in future studies some of their limitation requires to be improved. For instance, CA fibers are not wet stable and in case of cyclic evaporation of solvent molecules (e.g. changes in humidity) or immersion in liquids and subsequent ambient drying, their internal structure will collapse over time [60,61]. Additionally, the CA microfibers brittleness remains a challenge for further industrial textile production. These are the two main challenges for many biomedical application which needs to be overcome using physical or chemical modifications such as plasma treatment, layer by layer assembly, crosslinking, etc.

2.5 Conclusions

Herein, we successfully fabricated two different cellulose aerogel fibers (6 wt.%) from plant-derived microcrystalline cellulose powders. Fibers were prepared by dissolving the cellulose in calcium thiocyanate melt hydrate combined with wet spinning and scCO_2 drying methods. The aerogel fibers showed lower crystallinity and thermal stability in comparison to their original polysaccharides. The result showed that highly porous constructs were fabricated and proved that the properties of the fibers were affected by using different molecular weights of the polysaccharide. The microfiber originated from a high molecular weight with low crystallinity cellulose powder

showed thinner fibril diameter (~ 20 nm), higher surface area ($\sim 197\text{m}^2/\text{g}$) and pore volume (~ 1.03 cc/g) than the microfiber obtained from the low molecular weight with high crystallinity cellulose. Finally, it was confirmed that the cellulose aerogel fibers produced in this study is non-toxic and thus can be used in biomedical application such as tissue engineering and regenerative medicine applications.

References

1. Corrias, A.; Casula, M.; Aegerter, M.; N Leventis, M.K. Aerogel handbook. Aerogels containing metal, alloy and oxide nanoparticles in dielectric matrices. Springer, New York **2010**.
2. Montes, S.; Maleki, H. 12 - Aerogels and their applications. In *Colloidal Metal Oxide Nanoparticles*, Thomas, S., Tresa Sunny, A., Velayudhan, P., Eds. Elsevier: 2020; <https://doi.org/10.1016/B978-0-12-813357-6.00015-2>pp. 337-399.
3. Budtova, T. Cellulose II aerogels: a review. *Cellulose* **2019**, 26, 81-121, doi:10.1007/s10570-018-2189-1.
4. Abdul Khalil, H.P.S.; Adnan, A.S.; Yahya, E.B.; Olaiya, N.G.; Safrida, S.; Hossain, M.S.; Balakrishnan, V.; Gopakumar, D.A.; Abdullah, C.K.; Oyekanmi, A.A., et al. A Review on Plant Cellulose Nanofibre-Based Aerogels for Biomedical Applications. *Polymers* **2020**, 12, 1759.
5. García-González, C.A.; Budtova, T.; Durães, L.; Erkey, C.; Del Gaudio, P.; Gurikov, P.; Koebel, M.; Liebner, F.; Neagu, M.; Smirnova, I. An Opinion Paper on Aerogels for Biomedical and Environmental Applications. *Molecules* **2019**, 24, 1815.
6. Zhu, F. Starch based aerogels: Production, properties and applications. *Trends in Food Science & Technology* **2019**, 89, 1-10, doi:<https://doi.org/10.1016/j.tifs.2019.05.001>.
7. De Marco, I.; Reverchon, E. Starch aerogel loaded with poorly water-soluble vitamins through supercritical CO₂ adsorption. *Chemical Engineering Research and Design* **2017**, 119, 221-230, doi:<https://doi.org/10.1016/j.cherd.2017.01.024>.
8. Long, L.-Y.; Weng, Y.-X.; Wang, Y.-Z. Cellulose Aerogels: Synthesis, Applications, and Prospects. *Polymers* **2018**, 10, 623.
9. Li, M.; Jiang, H.; Xu, D.; Yang, Y. A facile method to prepare cellulose whiskers-silica aerogel composites. *Journal of Sol-Gel Science and Technology* **2017**, 83, 72-80, doi:10.1007/s10971-017-4384-1.
10. Ribeiro, N.; Soares, G.C.; Santos-Rosales, V.; Concheiro, A.; Alvarez-Lorenzo, C.; García-González, C.A.; Oliveira, A.L. A new era for sterilization based on supercritical CO₂ technology. *Journal of Biomedical Materials Research Part B: Applied Biomaterials* **2020**, 108, 399-428, doi:10.1002/jbm.b.34398.
11. Champeau, M.; Thomassin, J.M.; Tassaing, T.; Jérôme, C. Drug loading of polymer implants by supercritical CO₂ assisted impregnation: A review. *Journal of Controlled Release* **2015**, 209, 248-259, doi:<https://doi.org/10.1016/j.jconrel.2015.05.002>.
12. Kistler, S.S. Coherent Expanded Aerogels and Jellies. *Nature* **1931**, 127, 741-741, doi:10.1038/127741a0.
13. Tewari, P.H.; Hunt, A.J.; Lofftus, K.D. Ambient-temperature supercritical drying of transparent silica aerogels. *Materials Letters* **1985**, 3, 363-367, doi:[https://doi.org/10.1016/0167-577X\(85\)90077-1](https://doi.org/10.1016/0167-577X(85)90077-1).
14. van Bommel, M.J.; de Haan, A.B. Drying of silica gels with supercritical carbon dioxide. *Journal of Materials Science* **1994**, 29, 943-948, doi:10.1007/BF00351414.
15. Kikic, I.; Vecchione, F. Supercritical impregnation of polymers. *Current Opinion in Solid State and Materials Science* **2003**, 7, 399-405, doi:<https://doi.org/10.1016/j.cossms.2003.09.001>.
16. Vermerris, W.; Abril, A. Enhancing cellulose utilization for fuels and chemicals by genetic modification of plant cell wall architecture. *Current Opinion in Biotechnology* **2015**, 32, 104-112, doi:<https://doi.org/10.1016/j.copbio.2014.11.024>.
17. Festucci-Buselli, R.A.; Otoni, W.C.; Joshi, C.P. Structure, organization, and functions of cellulose synthase complexes in higher plants. *Brazilian Journal of Plant Physiology* **2007**, 19, 1-13.
18. Chu, H.-Y.; Hong, J.-Y.; Huang, C.-F.; Wu, J.-Y.; Wang, T.-L.; Wu, T.-M.; Lee, R.-H. Enhanced photovoltaic

- properties of perovskite solar cells by the addition of cellulose derivatives to MAPbI₃ based photoactive layer. *Cellulose* **2019**, *26*, 9229-9239, doi:10.1007/s10570-019-02724-2.
19. Jyothibasu, J.P.; Kuo, D.-W.; Lee, R.-H. Flexible and freestanding electrodes based on polypyrrole/carbon nanotube/cellulose composites for supercapacitor application. *Cellulose* **2019**, *26*, 4495-4513, doi:10.1007/s10570-019-02376-2.
 20. Huang, X.; Liu, Y.; Deng, J.; Yi, B.; Yu, X.; Shen, P.; Tan, S. A novel polymer gel electrolyte based on cyanoethylated cellulose for dye-sensitized solar cells. *Electrochimica Acta* **2012**, *80*, 219-226, doi:https://doi.org/10.1016/j.electacta.2012.07.014.
 21. Hoepfner, S.; Ratke, L. *Open porous cellulose aerogel fibers*; 2008; 10.13140/RG.2.2.12012.26246.
 22. Hoepfner, S.; Ratke, L.; Milow, B. Synthesis and characterisation of nanofibrillar cellulose aerogels. *Cellulose* **2008**, *15*, 121-129, doi:10.1007/s10570-007-9146-8.
 23. Wu, Z.-Y.; Li, C.; Liang, H.-W.; Chen, J.-F.; Yu, S.-H. Ultralight, Flexible, and Fire-Resistant Carbon Nanofiber Aerogels from Bacterial Cellulose. *Angewandte Chemie International Edition* **2013**, *52*, 2925-2929, doi:10.1002/anie.201209676.
 24. Gavillon, R.; Budtova, T. Aerocellulose: new highly porous cellulose prepared from cellulose-NaOH aqueous solutions. *Biomacromolecules* **2008**, *9*, 269-277, doi:10.1021/bm700972k.
 25. Sescousse, R.; Gavillon, R.; Budtova, T. Wet and dry highly porous cellulose beads from cellulose-NaOH-water solutions: influence of the preparation conditions on beads shape and encapsulation of inorganic particles. *Journal of Materials Science* **2011**, *46*, 759-765.
 26. Mohamed, S.M.K.; Ganesan, K.; Milow, B.; Ratke, L. The effect of zinc oxide (ZnO) addition on the physical and morphological properties of cellulose aerogel beads. *RSC Advances* **2015**, *5*, 90193-90201.
 27. Fischer, S.; Leipner, H.; Thümmel, K.; Brendler, E.; Peters, J. Inorganic molten salts as solvents for cellulose. *Cellulose* **2003**, *10*, 227-236.
 28. Jin, H.; Nishiyama, Y.; Wada, M.; Kuga, S. Nanofibrillar cellulose aerogels. *Colloids and Surfaces A: Physicochemical and Engineering Aspects* **2004**, *240*, 63-67.
 29. Karadagli, I.; Schulz, B.; Schestakow, M.; Milow, B.; Gries, T.; Ratke, L. Production of porous cellulose aerogel fibers by an extrusion process. *The Journal of Supercritical Fluids* **2015**, *106*, 105-114, doi:https://doi.org/10.1016/j.supflu.2015.06.011.
 30. Schulz, B.; Meinert, T.; Bierbüsse, D.; Busen, M.; Körtzinger, N.; Stankowski, M.; Seide, G. Cellulose Aerogel Fibers Tested on a REXUS 18 Rocket – The ACTOR Project. *Chemie Ingenieur Technik* **2016**, *88*, 1501-1507, doi:10.1002/cite.201600003.
 31. Mroszczok, J.; Schulz, B.; Wilsch, K.; Frenzer, G.; Kasper, S.; Seide, G. Cellulose Aerogel Fibres for Thermal Encapsulation of Diesel Hybrid Engines for Fuel Savings in Cars. *Materials Today: Proceedings* **2017**, *4*, S244-S248, doi:https://doi.org/10.1016/j.matpr.2017.09.194.
 32. Valo, H.; Arola, S.; Laaksonen, P.; Torkkeli, M.; Peltonen, L.; Linder, M.B.; Serimaa, R.; Kuga, S.; Hirvonen, J.; Laaksonen, T. Drug release from nanoparticles embedded in four different nanofibrillar cellulose aerogels. *European Journal of Pharmaceutical Sciences* **2013**, *50*, 69-77, doi:https://doi.org/10.1016/j.ejps.2013.02.023.
 33. Li, J.; Wang, Y.; Zhang, L.; Xu, Z.; Dai, H.; Wu, W. Nanocellulose/Gelatin Composite Cryogels for Controlled Drug Release. *ACS Sustainable Chemistry & Engineering* **2019**, *7*, 6381-6389, doi:10.1021/acssuschemeng.9b00161.
 34. Cai, H.; Sharma, S.; Liu, W.; Mu, W.; Liu, W.; Zhang, X.; Deng, Y. Aerogel Microspheres from Natural Cellulose

- Nanofibrils and Their Application as Cell Culture Scaffold. *Biomacromolecules* **2014**, *15*, 2540-2547, doi:10.1021/bm5003976.
35. Zhang, C.; Zhai, T.; Turng, L.-S. Aerogel microspheres based on cellulose nanofibrils as potential cell culture scaffolds. *Cellulose* **2017**, *24*, 2791-2799, doi:10.1007/s10570-017-1295-9.
36. Matsuyama, K.; Morotomi, K.; Inoue, S.; Nakashima, M.; Nakashima, H.; Okuyama, T.; Kato, T.; Muto, H.; Sugiyama, H. Antibacterial and antifungal properties of Ag nanoparticle-loaded cellulose nanofiber aerogels prepared by supercritical CO₂ drying. *The Journal of Supercritical Fluids* **2019**, *143*, 1-7, doi:https://doi.org/10.1016/j.supflu.2018.08.008.
37. Wang, X.; Cheng, F.; Liu, J.; Smått, J.-H.; Gepperth, D.; Lastusaari, M.; Xu, C.; Hupa, L. Biocomposites of copper-containing mesoporous bioactive glass and nanofibrillated cellulose: Biocompatibility and angiogenic promotion in chronic wound healing application. *Acta biomaterialia* **2016**, *46*, 286-298, doi:https://doi.org/10.1016/j.actbio.2016.09.021.
38. Hattori, M.; Koga, T.; Shimaya, Y.; Saito, M. Aqueous Calcium Thiocyanate Solution as a Cellulose Solvent. Structure and Interactions with Cellulose. *Polymer Journal* **1998**, *30*, 43, doi:10.1295/polymj.30.43.
39. Sjöholm, E. Size exclusion chromatography of cellulose and cellulose derivatives. 2004; Vol. 91, pp. 311-354.
40. Segal, L.; Creely, J.J.; Martin, A.E.; Conrad, C.M. An Empirical Method for Estimating the Degree of Crystallinity of Native Cellulose Using the X-Ray Diffractometer. *Textile Research Journal* **1959**, *29*, 786-794, doi:10.1177/004051755902901003.
41. Poletto, M.; Pistor, V.; Zattera, A.J. Structural characteristics and thermal properties of native cellulose. *Cellulose-fundamental aspects* **2013**, *2*, 45-68.
42. Nelson, M.L.; O'Connor, R.T. Relation of certain infrared bands to cellulose crystallinity and crystal latticed type. Part I. Spectra of lattice types I, II, III and of amorphous cellulose. *Journal of Applied Polymer Science* **1964**, *8*, 1311-1324, doi:10.1002/app.1964.070080322.
43. Yang, Y.; Zhang, Y.; Lang, Y.; Yu, M. Structural ATR-IR analysis of cellulose fibers prepared from a NaOH complex aqueous solution. *IOP Conference Series: Materials Science and Engineering* **2017**, *213*, 012039, doi:10.1088/1757-899X/213/1/012039.
44. Lu, X.; Shen, X. Solubility of bacteria cellulose in zinc chloride aqueous solutions. *Carbohydrate Polymers* **2011**, *86*, 239-244, doi:https://doi.org/10.1016/j.carbpol.2011.04.042.
45. Driemeier, C.; Bragatto, J. Crystallite Width Determines Monolayer Hydration across a Wide Spectrum of Celluloses Isolated from Plants. *The Journal of Physical Chemistry B* **2013**, *117*, 415-421, doi:10.1021/jp309948h.
46. Ye, S.; He, S.; Su, C.; Jiang, L.; Wen, Y.; Zhu, Z.; Shao, W. Morphological, Release and Antibacterial Performances of Amoxicillin-Loaded Cellulose Aerogels. *Molecules* **2018**, *23*, 2082.
47. Zhao, T.; Chen, Z.; Lin, X.; Ren, Z.; Li, B.; Zhang, Y. Preparation and characterization of microcrystalline cellulose (MCC) from tea waste. *Carbohydrate Polymers* **2018**, *184*, 164-170, doi:https://doi.org/10.1016/j.carbpol.2017.12.024.
48. Reichenauer, G. Structural Characterization of Aerogels. In *Aerogels Handbook*, Aegerter, M.A., Leventis, N., Koebel, M.M., Eds. Springer New York: New York, NY, 2011; 10.1007/978-1-4419-7589-8_21pp. 449-498.
49. Smirnova, I.; Gurikov, P. Aerogels in Chemical Engineering: Strategies Toward Tailor-Made Aerogels. *Annual Review of Chemical and Biomolecular Engineering* **2017**, *8*, 307-334, doi:10.1146/annurev-chembioeng-060816-101458.
50. Phillips, G.O.; Williams, P.A. *Handbook of hydrocolloids*; CRC press Boca Raton, FL: 2000.

51. García-González, C.A.; Alnaief, M.; Smirnova, I. Polysaccharide-based aerogels—Promising biodegradable carriers for drug delivery systems. *Carbohydrate Polymers* **2011**, *86*, 1425-1438, doi:<https://doi.org/10.1016/j.carbpol.2011.06.066>.
52. Bertini, I.; Sabatini, A. Infrared Spectra of Substituted Thiocyanate Complexes. The Effect of the Substituent on Bond Type. II. *Inorganic Chemistry* **1966**, *5*, 1025-1028, doi:[10.1021/ic50040a017](https://doi.org/10.1021/ic50040a017).
53. Chen, W.; Yu, H.; Li, Q.; Liu, Y.; Li, J. Ultralight and highly flexible aerogels with long cellulose I nanofibers. *Soft Matter* **2011**, *7*, 10360-10368, doi:[10.1039/C1SM06179H](https://doi.org/10.1039/C1SM06179H).
54. Maleki, H.; Durães, L.; García-González, C.A.; del Gaudio, P.; Portugal, A.; Mahmoudi, M. Synthesis and biomedical applications of aerogels: Possibilities and challenges. *Advances in Colloid and Interface Science* **2016**, *236*, 1-27, doi:<https://doi.org/10.1016/j.cis.2016.05.011>.
55. Schestakow, M.; Karadagli, I.; Ratke, L. Cellulose aerogels prepared from an aqueous zinc chloride salt hydrate melt. *Carbohydrate Polymers* **2016**, *137*, 642-649, doi:<https://doi.org/10.1016/j.carbpol.2015.10.097>.
56. Kampschulte, M.; Langheinrich, A.C.; Sender, J.; Litzlbauer, H.D.; Althöhn, U.; Schwab, J.D.; Alexandre-Lafont, E.; Martels, G.; Krombach, G.A. Nano-Computed Tomography: Technique and Applications. *Rofo* **2016**, *188*, 146-154, doi:[10.1055/s-0041-106541](https://doi.org/10.1055/s-0041-106541).
57. Coenen, A.M.J.; Bernaerts, K.V.; Harings, J.A.W.; Jockenhoevel, S.; Ghazanfari, S. Elastic materials for tissue engineering applications: Natural, synthetic, and hybrid polymers. *Acta biomaterialia* **2018**, *79*, 60-82, doi:<https://doi.org/10.1016/j.actbio.2018.08.027>.
58. Ozdemir, E.; Sendemir-Urkmez, A.; Yesil-Celiktas, O. Supercritical CO₂ processing of a chitosan-based scaffold: Can implantation of osteoblastic cells be enhanced? *The Journal of Supercritical Fluids* **2013**, *75*, 120-127, doi:<https://doi.org/10.1016/j.supflu.2012.12.031>.
59. Lindman, B.; Karlström, G.; Stigsson, L. On the mechanism of dissolution of cellulose. *Journal of Molecular Liquids* **2010**, *156*, 76-81, doi:<https://doi.org/10.1016/j.molliq.2010.04.016>.
60. Jiang, F.; Hsieh, Y.-L. Dual Wet and Dry Resilient Cellulose II Fibrous Aerogel for Hydrocarbon–Water Separation and Energy Storage Applications. *ACS Omega* **2018**, *3*, 3530-3539, doi:[10.1021/acsomega.8b00144](https://doi.org/10.1021/acsomega.8b00144).
61. Cervin, N.T.; Johansson, E.; Larsson, P.A.; Wågberg, L. Strong, Water-Durable, and Wet-Resilient Cellulose Nanofibril-Stabilized Foams from Oven Drying. *ACS Applied Materials & Interfaces* **2016**, *8*, 11682-11689, doi:[10.1021/acsami.6b00924](https://doi.org/10.1021/acsami.6b00924).



Chapter 3.

CELLULOSE AEROGEL MICROFIBERS FOR DRUG DELIVERY APPLICATIONS

This chapter is based on the following publication:

Rostamitabar, M.; Subrahmanyam, R.; Gurikov, P.; Seide, G.; Jockenhoevel, S.; Ghazanfari, S. Cellulose aerogel micro fibers for drug delivery applications. *Materials Science and Engineering: C* **2021**, 127, 112196

Abstract: Textile engineering can offer a multi-scale toolbox via various fiber or textile fabrication methods to obtain woven or nonwoven aerogels with different structural and mechanical properties to overcome the current limitations of polysaccharide-based aerogels, such as poor mechanical properties and undeveloped shaping techniques. Hereby, a high viscous solution of microcrystalline cellulose and zinc chloride hydrate was wet spun to produce mono and multi-filament alcogel microfibers. Subsequently, cellulose aerogel fibers (CAF) were produced and impregnated with model drugs using supercritical CO₂ processes. Fibers were characterized in terms of morphology and textural properties, thermal stability, mechanical properties, and *in vitro* biological and drug release assessments. Loaded and non-loaded CAFs proved to have a macro-porous outer shell and a nano-porous inner core with interconnected pore structure and a specific area in the range of 100-180 m²/g. The CAFs with larger diameter ($d \sim 235 \mu\text{m}$) were able to form knitted mesh while lower diameter fibers ($d \sim 70 \mu\text{m}$) formed needle punched nonwoven textiles. Humidity and water uptake assessments indicated that the fibrous structures were highly moisture absorbable and non-toxic with immediate drug release profiles due to the highly open interconnected porous structure of the fibers. Finally, CAFs are propitious to be further developed for biomedical applications such as drug delivery and wound care.

3.1 Introduction

There is a growing demand for nonwoven and woven materials that are mainly fabricated from petroleum-based resources; however, numerous research studies are trying to fabricate new value-added, sustainable, and competitive products originating from renewable materials such as cellulose [1-3]. Textile engineering is offering a multi-scale toolbox via various fabrication methods of fibers and fabrics for versatile biomedical applications. The current biomedical fibrous structures having a wide range of morphology, composition, and functionality are used in different applications, such as personal protective textiles, skin grafts, tissue engineering scaffolds, and wound dressings [3,4]. The high sensitivity of biomaterial and pharmaceutical agents to the processing condition requires the development of innovative technologies for processing and treatments. Mild temperature supercritical carbon dioxide (scCO₂) processes are currently utilized to produce highly porous and low-density material so-called aerogels [1,5]. Cellulose aerogels (CAs), due to their biocompatibility and biodegradability as ultra-lightweight material with 3D interconnected porous network structure, have been used in drug delivery [6,7], tissue engineering [8,9], and wound healing [10,11] applications.

CAs are typically fabricated in three steps: dissolving or dispersing cellulose, gel formation and aging followed by drying, which can be freeze-drying or scCO₂ drying. In the latter case, the 3D structure of the gel is merely retained [12,13]. The CAs are also suitable candidates to be loaded with various bioactive agents. Three aerogel impregnation processes have been evolved for loading drugs and bioactive agents, which are the incorporation of the drug to the dissolving mixture before the gelation (gel formation), the addition of the drug through the aging step (solvent exchange), and the inclusion of drug during adsorption/precipitation in the dried aerogels (post-treatment) [11, 29]. The solubility of the drug in the gel solvent and scCO₂ plays an important role in selecting the right impregnation technique.

Despite CAs outstanding properties, these bioaerogels typically suffer from poor mechanical properties as well as undeveloped fiber processing methods which have limited their shape mainly to monoliths [14,15], cylinders [16,17], and beads/microparticles [9,18,19]. The main limiting factor to produce fibers from most of the bio-based polymers, such as cellulose, is that they do not melt due to the existence of strong hydrogen bonding between macromolecule chains. These hydrogen bondings increase the melting point over the degradation temperature; therefore, processing these raw materials into fiber and finally textile requires dissolution, extrusion, gelation/solidification, and drawing.

Wet spinning is a method for the efficient fabrication of solid/gel fibers from cellulose solutions. Wet spun cellulose fibers often lead to microfibers with better mechanical properties than nanofibers fabricated by electrospinning [20]. In wet spinning, cellulose solution is pumped through a spinneret. Solid/gel fibers are formed when the stream reaches the coagulation bath and are subsequently drawn and collected on a bobbin. Inorganic salt melt hydrates, such as ZnCl_2 aqueous solution, are proved to be low-cost, non-derivatizing, and direct solvents for spinning cellulose [21-23]. Therefore, shaping CAs into fibers or filaments is appealing since utilizing textile fabrication methods can transform the fibers into woven, knitted, braided, or nonwoven fibrous structures that hold various structural and mechanical properties.

In literature, there are few studies on wet spun aerogel microfibers production from cellulose [23-27], silk fibroin [28,29], Kevlar [30], polyacrylonitrile [31], silica [32], and graphene [33,34] for versatile fields including thermal insulation, sensors, and flexible batteries and cells. In addition, recently Batista *et.al* fabricated alginate-chitosan aerogel fibers via emulsion gelation for wound healing applications [35]. Nevertheless, to the best of our knowledge, the usage and potential of wet spinning and textile formation of aerogel fibers for biomedical applications specifically from biobased materials, such as cellulose, have not been investigated. Furthermore, different drug loading techniques, drug-eluting behavior, release kinetics, and biological properties of the CAFs have not been studied.

In this study, the CAFs production with two different diameters from high viscose salt melt hydrate of ZnCl_2 (8.3 wt. %), fabricated by knitting and nonwoven textile formation, and impregnated with drug models has been investigated. Moreover, the effect of physio-chemical structure of microcrystalline cellulose (MCC) and CAFs, processing parameters such as the effect of scCO_2 depressurization rate, and the type of alcohol used for the regeneration of the fibers on the textural properties of the aerogels were studied. Solvent exchange and post-treatment impregnation processes using scCO_2 were investigated for loading of the drug models, methyl blue (MB), rhodamin B (RB), and fluorescein (FL).

MB is a triphenylmethane acid dye with antiseptic properties which can be utilized as a fluorescent probe, biological staining agent, and pH indicator [36]. RB and FL are well-known fluorophores which have been used as tracer diagnostic tools and labeling agent in the biomedical field [37-39]. Also, the difference between the polarity, molecular weight, water solubility, and chemical structure of the drug models could provide a closer description of appropriate solute/solvent systems and loading techniques to load

other bioactive agents within CAFs. After the solvent exchange, drug loading, drug release from the CAFs was measured over 24 h. The release data were rationalized with the kinetics models such as first-order and Peppas-Sahlin in order to define the mass transport mechanism of the drug release. In the end, *in vitro* assessments were performed to explore cytotoxicity, biocompatibility, and the interaction of the cellulose aerogel fibrous structures with the fibroblast cells.

3.2 Material and Methods

3.2.1 Materials

MCC with product number C6288 (degree of polymerization of 159), MB, cell proliferation kit II (XTT assay), and propidium iodide, as fluorescent cell staining, were obtained from Sigma-Aldrich. Calcein, a fluorescent probe for staining viable cells, was purchased from Biomol. Gibco™ Dulbecco's modified Eagle's medium (DMEM) with 10% Gibco™ fetal calf serum (FCS) were bought from Thermo Fisher Scientific. ZnCl_2 (97%), RB and FL were purchased from Alfa Aesar. For regeneration and washing the fiber samples, absolute isopropanol (iPrOH) ($\geq 99,7\%$, 2-Propanol CP) and ethanol (EtOH) from Biosolve were used. Carbon-dioxide (CO_2) cylinders (2.7 grade, 50 L) with a purity of 99.7 % from Linde Gas Benelux was used in the drying process. Finally, all materials were used without further purification.

3.2.2 Solution preparation

The MCC was dried at 100 °C in a vacuumed oven overnight to remove the moisture and achieve a constant weight. Spin dopes were prepared using 60 % zinc chloride (36 g), 31.66 % deionized water (19 mL), and 8.33 % microcrystalline cellulose (5 g). First, half of the deionized water was added to swell the cellulose chains and avoid agglomeration during mixing with the salt; subsequently, ZnCl_2 salt and the rest of the deionized water were added to the wet powder. Homogenous clear solutions were obtained by dissolving the cellulose at 70 °C and using a mechanical stirrer (100 rpm) after an approximate time of 45 min. Furthermore, two additional lower cellulose concentration solutions (3 and 6 wt%) were similarly prepared to inspect the effect of concentration increment on the cross-sectional morphology of the fibers by scanning electron microscopy.

3.2.3 Fiber spinning, gel washing, and textile fabrication

The spinning was carried out by a customized wet-spinning “LabLineCompact” unit (DIENES Apparatebau GmbH, Germany) (**Figure 3.1A-I**). To reduce the viscosity, the spinning dope required to be spun at an elevated temperature around 70 °C; therefore,

three heaters with suitable controllers were added to the tank, pump, and nozzle pipe. The air pressure (2-3 bar) and pump rate (1.5 mL/min) were applied during the spinning of the multifilament alcogel fibers (spinneret capillary diameter = 100 μm , 100 holes) (**Figure 3.1A-II**) and the monofilament alcogel fibers (spinneret capillary diameter = 330 μm) (**Figure 3.1A-III**). The spinning dope (50 mL) was added to the tank, and the fibers were spun in the iPrOH bath (30 L) without passing through an air gap between the nozzle and the regeneration bath. A customized winder was designed and placed directly in the regeneration bath to prevent alcogel fibers from drying (**Figure 3.1A-IV**).

Alcogel fibers were pulled and winded in the bath at the rate of 20-25 rpm. The wet spun fibers were transferred into a beaker containing fresh iPrOH. Moreover, to remove the residual salt from fibers and avoid excessive solvent consumption, fibers with their bobbins were placed in cellulose thimbles and washed in a customized soxhlet extractor system (NS 100) (**Figure 3.1B-I**). The extractor pipe (siphon return line) was designed 3 cm above the lowest part of the extraction chamber to keep a reasonable amount of solvent in the chamber and avoid gel drying during the periodical emptiness of the thimble. The presence of salt left-overs was checked by conductivity meter and spot test (**Figure 3.1B-II**). The spot test was performed with silver nitrate (1% wt/v) since acidified Ag^+ gives a white curdy precipitate with Cl^- .

The textiles were formed manually; knitted meshes were created by using a knitting loom and monofilament fibers, and needle punched nonwoven was produced by 3 felting needles purchased from Panduro (coarse, medium, and fine needles, each 7.5 cm long) with a needle base (8 \times 10 \times 1.8 cm, L \times W \times H) to punch the multifilament fibers.

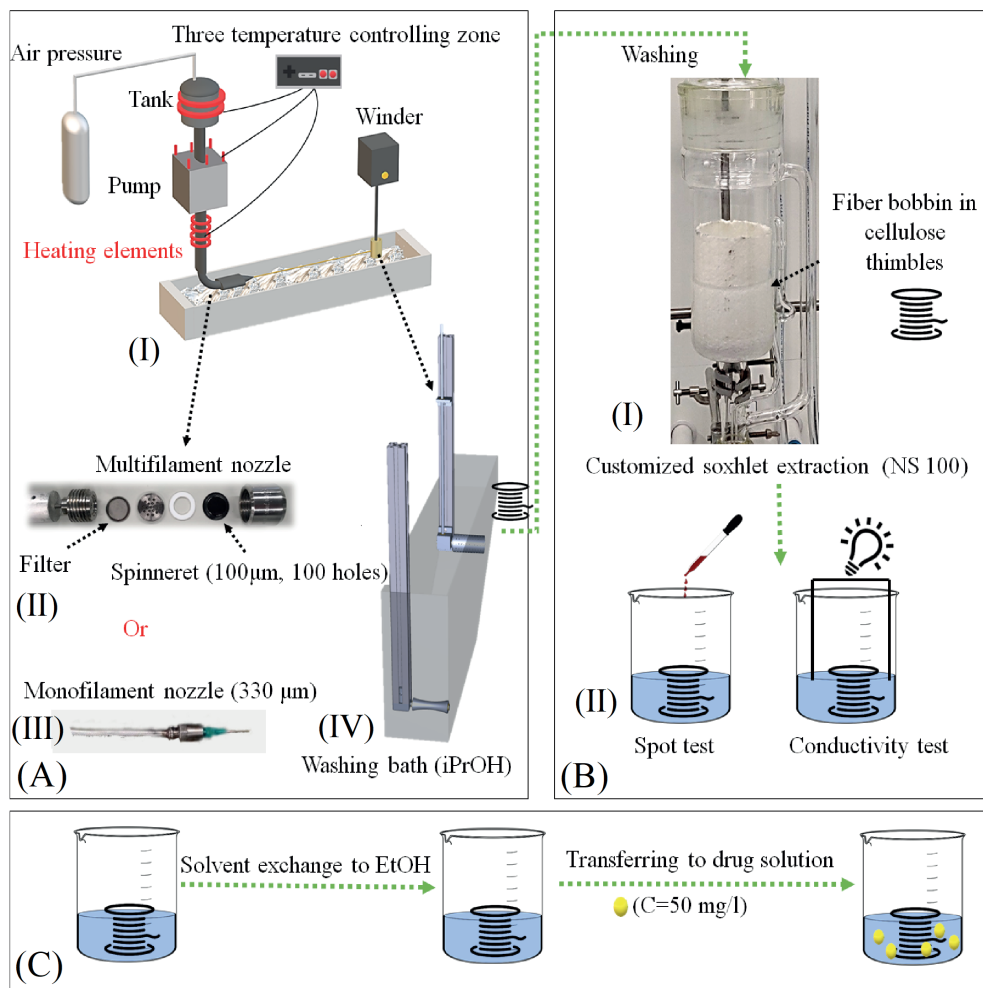
3.2.4 Supercritical CO_2 drying and drug loading

Supercritical CO_2 drying: The drying procedure was performed using scCO_2 dryer HPE 300 (EUROTECHNICA GmbH, Germany). The fabricated alcogel fibers were wrapped in the filter papers and placed in the drying vessel ($V=400$ ml) with a defined excess amount of iPrOH. Samples were dried at 120 bar and 50 $^\circ\text{C}$ over 60 min. During the drying process, the extraction valve of the vessel was manually opened to vent the alcohol-rich mixture of CO_2 into a plastic flask while the pressure and temperature of the vessel remained constant. The extraction cycle of the alcohol-rich stream was repeated 5 times for a duration of 3 min each. In the end, the vessel was depressurized in 10 min using a backpressure regulator, and the vessel was opened when it cooled down to room temperature. The CAFs were instantly placed in a tightly sealed sample

holder under dry N_2 purge to prevent the samples from absorbing the moisture of the environment.

Drug loading: For the impregnation of MB, RB and FL (**Figure Appendix 3.1.A**) by the solvent exchange step, salt-free alcogels in iPrOH were washed with absolute EtOH in a 1 L beaker two times since the aforementioned model drugs had very low solubility in iPrOH. 50 mg of each model drug was dissolved in 1 L of EtOH, and the solution was stirred at 50 °C with a rate of 200 rpm for 24 h. Around 500 mg of each alcogel fiber was immersed in 2 L of the drug solution and stirred at 50 rpm for 24 h so that the drug could diffuse into all gel bodies (**Figure 3.1C**). In the next step, drug-loaded alcogel fibers were wrapped in the filter paper and transferred to the vessel ($V=100$ mL) of the $scCO_2$ dryer. A defined excess amount of the same drug solution for each sample was added to the vessel to prevent ambient drying of the alcogels and $scCO_2$ drying was performed similarly to the unloaded CAFs.

For the post-treatment impregnation of dried aerogels with the model drugs, 25 mg of each drug was placed at the bottom of the high-pressure vessel ($V=100$ ml) with a magnetic bar. Then, 100 ± 10 mg of the dried aerogel fibers wrapped in filter papers were placed inside a porous cylinder that had a gap with the bottom of the vessel to avoid any contact between the fibers and the drug powders containing a rotating magnetic bar. A magnetic stirrer was placed under the vessel, and the pressure and temperature of CO_2 were set at 200 bar and 50 °C. After 24 h, the vessel was depressurized over 60 min.

**FIGURE 3.1.**

Schematic representation of wet spinning and fabrication of the salt-free alcogel fibers. (A) Wet spinning and designed components, (I) customized wet spinning line with heating elements, (II) multifilament nozzle with the filter and the spinneret containing 100 holes of 100 µm, (III) monofilament nozzle with an internal diameter of 330 µm. (IV) A custom made winder to collect the alcogel fibers within the bath to avoid drying of the alcogel fibers. (B) Washing process of the alcogel fibers using fresh iPrOH, (I) a customized soxhlet extraction (NS 100) loaded with cellulose thimbles containing alcogel fiber bobbins, (II) evaluation of the salt leftover in alcogel fibers using spot test and conductivity test. (C) Solvent exchange impregnation process of alcogel fiber by immersing them in 50 mg/L drug solutions.

3.2.5 FTIR

Fourier Transform Infrared (FTIR) spectroscopy was performed on the MCC and the fibers with a frontier FT-IR/NIR (Perkin Elmer, USA), and the spectrum was averaged over 32 spectra with a resolution of 2 cm⁻¹ from a range of 4000 till 500 cm⁻¹ in the reflectance mode.

3.2.6 XRD

Two-dimensional (2D) wide-angle X-ray diffraction (WAXD) analysis on samples was performed using a Ganesha diffractometer (SAXSLAB, Denmark) with a sample-to-detector distance of 116.536 mm. Cu K α radiation ($\lambda = 1.5406 \text{ \AA}$) and silver behenate ($d_{001} = 58.380 \text{ \AA}$) used for calibration were measured for 600 s. The diffraction spectrum was shown by the θ -2 θ geometry.

The crystallinity index percentage (CrI (%)) was determined by the empirical estimation method of Segal *et al.* [40] as the percentage of crystalline material in the sample expressed by the following equation:

$$\text{CrI}(\%) = \frac{I_{002} - I_{\text{am}}}{I_{002}} \times 100 \quad \text{Equation (3.1)}$$

where for cellulose I, I_{002} is the maximum intensity of the (0 0 2) lattice diffraction at $2\theta \approx 22.6^\circ$ and I_{am} is the intensity at $2\theta \approx 18.7^\circ$ representing the amorphous part in the cellulose fibers. For cellulose II, I_{002} and I_{am} is the intensity at $2\theta \approx 20^\circ$ and 16° , respectively.

3.2.7 Thermal gravimetric analysis

The thermal stability and degradation of the MCC and loaded and non-loaded fibers were studied by a TA Q500 thermo-gravimetric instrument (TA Instruments, USA). Samples were heated from 20 °C to 500 °C with a rate of 10 °C min⁻¹ under N₂ purge.

3.2.8 Scanning electron microscopy and Micro-computed tomography

Scanning Electron Microscopy (SEM): Micrograph images of the CAFs' cross-sections and surface were acquired by Teneo scanning electron microscope (Thermo Fisher Scientific, USA). All fibers were broken in liquid nitrogen and coated with a 3 nm thick layer of iridium. Images were obtained using 5 kV voltage at a working distance of 10 mm. SEM images were analyzed using Image J (version 1.8.0_172, NIH, USA).

Linear shrinkage ΔL of samples were determined from the SEM images by measuring the diameter of the samples after spinning (D_i) and after drying (D_f) using equation (2):

$$\Delta L (\%) = \frac{D_i - D_f}{D_i} \times 100 \quad \text{Equation (3.2)}$$

X-ray microtomography (μ -CT): Stack images were obtained using Skyscann 127211MP (Bruker, USA) at the source voltage and current of 40 kV and 200 μ A, respectively, with an exposure time of 1.5 s and the image pixel size of 0.8 μ m. A CTAn analyzer (version

1.18.8.0+) was utilized to calculate the macroporosity from 2D aerogel structures within three different regions of interest for each sample. In order to visualize 3D images of the samples, CTvox software (version 3.3.0 r1403) was used.

3.2.9 Textural properties (porosity, surface area, and pore volume)

Porosity: The porosity (\emptyset) was estimated from the bulk density and skeletal density as follows:

$$\emptyset(\%) = \frac{V_{\text{pores}}}{V_{\text{material}}} = 1 - \frac{\rho_{\text{bulk}}}{\rho_{\text{skeletal}}} \times 100 \quad \text{Equation (3.3)}$$

Where the skeletal density (ρ_{skeletal}) of cellulose is 1.501 g.cm⁻³ [41], and the bulk density (ρ_{density}) was estimated as the mass to volume ratio of the three small cylindrical samples. The samples' diameters and lengths were in the range of 1.8-2 mm and 2.3-2.7 mm, respectively. The dimension of the samples was measured by a digital vernier calipers.

Surface area and pore volume: The specific surface area of the CAFs were measured by using the Nova 4200e Surface Area Analyzer (Quantachrome GmbH and Co. KG, Germany). The samples were degassed at 80 °C over 24 h, and the Brunauer–Emmett–Teller (BET) method was utilized to determine the specific surface area (SA_{BET}). Moreover, the pore size distribution and average pore size were obtained from the Barrett-Joyner-Halenda (BJH) model.

3.2.10 Mechanical properties

The linear density, tensile strength, and elongation measurements of the CAFs were performed using Textechno Favimat+ single fiber testing machine (Herbert Stein GmbH & Co., KG, Germany). The device was equipped with a load cell of 210 cN, and the linear density and tensile measurements were carried out at the rate of 10 mm/min. To address the coarse structure of the fibers and the resulting stiffness, high gauge lengths (20 mm) and high pretensions (1cN/tex) were used.

3.2.11 Humidity absorbance and water uptake

Humidity absorbance: Three replicates of CAFs (each 100 ± 10 mg) with two different diameters were dried in a vacuum oven at 90 °C around 24 h to reach a constant weight. Subsequently, they were placed for 24 h in a humidity chamber at 25 °C with relative humidity (RH) of 50% and 80%. The weight of the samples was instantly measured before (W_{oven}) and after keeping it in the humidity chamber (W_{chamber}).

Humidity absorbance weight ratio ($W_{RH\%}$) was measured by:

$$W_{RH\%} = \frac{W_{chamber} - W_{oven}}{W_{oven}} \times 100 \quad \text{Equation (3.4)}$$

$W_{RH\%}$ is the weight ratio of the absorbed humidity at the relative humidity of (X), (W_{oven}) is the weight after drying the CAFs in the vacuum oven and $W_{chamber}$ is the weight of the fibers after removing from the humidity chamber.

Water uptake: The water uptake was measured after 1, 8, and 24 h and performed on the knitted mesh and nonwoven patch in the PBS solution (pH 7.4, 37 °C) to avoid single fibers breakage and agglomeration. The weight of the swollen samples (W_{wet}) was measured after removing excess water with filter paper for each time point utilizing three replicates. The water uptake weight ratio (WU) (%) was calculated as follows:

$$WU(\%) = \frac{W_{wet} - W_{oven}}{W_{wet}} \times 100 \quad \text{Equation (3.5)}$$

3.2.12 In vitro drug loading efficiency, release, and kinetics

Drug loading efficiency: In order to calculate the drug loading efficiency of the solvent exchange impregnation, several assumptions were taken into account. It was assumed that fibers had perfect cylindrical shapes, and the alcogel fiber volume was mainly equal to the ethanol volume since ethanol filled up the majority of the gel matrix. Furthermore, it was assumed that the diffusion of the drugs into the alcogel fibers was complete, meaning that the concentration of the drug in the solution was equal to that in the alcogel fiber ($C_{alcogel} = C_{ethanol}$) and the drug mass loss during $scCO_2$ drying was negligible. The theoretical drug dose (M_{theo}) can be then expressed as:

$$M_{theo}(mg) = V_{alcogel}(cm^3) \times C_{ethanol} \left(\frac{mg}{cm^3} \right) \quad \text{Equation (3.6)}$$

Experimental drug doses (M_{exp}) were obtained after washing 100 ± 10 mg of the fibers using 1 L of ethanol in a soxhlet extraction system for 72 h and subsequently measuring the concentration of the drug in the final solution. Drug loading efficiency (%), aerogel loading capacity (wt.%), and aerogel specific loading (mg/m²) can be defined as:

$$\text{Drug loading efficiency (\%)} = \frac{M_{exp}(g)}{M_{theo}(g)} \times 100 \quad \text{Equation (3.7)}$$

$$\text{Drug loading capacity (wt.\%)} = \frac{M_{exp}(g)}{M_{aerogl}(g)} \times 100 \quad \text{Equation (3.8)}$$

$$\text{Aerogel specific loading } \left(\frac{\text{mg}}{\text{m}^2} \right) = \frac{\text{Aerogel loading capacity (wt\%)}}{\text{Specific surface area } \left(\frac{\text{m}^2}{\text{g}} \right)} \times 1000 \text{ Equation (3.9)}$$

The drug loading efficiency of the post-treatment method (in scCO_2) was obtained by measuring the weight of the aerogel fibers before (M_i) and after (M_f) the impregnation as expressed by:

$$\text{Drug loading efficiency (\%)} = \frac{M_i (\text{g})}{M_f (\text{g})} \times 100 \text{ Equation (3.10)}$$

Nevertheless, the drug loading efficiency of the post-treatment method was very low (0.01 %) and the drugs were slightly adsorbed only on the surface of the fibers. Thus, the post-treatment loaded fibers were not investigated in further characterization steps.

In the result and discussion part, the CAF samples were named as ($F_{\text{diameter-solvent or drug}}$) in which the subscript refers to the wet spun initial diameter of the nozzle, the final solvent before drying, and the type of the drug that the fiber was loaded with. **Table 3.1** summarizes the fabricated samples and their corresponding abbreviation and characteristics.

TABLE 3.1.

Fabricated samples and their labels.

SAMPLE NAME	SPINNING NOZZLE DIAMETER (μm)	SOLVENT PRIOR TO THE scCO_2 DRYING	TYPE OF THE LOADED DRUG
$F_{330iPrOH}$	330	Isopropanol	-
$F_{330EtOH}$	330	Ethanol	-
$F_{100iPrOH}$	100	Isopropanol	-
$F_{100EtOH}$	100	Ethanol	-
F_{330RB}	330	Ethanol	Rhodamine B
F_{100RB}	100	Ethanol	Rhodamine B
F_{330FL}	330	Ethanol	Fluorescein
F_{100FL}	100	Ethanol	Fluorescein
F_{330MB}	330	Ethanol	Methyl blue
F_{100MB}	100	Ethanol	Methyl blue

Drug release: 100 ± 10 mg of drug-loaded CAFs were immersed in 100 ml PBS solution ($\text{pH} = 7.4$) at 37°C and stirred at a rate of 50 rpm. 16 samples over 24 h at various time intervals were measured as follows: 2 ml from the PBS and sample solution was

transferred into a vial and subsequently, 2 ml of fresh PBS was added to the solution to maintain a constant medium volume. The measurements were performed in triplicate. Using a UV-visible UV3600 spectrophotometer (Shimadzu, Japan), the maximum absorption peaks for MB, RB, and FL in PBS solution were at the wavelengths of 306, 554, and 490 nm, respectively.

The blank, calibration material, and all the collected samples over time were placed in 96 well plates, and Synergy™ HTX multi-mode microplate reader (BioTek, USA) was used to obtain the intensities. The Beer-Lambert law was utilized to obtain the concentration of the drug, and cumulative drug release was calculated by:

$$Q(\%) = \frac{C_n V + V_i \sum_{i=0}^{n-1} C_i}{M_{\text{exp}}} \times 100 \quad \text{Equation (3.11)}$$

Q (%) is the percentage of the cumulative released drug, and V (mL) was the total volume of the samples. C_n (mg/mL) and V_i (mL) were the concentration and the volume of the samples taken at n and i time points. M_{exp} (mg) was the actual weight of the drug in the fibers, and the number of times that the drug release media was replaced is shown as n .

Kinetics of release: First-order and Korsmeyer-Peppas were selected as the mathematical models to fit the experimental data obtained from the drug release measurements from the CAFs since previous drug release studies showed CAs were stable (no erosion) in aqueous media [42]. The correlation coefficient (R^2) was calculated to define the accuracy of each model.

First-order: The first-order release kinetics is corresponding to the amount of the loaded drug in the fiber matrix. This model results in a constant release over time, and the rate is only reliant on the initial drug concentration [43,44]. The cumulative released fraction ($Q(t)$) can be described by:

$$Q_{(t)} = 1 - \exp(-k_1 t) \quad \text{Equation (3.12)}$$

where $(1 - Q_{(t)})$ represents the remaining fraction of the drug at the time t in the system, and k_1 is the first-order constant.

Korsmeyer-Peppas: The Korsmeyer-Peppas, known as the power-law model, explains the exponential relationship between the release and the time [44,45]. The model is expressed by:

$$Q_{(t)} = \frac{M_t}{M_{\text{tot}}} = K_{\text{KP}} t^n \quad \text{Equation (3.13)}$$

Where M_t is the amount of the drug at the time t , M_{tot} is the total amount of the loaded drug, K_{kp} is the constant accounting for the structural and geometrical characteristics of the system, and m is the exponent of the release related to the drug release mechanism. This model is limited to the first 60% of cumulative release or $Q(\%) < 60\%$. In case of $n < 0.45$, Fickian diffusion takes place by the typical molecular diffusion of the drug due to a chemical potential gradient. When $0.45 < n < 0.89$, the release is controlled by the effect of both diffusion and polymer relaxation (swelling or erosion).

3.2.13 In Vitro cell viability and proliferation studies

Human dermal fibroblasts were isolated from the adult skin biopsies as previously described by Kreimendahl *et al.* [46]. Cells were cultured at 37 °C and 5% CO₂ in DMEM with 10% fetal calf serum (FCS). Cells at passage 4 were used for the viability and proliferation experiments using XTT and live dead staining. The CAFs samples were sterilized in 70% ethanol and washed in PBS prior to the tests.

XTT assay was performed according to the ISO 10993-12. In short, samples, positive control, and negative control were incubated in a culture medium for 72 h. The negative control was a piece of polyethylene tube, and the positive control was a piece of a latex glove. Cells were seeded in 96-well plates (1×10^4 cells per well) and were allowed to adhere to the wells for 24 h. After 24 h, cell medium was exchanged with sample medium, positive control, and negative control or blank. After different incubation periods of 1, 3, and 7 days, the XTT assay was performed according to the manufacturer's protocol. The absorbance was measured in a multimode microplate reader M200 (Tecan, Switzerland) at 450 nm with a reference wavelength of 630 nm. The assessment was performed in three replicates.

For the live-dead assay, nonwoven textiles were punched using a biopsy punch and were placed in 96-well plates. Cells were seeded on the textile with a concentration of 5×10^4 cells per well. Live-dead assay on days 1 and 7 was performed according to the manufacturer's protocol as described previously [47]. Images were obtained using an inverted confocal microscope (Leica SP8, Germany).

3.2.14 Statistical analysis

All the experimental data are expressed as means \pm standard errors (SD). The statistical analysis was done by Originlab (2019 b) using a significance level of $p < 0.05$. Student t-test and one-way ANOVA based on the Tukey test was performed to determine the differences between different data groups.

3.3 Results and Discussion

3.3.1 Estimation of cellulose aerogel fibers density and porosity

The salt-free alcogel fibers and cylinders were successfully prepared. After scCO_2 drying, white opaque mono and multifilament CAFs (8.3 wt.%) were obtained (**Figure 3.2A-I and II**). The bulk density and porosity of the fibers were estimated from the small fabricated cylinders (8.3 wt.%) (**Figure 3.2A-III**) as $0.188 \pm 0.025 \text{ g/cm}^3$ and $87.5 \pm 1.7 \text{ (\%)}$, respectively. By considering the higher cellulose concentration of the fabricated CA cylinders and comparing them to the reported values for the density of the lower concentration CAs (e.g., 0.14 g/cm^3 for 6 wt.%) produced from similar salt melt hydrates, it can be concluded that the obtained density and porosity data are in agreements with previous studies [25,48].

3.3.2 Structural properties and crystallinity by FTIR and WAXS

Fourier transform infrared spectroscopy: FTIR spectra of the cellulose powders and fabricated CAFs in the wave number region of $4000\text{--}500 \text{ cm}^{-1}$ are exhibited in (**Figure 3.2B**). The cellulose spectra showed bands at $3650\text{--}3000 \text{ cm}^{-1}$ (O-H hydroxyl group stretching vibration), $2900\text{--}2800 \text{ cm}^{-1}$ ($-\text{CH}_2-$ alkyl stretching vibration), 1645 cm^{-1} (C=O stretching), and 1020 cm^{-1} (C-O stretching). The presence of numerous intra- and inter-molecular hydrogen bonds between hydroxyl groups organize cellulose chains in a semi-crystalline structure with a low ordered amorphous region in two polymorphs of cellulose I and cellulose II (**Figure 3.2C-I**) [49]. The crystalline structural transformation of cellulose from cellulose I to cellulose II were studied with the investigation of absorption bands at 897 , 1107 , 1161 and 1430 cm^{-1} , which are attributed to group C_1 frequency, ring asymmetric stretching, C-O-C asymmetric stretching, and CH_2 symmetric bending vibration mainly in cellulose I, respectively.

In addition, the 893 cm^{-1} absorption band (β -glucosidic linkages between the sugar units) confirmed that the crystalline cellulose I can be almost insignificant in the regenerated cellulose fibers since the 893 cm^{-1} is allocated to group C_1 frequency in cellulose II [30,31]. In comparison with the MCC, the CAFs retained the most original FTIR peaks in a broader form, except for the cellulose I peaks, which were mainly vanished or decreased significantly. Besides, to ensure that the salt-free CAFs were produced, no chlorinated compound peaks were observed [50,51]. The peaks from CAF_{EtOH} and $\text{CAF}_{\text{iPrOH}}$ were similar. Furthermore, the FTIR spectra of the drug-loaded CAFs showed a similar pattern to the CAF_{EtOH} (**Figure Appendix 3.1. B, C and D**). However, the main bands of the drug models, such as -OH, C=O, and phenolic C-O stretching's, could not be observed in the FTIR spectrum of the loaded CAFs due to the overlapping

with cellulose bands. The low intensified shoulders in the wavelength range of 700-1000 cm^{-1} can prove the presence of drug models in the aerogels.

Wide-angle X-ray scattering: The spectral detector image (**Figure 3.2C-I**) and XRD diffractogram (**Figure 3.2C-II**) of microcrystalline cellulose exhibited five major diffraction peaks at $2\theta = 14.9$ (1 0 1), 15.9 (1 0 $\bar{1}$), 21 (0 2 1), 22.5 (0 0 2), and 34.6 (0 0 4), which are in agreement with values reported in the literature for cellulose [52,53]. The CAFs samples gave a diffractogram which clearly represented an amorphous structure. This character is validated by the absence or notable reduction of all peaks standing for planes (1 0 1) and (0 0 2) as the characteristic peaks of cellulose I. Moreover, the cellulose aerogels diffractogram shows peaks at $2\theta = 13^\circ$ and 20° , which are the corresponding properties of cellulose II [54]. The crystallite index for the MCC, F_{330} , and F_{100} was 81.15, 27.58, and 28.78 (%), respectively. It is important to mention that no effect of the subsequent solvent change from iPrOH to EtOH was observed on the XRD patterns.

The FTIR and XRD indicated a clear conversion of MCC from cellulose I to cellulose II structure with forming aerogel fibers in the amorphous phase. This notable reduction in crystallinity can be interpreted in the modified hydrogen bonding and antiparallel orientation of cellulose chains, which occurred during dissolving the MCC in the salt melt hydrate and led to the continuous transformation of cellulose I into an amorphous state [22].

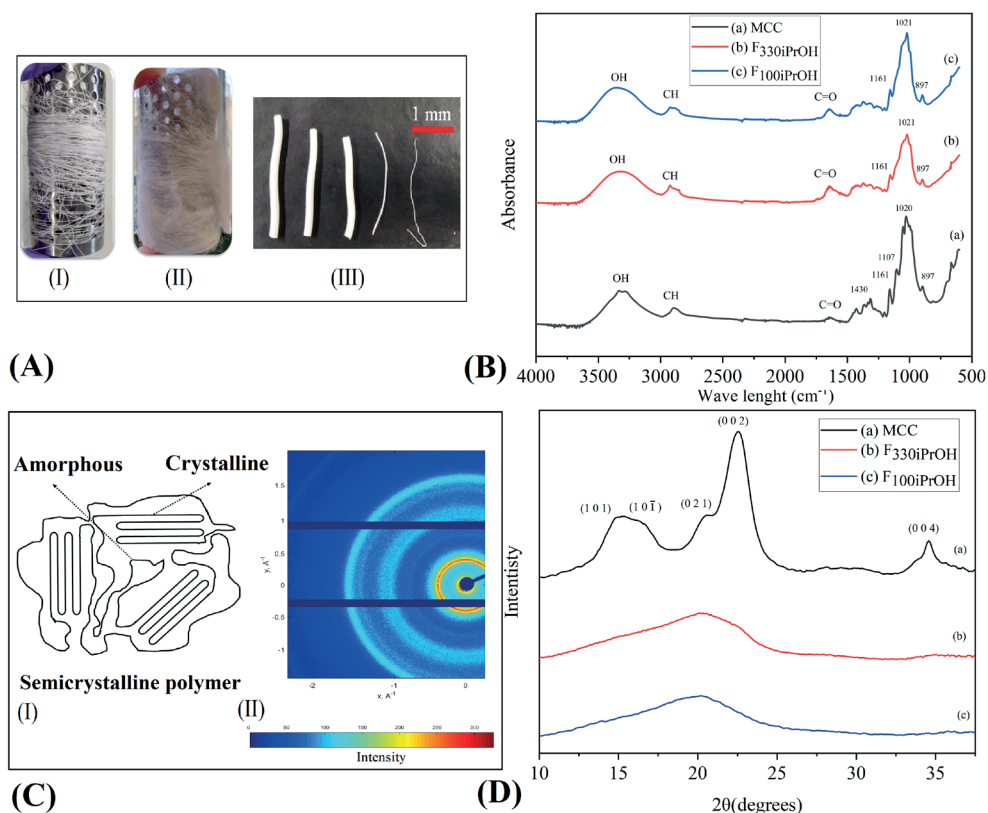


FIGURE 3.2.

(A) The macroscopic images of the produced aerogel; (I) CAF₃₃₀, (II) CAF₁₀₀, and (III) on the left three small cylinders produced for bulk density measurement and CAF₃₃₀ and CAF₁₀₀ on the right. (B) FTIR spectra of MCC and CAFs exhibiting transformation of cellulose I to cellulose II. (C) Crystalline properties of the MCC and the produced fibers; (I) schematic representation of a semicrystalline polymer, (II) the detector image of the MCC exhibiting high crystalline regions (the color bar indicates the intensity of the adsorbed radiation, low is blue and high is red). (D) XRD pattern of the MCC and the CAFs proving amorphous structure of the CAFs and the highly crystalline structure of the MCC.

3.3.3 Thermal analysis utilizing TGA and DTA

Thermogravimetric analysis (TGA) curves depicted in **(Figure 3.3A)** showed a first decomposition stage in the range of 30–105 °C for the MCC and the CAFs regenerated in iPrOH due to the loss of moisture and other volatile solvents. A second decomposition stage was found in the range of 220–350 °C for the CAFs and 265–350 °C for the MCC, indicating lower thermal stabilities of the fibers. The differential thermal analysis (DTA) curves shown in **(Figure 3.3B)** implies that the CAFs exhibited a slower degradation rate compared to the MCC. No difference between CAF_{EtOH} and CAF_{iPrOH} was observed.

In the TGA profiles, the fibers exhibited greater weight loss in the first absorbance stage, mainly due to interconnected highly porous structure and higher accessibility

of hydroxyl groups of the cellulose chains to the water molecules. However, the fibers had slightly lower thermal stability in comparison to the MCC because of the lower crystallinity and degradation of the cellulose chains which occurs during the cellulose dissolving process in salt melt hydrates [22].

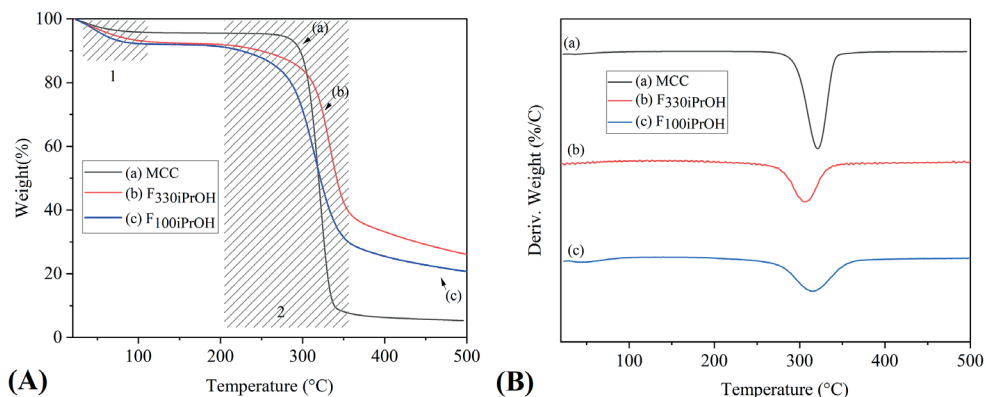


FIGURE 3.3.

A) TGA graphs of the MCC and the CAFs regenerated in iPrOH. The first step (from 30 to 105 °C) in the mass loss was due to the evaporation of water molecules, and the second step at 220–350 °C was the relatively rapid decomposition of the cellulose chains. (B) DTA of the regenerated fibers and the MCC showed that the decomposition range was broader and the rate was slower in the fibers compared to the MCC.

3.3.4 Morphology and structural studies using SEM and μ -CT

Scanning electron microscope: Cellulose aerogels produced in lower concentration (3 wt.%) had a randomly oriented nanofibrillar structure (**Figure 3.4A-I**) while increasing the concentration showed nanofibrils agglomeration in the form of “strands” (6 wt.%) (**Figure 3.4A-II**). With further increase of the cellulose concentration (8.3 wt%), the strands were condensed and the fibers exhibited lower pore size dimensions (**Figure 3.4A-III**) [17,55]. The knotability of the fibers without fibrillation or breakage of the fiber surface is displayed in **Figure 3.4B-I**.

Open porous surface morphologies of the CAFs with the direction of the fibers are shown in **Figure 3.4B-II and III**. Since there was no air gap between the nozzle and the bath, no film formation occurred on the surface of the CAFs; however, F_{330iPrOH} and F_{100iPrOH} exhibited different surface structures. F_{100iPrOH} displayed a porous surface with elongated pores perpendicular to the fiber axis, while F_{330iPrOH} had more elongated pores in the direction of the fiber axis besides more irregular distribution of the pores on the surface. This dissimilarity in the surface morphology and pores elongation alignment can originate from the spinning nozzle compartments. Monofilament spinneret

($F_{100iPrOH}$) benefited from a more complex spinning pack with conical shape spinneret holes. In particular, the spinning dope passed through the multifilament spinning pack in which filter plates caused fluid breakage and better achievement of gel uniformity before being extruded in the coagulation bath.

The textile structure investigated under the microscope showed that the knitted mesh formed by several loops and knots alongside the fiber axis had no sign of breakage or deformation of the fibers (**Figure 3.4C-I**), and the needle punched nonwoven formed a highly condensed patch (**Figure 3.4C-II**).

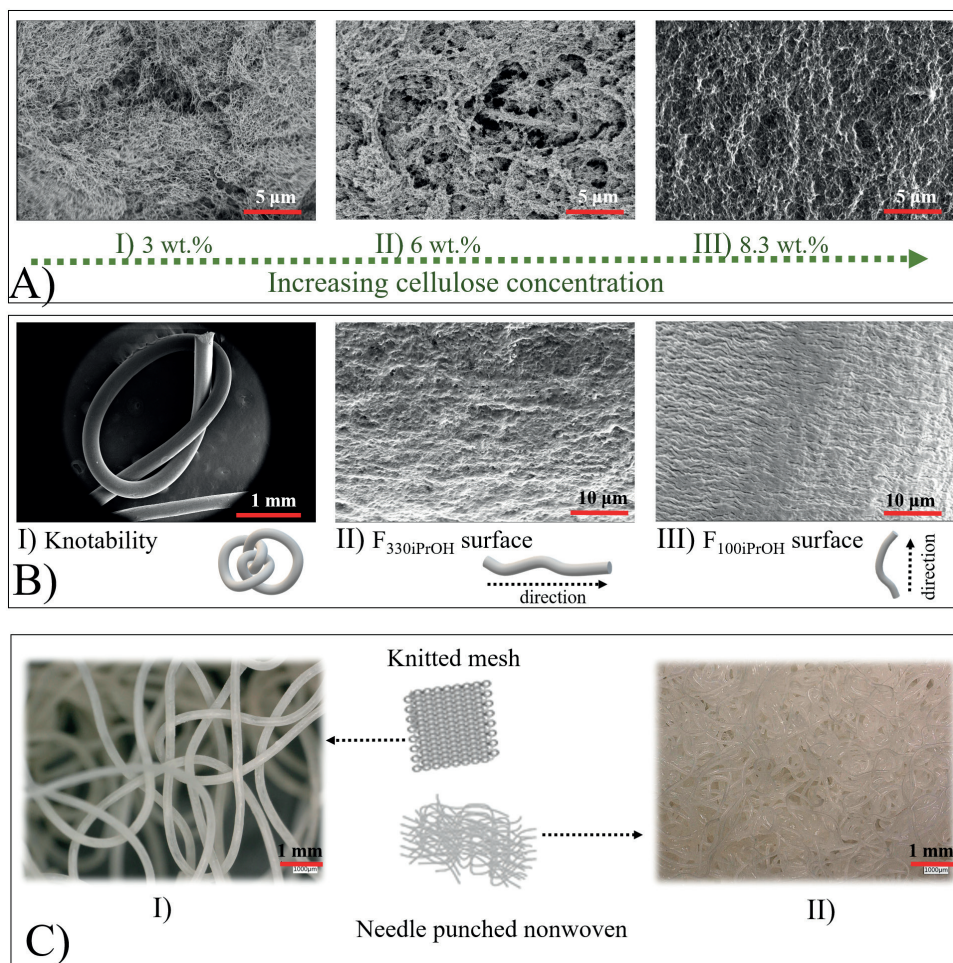


FIGURE 3.4.

(A) SEM images of various concentrations of cellulose showed (I) a random nanofibrillated morphology in 3 wt.%, (II) strand-like morphology in 6 wt.%, and (III) highly condensed structure in 8.3 wt% CAFs with porous structure. (B) The SEM images of the knot made from the $F_{330iPrOH}$ (scale bar 1 mm) (I), (II) porous surface of the $F_{330iPrOH}$ (scale bar 10 μm) alongside the fiber direction, and (III) open surface pores of

the $F_{330iPrOH}$ with perpendicular alignment to the fiber axis (scale bar 10 μm). (C) Microscope images of (I) a knitted mesh with several loops and knots of the CAF_{300} (scale bar 1 mm) and (II) a needle punched nonwoven patch (scale bar 1 mm).

The CAFs cross-sections consisted of a macro-porous outer shell and a nano-porous inner core (**Figure 3.5A-I, II, III, and IV**). The CAFs (8.3 wt%) regenerated in *iPrOH* and ethanol exhibited no specific morphological distinction, and fibers' morphologies were similar to those reported in the CAFs studies [24,25,48]. It is likely that the core-shell structural difference was formed when the hot spinning dope entered the regeneration bath and the alcohol began to vaporize. The alcohol vapor then diffused through the gel matrix and generated macropores in the shell region and accessible pores on the surface of the fiber. With cooling down the fiber in ethanol, this process terminated and was limited to the outer shell of the fiber. In the fibers with a larger diameter, a slightly larger macropore shell is formed as the cooling time is proportional to the fiber diameter. Similar cross-sectional morphology was observed in the fibers impregnated with MB, RB, and FL (**Figure Appendix 3.2**). Also, it can be concluded that the solvent exchange impregnation of the drug models did not lead to the significant collapse of the pores and thus its influence on the morphological properties of the fibers is negligible. The total linear shrinkage of the CAFs after gelation, washing, and scCO_2 drying steps were $25.1 \pm 1.5\%$ and $28.7 \pm 1.1\%$ for CAF_{100} and CAF_{330} , respectively.

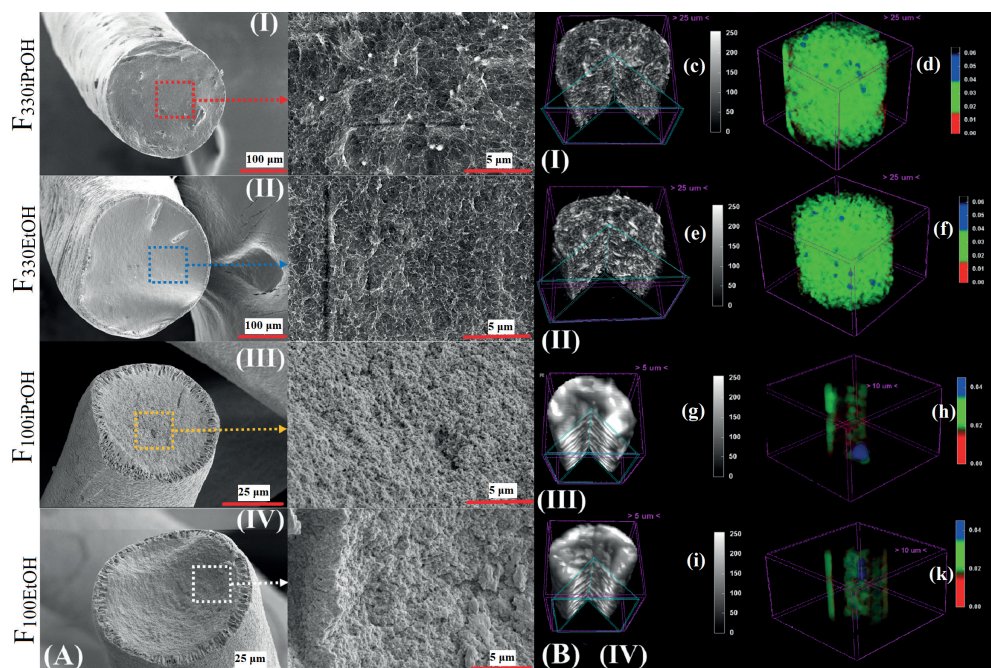


FIGURE 3.5.

(A) Cross-sectional morphology of the cellulose fibers exhibiting a macro-porous outer shell with a nano-porous inner core of (I) $F_{330iPrOH}$ and (II) $F_{330EtOH}$ (magnification and scale bars in the left column (100 μm) and right column images (5 μm)) and (III) $F_{100iPrOH}$ and (IV) $F_{100EtOH}$ (magnification and scale bars in the left side (25 μm) and the right side images (5 μm)). (B) μ -CT computed tomography 3D reconstructions of the CAFs with cut prism shape of the volume indicating interconnected porous structure within the whole volume of the fibers; (I-c) $F_{330iPrOH}$, (II-e) $F_{330EtOH}$, (III-g) $F_{100iPrOH}$, and (IV-i) $F_{100EtOH}$. Defect volume analysis for estimation of the porosity where the macropores have been divided into RGB colors as an indication of the size distribution of the macropores for (I-d) $F_{330iPrOH}$, (II-f) $F_{330EtOH}$, (III-h) $F_{100iPrOH}$, and (IV-k) $F_{100EtOH}$.

X-ray microtomography: μ -CT was used to investigate the 3D microporous architecture of the CAFs (8.3 wt%) regenerated in iPrOH (Figure 3.5B-I-c and III-g) and those subsequently solvent exchanged to ethanol (Figure 3.5B-III-e and IV-i). The reconstructed images of the CAFs volumes indicated that the pores were distributed throughout the fiber matrix. Similarly, defect volume analyses were performed for the CAF_{iPrOH} (Figure 3.5B-V-d and VI-h) and CAF_{EtOH} (Figure 3.5B-VII-f and VIII-k) estimation of porosity where the macropores have been divided into three regions of red, green, and blue as an indication of the macropores size distribution. Detailed information on the percentage of the open and closed pores, the average structural thickness (cellulosic walls between macropores) within the CAFs volume, and the average macropores diameter calculated from μ -CT image stacks are provided in Table 3.2.

TABLE 3.2.

The percentage of the open and closed pores, the average structural thickness (cellulosic walls between macropores) within the CAFs volume, and the average macropores diameter calculated by CTAn software from μ -CT image stacks in different regions of interests.

SAMPLE NAME	OPEN POROSITY (%)	CLOSED POROSITY (%)	STRUCTURE THICKNESS (μm)	AVERAGE DIAMETER OF MACROPORES (μm)
F _{330iPrOH}	59.0 \pm 1.0	0.020 \pm 0.001	7.90 \pm 0.31	9.51 \pm 0.97
F _{330EtOH}	56.29 \pm 0.99	0.021 \pm 0.003	8.51 \pm 0.20	10.0 \pm 1.4
F _{100iPrOH}	38.87 \pm 0.94	0.024 \pm 0.004	13.05 \pm 0.44	7.8 \pm 1.4
F _{100EtOH}	37.201 \pm 0.055	0.031 \pm 0.0043	12.87 \pm 0.38	6.3 \pm 1.9

Overall, the CAF₃₃₀ samples had higher porosity and lower average pore diameter with higher structure thickness than the CAF₁₀₀, and no significant difference between two regeneration alcohols for the same CAF diameter was observed. However, one might notice the resolution of the μ -CT detector is limited to 0.8 μm , and therefore the pores less than this resolution are not considered in the image stacks calculation. The porosity of the fibers is closer to the porosity obtained from the bulk density in section 3.3.1. However, μ -CT is still a very useful tool to investigate the interconnectivity of the pores and the macropore size distribution within the matrix. For instance, macroporosity is essential for the diffusion of nutrients and gases and the proliferation of cells in biomedical applications such as tissue engineering scaffolds [52]. It is worthy to mention that since aerogels have a broad range (from nm to μm) of morphological characteristics, such as pore lengths and diameters, multiple characterization methods are required to quantify both nanoscale and macroscale parameters and provide a consistent overall view of the aerogels textural properties. In the next section, for a better understanding of porosity, N₂ adsorption was performed as an additional tool to cover the mesoporosity.

3.3.5 Textural properties by N₂ adsorption-desorption

The N₂ adsorption-desorption isotherms of the CAFs regenerated in iPrOH and those subsequently solvent exchanged with EtOH are shown in **Figure 3.6A and B**. The CAF_{EtOH} and fibers with thicker diameters absorbed higher quantities of N₂. Nevertheless, the isotherms curves in all samples are similar to IUPAC type IV with a hysteresis loop in the range of 0.7– 1.0, representing the presence of meso- and macro-porous structure, which is pursuant to the SEM and μ -CT results [56].

The multi-point BET of CAFs specified that the successive solvent exchange to EtOH enhanced the SA_{BET} in the CAF₁₀₀ and CAF₃₀₀ (**Figure 3.6C**). The CAF_{330EtOH} (177 ± 16 m²/g) had significantly higher SA_{BET} than the CAF_{100EtOH} (103 ± 5 m²/g). The solvent exchange drug loading of the fibers did not have a significant impact on the SA_{BET} of the drug-loaded CAF₃₃₀ samples but the results were rather different in the drug-loaded CAF₁₀₀ (**Figure 3.6D**). Lower diameter fibers impregnated by FL and MB showed significantly lower SA_{BET} in comparison to the CAF₃₃₀ and RB loaded CAF₁₀₀. The relative SA_{BET} data of the CAFs and the loaded CAFs are shown in **Table 3.3**.

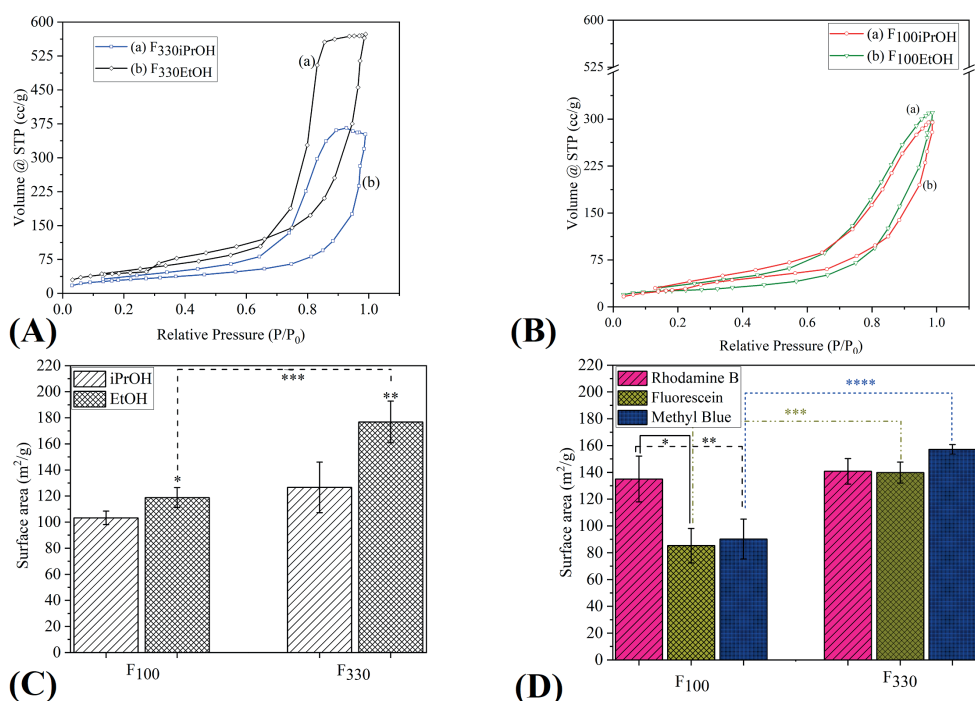
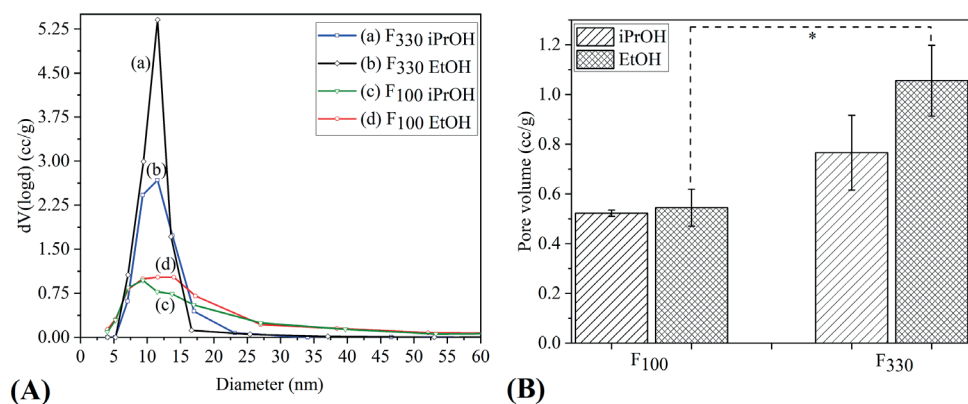


FIGURE 3.6.

The N₂ adsorption-desorption isotherm curves of the CAFs regenerated in iPrOH (A) and solvent exchanged to EtOH (B). (C) The surface area of CAF₁₀₀ and CAF₃₀₀ regenerated in iPrOH and solvent exchanged to EtOH. (D) The surface area of rhodamine B (RB), fluorescein (FL), and methyl blue (MB) loaded CAFs by solvent exchange impregnation. In all diagrams (* data statistically significant $p < 0.05$).

The BJH revealed that the size of nanopores was mainly distributed between 5-20 nm in all samples (**Figure 3.7A**). The pore volume of the CAF_{330EtOH} (1.055 ± 0.142 cc/g) was not significantly different from the CAF_{330iPrOH} (0.765 ± 0.15 cc/g). However, the higher fiber diameter exhibited higher pore volume than lower diameter fibers, indicating the effect of the fiber thickness on the pore volume (**Figure 3.7B**). All average pore diameter and pore volume data of the pure and drug-loaded CAFs are shown in **Table 3.3**.

**FIGURE 3.7.**

(A) Representative curves of the pore-size distribution determined by N₂ adsorption-desorption for the CAFs regenerated in iPrOH and those subsequently exchanged to EtOH. Most of the pores were within the range of 5–20 nm. (B) The pore volume of the CAFs, higher diameter fibers exhibited higher pore volume. (* p < 0.05).

TABLE 3.3.

The surface area (m²/g), pore volume (cc/g), and average pore diameter (nm) of the non-loaded and loaded CAFs.

SAMPLE NAME	BET SURFACE AREA (m ² /g)	PORE VOLUME (cc/g)	AVERAGE PORE DIAMETER (nm)
F ₃₃₀ iPrOH	127±19	0.77±0.15	9.285±0.037
F ₃₃₀ EtOH	177±16	1.06±0.14	11.625±0.055
F ₁₀₀ iPrOH	103±5	0.522±0.012	7.157±0.066
F ₁₀₀ EtOH	119±8	0.544±0.074	7.099±0.042
F ₃₃₀ RB	141±9	0.927±0.051	11.6±2.3
F ₁₀₀ RB	135±17	0.472±0.060	7.106±0.012
F ₃₃₀ FL	140±8	0.871±0.035	7.5±5.2
F ₁₀₀ FL	85±13	0.371±0.047	13.75±0.17
F ₃₃₀ MB	157±4	0.939±0.032	10.9±1.3
F ₁₀₀ MB	90±15	0.412±0.057	8.6±1.3

The subsequent solvent exchange from iPrOH (relative polarity of 0.546) to more polar alcohol EtOH (0.654) increased the SA_{BET} of the fibers. The observed increase in the SA_{BET} could be attributed to EtOH higher polarity causing fibrils linking zones to disintegrate and release loosely packed fibrils from the alcogel body [48,57]. Moreover, the pore volume difference in the CAF₃₃₀ samples with the CAF₁₀₀ can be explained based on the fact that the CAF₃₃₀ nano-porosity (core) to macro-porosity (shell) ratio

was higher than that of the CAF₁₀₀ due to the higher diameter of the fibers during fiber regeneration and alcohol evaporation as discussed in section 3.3.4.

In the end, the effect of depressurization time over 10, 20 and 60 min on the fabricated samples were explored and no significant effect on the textural properties of the CAFs was observed; though, depressurization time of less than 10 min could cause freezing of the samples and further collapsing of the pores due to the fast expansion of CO₂ within the vessel.

It should be noted that due to the variation in the BET and BJH data, these data must be interpreted with caution since there are some challenges within the sample preparation and measurements. For instance, aerogel fibers were very lightweight with high electrostatic charges. In order to add enough weight of the aerogel fibers to the measurement tube, the aerogel fibers had to be densely filled in the test tube. Since controlling this process was hard, there might be some extent of compression when samples were filled in the test tube.

3.3.6 Mechanical properties

Figure 3.8A represents the amount of forces that the CAFs with two different diameters could withstand. The CAF₃₃₀ fibers could withstand greater forces (159 ± 14 cN) than the CAF₁₀₀ samples (6.9 ± 1.6 cN) due to their larger diameter. **Figure 3.8B** shows the representative curves of tenacity versus elongation (%) with an indication of data spread for the maximum tenacity (cN/dtex) and maximum elongation (%) of the CAF₃₃₀ and CAF₁₀₀ samples. The aerogel fibers had similar behavior to the previously reported studies on cellulose aerogel fibers in which a linear regime was followed by an irreversible plastic deformation until the fracture happened [25]. Both fibers showed a wide range of mechanical data, but their maximum tenacity was in close range to each other, 0.34 ± 0.17 and 0.36 ± 0.18 (cN/dtex) for the CAF₃₃₀ and CAF₁₀₀ samples, respectively. The maximum elongation of the CAF₁₀₀ (16.3 ± 4.5 %) was significantly higher than the CAF₃₀₀ (9.2 ± 4.5 %). It seems likely that the difference in the maximum elongation results arose due to the difference in the stiffness of the samples. One possible explanation could be that the thinner fibers are denser and/or have more strongly connected nanofibrils than thick fibers, as it was also perceived by BJH analysis that the CAF₁₀₀ had lower pore volume than CAF₃₀₀. Furthermore, the data outspread in both samples could be attributed to several reasons including highly open non-homogeneous distribution of the pores, coarse nature of the fibers, slight diameter variation along the fiber axis, slight residual stiffness during the measurement, misalignment and kinking in the fiber matrix.

3.3.7 Humidity absorbance and water uptake properties

The CAF₃₃₀ fibers showed a superior moisture weight ratio than the CAF₁₀₀ because of their higher SA_{BET} and pore volume which provided more accessible hydroxyl groups for the water molecules (**Figure 3.8C**). Furthermore, with increasing the relative humidity from 50 to 80% in both samples, the weight ratio of the adsorbed humidity increased from 5.54 ± 0.53 and 7.9 ± 1.1 to 13.54 ± 0.13 and 15.9 ± 1.3 for CAF₁₀₀ and CAF₃₃₀, respectively.

The water uptake tests (**Figure 3.8D**) indicated superabsorbent property for the nonwoven textile made of the CAF₁₀₀ since 1 g of the cellulose aerogel could absorb around 100 g of water; whereas the water uptake weight ratio of the knitted mesh of CAF₃₃₀ was almost three times lower. This phenomenon was presumably because of the macrostructure of the nonwoven patch rather than textural properties of the fibers as the higher surface to volume ratio of the CAF₁₀₀ within the condensed framework of the needle punched nonwoven can entrap more water molecules compared to the loosely packed structure of the knitted mesh.

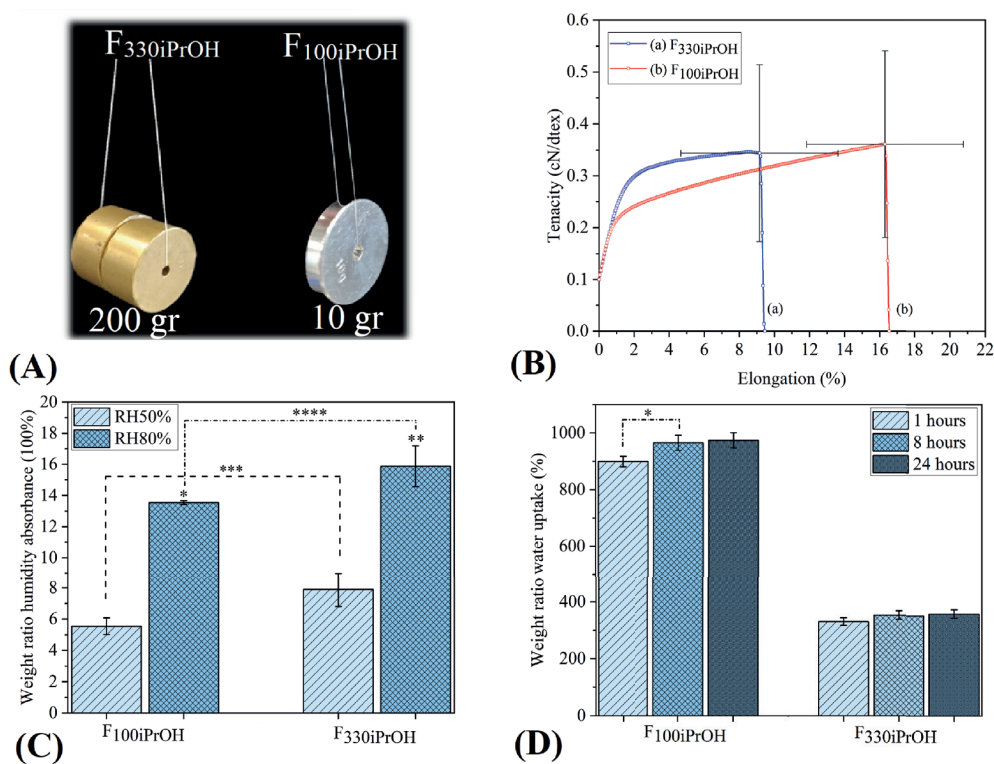


FIGURE 3.8.

(A) The $CAF_{F330iPrOH}$ holding 200 gr and the $CAF_{F100iPrOH}$ carrying 10 g weight, fibers with higher diameter withstood higher forces. (B) Representative curves of tenacity-elongation for $CAF_{F330iPrOH}$ and $CAF_{F100iPrOH}$ with tenacity and the maximum elongation over 20 tensile measurements of the CAFs. $CAF_{F330iPrOH}$ and $CAF_{F100iPrOH}$ showed very close maximum tenacity (~ 0.36 cN); however, the CAFs with the lower diameter had higher elongation ($\sim 16\%$). (C) Humidity absorbance of the CAFs within 50 and 80 RH%, the relative humidity in the CAF_{330} was higher and would increase by enhancing the RH%. (D) Water uptake of the knitted and needle punched samples made from $CAF_{F330iPrOH}$ and $CAF_{F100iPrOH}$ at 1, 8, 24 h. Needle punched samples had superior water uptake capacity up to 1000 wt.%.

3.3.8 Drug loading, release, and kinetic models

The fibers were loaded during the solvent exchange step and the post-treatment process in $scCO_2$. The theoretical amount of the solvent exchange impregnation using Equation 3.6 was estimated to be 5.11 ± 0.19 mg/cm³ for all samples. The experimental amount of the loaded drug (M_{exp}), calculated drug loading efficiency, aerogel loading capacity, and specific loading of the solvent exchange impregnation for RB, MB, and FL are shown in Table 3.4. The CAF_{330} samples indicated slightly higher drug loading efficiency than the CAF_{100} samples in all drug models. Aerogel loading capacity and specific loading were in the sequence of RB > MB > FL.

TABLE 3.4.

The experimental amount of loaded drug, drug loading efficiency (%), aerogel loading capacity (wt. %), and specific loading (mg/m²) of the solvent exchange impregnation process for the loaded CAFs.

SAMPLE NAME	M _{exp} (mg)	DRUG LOADING EFFICIENCY (%)	AEROGEL LOADING CAPACITY (wt.%)	SPECIFIC LOADING (mg/m ²)
F _{330RB}	1.860 ± 0.069	36.4 ± 1.4	1.898 ± 0.071	13.5
F _{100RB}	1.666 ± 0.069	34.6 ± 1.4	1.701 ± 0.070	12.6
F _{330FL}	0.751 ± 0.0082	14.69 ± 0.16	0.7653 ± 0.0083	5.47
F _{100FL}	0.651 ± 0.0216	13.32 ± 0.42	0.663 ± 0.022	30.1
F _{330MB}	0.973 ± 0.057	17.8 ± 1.1	0.993 ± 0.059	6.32
F _{100MB}	0.84 ± 0.077	14.7 ± 1.5	0.857 ± 0.079	9.51

It seems possible that these differences in the drug loading efficiency are due to the interaction and solubility of these molecular probes with the alcohol and the affinity of the drug models with cellulose macromolecules since they can bind to the cellulose chains by electrostatic interactions and hydrogen bonding [58,59]. Furthermore, at a low concentration of the drug (50 mg/L), sorption plays an important role since every hydroglucose unit within cellulose chain have three hydroxyl groups that give active binding sites to the dyes. For instance, in this case, FL is slightly soluble in hot ethanol while RB and MB are both soluble in alcohol at room temperature and have better access to the hydrogen bonding sites, and cellulose is known for being an effective sorbent of RB [60].

In this research, gel formation impregnation was not inspected purposely since the solubility of the model drugs in the alcohol can wash away most of the drug in the fiber production steps, namely regeneration and washing steps. Furthermore, a likely explanation for the inadequate drug loading efficiency of the post-treatment process as mentioned in section 3.2.12 can be due to the low solubility of the compounds in the scCO₂ because of the presence of the polar groups in the drugs chemical structure. Therefore, solvent exchange loading is the best method for loading the aforementioned drug models or bioactive compounds with similar chemical structures. Using the solvent exchange process, both fabrication and loading of the aerogels can be conducted in one single preparation step.

Drug release data of the loaded CAF₃₀₀ and CAF₁₀₀ (**Figure 3.9A and B**) exhibited an immediate release since most of the drug incorporated within the aerogel body was released in 300 min ($Q(\%) \geq 70\%$). When evaluating the drug release from

aerogels, the specific surface area is one of the most important variables governing both the dissolution rate of the drug and its absorption in the aerogel body [61]. Other major factors are the diffusion path length and the solubility of the drug models in the release media as the chosen compounds have different solubility in water (in this study $MB > RB > FL$) [62]. The CAF_{330} drug-loaded samples have a similar range of surface area and diffusion path length, the drug model water solubility will have a more significant role in the drug release. For instance, the slower release rate of the F_{330FL} arose from a more hydrophobic nature of FL and lowest water solubility in comparison to F_{330MB} and F_{330RB} . F_{330MB} higher drug released amount above 300 min can be also attributed to the highest solubility of MB in water. However, the CAF_{100} samples had a faster release rate in comparison to the CAF_{330} presumably due to the smaller diffusion path length and lower surface area and pore volume. The F_{100RB} had the highest surface area and pore volume between the CAF_{100} samples and displayed a slower release rate than the F_{100MB} . Nevertheless, the F_{100FL} exhibited the slowest release pace due to the significantly lower solubility of FL.

Therefore, the CAFs high specific surface area and the porous structure can lead to a rapid drug release for poorly water-soluble drugs such as FL. Such fast release of poorly water-soluble drugs has been investigated in other drug-eluting textiles such as nanofibers produced by the electrospinning technique [63,64]. This type of medical textiles with immediate drug release have been utilized for oral delivery or some circumstances where an instant reaction is required. For example, a fast release rate of antibiotics in the first hours following the biomaterial implantation is essential to prevent implant-related infection [20].

First-order kinetic model was not able to explain the drug release mechanism due to poor fitting of experimental data with the model and R^2 lower than 0.7 for all sample. Korsmeyer-Peppas could justify the release behavior better since R^2 was higher than 0.9 for all samples. The data of m and rate constant are shown in **Table 3.5**. The samples mainly exhibited Fickian diffusion, which occurs by the typical molecular diffusion of the drug due to a chemical potential gradient.

TABLE 3.5.

The power value of n and K_{kp} (constant of release rate) as parameters of Korsmeyer-Peppas for the drug-loaded fibers. The value of m determines the mechanism of release.

SAMPLE NAME	m	R^2	MECHANISM OF RELEASE
F _{330RB}	0.12	0.98	Fickian
F _{100RB}	0.15	0.93	Fickian
F _{330FL}	0.84	0.93	non-Fickian
F _{100FL}	0.33	0.94	Fickian
F _{330MB}	0.35	0.98	Fickian
F _{100MB}	0.31	0.93	Fickian

Modification of the cellulose aerogel fibers is necessary for tuning and extending the drug release since the storage and shipping of immediate drug-eluting textiles might be difficult. Furthermore, their inherent hydrophilicity and lack of cyclic wet stability can lower the long-term steadiness or limit the range of their application. Therefore, several chemical modifications, such as grafting with various hydrophobic groups and esterification, or physical treatments, such as plasma and polymeric coating, are possible strategies to achieve hydrophobized cellulose and overcome these issues.

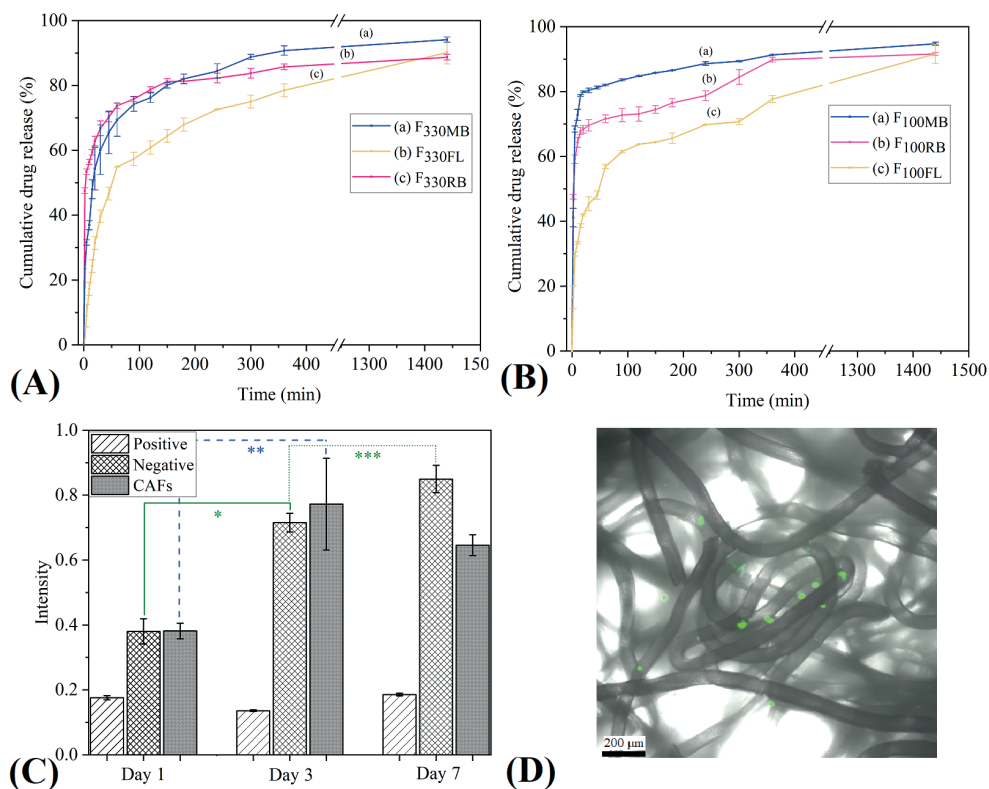


FIGURE 3.9.

Immediate drug release behavior of three model drugs of RB, FL, MB from (A) CAF₃₀₀ and (B) CAF₁₀₀. (C) XTT assay of the cellulose aerogel fibers; cell viability was observed in the samples in day 1, 3 and 7 of the experiment. Cell proliferation was detected from day 1 to day 3. The negative sample was polyethylene and the positive sample was a piece of a latex glove. (D) A representative confocal microscope image displaying live but poorly attached cells to the fibers. (* $p < 0.05$)

3.3.9 Cytotoxicity and cell viability analysis

The cell viability was observed in the CAFs after 1, 3 and 7 days of cell culture demonstrating that the fibrous meshes provided excellent conditions for cell viability and proliferation (**Figure 3.9C**). The proliferation of fibroblast cells in the fibrous structure took place only from day 1 to day 3. This could be due to the fact that the cells reached a confluent layer after 3 days and thus there was no room for further proliferation of the cells. Moreover, 3D projection of the confocal microscopy images of the cells stained with live-dead staining with an imaging depth of 200 μ m displayed no dead cells (in red) within the meshes after 7 days of culture (**Figure 3.9D**).

The open porous structure of the CAFs allowed cell infiltration within the meshes. However, cell attachment was poor and therefore cells showed round morphology

and did not proliferate inside the mesh. Fibroblast cells show elongated morphology both on adherent films and fibers [46][65]. For applications such as tissue engineering in which cell attachment is crucial, further physio-chemical surface modification is required. However, non-adherent meshes can be favorable products for some biomedical applications, such as wound dressing, to avoid damaging the newly formed tissue during the dressing removal [11,66].

3.4 Conclusion

In this study, wet spinning and scCO_2 drying were used to produce highly porous cellulose aerogel microfibers with large surface area ($\sim 100\text{-}180\text{ m}^2/\text{g}$), high humidity absorption ($\sim 10\text{-}18\text{ wt.}\%$), high water uptake capacity ($300\text{-}1000\text{ wt.}\%$), low bulk density ($\sim 0.188\text{ g/cm}^3$), and interconnected pores structures. The microfibers with different diameter were able to be transformed into knitted and needle punched textiles. Impregnation during the solvent exchange step was employed to load the three model drugs. The drug-loaded fibers exhibited an immediate release while more than 70% of the loaded drugs were released within 300 min. The drug release mechanism was mainly Fickian based on the Korsmeyer-Peppas kinetic models. Cell studies demonstrated that the fibrous meshes have a great potential to be used for biomedical applications.

References

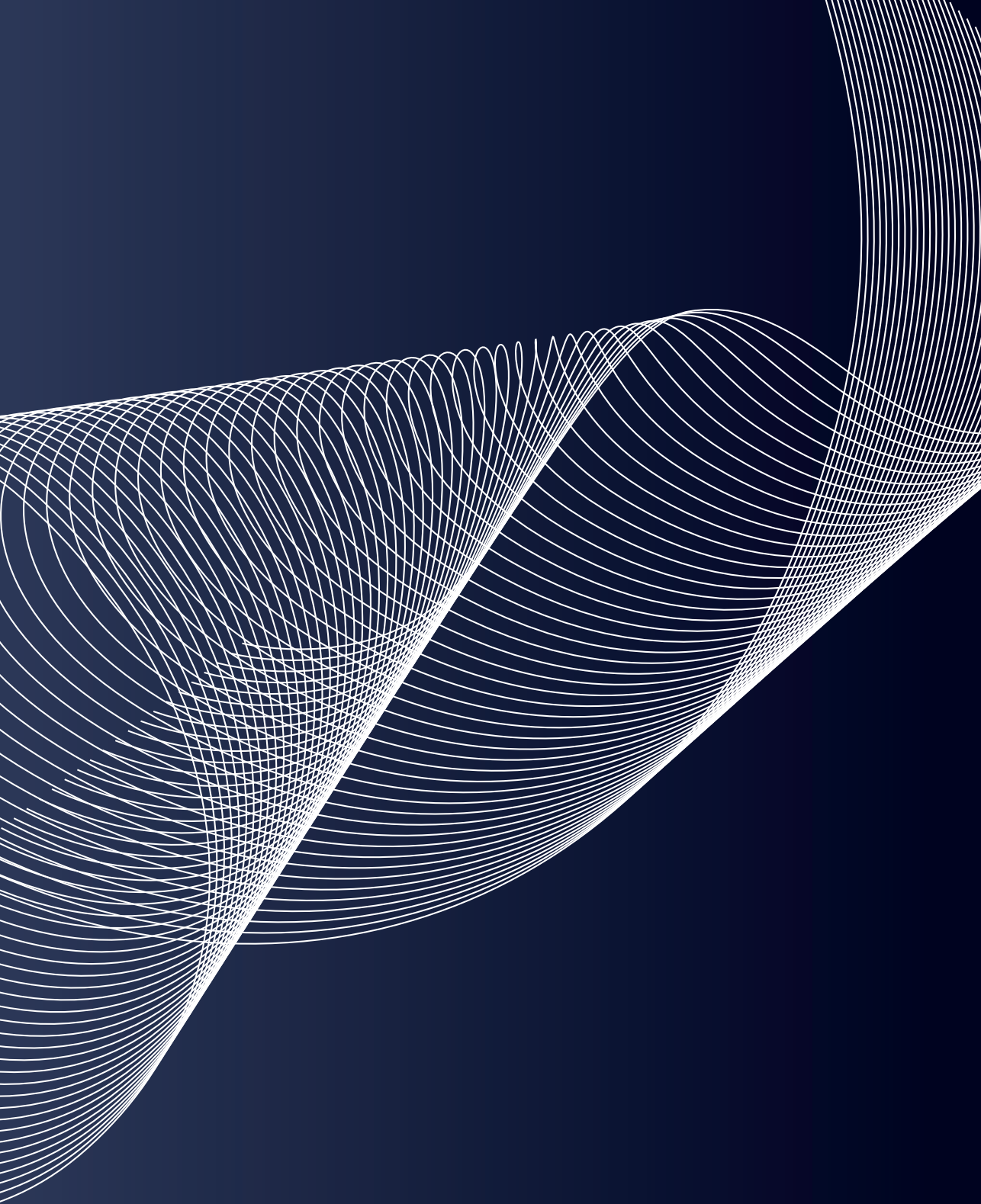
1. Budtova, T. Cellulose II aerogels: a review. *Cellulose* **2019**, *26*, 81-121, doi:10.1007/s10570-018-2189-1.
2. Long, L.-Y.; Weng, Y.-X.; Wang, Y.-Z. Cellulose Aerogels: Synthesis, Applications, and Prospects. *Polymers* **2018**, *10*, 623.
3. VTBartels. *Handbook of medical textiles*; Woodhead publishing: 2011.
4. Gupta, B.S. 1 - Manufacture, types and properties of biotextiles for medical applications. In *Biotextiles as Medical Implants*, King, M.W., Gupta, B.S., Guidoin, R., Eds. Woodhead Publishing: 2013; <https://doi.org/10.1533/9780857095602.1.3pp>. 3-47.
5. Corrias, A.; Casula, M.; Aegerter, M.; N Leventis, M.K. Aerogel handbook. Aerogels containing metal, alloy and oxide nanoparticles in dielectric matrices. Springer, New York **2010**.
6. García-González, C.A.; Alnaief, M.; Smirnova, I. Polysaccharide-based aerogels—Promising biodegradable carriers for drug delivery systems. *Carbohydrate Polymers* **2011**, *86*, 1425-1438, doi:<https://doi.org/10.1016/j.carbpol.2011.06.066>.
7. Valo, H.; Arola, S.; Laaksonen, P.; Torkkeli, M.; Peltonen, L.; Linder, M.B.; Serimaa, R.; Kuga, S.; Hirvonen, J.; Laaksonen, T. Drug release from nanoparticles embedded in four different nanofibrillar cellulose aerogels. *European Journal of Pharmaceutical Sciences* **2013**, *50*, 69-77, doi:<https://doi.org/10.1016/j.ejps.2013.02.023>.
8. Liu, J.; Cheng, F.; Grénman, H.; Spoljaric, S.; Seppälä, J.; E. Eriksson, J.; Willför, S.; Xu, C. Development of nanocellulose scaffolds with tunable structures to support 3D cell culture. *Carbohydrate Polymers* **2016**, *148*, 259-271, doi:<https://doi.org/10.1016/j.carbpol.2016.04.064>.
9. Cai, H.; Sharma, S.; Liu, W.; Mu, W.; Liu, W.; Zhang, X.; Deng, Y. Aerogel Microspheres from Natural Cellulose Nanofibrils and Their Application as Cell Culture Scaffold. *Biomacromolecules* **2014**, *15*, 2540-2547, doi:10.1021/bm5003976.
10. Hakkarainen, T.; Koivuniemi, R.; Kosonen, M.; Escobedo-Lucea, C.; Sanz-Garcia, A.; Vuola, J.; Valtonen, J.; Tammela, P.; Mäkitie, A.; Luukko, K., et al. Nanofibrillar cellulose wound dressing in skin graft donor site treatment. *Journal of Controlled Release* **2016**, *244*, 292-301, doi:<https://doi.org/10.1016/j.jconrel.2016.07.053>.
11. Soorbaghi, F.P.; Isanejad, M.; Salatin, S.; Ghorbani, M.; Jafari, S.; Derakhshankhah, H. Bioaerogels: Synthesis approaches, cellular uptake, and the biomedical applications. *Biomedicine & Pharmacotherapy* **2019**, *111*, 964-975, doi:<https://doi.org/10.1016/j.biopha.2019.01.014>.
12. Subrahmanyam, R.; Gurikov, P.; Meissner, I.; Smirnova, I. Preparation of Biopolymer Aerogels Using Green Solvents. *JoVE* **2016**, doi:10.3791/54116, e54116, doi:doi:10.3791/54116.
13. Martins, M.; Barros, A.A.; Quraishi, S.; Gurikov, P.; Raman, S.P.; Smirnova, I.; Duarte, A.R.C.; Reis, R.L. Preparation of macroporous alginate-based aerogels for biomedical applications. *The Journal of Supercritical Fluids* **2015**, *106*, 152-159, doi:<https://doi.org/10.1016/j.supflu.2015.05.010>.
14. Jin, H.; Nishiyama, Y.; Wada, M.; Kuga, S. Nanofibrillar cellulose aerogels. *Colloids and Surfaces A: Physicochemical and Engineering Aspects* **2004**, *240*, 63-67.
15. Hoepfner, S.; Ratke, L.; Milow, B. Synthesis and characterisation of nanofibrillar cellulose aerogels. *Cellulose* **2008**, *15*, 121-129, doi:10.1007/s10570-007-9146-8.
16. Zhou, S.; Liu, P.; Wang, M.; Zhao, H.; Yang, J.; Xu, F. Sustainable, Reusable, and Superhydrophobic Aerogels from Microfibrillated Cellulose for Highly Effective Oil/Water Separation. *ACS Sustainable Chemistry & Engineering* **2016**, *4*, 6409-6416, doi:10.1021/acssuschemeng.6b01075.
17. Gavillon, R.; Budtova, T. Aerocellulose: new highly porous cellulose prepared from cellulose-NaOH aqueous

- solutions. *Biomacromolecules* **2008**, *9*, 269-277, doi:10.1021/bm700972k.
18. Sescousse, R.; Gavillon, R.; Budtova, T. Wet and dry highly porous cellulose beads from cellulose–NaOH–water solutions: influence of the preparation conditions on beads shape and encapsulation of inorganic particles. *Journal of Materials Science* **2011**, *46*, 759-765.
 19. Mohamed, S.M.K.; Ganesan, K.; Milow, B.; Ratke, L. The effect of zinc oxide (ZnO) addition on the physical and morphological properties of cellulose aerogel beads. *RSC Advances* **2015**, *5*, 90193-90201.
 20. Rostamitabar, M.; Abdelgawad, A.M.; Jockenhoevel, S.; Ghazanfari, S. Drug-Eluting Medical Textiles: From Fiber Production and Textile Fabrication to Drug Loading and Delivery. *Macromolecular bioscience* **2021**, *n/a*, 2100021, doi:https://doi.org/10.1002/mabi.202100021.
 21. Lu, X.; Shen, X. Solubility of bacteria cellulose in zinc chloride aqueous solutions. *Carbohydrate Polymers* **2011**, *86*, 239-244, doi:https://doi.org/10.1016/j.carbpol.2011.04.042.
 22. Fischer, S.; Leipner, H.; Thümmeler, K.; Brendler, E.; Peters, J. Inorganic molten salts as solvents for cellulose. *Cellulose* **2003**, *10*, 227-236.
 23. Rostamitabar, M.; Seide, G.; Jockenhoevel, S.; Ghazanfari, S. Effect of Cellulose Characteristics on the Properties of the Wet-Spun Aerogel Fibers. *Applied Sciences* **2021**, *11*, 1525, doi:https://doi.org/10.3390/app11041525.
 24. Hoepfner, S.; Ratke, L. *Open porous cellulose aerogel fibers*; 2008; 10.13140/RG.2.2.12012.26246.
 25. Karadagli, I.; Schulz, B.; Schestakow, M.; Milow, B.; Gries, T.; Ratke, L. Production of porous cellulose aerogel fibers by an extrusion process. *The Journal of Supercritical Fluids* **2015**, *106*, 105-114, doi:https://doi.org/10.1016/j.supflu.2015.06.011.
 26. Zhou, J.; Hsieh, Y.-L. Nanocellulose aerogel-based porous coaxial fibers for thermal insulation. *Nano Energy* **2020**, *68*, 104305, doi:https://doi.org/10.1016/j.nanoen.2019.104305.
 27. Schulz, B.; Meinert, T.; Bierbüsse, D.; Busen, M.; Körtzinger, N.; Stankowski, M.; Seide, G. Cellulose Aerogel Fibers Tested on a REXUS 18 Rocket – The ACTOR Project. *Chemie Ingenieur Technik* **2016**, *88*, 1501-1507, doi:10.1002/cite.201600003.
 28. Wang, Z.; Yang, H.; Li, Y.; Zheng, X. Robust Silk Fibroin/Graphene Oxide Aerogel Fiber for Radiative Heating Textiles. *ACS Applied Materials & Interfaces* **2020**, *12*, 15726-15736, doi:10.1021/acsami.0c01330.
 29. Yang, H.; Wang, Z.; Liu, Z.; Cheng, H.; Li, C. Continuous, Strong, Porous Silk Fibroin-Based Aerogel Fibers toward Textile Thermal Insulation. *Polymers* **2019**, *11*, 1899.
 30. Liu, Z.; Lyu, J.; Fang, D.; Zhang, X. Nanofibrous Kevlar Aerogel Threads for Thermal Insulation in Harsh Environments. *ACS Nano* **2019**, *13*, 5703-5711, doi:10.1021/acsnano.9b01094.
 31. Li, J.; Wang, J.; Wang, W.; Zhang, X. Symbiotic Aerogel Fibers Made via In-Situ Gelation of Aramid Nanofibers with Polyamidoxime for Uranium Extraction. *Molecules* **2019**, *24*, 1821.
 32. Du, Y.; Zhang, X.; Wang, J.; Liu, Z.; Zhang, K.; Ji, X.; You, Y.; Zhang, X. Reaction-Spun Transparent Silica Aerogel Fibers. *ACS Nano* **2020**, *14*, 11919-11928, doi:10.1021/acsnano.0c05016.
 33. Li, G.; Hong, G.; Dong, D.; Song, W.; Zhang, X. Multiresponsive Graphene-Aerogel-Directed Phase-Change Smart Fibers. *Advanced Materials* **2018**, *30*, 1801754, doi:10.1002/adma.201801754.
 34. Xu, Z.; Zhang, Y.; Li, P.; Gao, C. Strong, Conductive, Lightweight, Neat Graphene Aerogel Fibers with Aligned Pores. *ACS Nano* **2012**, *6*, 7103-7113, doi:10.1021/nn3021772.
 35. Batista, M.P.; Gonçalves, V.S.S.; Gaspar, F.B.; Nogueira, I.D.; Matias, A.A.; Gurikov, P. Novel alginate-chitosan aerogel fibres for potential wound healing applications. *International journal of biological macromolecules*

- 2020, 156, 773-782, doi:<https://doi.org/10.1016/j.ijbiomac.2020.04.089>.
36. Song, S.-m.; Hou, X.-l.; Wu, Y.-b.; Shuang, S.-m.; Yang, C.; Inoue, Y.; Dong, C. Study on the interaction between methyl blue and human serum albumin by fluorescence spectrometry. *Journal of Luminescence* **2009**, 129, 169-175, doi:<https://doi.org/10.1016/j.jlumin.2008.09.008>.
 37. Moreau, D.; Lefort, C.; Burke, R.; Leveque, P.; O'Connor, R.P. Rhodamine B as an optical thermometer in cells focally exposed to infrared laser light or nanosecond pulsed electric fields. *Biomed Opt Express* **2015**, 6, 4105-4117, doi:[10.1364/BOE.6.004105](https://doi.org/10.1364/BOE.6.004105).
 38. Morsi, R.E.; Elsayw, M.; Manet, I.; Ventura, B. Cellulose Acetate Fabrics Loaded with Rhodamine B Hydrazide for Optical Detection of Cu(II). *Molecules* **2020**, 25, 3751.
 39. Okuno, Y.; Yamazaki, Y.; Fukutomi, H.; Kuno, S.; Yasutake, M.; Sugiura, M.; Kim, C.J.; Kimura, S.; Uji, H. A Novel Surface Modification and Immobilization Method of Anti-CD25 Antibody on Nonwoven Fabric Filter Removing Regulatory T Cells Selectively. *ACS Omega* **2020**, 5, 772-780, doi:[10.1021/acsomega.9b03494](https://doi.org/10.1021/acsomega.9b03494).
 40. Segal, L.; Creely, J.J.; Martin, A.E.; Conrad, C.M. An Empirical Method for Estimating the Degree of Crystallinity of Native Cellulose Using the X-Ray Diffractometer. *Textile Research Journal* **1959**, 29, 786-794, doi:[10.1177/004051755902901003](https://doi.org/10.1177/004051755902901003).
 41. Fischer, E.; Rigacci, A.; Pirard, R.; Berthon-Fabry, S.; Achard, P. Cellulose-based aerogels. *Polymer* **2006**, 47, 7636-7645, doi:<https://doi.org/10.1016/j.polymer.2006.09.004>.
 42. Haimer, E.; Wendland, M.; Schlufte, K.; Frankenfeld, K.; Miethe, P.; Potthast, A.; Rosenau, T.; Liebner, F. Loading of Bacterial Cellulose Aerogels with Bioactive Compounds by Antisolvent Precipitation with Supercritical Carbon Dioxide. *Macromolecular Symposia* **2010**, 294, 64-74, doi:[10.1002/masy.201000008](https://doi.org/10.1002/masy.201000008).
 43. Mulye, N.V.; Turco, S.J. A Simple Model Based on First Order Kinetics to Explain Release of Highly Water Soluble Drugs from Porous Dicalcium Phosphate Dihydrate Matrices. *Drug Development and Industrial Pharmacy* **1995**, 21, 943-953, doi:[10.3109/03639049509026658](https://doi.org/10.3109/03639049509026658).
 44. 5 - Mathematical models of drug release. In *Strategies to Modify the Drug Release from Pharmaceutical Systems*, Bruschi, M.L., Ed. Woodhead Publishing: 2015; <https://doi.org/10.1016/B978-0-08-100092-2.00005-9>pp. 63-86.
 45. Korsmeyer, R.W.; Gurny, R.; Doelker, E.; Buri, P.; Peppas, N.A. Mechanisms of solute release from porous hydrophilic polymers. *International journal of pharmaceutics* **1983**, 15, 25-35, doi:[https://doi.org/10.1016/0378-5173\(83\)90064-9](https://doi.org/10.1016/0378-5173(83)90064-9).
 46. Kreimendahl, F.; Marquardt, Y.; Apel, C.; Bartneck, M.; Zwadlo-Klarwasser, G.; Hepp, J.; Jockenhoevel, S.; Baron, J.M. Macrophages significantly enhance wound healing in a vascularized skin model. *Journal of Biomedical Materials Research Part A* **2019**, 107, 1340-1350, doi:<https://doi.org/10.1002/jbm.a.36648>.
 47. Ghazanfari, S.; Alberti, K.A.; Xu, Q.; Khademhosseini, A. Evaluation of an elastic decellularized tendon-derived scaffold for the vascular tissue engineering application. *Journal of Biomedical Materials Research Part A* **2019**, 107, 1225-1234, doi:[10.1002/jbm.a.36622](https://doi.org/10.1002/jbm.a.36622).
 48. Schestakow, M.; Karadagli, I.; Ratke, L. Cellulose aerogels prepared from an aqueous zinc chloride salt hydrate melt. *Carbohydrate Polymers* **2016**, 137, 642-649, doi:<https://doi.org/10.1016/j.carbpol.2015.10.097>.
 49. Poletto, M.; Pistor, V.; Zattera, A.J. Structural characteristics and thermal properties of native cellulose. *Cellulose-fundamental aspects* **2013**, 2, 45-68.
 50. Kadokawa, J.-i.; Murakami, M.-a.; Takegawa, A.; Kaneko, Y. Preparation of cellulose-starch composite gel and fibrous material from a mixture of the polysaccharides in ionic liquid. *Carbohydrate Polymers* **2009**, 75, 180-183.
 51. Shang, X.; Jiang, H.; Wang, Q.; Liu, P.; Xie, F. Cellulose-starch Hybrid Films Plasticized by Aqueous ZnCl₂

Solution. *International Journal of Molecular Sciences* **2019**, *20*, 474.

52. Park, S.; Baker, J.O.; Himmel, M.E.; Parilla, P.A.; Johnson, D.K. Cellulose crystallinity index: measurement techniques and their impact on interpreting cellulase performance. *Biotechnology for biofuels* **2010**, *3*, 10.
53. Dassanayake, R.S.; Acharya, S.; Abidi, N. Biopolymer-based materials from polysaccharides: Properties, processing, characterization and sorption applications. In *Advanced Sorption Process Applications*, IntechOpen: 2018.
54. Abdulkhali, A.; Hojati Marvast, E.; Ashori, A.; Hamzeh, Y.; Karimi, A.N. Preparation of cellulose/polyvinyl alcohol biocomposite films using 1-n-butyl-3-methylimidazolium chloride. *International journal of biological macromolecules* **2013**, *62*, 379-386, doi:<https://doi.org/10.1016/j.ijbiomac.2013.08.050>.
55. Sescousse, R.; Gavillon, R.; Budtova, T. Aerocellulose from cellulose-ionic liquid solutions: Preparation, properties and comparison with cellulose-NaOH and cellulose-NMMO routes. *Carbohydrate Polymers* **2011**, *83*, 1766-1774, doi:<https://doi.org/10.1016/j.carbpol.2010.10.043>.
56. Reichenauer, G. Structural Characterization of Aerogels. In *Aerogels Handbook*, Aegerter, M.A., Leventis, N., Koebel, M.M., Eds. Springer New York: New York, NY, 2011; 10.1007/978-1-4419-7589-8_21pp. 449-498.
57. Empirical Parameters of Solvent Polarity. In *Solvents and Solvent Effects in Organic Chemistry*, 2010; <https://doi.org/10.1002/9783527632220.ch7pp>. 425-508.
58. Champeau, M.; Thomassin, J.M.; Tassaing, T.; Jérôme, C. Drug loading of polymer implants by supercritical CO₂ assisted impregnation: A review. *Journal of Controlled Release* **2015**, *209*, 248-259, doi:<https://doi.org/10.1016/j.jconrel.2015.05.002>.
59. Ulker, Z.; Erkey, C. An advantageous technique to load drugs into aerogels: Gas antisolvent crystallization inside the pores. *The Journal of Supercritical Fluids* **2017**, *120*, 310-319, doi:<https://doi.org/10.1016/j.supflu.2016.05.033>.
60. Kausar, A.; Shahzad, R.; Asim, S.; BiBi, S.; Iqbal, J.; Muhammad, N.; Sillanpää, M.; Din, I.U. Experimental and theoretical studies of Rhodamine B direct dye sorption onto clay-cellulose composite. *Journal of Molecular Liquids* **2021**, *328*, 115165, doi:<https://doi.org/10.1016/j.molliq.2020.115165>.
61. Esquivel-Castro, T.A.; Ibarra-Alonso, M.C.; Oliva, J.; Martínez-Luévanos, A. Porous aerogel and core/shell nanoparticles for controlled drug delivery: A review. *Materials Science and Engineering: C* **2019**, *96*, 915-940, doi:<https://doi.org/10.1016/j.msec.2018.11.067>.
62. Lillie, R.D.; Conn, H.J. *HJ Conn's biological stains*; Sigma Chemical Co.: 1991.
63. Bai, Y.; Wang, D.; Zhang, Z.; Pan, J.; Cui, Z.; Yu, D.-G.; Annie Bligh, S.-W. Testing of fast dissolution of ibuprofen from its electrospun hydrophilic polymer nanocomposites. *Polymer Testing* **2021**, *93*, 106872, doi:<https://doi.org/10.1016/j.polymertesting.2020.106872>.
64. Kang, S.; Hou, S.; Chen, X.; Yu, D.-G.; Wang, L.; Li, X.; R. Williams, G. Energy-Saving Electrospinning with a Concentric Teflon-Core Rod Spinneret to Create Medicated Nanofibers. *Polymers* **2020**, *12*, 2421.
65. Ghazanfari, S.; TAFAZOLI, S.M.; Shokrgozar, M.A.; Haghighipour, N.; Amirzadeh, N.; JAFARGHOLI, R.E. Analysis of alterations in morphologic characteristics of mesenchymal stem cells by mechanical stimulation during differentiation into smooth muscle cells. **2010**.
66. Saghazadeh, S.; Rinoldi, C.; Schot, M.; Kashaf, S.S.; Sharifi, F.; Jalilian, E.; Nuutila, K.; Giatsidis, G.; Mostafalu, P.; Derakhshandeh, H., et al. Drug delivery systems and materials for wound healing applications. *Advanced drug delivery reviews* **2018**, *127*, 138-166, doi:[10.1016/j.addr.2018.04.008](https://doi.org/10.1016/j.addr.2018.04.008).



Chapter 4.

DRUG LOADED CELLULOSE-CHITOSAN AEROGEL MICROFIBERS FOR WOUND DRESSING APPLICATIONS

This chapter is based on the following publication:

Rostamitabar, M.; Gharamani A.; Seide, G.; Jockenhoevel, S.; Ghazanfari, S. Drug Loaded Cellulose-Chitosan Aerogel Microfibers for Wound Dressing Applications. *Cellulose*, **2022**, 29, 6261–6281.

Abstract: Cellulose and chitosan have been studied for wound dressing due to their biocompatibility, biodegradability, lower antigenicity, and renewability. The functional and structural characteristics of such biopolymers can be dramatically improved by their transformation into fibrous bioaerogels due to their outstanding characteristics such as low density, high porosity, and large specific surface area. Producing aerogels in the form of fibers and textiles not only can enhance mechanical properties, stiffness, and shapeability of aerogels but also lead to short drying times and scalable production processes. Hereby, wet spun chitosan-cellulose aerogel microfibers (CHCLAF) in two ratios of 1:5 and 1:10 have been produced by supercritical CO₂ (scCO₂) drying for wound dressing application. The fibers were also loaded with ibuprofen (IBU) through post-treatment scCO₂ impregnation. CHCLAF characteristics in terms of morphology, textural properties, thermal stability, mechanical properties, and *in vitro* assessment such as drug release, antibacterial properties, cytotoxicity, and wound exudate uptake were analyzed and compared to pure cellulose aerogel microfibers (CLF). Blended CHCLAF showed a low density (~ 0.18 g/cm³), high porosity ($\sim 85\%$), and large specific surface area (~ 300 m²/g) with a macro-porous outer shell and a nano-porous inner core. The fibers were transformed into braided meshes that were highly water absorbable (~ 400 wt.%) and bactericidal against *escherichia coli* and *staphylococcus aureus*. Furthermore, the fibrous structures showed no cytotoxicity using fibroblast cells, and the hybrid fibers were able to release IBU over 48 hours in a sustained manner. The results showed that the CHCLAF could be used as a promising candidate for wound dressing materials.

4.1 Introduction

It has been forecast that the global wound dressing market can exceed \$15 billion by 2022. Moreover, the advanced wound care market aiming for surgical wounds and chronic ulcers is expected to exceed \$22 billion by 2024 [1]. Medical textile plays an important role in wound dressings, and such a continuing rise in the need for wounds products requires the fabrication of sustainable added-value products originating from renewable materials such as cellulose and chitosan [2,3]. Cellulose the most abundant biopolymer present in plant cell walls is made of β -D-glucose held by β -1, 4-glycosidic linkages [4]. Cellulose has been widely used in wound dressing products due to its high flexibility, excellent physical barrier for microbial pathogens, and especially its moisture-retaining properties thanks to presence of numerous hydroxyl functional groups [5,6]. Wounds are well known to heal more quickly in a moist environment since a sufficient supply of growth factors and other molecules to the healing tissues is more likely to happen [7]. Furthermore, cellulose can assist in the absorption of wound exudates evolving in the uptake of cell debris [7,8]. However, cellulose by itself does not possess any antibacterial and antifungal properties, which can be a drawback for infectious wound sites.

Chitosan is the active form and deacetylated substance of chitin biomacromolecules made up of n-acetyl glucosamine residues held by β -1, 4 linkages. Chitin is a natural biopolymer that typically occurs in fungi, crustaceans, mollusks, and insects. Chitosan has been widely investigated as an antimicrobial agent to prevent bacterial and fungal infections of the wound site [9,10]. Chitosan has also exhibited fibroblast proliferative characteristics necessary to accelerate wound healing [11] and can lead to activation of polymorphonuclear leukocytes and macrophages for phagocytosis and expression of interleukin-1 (IL-1), transforming growth factor beta (TGF- β), and platelet-derived growth factor (PDGF) [9,12].

The functional and structural characteristics of such biopolymers can be dramatically enhanced by producing fibrous aerogels due to their outstanding characteristics such as low density, high porosity, and large specific surface area. Aerogels are produced from wet gels in delicate drying processes such as freeze-drying or supercritical CO₂ (scCO₂) so that the gel structure is merely conserved. In contrast to other drying techniques, scCO₂ is a mild temperature process that leads to better textural properties as well as sterilization [13] and drug loading possibilities of fabricated aerogels [3]. Drug impregnation in the aerogel fibers can be performed either during gel preparation or during the network formation (solvent exchange) or after drying the aerogel through the post-treatment method which utilizes scCO₂ as a medium to dissolve and impregnate

the drug [14]. In addition, producing microfiber aerogels not only can enhance the mechanical properties, stiffness, and shapeability of aerogels but also lead to short scCO_2 drying times and scalable production processes [15].

The design and fabrication of new biomaterials from renewable resources to promote the wound healing process are a constant demand from the health sector. To the best of our knowledge, no cellulose-chitosan hybrid aerogel in the geometry of microfiber or textile has been fabricated or studied for wound dressing application. Such bioaerogel microfibers have the combination of unique characteristics of biopolymers, microfibers, and aerogels in one single product. Moreover, these products have a great potential to be further functionalized and tuned for not only different types of wounds but also other biomedical applications.

In this study, cellulose-chitosan aerogel microfibers (CHCLAFs) were produced by blending microcrystalline cellulose (MCC) with low molecular weight chitosan powder (CHP) using $\text{ZnCl}_2 \cdot 3\text{H}_2\text{O}$ as a dissolving agent. This low-cost hydrated salt is able to simultaneously dissolve cellulose and chitosan and has the potential to be extended to industrial processes [16]. Hybrid aerogel fibers in two different ratios of 1:10 and 1:5 (CHP:MCC), referred to as CH1CL10 and CH1CL5 respectively, were fabricated. Moreover, cellulose aerogel fibers (CLF) were created through a similar processing route to be compared with hybrid aerogel fibers. Ibuprofen (IBU) is an anti-inflammatory, non-steroidal analgesic, and antipyretic drug which can promote wound healing by preventing excessive inflammation. Fibers were loaded with IBU through scCO_2 post-treatment impregnation since the solubility of ibuprofen in scCO_2 is satisfactory as reported to be 0.98% (w/w) at $40 \pm 1^\circ\text{C}$ and 180 ± 2 bar [17].

CLF and CHCLAF characteristics were investigated in terms of morphology, physico-chemical structure, textural properties, thermal stability, mechanical properties, and *in vitro* assessments including humidity and water uptake, wound exudate uptake, drug release, cytotoxicity, and antibacterial properties.

4.2 Materials and Methods

4.2.1 Materials

Microcrystalline cellulose (MCC) with the product number C6288 (degree of polymerization of 159) [15], CHP (50–190 kDa, 75–85% deacetylated), dialysis tubing cellulose membrane (typical molecular weight cut-off = 14,000), dimethyl sulfoxide (DMSO) and cell proliferation kit II (XTT) all from Sigma–Aldrich (Germany) were

purchased. ZnCl_2 (97%) and 4-Isobutyl-alpha-methylphenylacetic acid (IBU) were obtained from Alfa Aesar (Germany). For regeneration and washing of the samples, the absolute isopropanol (iPrOH) ($\geq 99,8\%$, 2-Propanol CP) from Biosolve BV (The Netherlands) were used. Carbon-dioxide (CO_2) cylinders (2.7, 50 liter) with a purity of 99.5 % from Linde Gas Benelux (The Netherlands) was used in the scCO_2 drying process. Gibco™ Dulbecco's modified Eagle's medium (DMEM) with 10% Gibco™ fetal calf serum (FCS) were purchased from Thermo Fisher Scientific (USA). For antibacterial studies, ampicillin and lysogeny broth (LB) medium which was created by a mixture of trypton (10 g/L), yeast extract (5 g/L), NaCl (5 g/L) and agar-agar (12 g/L) were all purchased from Carl Roth (Germany). *E. coli* from New England Biolabs (Germany) and *S. aureus* from DSMZ (German Collection of Microorganisms and Cell Cultures GmbH, Germany) were obtained. Finally, all materials were used without further purification.

4.2.2 Fabrication of the aerogel fibers, textiles, and cylinders

4.2.2.1 Spinning dope

MCC and CHP were dried at 100 °C in a vacuum oven overnight to remove the moisture and achieve a constant weight. Two various spinning dopes of 10:1 and 5:1 of MCC:CHP were prepared using 60 % zinc chloride (36 g), 31.66 % of deionized water (19 mL), and 8.33 % of polymer powders of MCC and CHP (5 g). Pure CLFs were fabricated by using 8.33% (5 g) of MCC. Homogenous clear solutions were achieved by dissolving the polymers at 75 °C and using a mechanical stirrer (100 rpm) after approximately 90 min.

4.2.2.2 Wet spinning and washing

The spinning was done by a customized wet-spinning “DIENES LabLineCompact” unit as thoroughly explained previously [18]. In brief, monofilament alcogel fibers (fibers regenerated in alcohol) were obtained by spinning the dope through a spinneret with a capillary diameter of 330 μm in the iPrOH bath (30 L) without passing through an air gap between the nozzle and the regeneration bath. The pump rate of 1 mL/min and pressure of 2-3 bar were used. The fibers were collected in the coagulation bath on a porous stainless steel bobbin with a winding rate of 50 rpm. Fibers were washed in a customized soxhlet extractor system (NS 100) and the presence of salt leftovers was checked by conductivity meter and spot test as explained elsewhere [15].

4.2.2.3 scCO_2 drying

The drying procedure was performed using scCO_2 dryer HPE 300 (EUROTECHNICA GmbH, Germany) at 130 bar and 50 °C over 45 min as described more completely elsewhere [18].

4.2.2.4 Braided textiles

The dried fibers were manually turned into a braided construct containing at least 27 monofilaments in each mesh.

4.2.2.5 Aerogel cylinders

Cellulose and cellulose-chitosan cylinders were prepared in two different ratios of 10:1 and 5:1 (MCC:CHP) for density assessment and antibacterial assay. To obtain such cylinders, the warm solution was poured into cylindrical molds with an inner diameter of 14.5 mm and was centrifuged to remove air bubbles. Subsequently, they were regenerated in iPrOH and placed on a shaker (50 rpm) to increase the rate of solvent diffusion into the gel body. After 3 days and 6 cycles of solvent exchange, they were supercritically dried over 8 hours in a similar condition to the fibers.

4.2.3 Post-treatment scCO_2 drug impregnation and drug loading efficiency

4.2.3.1 Post-treatment scCO_2 drug impregnation

30 ± 5 mg of IBU was placed at the bottom of the high-pressure vessel ($V = 100$ mL) with a magnetic bar. Then, 100 ± 10 mg of the dried aerogel fibers wrapped in filter papers were placed inside a porous cylinder that had a gap with the bottom of the vessel to avoid any contact between the fibers and the drug powders containing a rotating magnetic bar. A magnetic stirrer was placed under the vessel, and the pressure and temperature of CO_2 were set at 200 bar and 50 °C. After 24 h, the vessel was depressurized over 60 min. **Table 4.1** summarizes the abbreviation for the samples fabricated in the current study.

TABLE 4.1.

The label of fiber samples was produced by using a spinning nozzle diameter of 330 (μm) and iPrOH as regeneration and washing solvent.

SAMPLE NAME	CELLULOSE RATIO	CHITOSAN RATIO	LOADED DRUG
CLF	1	0	-
CH1CL10	10	1	-
CH1CL5	5	1	-
CLF _{IBU}	1	0	ibuprofen
CH1CL10 _{IBU}	10	1	ibuprofen
CH1CL5 _{IBU}	5	1	ibuprofen

4.2.3.2 Drug loading efficiency

The drug loading efficiency (entrapment) of the post-treatment method (in scCO_2) was obtained by measuring the weight of the aerogel fibers before (M_i) and after (M_f) the impregnation as expressed by:

$$\text{Drug loading efficiency (\%)} = \frac{M_i}{M_f} \times 100 \quad \text{Equation (4.1)}$$

4.2.4 Material and structural characterizations

4.2.4.1 Density and porosity

The porosity (\emptyset) was estimated from the bulk density and skeletal density as follows:

$$\emptyset(\%) = \frac{V_{\text{pores}}}{V_{\text{material}}} = 1 - \frac{\rho_{\text{bulk}}}{R \times \rho_{\text{skeletalCHP}} + (1-R) \times \rho_{\text{skeletalMCC}}} \times 100 \quad \text{Equation (4.2)}$$

Where the skeletal density of cellulose ($\rho_{\text{skeletalMCC}}$) is 1.501 g.cm^{-3} [19], and the skeletal density of chitosan ($\rho_{\text{skeletalCHP}}$) is 1.42 g.cm^{-1} [20] and R is the ratio of CHP:MCC in the samples. The bulk density (ρ_{density}) was estimated as the mass to volume ratio of the three small cylindrical samples. The samples' diameters and lengths were in the range of 0.75-1 cm and 2-2.2 cm, respectively. The dimension of the samples was measured by a digital vernier caliper.

4.2.4.2 Electron microscopy

The surface and cross-sectional morphologies of the aerogels were observed by using a Teneo scanning electron microscope (Thermo Fisher Scientific, USA). All fibers were broken in liquid nitrogen and coated with a 3 nm thick layer of iridium. Images were

obtained using 5 kV voltage at a working distance of 10 mm. To obtain the average diameter of fibers SEM images were analyzed using Image J (version 1.8.0_172, NIH, USA). The diameter measurement was repeated 10 times at different points for each fiber.

Linear shrinkage ΔL of samples was determined from the SEM images by measuring the diameter of the samples after spinning (D_i) and after drying (D_f) using the following equation:

$$\Delta L (\%) = \frac{D_i - D_f}{D_i} \times 100 \quad \text{Equation (4.3)}$$

4.2.4.3 Elemental analysis

The nitrogen percentage in the CHCLAF was quantified by elemental analysis using an Elemental Analyzer vario MICRO cube (Elementar, Germany). Sulfanilamide and helium were used as the calibration standard and carrier gas, respectively. The weight of the samples was 2–3 mg, and the total time of analysis was 10 min. The nitrogen content was converted to chitosan content (on a weight percentage basis, wt.%) as described in the literature [21,22], and calculated as follows:

$$\text{Chitosan (wt. \%)} = \frac{P_N \times C}{N} \quad \text{Equation (4.4)}$$

Where P_N (wt.%) is the weight percentage of nitrogen in the fibers, C (g/mol) is the relative molecular weight of the chitosan repeating unit considering the deacetylation degree; N (g/mol) is the molecular weight of elemental nitrogen.

4.2.4.4 FTIR

Fourier transform infrared spectroscopy (FTIR) (Perkin Elmer, USA) was used to study inter/intra chemical interactions between the macromolecules. The spectrum was averaged over 32 spectra with a resolution of 2 cm^{-1} from a range of 4000 till 500 cm^{-1} in the reflectance mode.

4.2.4.5 X-ray diffraction

Wide-angle X-ray diffraction (WAXD) analysis on samples including microcrystalline cellulose powder and aerogel fibers were performed using a Ganesha diffractometer (SAXSLAB, Denmark) with a sample-to-detector distance of 116.536 mm . Cu K α radiation ($\lambda = 1.5406 \text{ \AA}$) and silver behenate ($d_{001} = 58.380 \text{ \AA}$) used for calibration and samples were measured for 600 s. The diffraction spectrums were analyzed in transmission mode by saxsgui v2.23.23 software and environmental

background were removed from spectrums. The graphs were shown in the θ -2 θ geometry.

4.2.4.6 TGA

The thermal properties of the aerogels were studied using a TA Q500 thermo-gravimetric instrument (TA Instruments, USA). Samples were heated from 20 °C to 500 °C with a rate of 10 °C min⁻¹ under N₂ purge.

4.2.4.7 Nitrogen adsorption-desorption

Surface area and porosimetry measurements of the aerogel fibers were performed by ASAP™ 2020 (micrometrics, Norcross (Atlanta), GA, USA). Samples were degassed at 80 °C over 24 h and the Brunauer–Emmet–Teller (BET) method was utilized to determine the specific surface area. The pore volume and average pore size were obtained by Barrett-Joyner-Halenda (BJH).

4.2.4.8 Mechanical properties

The linear density, tensile strength, and elongation measurements of the fibers were analyzed using Texttechno Favimat+ single fiber testing machine (Herbert Stein GmbH & Co., KG, Germany). The device was equipped with a load cell of 210 cN, and the linear density and tensile measurements were carried out at the rate of 10 mm/min. To address the coarse structure of the fibers and the resulting stiffness, high gauge lengths (20 mm) and high pretensions (0.1cN/dtex) using 20 samples per group were used.

4.2.5 In vitro characterization

4.2.5.1 Humidity absorbance and water uptake

Three replicates of braided fibers were dried in a vacuum oven at 90 °C for around 24 h to reach a constant weight. Subsequently, they were placed for 24 h in a humidity chamber at 25 °C with relative humidity (RH) of 50% and 80%. The weight of the samples was instantly measured before (W_{dry}) and after (W_{humid}) keeping it in the humidity chamber. Humidity absorbance weight ratio ($W_{RH\%}$) was measured by:

$$W_{RH\%} = \frac{W_{humid} - W_{dry}}{W_{dry}} \times 100 \quad \text{Equation (4.5)}$$

Similarly, the dried braided fiber samples were placed in PBS solution (pH 7.4, 37 °C) and their weights were measured after removing the excess amount of water by filter papers. The wet weight (W_{wet}) was measured after 1, 8 and 24 hours, and the water uptake (WU(%)) was calculated as below:

$$WU(\%) = \frac{W_{wet} - W_{dry}}{W_{dry}} \times 100 \quad \text{Equation (4.6)}$$

To investigate the water droplet sorption time on single aerogel fibers, three droplets with an approximate volume of 3 μL were placed on each fiber. Photographs were captured by FLIR chameleon®3 monochrome camera (1.3 megapixels) at four different time points of 5 s, 3 min, 5 min, and 10 min.

4.2.5.2 Wound exudate uptake

In order to investigate the capability of the braided structures to absorb wound exudate, the skin mimicking layers were created as explained in previous studies [23,24]. In summary, the artificial skin consisted of a dermis mimicking layer and an underneath hypodermis mimicking layer to avoid excessive drying over time was used as a skin model. The hypodermis was created by mixing gelatin (2 wt. %) and agar (0.4 wt. %) in deionized water on a heating stirrer at 50 °C and 100 rpm to achieve a homogeneous solution. The hot solution was poured into a cylindrical mold with an inner diameter of 75 mm to reach the height of 15 mm and left for 30 min to solidify. Similarly, the dermis layer was made of gelatin (24 wt. %) and agar (2 wt. %) and it was subsequently poured on top of the hypodermis layer to reach a thickness of 5 mm and left to solidify. The braided structures were placed on the surface of the top layer and covered with parafilm tape. The weight of samples was measured at 8 different time points up to 48 hours. The uptake weight percentage was reported based on equation 6 and the experiment was performed in triplicates.

4.2.5.3 Drug release

In vitro IBU release studies were performed in phosphate-buffered media of pH 7.4 using the dialysis bag technique similar to previously reported studies for wound dressing materials [25,26]. Dialysis bags were equilibrated with dissolution medium for 2 hours prior to experiments. 100 ± 10 mg of CLF_{IBU} , $\text{CH1CL10}_{\text{IBU}}$ and $\text{CH1CL5}_{\text{IBU}}$ were suspended in dialysis bags containing 5 mL of release medium. Dialysis bags were dipped into the separate beakers containing 100 mL of PBS solution at 37 °C and stirred at a rate of 50 rpm. 12 samples over 72h at various time intervals were measured as follows: 2 mL from the PBS and sample solution was transferred into a vial and subsequently, 2 mL of fresh PBS was added to the solution to maintain a constant medium volume. The measurements were performed in triplicate. Using a UV-visible UV3600 spectrophotometer (Shimadzu, Japan), the maximum absorption peaks (264 nm) for IBU in PBS solution and samples at different time intervals were measured. The Beer-Lambert law was utilized to obtain the concentration of the drug, and cumulative drug release was calculated by:

$$Q(\%) = \frac{C_n V + V_i \sum_{i=0}^{n-1} C_i}{M_f} \times 100 \quad \text{Equation (4.7)}$$

Q (%) is the percentage of the cumulative released drug, and V (mL) was the total volume of the samples. C_n (mg/mL) and V_i (mL) were the concentration and the volume of the samples taken at n and i time points. M_f (mg) was the weight of the loaded drug in the fibers, and the number of times that the drug release media was replaced is shown as n.

4.2.5.4 Cytotoxicity

Human dermal fibroblasts were isolated from the adult skin biopsies as previously described by Kreimendahl *et al.* [27]. Cells were cultured at 37 °C and 5% CO₂ in DMEM with 10% FCS. Cells at passage 4 were used for the viability experiment using XTT assay. The CLF and CHCLAF samples were sterilized in 70% ethanol and washed in PBS prior to the tests.

XTT assay was performed according to the ISO 10993-12. In short, aerogel fiber samples and negative control were incubated in a culture medium for 72 h. The negative control was a piece of polyethylene tube, and the positive control was DMSO. Cells were seeded in 96-well plates (1 × 10⁴ cells per well) and were allowed to adhere to the wells for 24 h. After 24 h, cell medium was exchanged with the samples medium, positive control, and negative control or blank. After 1 day of incubation, the XTT assay was performed according to the manufacturer's protocol. The absorbance was measured in a multimode microplate reader M200 (Tecan, Switzerland) at 450 nm with a reference wavelength of 630 nm after 4 hours of adding the salts to the cells. The assessment was performed in five replicates.

4.2.6 Antibacterial activity

4.2.6.1 Disk diffusion method

In order to keep a constant contact area of samples with agar diffusion disks, cylindrical geometries of cellulose and cellulose-chitosan aerogels were utilized. Diffusion disks were used for determining the antibacterial properties of the CHP and cylindrical aerogel samples.

Escherichia coli DH5a and *Staphylococcus aureus* were grown on the nutrient agar slant and kept at 4 °C. Liquid cultures of both bacteria were inoculated from previously established cultures on lysogeny broth (LB) agar plates using 200 mL sterile LB medium

with two different pHs of 5.8 and 6.3. The pH of the media was adjusted using a 1 M HCL solution before autoclavation. Cultures were incubated at 180 rpm and 37° C for 16 h in a shaking incubator; and the agar plates were seeded with 0.1 mL of saturated bacteria suspension. Subsequently, a triplicate of cylindrical samples was placed on the agar plates with two different pHs. Ampicillin (100 µg/mL) was used as the positive control and non-treated plates as a negative control. Results were reported as the radius of the bacterial inhibition zone from the contact area with aerogel cylinders.

4.2.6.2 Determination of optical density of bacterial liquid cultures

This method was adopted from elsewhere [28] to assess the antibacterial activity of the CHP and aerogel fiber samples. One colony from *E. coli* and *S. aureus* was scratched from their agar plate using a sterile pipette tip, and the pipette tip was ejected in a culture tube containing 5 mL of sterile LB medium with two different pHs of 5.8 and 6.3. Then, 20 mg of all samples were incubated in contact with the bacterial suspensions under orbital shaking (180 rpm) for 16 h at 37° C. Ampicillin and sample-free bacterial tubes were used as the positive and negative control. The optical density (OD600) of the samples was measured in 96 well plates at a wavelength of 600 nm using Synergy™ HTX multi-mode microplate reader (BioTek, USA).

4.2.7 Statistical analysis

All the experimental data are expressed as means \pm standard errors (SD). The statistical analysis was done by Originlab (2019 b) using a significance level of $p < 0.05$. Student t-test and one-way ANOVA based on the Tukey post hoc test were performed to determine the differences between different experimental groups.

4.3 Results and Discussions

4.3.1 Fabrication and morphological characterization

After wet spinning, regeneration, washing, and scCO_2 drying processes, the aerogel fibers preserved their white and round cross-sectional shape. **Figure 4.1A-I** shows the schematic of the fabrication process of the CHCLAF prepared from 8.3 wt. % of chitosan and cellulose. A representative example of manually braided textile produced from CHCLAF consisting a minimum of 27 monofilaments is shown in **Figure 4.1A-II**. It also shows the flexibility and strength of the aerogel fibers which could be easily transformed into different textiles for practical applications. **Figure 4.1A-III** is a representative photograph of light yellow cylindrical chitosan-cellulose aerogel fabricated for evaluation of density and antibacterial assessment. The density and porosity of cylindrical aerogel samples were estimated based on equation 4.2 and are

shown in **Table 4.2**. No significant difference was observed between different samples.

The porous cross-section and surface morphologies of CH1CL10 and CH1CL5 aerogel fibers were revealed by SEM as shown in **Figure 4.1B-I, II and III** and **Figure 4.1C-I, II and III**, respectively. Cross-sectional pores consist of mesopores (2–50 nm) and macropores (>50 nm) according to the IUPAC classification. The fabricated aerogel fibers present good integrity and a wrinkled open porous surface. Both CHCLAF cross-sections consisted of a macro-porous outer shell and a nano-porous inner core similar to reported CLFs [18,19]. No significant difference between CHCLAF morphology is observable.

The CH1CL5 and CH1CL10 had a close linear shrinkage range of $20.4 \pm 4.9 \%$ and $22.1 \pm 2.1 \%$, respectively, based on the SEM images. This shrinkage could be attributed to the flexibility of the macromolecules chains of cellulose and chitosan that are slightly compacted during the regeneration process and also the removal of loosely packed fibrils of the gel matrix during washing of the fibers [29]. The hybrid fibers showed lower shrinkage in comparison to the reported value for the pure CLF ($28.7 \pm 1.1 \%$). This can arise from the chitosan interaction with the cellulose nano/microfibrils, which may affect the final physicochemical properties and network structure [12,30].

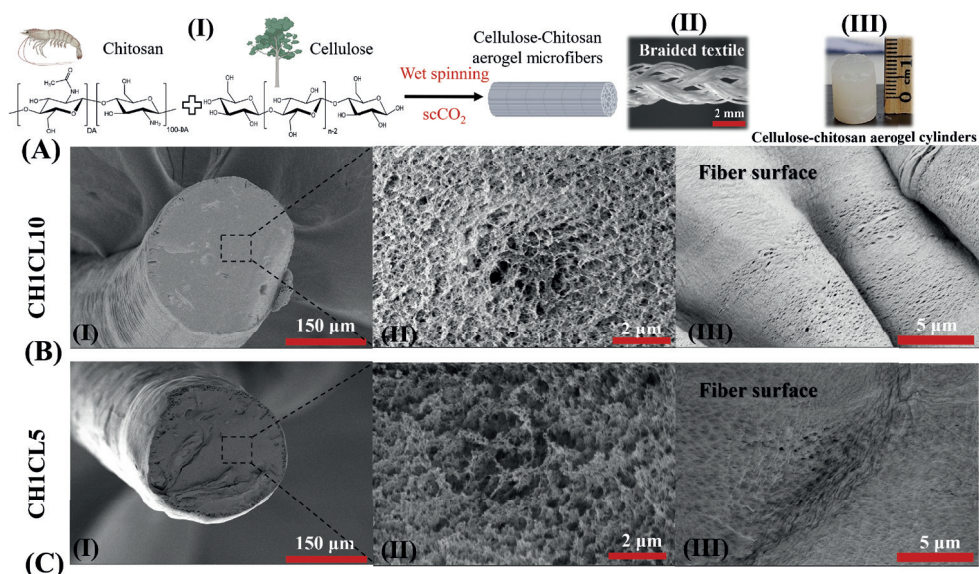


FIGURE 4.1.

(A) Fabrication process of chitosan-cellulose aerogel microfibers (I), a representative image of the chitosan-cellulose aerogel microfibers transformed into a braided textile (II) and examples of produced chitosan-cellulose cylindrical aerogel samples for density and porosity measurements (III). Cross-sectional morphology of the chitosan-cellulose fibers exhibiting a macro-porous outer shell (B-I, C-I) with a nano-porous inner core (B-II, C-II) of CH1CL10 and CH1CL5, respectively. Open porous surface of aerogel CH1CL10 fibers (B-III) and CH1CL5 fibers (C-III). Graphical elements were created using "BioRender.com".

4.3.2 Structural and thermal properties

The elemental analysis proved the presence of nitrogen and chitosan in the structure of CHCLAF. The CH1CL10 and CH1CL5 showed average nitrogen content of 0.59 ± 0.01 wt.% and 1.08 ± 0.01 wt.%, respectively. The calculated chitosan content was 7.23 ± 0.1 wt.% and 13.24 ± 0.1 wt.% for CH1CL10 and CH1CL5, respectively, indicating that both fibers had significantly different chitosan content.

Figure 4.2A describes the FTIR spectra of polysaccharides and aerogel fibers. For all five samples, the broad bands at $3500\text{--}3100\text{ cm}^{-1}$ and $2800\text{--}2900\text{ cm}^{-1}$ were attributed to the --OH stretching and --CH stretching vibrations, respectively [30]. In the case of chitosan powder and fibers, NH_2 groups have overlapped at the same range with --OH bands [16]. Similarly, in all samples, C=O stretching and C-O stretching emerged at $1645\text{--}1650\text{ cm}^{-1}$ and $1014\text{--}1020\text{ cm}^{-1}$. In the CHP, the characteristic amide groups of chitosan appeared at 1615 cm^{-1} (amide I), 1554 cm^{-1} (amide II), and 1380 cm^{-1} (amide III). Such peaks intensity decreased noticeably in the CHCLAF. In the case of MCC and CHP in the range from 3000 to 3600 cm^{-1} , the band at 3300 cm^{-1} disappeared and the 3359 cm^{-1} band shifted to higher wavenumbers (3367 cm^{-1}). It has been reported that

such phenomena can occur due to the intermolecular interaction between the OH and NH groups of cellulose and chitosan during the process of dissolution and regeneration [12,31]. Overall, the FTIR spectra aided to confirm the presence of chitosan molecules in the CHCLAF.

The XRD measurements were performed in order to investigate the microstructural changes in the CHCLAF caused during processing. XRD patterns of MCC, CHP, CLF and blended aerogel microfibers are shown in **Figure 4.2B**. MCC exhibited the peaks at $2\theta = 14.8^\circ, 16.4^\circ, 20.4^\circ, 22.7^\circ$, and 34.5° which were indexed as the cellulose crystalline plane (1–10), (110), (102)/(012), (200), and (004) [32]. The diffraction pattern of the CHP showed a prominent peak at 20.3° and was assigned to (1 1 0) as has been reported for chitosan [33]. In the CLF, CH1CL10 and CH1CL5, remarkable changes were observed in their diffraction pattern of aerogels samples as the aforementioned peaks were transformed into a broad low-intensity peak between $15\text{--}20^\circ$. The results demonstrate that the crystal structure of the MCC and CHP was disrupted during the processes of dissolving in ZnCl_2 and regeneration in iPrOH. This is in accordance with some previous studies which showed that the dissolution in salt melt hydrate and blending MCC and CHP usually resulted in decreased crystallinity [30,31]. The broad peaks of blended samples could be also attributed to the reformation of hydrogen bonds between cellulose and chitosan and support the FTIR results [16].

TGA graphs of initial materials and fabricated aerogel fibers are shown in **Figure 4.2C**. The graphs exhibited the weight decline in two main steps. The initial weight loss below 100°C arose from the vaporization of unbound and capillary water and the second step at $220\text{--}350^\circ\text{C}$ was the relatively rapid decomposition of the cellulose and chitosan chains. The results indicated that the thermal stabilities and onset thermal degradation of the MCC and CLF were inferior to those of the CHP and CHCLAF.

The derivative thermogravimetry (DTG) curves are shown in **Figure 4.2D**. In the first region (I), the increase of peak intensity and area demonstrated higher moisture uptake of the aerogel fiber samples apparently due to their porous nature providing a more accessible hydroxyl group for water molecules. The peaks in the second step (II) have shifted toward lower temperature and the peak area has decreased, which implies that the CHCLAF exhibited a slower degradation rate compared to the MCC and CLF. These thermal stability data at high temperatures could be used to avoid degradation in aerogel samples involved in high temperature processes for instance heat sterilization or some characterization measurements such as high temperature degassing of samples before N_2 adsorption-desorption.

Therefore, it can be justified that the disrupted crystalline structure, addition of chitosan, and interactions between cellulose and chitosan chains after dissolving and processing in the ZnCl_2 solution affected the thermal decomposition properties of the fibers in comparison to macromolecular powders. Moreover, it was observed that the residual amount of the CHCLAF blend fibers escalated with the increase of the chitosan contents. This could be possibly explained by the greater interaction between amino groups of the chitosan and the hydroxyl groups of the cellulose as found in FTIR and XRD results [16].

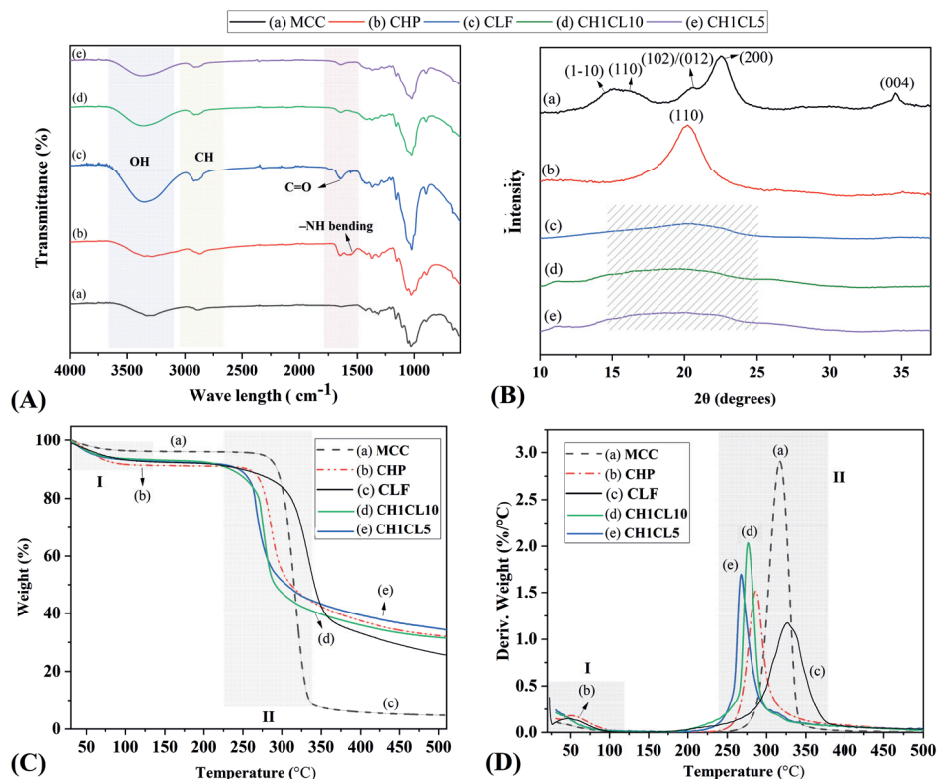


FIGURE 4.2.

(A) FTIR spectra of the MCC, CHP and aerogel microfiber samples indicating the presence of amide groups (-NH) in the blended aerogel fiber samples as well as the disruption of the crystalline structure of powders after dissolution and wet spinning. (B) XRD pattern of the MCC, CHP, and the aerogel fibers proving the amorphous structure (cross-hatched region) of the fabricated samples and the highly crystalline structure of the initial powders. (C) TGA graphs of the powders and aerogel fibers. The initial weight loss below 100 $^{\circ}\text{C}$ (I, cross-hatched region) arose from the vaporization of unbound and capillary water and the second step at 220–350 $^{\circ}\text{C}$ (II, cross-hatched region) was the relatively rapid decomposition of the cellulose and chitosan chains. Addition of chitosan to cellulose fibers decreased the thermal stability of fibers. (D) DTG of the powders and fibers showed that the decomposition range was broader and the rate was slower in the fibers; the chitosan addition increased the degradation rate in comparison to pure cellulose fibers.

4.3.3 Textural properties of aerogel fibers

The N₂ adsorption-desorption isotherms of the aerogel fibers are displayed in **Figure 4.3A**. The higher quantities of N₂ were absorbed in CHCLAF compared to the CLFs. Nevertheless, the isotherms graphs for samples are comparable to IUPAC type IV with a hysteresis loop in the range of 0.7–1.0, representing the presence of meso- and macroporous structure, which is pursuant to the SEM results [18,34].

The textural properties including BET specific surface area (**Figure 4.3B**), BJH desorption pore volume (**Figure 4.3C**), and BJH desorption average pore width diameter of the aerogel fibers were analyzed by nitrogen adsorption-desorption. In general, the analyzed CHCLAF possess surface area in the range of 288–305 m²/g and pore volume in the range of 1.14–1.31 cm³/g, comparable with the corresponding values for polysaccharide-based aerogels reported in the literature [35,36]. On the other hand, the reported value for CLFs surface area (127 ± 19 m²/g) and pore volume (288–305 m²/g) was noticeably lower than CHCLAFs. The average pore width diameter of the aerogel fibers is in the range of 9–12 nm. These results imply “no convection” effect since aerogel fibers’ pore sizes are typically smaller than the mean free path of gas molecules (69 nm), making them interesting thermal insulation material [37]. Finally, the values of textural properties of aerogel microfiber samples is presented in **Table 4.2**.

The relatively higher specific surface area and pore volume of CHCLAFs in comparison to CLF could possibly be attributed to different macromolecule phases of the blend in the gelation and during the regeneration procedure [37]. However, such conclusions need further assessment of the current system by other techniques such as SAXS. In addition, in the majority of bioaerogel studies, the structure establishment is presumed to happen during solution gelation and/or solvent-exchange steps, and the subsequent scCO₂ drying leads to slight alterations. However, this has not been proven thoroughly and experimentally in most biopolymer systems and some recent studies challenge the common perception [38]. Overall, the formation of porous structures is more complicated for hybrid aerogels from biomacromolecules and requires further research and it is not within the focus of the current study.

TABLE 4.2.

Linear diameter shrinkage (%) and textural properties of aerogel microfiber samples including estimated density (g/cm^3) and porosity (%) as well as BET surface area (m^2/g), BJH desorption pore volume (cm^3/g), and BJH desorption average pore diameter (nm).

SAMPLE NAME	LINEAR SHRINKAGE (%)	DENSITY* (g/cm^3)	POROSITY * (%)	SURFACE AREA (m^2/g)	PORE VOLUME (cc/g)	AVERAGE PORE WIDTH DIAMETER (nm)
CLF	28.7 ± 1.1	0.18 ± 0.025	87.5 ± 1.7	127 ± 19	0.77 ± 0.15	9.28 ± 0.037
CH1CL10	20.4 ± 4.9	0.17 ± 0.012	88.4 ± 0.8	288 ± 10	1.14 ± 0.07	11.1 ± 1.053
CH1CL5	22.1 ± 2.1	0.19 ± 0.033	86.8 ± 2.2	305 ± 13	1.31 ± 0.04	$11.06 \pm .048$

*Estimated for cylindrical geometries

4.3.4 Mechanical properties

The CLF, CH1CL10, and CH1CL5 fibers showed maximum forces of 159 ± 14 cN, 123 ± 15 cN, and 56 ± 9 cN, respectively. **Figure 4.3D** shows the representative curves of tenacity versus elongation (%) with an indication of standard deviation for the maximum tenacity (cN/dtex) and maximum elongation (%) of all fibers. The CHCLAF exhibited a similar tensile profile in comparison to the previously disclosed assessments on CLFs in which an elastic region was followed by a plastic deformation until failure happened [18,19]. CLF, CH1CL10, and CH1CL5 exhibited maximum tenacity of 0.43 ± 0.052 , 0.28 ± 0.021 , and 0.24 ± 0.024 cN/dtex , respectively. The maximum elongation was 16.2 ± 5.33 , 4.2 ± 2.06 , and 2.1 ± 1.02 % for CLF, CH1CL10 and CH1CL5, respectively.

In the CLFs, it has been observed that by increasing the initial cellulose concentration, the ultimate tenacity was enhanced which could be attributed to the increased amount of cellulose in the skeleton structure [18,39]. Furthermore, cellulose is well-known for its outstanding intrinsic mechanical properties with a theoretical modulus of about 100–200 GPa (~ 63 – 125 GPa g/cm^3) and tensile strength of about 4.9–7.5 GPa (~ 3.0 – 4.7 GPa g/cm^3) in its crystalline form. It has been reported that the addition of chitosan can lower the tensile strength of the blend due to the lower bonding strength of chitosan [40]. In the case of CH1CL10 and CH1CL5, the cellulose amount was decreased and replaced by chitosan which consequently lowered the mechanical properties. This indicates that the blending ratio of hybrid aerogel fibers should be optimized based on the required textural and antibacterial properties without lowering their mechanical properties significantly.

The results also indicated that the maximum tenacity and elongation values had large standard deviations. One possible explanation could be the presence of the pores and wrinkles on the surface of fibers, minor diameter changes along the fiber axis, slight

residual stiffness during the measurement, and variations in the structure of fibers. To enhance the mechanical properties of the fibers, chemical crosslinking between hydroxyl groups of cellulose and chitosan could be performed utilizing solvent-free and non-invasive techniques to prevent the structural collapse of the fibers and prevent loss of amino groups, responsible for antibacterial activities.

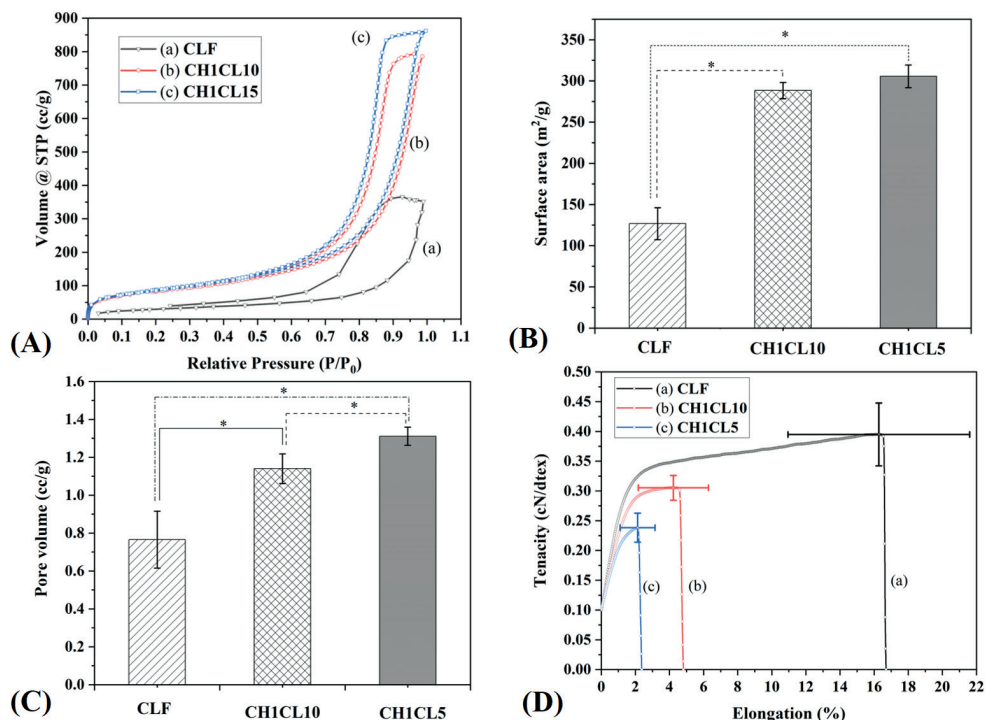


FIGURE 4.3.

(A) The N_2 adsorption-desorption isotherm curves of the aerogel fibers. (B) The BET specific surface area; the CHCLAFs showed a higher quantity than the CLFs. (C) BJH pore volume of aerogel fibers; fibers with higher chitosan quantity showed higher pore volume. (D) Representative curves of tenacity-elongation for the CLF, CH1CL10, and CH1CL5 with the maximum tenacity and the maximum elongation including the standard deviations. Addition of chitosan decreased the mechanical properties of the fibers. In all diagrams (* $p < 0.05$).

4.3.5 Humidity, water and wound exudate uptake

The CHCLAF fibers exhibited a high moisture absorbance weight ratio due to the presence of accessible hydroxyl groups in their porous structure (**Figure 4.4A**). Moreover, with increasing the relative humidity from 50 to 80% in all samples, the weight ratio of the adsorbed humidity increased; however, the absorbed amount of humidity by CLFs (15.8 ± 1.32 wt.%) was significantly lower than CH1CL10 (19.5 ± 1.57 wt.%) and CH1CL5 (19.3 ± 1.52 wt.%) at 80% RH. The lower pore volume of CLFs could be the main reason for the lower humidity absorption.

The water uptake capacity of the aerogel braided meshes was studied in PBS and results are shown in **Figure 4.4B**. The PBS solution is utilized to simulate the human body fluid environment in terms of ion concentration and osmolarity. The water uptake for each braided CHCLAF samples after 24 hours of immersion (~ 400 wt.%) is slightly higher than the first hour. Although no striking difference is observed between various samples at similar time points.

Although crystalline domains of cellulose are inaccessible to water, non-crystalline domains are easily accessible to water. As shown in XRD results, the regenerated fibers were mainly in amorphous form, making them more susceptible to water absorption [41]. Furthermore, despite differences in textural properties of aerogel fibers, their water uptake behavior was similar. This could be possibly because of the differences in the macrostructure of the braided patches rather than the microstructural properties of individual fibers as the water can be entrapped in between the filaments and thus have a huge impact on the final total weight.

Furthermore, fibers did not show any disintegration or matrix deterioration in PBS after 1 week (**Figure 4.4C**). Droplet sorption by single aerogel fiber samples was observed by a macroscopic camera and all the samples absorbed the droplets completely after 10 mins (**Figure 4.4D**). These photographs also confirm that the measured time points in water uptake and humidity absorbance were long enough for fibers to get saturated with water molecules.

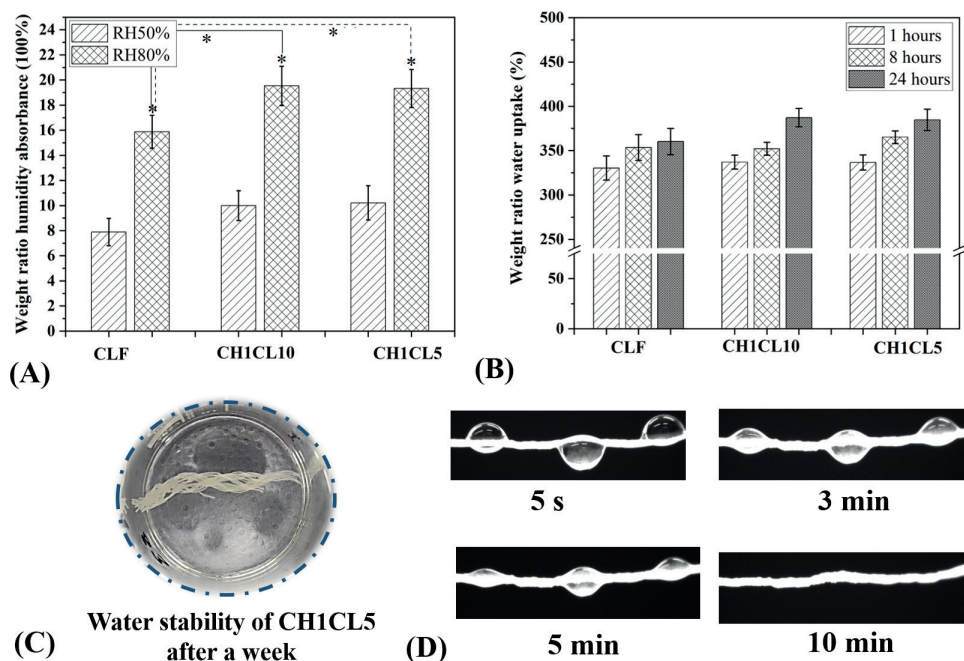


FIGURE 4.4.

(A) The humidity absorbance weight ratio of the aerogel fibers at 50 and 80 RH% after 24 h. (B) Water uptake of the braided aerogel fiber samples at 1, 8, and 24 h. (C) An exemplary image showing the wet stability of the CHCLAF, CH1CL5 in this picture, after a week of being immersed in PBS. (D) Representative images of droplet sorption by aerogel fiber samples (here CH1CL5) at 5 s, 3, 5 and 10 min. In all diagrams (* $p < 0.05$).

By using skin-mimicking layers, wound exudate uptake assessment on braided samples was conducted to simulate the *in vivo* conditions. A gel made of agar-gelatin with a hypodermis and a dermis mimicking layer was created as illustrated in **Figure 4.5A** and **B**. In the first 3 hours, a rapid exudate uptake up to 49.6 ± 2.71 and 51.7 ± 2.83 wt.% is observed for CHCL10 and CH1CL5 braided patches, respectively (**Figure 4.5C**). Overall the uptake values were found to be lower for CLF mesh and it was 43.1 ± 5.36 wt.% after three hours. Following a rapid uptake of water in the structure, the rate declined and stabilized after 48 hours. The maximum uptake of braided meshes was 73.4 ± 3.51 , 94.8 ± 4.95 , and 93.95 ± 7.01 for CLF, CHCL10 and CH1CL5 braided samples, respectively.

The exudate uptake values in comparison to water uptake ones were significantly lower due to the lower water accessibility and restricted diffusion of water molecules which occurs only through the surface that was in contact with the gelatin-agar layers. The CLFs presumably due to it is lower specific surface area and pore volume absorbed lower

quantities of water in the wound exudate uptake test. Overall, it can be concluded that the CHCLAF are better candidates than CLFs as wound dressing products since they can provide a moister environment at the wound site and absorb large amounts of exudate.

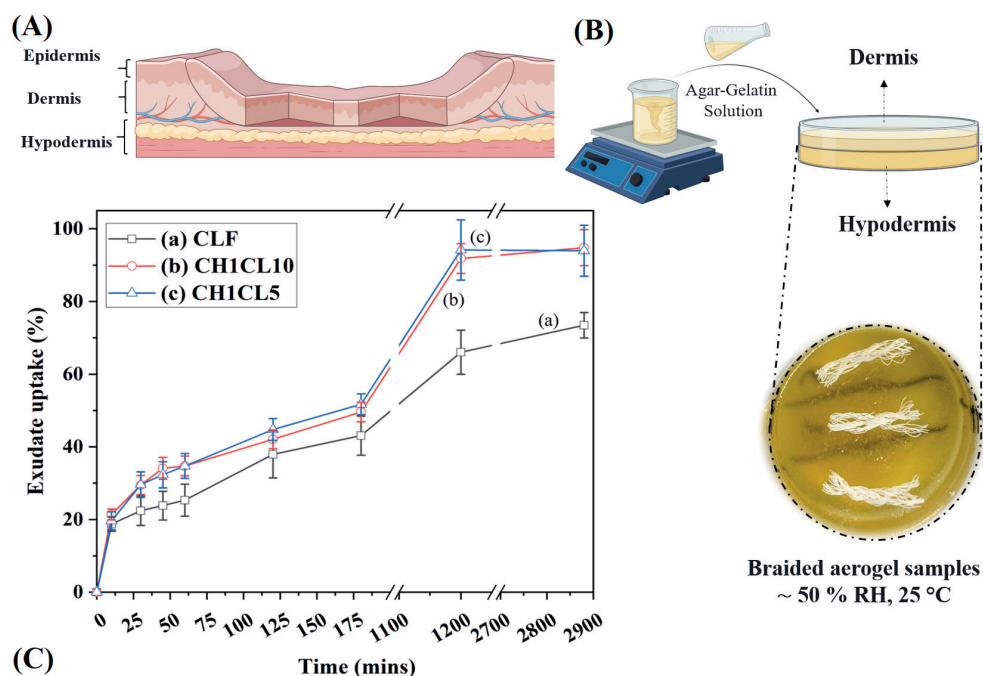


FIGURE 4.5

(A) The graphical representation of the 3 skin layers. (B) Skin mimicking fabrication process and a photograph of the hypodermis and dermis layers in the dish including the braided meshes on the surface. (C) The exudate uptake graph for the aerogel braided samples exhibits better exudate uptake capability of the CHCL10 and CHCL5 braided meshes compared to the CLF samples. Graphical elements were created with “BioRender.com”.

4.3.6 Drug loading efficiency and drug release profiles

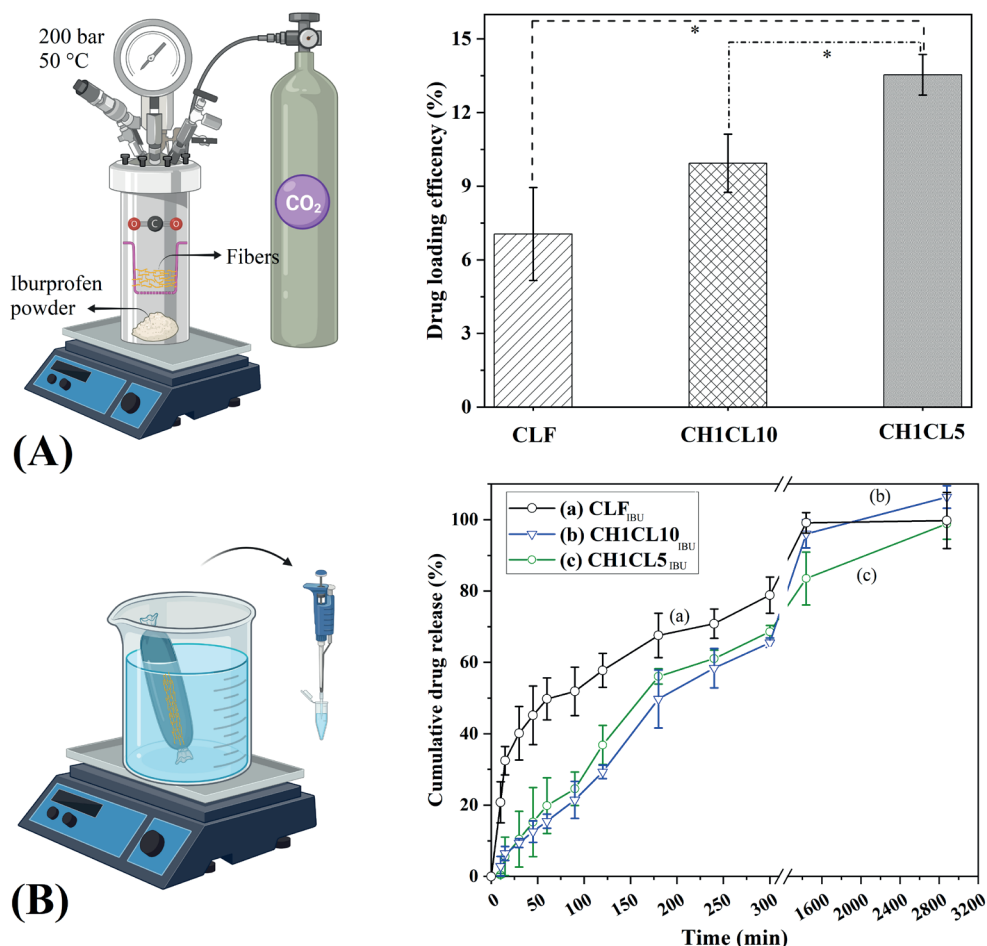
Figure 4.6A displays the drug loading efficiency of aerogel fibers impregnated by the post-treatment technique. The highest entrapment values up to 13.54 ± 0.825 % were achieved for CH1CL5. It is clear that IBU loading efficiency improved with the increase of aerogel fibers' specific surface area and pore volume. Such higher loading yield occurs based on a direct correlation between the impregnation efficiency and specific surface area, which is due to the amount of internal pores' surface available for drug deposition [42,43].

The drug release profiles for CLF_{IBU}, CH1CL10_{IBU}, and CH1CL5_{IBU} are shown in **Figure 4.6B**. CH1CL10_{IBU} and CH1CL5_{IBU} exhibited a similar and more sustained release

profile in comparison to the CLF_{IBU}. In the first hour, only 15.5 ± 1.97 and 21.4 ± 5.18 % of IBU from CH1CL10_{IBU} and CH1CL5_{IBU}, respectively, were released while CLF_{IBU} exhibited burst effect since 49.8 ± 5.89 % was released. The drug eluted fractions for CH1CL10_{IBU} and CH1CL5_{IBU} were in the same range over the 600 min; however, after 24 h, the CH1CL10_{IBU} drug release was slightly higher possibly due to a lower pore volume in comparison to CH1CL5_{IBU}. Also, CLF_{IBU} possessed significantly lower specific surface area and pore volume in comparison to CH1CL10_{IBU} and CH1CL5_{IBU} which could be the main reason for the observed burst effect.

As previously reported in the literature, loading of the IBU using post-treatment scCO₂ is mainly adsorbed on a molecular level. In comparison to other loading techniques, using the scCO₂ impregnation technique can be considered favorable to obtain targeted application products and sustained release [17,44,45]. In the case of CLFs and CHCLAF aerogels loaded by post-treatment scCO₂, no chemical interactions between the macromolecules and the drug can be noticed which have been confirmed by two main findings. First, the IBU release from the aerogels is complete, and the residual drug in the polymer matrix is negligible. Second, the IBU can be washed out from the aerogel networks by scCO₂ extraction [42].

The release rate from polysaccharide aerogels also depends on the stability of the aerogel matrix in the release medium. Since CHCLAF exhibited very well dimensional stability in the wet environment even after a week, it makes them more suitable for drug delivery purposes compared to some polysaccharides reported from cellulose nanofibers [24], and alginate and starch aerogel [17]. Moreover, the final aerogel wound dressing can be composed of CLFs and CHCLAF fibers with two different drug release profiles. For instance, fast local administration of the antibiotic at the wound site to prevent infections shortly after wound debridement can be obtained by antibiotic eluting from CLFs while longer sustained anti-inflammatory substances can be released via CHCLAF.

**FIGURE 4.6.**

(A) Post-treatment scCO₂ IBU loading of the aerogel fibers. The chitosan-cellulose fibers showed higher loading efficiency than pure cellulose aerogel fibers. (B) IBU release from CLF, CH1CL10, and CH1CL5. An improved sustained release profile was observed in CH1CL10 and CH1CL5 samples in comparison to the CLF samples. (* $p < 0.05$). Graphical elements were created using "BioRender.com".

4.3.7 Cytotoxicity

The human fibroblast cell viability was observed in the CLF, CH1CL5, and CH1CL10 samples after 1 day of cell culture demonstrating that the fibrous meshes provided suitable conditions for cell growth (**Figure 4.7**). The increase of chitosan content in the CH1CL5 decreased the cell viability compared to the negative control, CLF, and CH1CL10 but was still significantly higher than the positive control. Even though these hybrid aerogel fibers have been produced for the first time, previously reported studies already proved the non-toxic nature of other types of chitosan-cellulose hybrid materials too [10,46].

In future studies, the cells viability dependency on chitosan concentration can be investigated comprehensively. In addition, *in vitro* and *in vivo* assays to analyze the effect of aerogel fibers on healing progression and rate in acute and chronic conditions could also be performed to obtain a broader perspective about their wound dressing application.

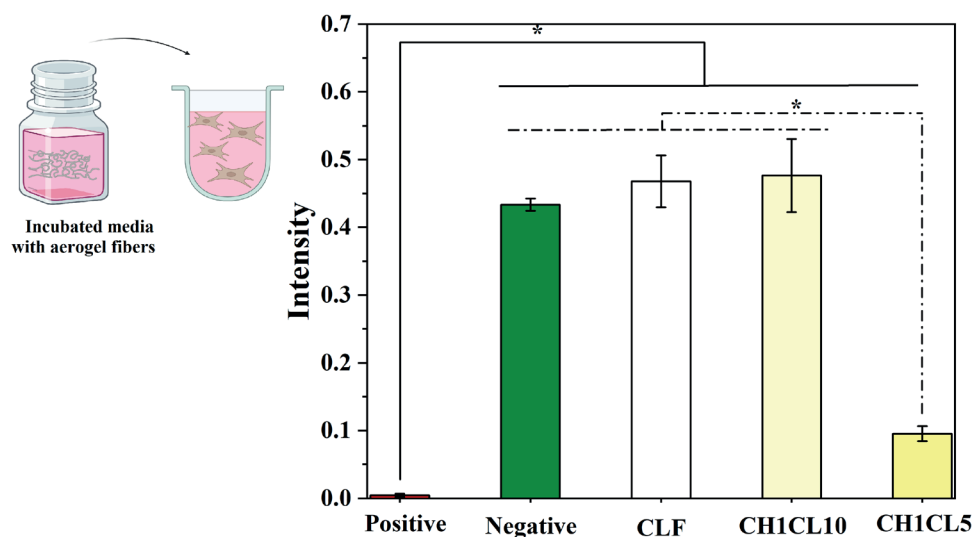


FIGURE 4.7.

XTT assay of the aerogel fibers; cell viability was observed in the samples on day 1 of the experiment. The negative sample was a piece of polyethylene and the positive sample was DMSO. (* data statistically significantly different, $p < 0.05$). Graphical elements were created with “BioRender.com”.

4.3.8 Antimicrobial characteristics

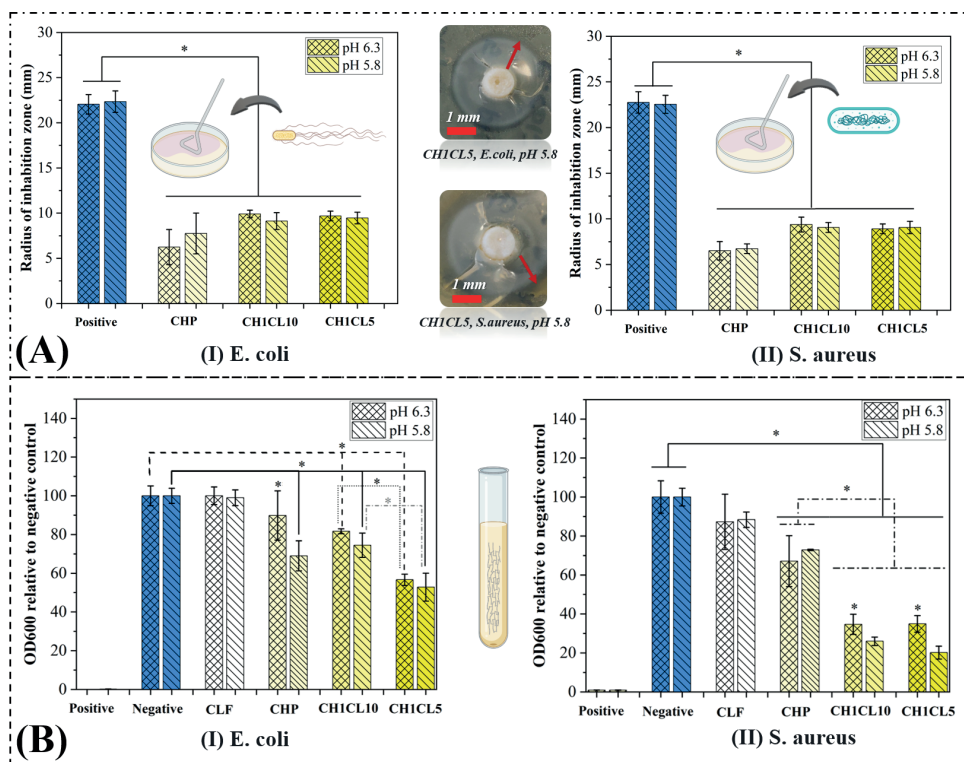
Based on a disc diffusion method, the antibacterial activity of the powders and aerogel cylinders were tested by *E. coli* (Figure 4.8A-I) and *S. aureus* (Figure 4.8A-II) in two different pHs of 5.8 and 6.3. An inhibition zone up to approximately 10 mm was observed around the CHP and two chitosan-cellulose cylinders while no inhibition zone was spotted for the pure cellulose cylinder and therefore not shown in the diagram. No significant difference in inhibition radius zones of the CHP and chitosan and cellulose cylinders between pH 5.8 and 6.3 for both bacteria were detected.

Aerogel fibers and CHP antibacterial properties were also investigated in the bacterial suspension of *E. coli* (Figure 4.8B-I) and *S. aureus* (Figure 4.8B-II) at two different acidic pHs of 5.8 and 6.3. The Bacterial growth monitored by OD600 revealed that the CLFs in both pHs did not affect the *E. Coli* and *S. aureus* growth and had similar performance to the negative control. However, the bacteria proliferation significantly

decreased in CH1CL10, and CH1CL5 and CHP (except in *E. coli* and pH 6.3), in comparison to negative control in both pHs and bacteria. Although the CHP prevented the *E. Coli* growth significantly at the lower pH, *S. aureus* growth in the CHP suspension medium was not pH dependent. Moreover, CH1CL5 had higher *E. Coli* inhibition activity than CH1CL10 apparently due to the higher content of chitosan in the aerogel fiber matrix, but their activity did not seem to be different in various pHs. In the case of *S. aureus*, the antibacterial growth of CHP was lower in comparison to other aerogel fiber samples. Also at lower pH of 5.8, the CHCLAF showed better antibacterial performance in comparison to pH 6.3. However, both CH1CL10 and CH1CL5 had a similar range of the *S. aureus* inhibition activity in both pHs.

Though the exact antibacterial mechanism of chitosan is still debatable, many studies have suggested that the negatively charged cell wall of a bacterium can be disrupted by the chitosan protonated amino groups due to the interaction between opposite charges [47]. It is known that the chitosan's antimicrobial activity is influenced by several factors including the type of microorganism, the source of chitosan, temperature, molecular weight, degree of deacetylation and pH [48]. It has been proposed that the glucosamine monomer of chitosan obtains a positive charge (NH^{3+}) at the pH lower than 6.3-6.5 and that the antibacterial activity of chitosan increases as the pH decrease which can justify the higher *S. aureus* inhibition of the CHCLAF in the lower pH media [49]. Regarding *E. Coli*, CLCHAF bacterial inhibition did not seem to be pH dependent possibly due to the porous nature of the fibers which allows the amino groups to get protonated easier. Similarly, it can be the probable explanation for better performance of CHCLAFs in *S. aureus* in comparison to CHP in both pHs.

Traditional wound dressings mainly suffer from the lack of stability and the risk of infection. For instance, gram-positive bacteria, such as *S.aureus*, are mainly found in the initial stage of wound infection and are responsible for over 90% of infectious wound ulcers; however, gram-negative bacteria, such as *E.coli*, can be found when the wound is already developed [50,51]. Therefore, due to favorable antibacterial properties of CHCLAFs, they can be considered as promising materials for wound dressing applications especially with the pathological acidic environment ($\text{pH} < 6.3\text{-}6.5$) of the infected chronic wounds. Future works can be devoted to loading of the fibers with various antibiotics to increase the bactericidal activity and obtain pH nondependent patches.

**FIGURE 4.8.**

(A) Disk diffusion antibacterial assessment of the CHP, CHICL10 and CHICL5 cylindrical aerogels against *E. coli* (I) and *S. aureus* (II). Chitosan containing cylindrical aerogel samples showed inhibition zone, and their performance was not different at two pHs of 5.8 and 6.3; however, cellulose cylinders did not show any antibacterial activity. (B) Liquid culture and the optical density (600 nm) of the CLF, CHP, CHICL10, and CHICL5 samples in the bacterial suspension of *E. coli* (I) and *S. aureus* (II). In both measurements, ampicillin was used as a positive control. Aerogel fibers containing chitosan showed inhibition activity while CLF did not show any antibacterial properties. In all diagrams (* data statistically significantly different, $p < 0.05$). Graphical elements were created with “BioRender.com”.

4.4 Conclusion

Chitosan-cellulose aerogel microfibers have been prepared successfully by wet spinning of salt melt hydrate of ZnCl_2 and consequent scCO_2 drying. The CHCLAF showed a low density ($\sim 0.18 \text{ g/cm}^3$), high porosity ($\sim 85\%$), and large specific surface area ($\sim 300 \text{ m}^2/\text{g}$) with a macro-porous outer shell and a nano-porous inner core. Better-sustained release of ibuprofen was observed in the CHCLAF in comparison to the CLFs. Also, the CHCLAF were non-toxic and bactericidal against *E. Coli* and *S. aureus*. In conclusion, addition of chitosan to cellulose in order to form hybrid aerogel microfibers led to a new class of wound dressing materials with significantly improved textural characteristics, antibacterial properties, and more sustained drug release behavior.

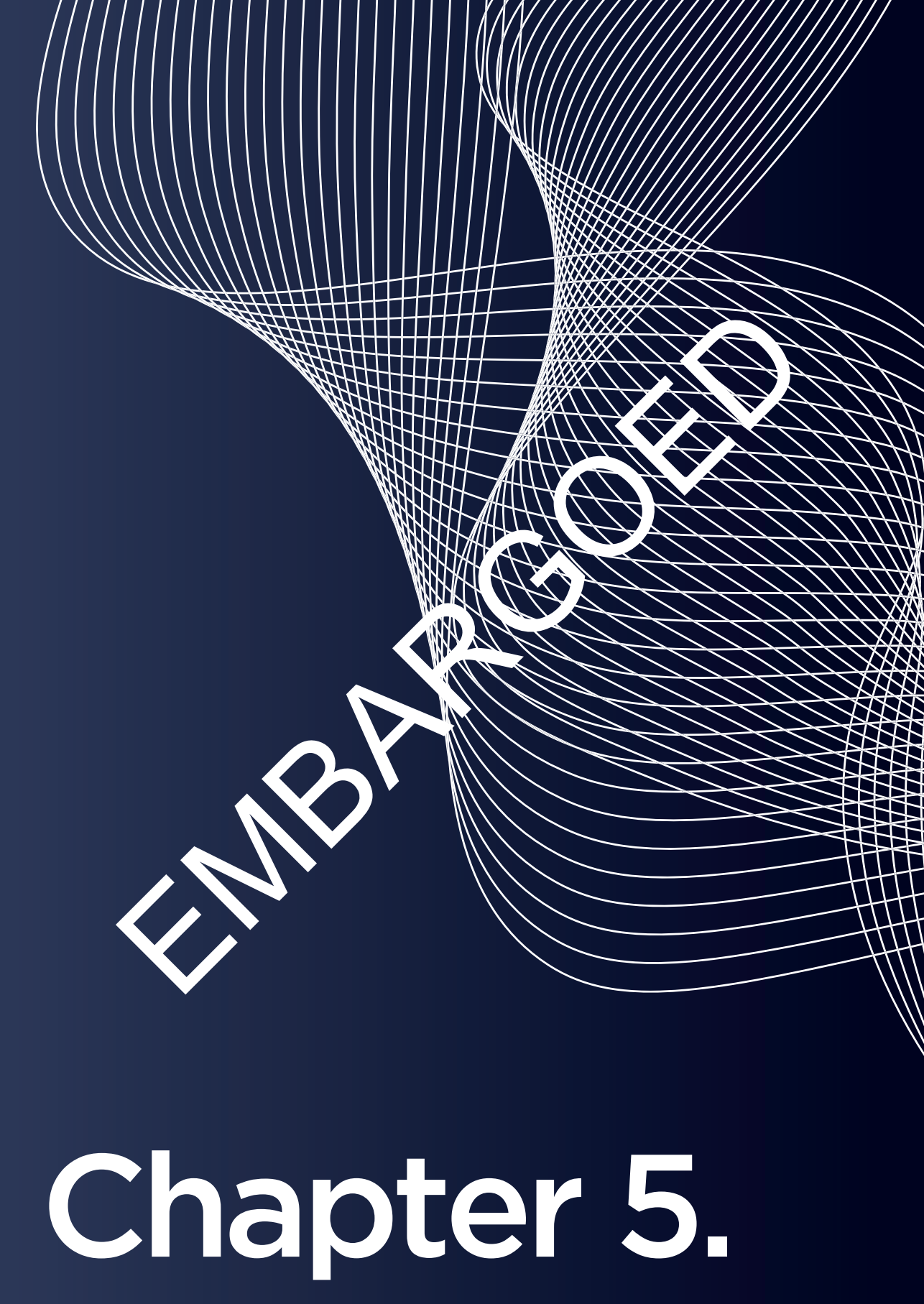
References

1. Sen, C.K. Human Wounds and Its Burden: An Updated Compendium of Estimates. *Adv Wound Care (New Rochelle)* **2019**, *8*, 39-48, doi:10.1089/wound.2019.0946.
2. VTBartels. *Handbook of medical textiles*; Woodhead publishing: 2011.
3. Rostamitabar, M.; Abdelgawad, A.M.; Jockenhoevel, S.; Ghazanfari, S. Drug-Eluting Medical Textiles: From Fiber Production and Textile Fabrication to Drug Loading and Delivery. *Macromolecular bioscience* **2021**, *n/a*, 2100021, doi:https://doi.org/10.1002/mabi.202100021.
4. French, A.D. Glucose, not cellobiose, is the repeating unit of cellulose and why that is important. *Cellulose* **2017**, *24*, 4605-4609, doi:10.1007/s10570-017-1450-3.
5. Dassanayake, R.S.; Acharya, S.; Abidi, N. Biopolymer-based materials from polysaccharides: Properties, processing, characterization and sorption applications. In *Advanced Sorption Process Applications*, IntechOpen: 2018.
6. Yuan, Z.; Cheng, J.; Lan, G.; Lu, F. A cellulose/Konjac glucomannan-based macroporous antibacterial wound dressing with synergistic and complementary effects for accelerated wound healing. *Cellulose* **2021**, *28*, 5591-5609, doi:https://doi.org/10.1007/s10570-021-03821-x.
7. Sahana, T.G.; Rekha, P.D. Biopolymers: Applications in wound healing and skin tissue engineering. *Molecular Biology Reports* **2018**, *45*, 2857-2867, doi:10.1007/s11033-018-4296-3.
8. Sulaeva, I.; Henniges, U.; Rosenau, T.; Potthast, A. Bacterial cellulose as a material for wound treatment: Properties and modifications. A review. *Biotechnology advances* **2015**, *33*, 1547-1571, doi:https://doi.org/10.1016/j.biotechadv.2015.07.009.
9. Bano, I.; Arshad, M.; Yasin, T.; Ghauri, M.A.; Younus, M. Chitosan: A potential biopolymer for wound management. *International journal of biological macromolecules* **2017**, *102*, 380-383, doi:https://doi.org/10.1016/j.ijbiomac.2017.04.047.
10. Fan, X.; Li, Y.; Li, X.; Wu, Y.; Tang, K.; Liu, J.; Zheng, X.; Wan, G. Injectable antibacterial cellulose nanofiber/chitosan aerogel with rapid shape recovery for noncompressible hemorrhage. *International journal of biological macromolecules* **2020**, *154*, 1185-1193, doi:https://doi.org/10.1016/j.ijbiomac.2019.10.273.
11. Minagawa, T.; Okamura, Y.; Shigemasa, Y.; Minami, S.; Okamoto, Y. Effects of molecular weight and deacetylation degree of chitin/chitosan on wound healing. *Carbohydrate Polymers* **2007**, *67*, 640-644, doi:https://doi.org/10.1016/j.carbpol.2006.07.007.
12. Lin, W.-C.; Lien, C.-C.; Yeh, H.-J.; Yu, C.-M.; Hsu, S.-h. Bacterial cellulose and bacterial cellulose-chitosan membranes for wound dressing applications. *Carbohydrate Polymers* **2013**, *94*, 603-611, doi:https://doi.org/10.1016/j.carbpol.2013.01.076.
13. Ribeiro, N.; Soares, G.C.; Santos-Rosales, V.; Concheiro, A.; Alvarez-Lorenzo, C.; García-González, C.A.; Oliveira, A.L. A new era for sterilization based on supercritical CO₂ technology. *Journal of Biomedical Materials Research Part B: Applied Biomaterials* **2020**, *108*, 399-428, doi:10.1002/jbm.b.34398.
14. Ulker, Z.; Erkey, C. An advantageous technique to load drugs into aerogels: Gas antisolvent crystallization inside the pores. *The Journal of Supercritical Fluids* **2017**, *120*, 310-319, doi:https://doi.org/10.1016/j.supflu.2016.05.033.
15. Rostamitabar, M.; Seide, G.; Jockenhoevel, S.; Ghazanfari, S. Effect of Cellulose Characteristics on the Properties of the Wet-Spun Aerogel Fibers. *Applied Sciences* **2021**, *11*, 1525, doi:https://doi.org/10.3390/app11041525.
16. Lin, S.; Chen, L.; Huang, L.; Cao, S.; Luo, X.; Liu, K.; Huang, Z. Preparation and characterization of chitosan/

- cellulose blend films using $\text{ZnCl}_2 \cdot 3\text{H}_2\text{O}$ as a solvent. *Bioresources* **2012**, *7*, 5488-5499, doi:<https://doi.org/10.15376/biores.7.4.5488-5499>.
17. Mehling, T.; Smirnova, I.; Guenther, U.; Neubert, R. Polysaccharide-based aerogels as drug carriers. *Journal of Non-Crystalline Solids* **2009**, *355*, 2472-2479, doi:<https://doi.org/10.1016/j.jnoncrysol.2009.08.038>.
 18. Rostamitabar, M.; Subrahmanyam, R.; Gurikov, P.; Seide, G.; Jockenhoevel, S.; Ghazanfari, S. Cellulose aerogel micro fibers for drug delivery applications. *Materials Science and Engineering: C* **2021**, *127*, 112196, doi:<https://doi.org/10.1016/j.msec.2021.112196>.
 19. Karadagli, I.; Schulz, B.; Schestakow, M.; Milow, B.; Gries, T.; Ratke, L. Production of porous cellulose aerogel fibers by an extrusion process. *The Journal of Supercritical Fluids* **2015**, *106*, 105-114, doi:<https://doi.org/10.1016/j.supflu.2015.06.011>.
 20. Bilbao-Sainz, C.; Chiou, B.-S.; Williams, T.; Wood, D.; Du, W.-X.; Sedej, I.; Ban, Z.; Rodov, V.; Poverenov, E.; Vinokur, Y., et al. Vitamin D-fortified chitosan films from mushroom waste. *Carbohydrate Polymers* **2017**, *167*, 97-104, doi:<https://doi.org/10.1016/j.carbpol.2017.03.010>.
 21. Yen, M.-T.; Yang, J.-H.; Mau, J.-L. Physicochemical characterization of chitin and chitosan from crab shells. *Carbohydrate Polymers* **2009**, *75*, 15-21, doi:<https://doi.org/10.1016/j.carbpol.2008.06.006>.
 22. Batista, M.P.; Gonçalves, V.S.S.; Gaspar, F.B.; Nogueira, I.D.; Matias, A.A.; Gurikov, P. Novel alginate-chitosan aerogel fibres for potential wound healing applications. *International journal of biological macromolecules* **2020**, *156*, 773-782, doi:<https://doi.org/10.1016/j.ijbiomac.2020.04.089>.
 23. Chen, A.I.; Balter, M.L.; Chen, M.I.; Gross, D.; Alam, S.K.; Maguire, T.J.; Yarmush, M.L. Multilayered tissue mimicking skin and vessel phantoms with tunable mechanical, optical, and acoustic properties. *Medical Physics* **2016**, *43*, 3117-3131, doi:<https://doi.org/10.1118/1.4951729>.
 24. Darpentigny, C.; Nonglaton, G.; Bras, J.; Jean, B. Highly absorbent cellulose nanofibrils aerogels prepared by supercritical drying. *Carbohydrate Polymers* **2020**, *229*, 115560, doi:<https://doi.org/10.1016/j.carbpol.2019.115560>.
 25. Kevadiya, B.D.; Rajkumar, S.; Bajaj, H.C.; Chettiar, S.S.; Gosai, K.; Brahmbhatt, H.; Bhatt, A.S.; Barvaliya, Y.K.; Dave, G.S.; Kothari, R.K. Biodegradable gelatin-ciprofloxacin-montmorillonite composite hydrogels for controlled drug release and wound dressing application. *Colloids and Surfaces B: Biointerfaces* **2014**, *122*, 175-183, doi:<https://doi.org/10.1016/j.colsurfb.2014.06.051>.
 26. Ganesan, P. Natural and bio polymer curative films for wound dressing medical applications. *Wound Medicine* **2017**, *18*, 33-40, doi:<https://doi.org/10.1016/j.wndm.2017.07.002>.
 27. Kreimendahl, F.; Marquardt, Y.; Apel, C.; Bartneck, M.; Zwadlo-Klarwasser, G.; Hepp, J.; Jockenhoevel, S.; Baron, J.M. Macrophages significantly enhance wound healing in a vascularized skin model. *Journal of Biomedical Materials Research Part A* **2019**, *107*, 1340-1350, doi:<https://doi.org/10.1002/jbm.a.36648>.
 28. Heller, A.A.; Spence, D.M. A rapid method for post-antibiotic bacterial susceptibility testing. *PLOS ONE* **2019**, *14*, e0210534, doi:<https://doi.org/10.1371/journal.pone.0210534>.
 29. López-Iglesias, C.; Barros, J.; Ardao, I.; Monteiro, F.J.; Álvarez-Lorenzo, C.; Gómez-Amoza, J.L.; García-González, C.A. Vancomycin-loaded chitosan aerogel particles for chronic wound applications. *Carbohydrate Polymers* **2019**, *204*, 223-231, doi:<https://doi.org/10.1016/j.carbpol.2018.10.012>.
 30. Ul-Islam, M.; Shah, N.; Ha, J.H.; Park, J.K. Effect of chitosan penetration on physico-chemical and mechanical properties of bacterial cellulose. *Korean Journal of Chemical Engineering* **2011**, *28*, 1736, doi:[10.1007/s11814-011-0042-4](https://doi.org/10.1007/s11814-011-0042-4).
 31. Yang, J.; Kwon, G.-J.; Hwang, K.; Kim, D.-Y. Cellulose-Chitosan Antibacterial Composite Films Prepared from

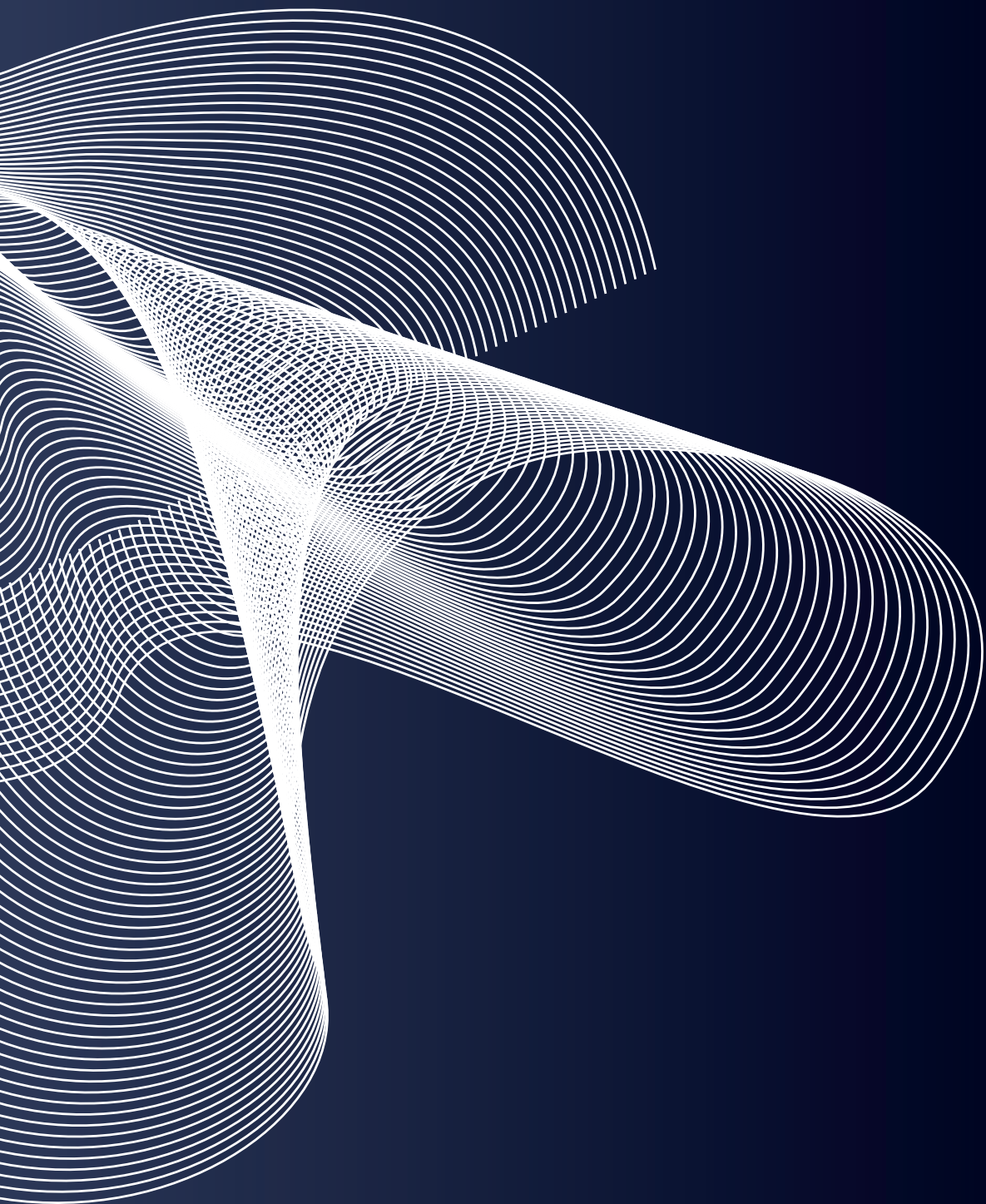
- LiBr Solution. *Polymers* **2018**, *10*, 1058, doi:<https://doi.org/10.3390/polym10101058>.
32. French, A.D. Idealized powder diffraction patterns for cellulose polymorphs. *Cellulose* **2014**, *21*, 885-896, doi:[10.1007/s10570-013-0030-4](https://doi.org/10.1007/s10570-013-0030-4).
 33. Kim, S.J.; Hong, B.M.; Park, W.H. The effects of chitin/chitosan nanowhiskers on the thermal, mechanical and dye adsorption properties of electrospun PVA nanofibrous membranes. *Cellulose* **2020**, *27*, 5771-5783, doi:[10.1007/s10570-020-03191-w](https://doi.org/10.1007/s10570-020-03191-w).
 34. Reichenauer, G. Structural Characterization of Aerogels. In *Aerogels Handbook*, Aegerter, M.A., Leventis, N., Koebel, M.M., Eds. Springer New York: New York, NY, 2011; 10.1007/978-1-4419-7589-8_21pp. 449-498.
 35. Maleki, H.; Durães, L.; García-González, C.A.; del Gaudio, P.; Portugal, A.; Mahmoudi, M. Synthesis and biomedical applications of aerogels: Possibilities and challenges. *Advances in Colloid and Interface Science* **2016**, *236*, 1-27, doi:<https://doi.org/10.1016/j.cis.2016.05.011>.
 36. Soorbaghi, F.P.; Isanejad, M.; Salatin, S.; Ghorbani, M.; Jafari, S.; Derakhshankhah, H. Bioaerogels: Synthesis approaches, cellular uptake, and the biomedical applications. *Biomedicine & Pharmacotherapy* **2019**, *111*, 964-975, doi:<https://doi.org/10.1016/j.biopha.2019.01.014>.
 37. Zhang, S.; He, J.; Xiong, S.; Xiao, Q.; Xiao, Y.; Ding, F.; Ji, H.; Yang, Z.; Li, Z. Construction and Nanostructure of Chitosan/Nanocellulose Hybrid Aerogels. *Biomacromolecules* **2021**, *22*, 3216-3222, doi:<https://doi.org/10.1021/acs.biomac.1c00266>.
 38. Takeshita, S.; Sadeghpour, A.; Malfait, W.J.; Konishi, A.; Otake, K.; Yoda, S. Formation of Nanofibrous Structure in Biopolymer Aerogel during Supercritical CO₂ Processing: The Case of Chitosan Aerogel. *Biomacromolecules* **2019**, *20*, 2051-2057, doi:[10.1021/acs.biomac.9b00246](https://doi.org/10.1021/acs.biomac.9b00246).
 39. Schestakow, M.; Karadagli, I.; Ratke, L. Cellulose aerogels prepared from an aqueous zinc chloride salt hydrate melt. *Carbohydrate Polymers* **2016**, *137*, 642-649, doi:<https://doi.org/10.1016/j.carbpol.2015.10.097>.
 40. Wu, Y.-B.; Yu, S.-H.; Mi, F.-L.; Wu, C.-W.; Shyu, S.-S.; Peng, C.-K.; Chao, A.-C. Preparation and characterization on mechanical and antibacterial properties of chitsoan/cellulose blends. *Carbohydrate Polymers* **2004**, *57*, 435-440, doi:<https://doi.org/10.1016/j.carbpol.2004.05.013>.
 41. Ioelovich, M.; Leykin, A. Study of sorption properties of cellulose and its derivatives. *Bioresources* **2011**, *6*, 178-195, doi:[10.15376/biores.6.1.178-195](https://doi.org/10.15376/biores.6.1.178-195).
 42. Groult, S.; Buwalda, S.; Budtova, T. Tuning bio-aerogel properties for controlling theophylline delivery. Part 1: Pectin aerogels. *Materials Science and Engineering: C* **2021**, *126*, 112148, doi:<https://doi.org/10.1016/j.msec.2021.112148>.
 43. Gurikov, P.; Smirnova, I. Amorphization of drugs by adsorptive precipitation from supercritical solutions: A review. *The Journal of Supercritical Fluids* **2018**, *132*, 105-125, doi:<https://doi.org/10.1016/j.supflu.2017.03.005>.
 44. Smirnova, I.; Suttiruangwong, S.; Arlt, W. Aerogels: Tailor-made Carriers for Immediate and Prolonged Drug Release. *KONA Powder and Particle Journal* **2005**, *23*, 86-97, doi:[10.14356/kona.2005012](https://doi.org/10.14356/kona.2005012).
 45. García-González, C.A.; Alnaief, M.; Smirnova, I. Polysaccharide-based aerogels—Promising biodegradable carriers for drug delivery systems. *Carbohydrate Polymers* **2011**, *86*, 1425-1438, doi:<https://doi.org/10.1016/j.carbpol.2011.06.066>.
 46. Naseri-Nosar, M.; Ziora, Z.M. Wound dressings from naturally-occurring polymers: A review on homopolysaccharide-based composites. *Carbohydrate Polymers* **2018**, *189*, 379-398, doi:<https://doi.org/10.1016/j.carbpol.2018.02.003>.
 47. Yilmaz Atay, H. Antibacterial Activity of Chitosan-Based Systems. In *Functional Chitosan: Drug Delivery*

- and Biomedical Applications*, Jana, S., Jana, S., Eds. Springer Singapore: Singapore, 2019; 10.1007/978-981-15-0263-7_15pp. 457-489.
48. Hosseinnejad, M.; Jafari, S.M. Evaluation of different factors affecting antimicrobial properties of chitosan. *International journal of biological macromolecules* **2016**, *85*, 467-475, doi:<https://doi.org/10.1016/j.ijbiomac.2016.01.022>.
49. Chang, S.-H.; Lin, H.-T.V.; Wu, G.-J.; Tsai, G.J. pH Effects on solubility, zeta potential, and correlation between antibacterial activity and molecular weight of chitosan. *Carbohydrate Polymers* **2015**, *134*, 74-81, doi:<https://doi.org/10.1016/j.carbpol.2015.07.072>.
50. Boateng, J.S.; Matthews, K.H.; Stevens, H.N.; Eccleston, G.M. Wound healing dressings and drug delivery systems: a review. *Journal of pharmaceutical sciences* **2008**, *97*, 2892-2923, doi:<https://doi.org/10.1002/jps.21210>.
51. Moeini, A.; Pedram, P.; Makvandi, P.; Malinconico, M.; Gomez d'Ayala, G. Wound healing and antimicrobial effect of active secondary metabolites in chitosan-based wound dressings: A review. *Carbohydrate Polymers* **2020**, *233*, 115839, doi:<https://doi.org/10.1016/j.carbpol.2020.115839>.



EMBARGOED

Chapter 5.



Chapter 6.

General discussion

Innovative material design and nano-structural engineering have been utilized by researchers to address the challenges of the chronic wound healing process [1]. In the past decade, aerogels have been significantly used as wound dressing materials due to their outstanding structures such as high porosity, low density, and large specific surface area [2]. Aerogels based on hydrophilic materials are favorable as wound dressings since providing a moist wound environment and absorbing wound exudates is an essential part of the wound healing process. Therefore, the fabrication of aerogels from natural hydrophilic polymers especially from polysaccharides would be suitable for producing biocompatible, biodegradable, and drug-loaded bioaerogels for wound dressing applications [3].

Cellulose is the most abundant natural polymer and can be found in the plant cell wall, biofilms secreted from bacteria, and in some species such as tunicates and algae as a primary structural component [4]. The presence of strong intra- and inter-molecular hydrogen bonds in cellulose structures leads to the formation of a cross-linking network which makes cellulose favorable material for preparation of aerogel materials. The production of cellulose aerogels in form of the monolith, cylinder, and film is a steadily developing direction in the biomedical field including wound healing, tissue engineering and drug delivery [5]. However, such aerogels typically suffer from poor mechanical properties such as brittleness, low flexibility, and time-consuming drying processes.

By transforming cellulose aerogels into the shape of fibers, using various fiber spinning and textile fabrication methods, it is possible to achieve enhanced mechanical performance and high flexibility [6]. Furthermore, it is possible to load the aerogel fibers by different supercritical CO₂ methods. To the best of our knowledge, comprehensive studies on cellulose based aerogel microfibers fabrication and their potential for biomedical applications such as wound dressing and drug delivery have not been conducted. Therefore, in this PhD project, cellulose was used to fabricate aerogel microfibers for biomedical applications of drug delivery and wound dressing. Three main objectives were achieved:

- I. Evaluating the effect of the cellulose properties and the preparation conditions on the internal structure of the aerogel and its physicochemical properties.
- II. Optimizing and designing the fiber processing conditions and textile fabrication techniques for cellulose aerogel microfibers (CAFs) production.

III. Investigating the feasibility of using cellulose aerogels as advanced biomaterials for drug delivery and wound dressing applications.

During this thesis work, it was proven that due to the presence of various fiber spinning and textile formation techniques, cellulose based aerogels fibers have a high shapeability and flexibility which enables them to adapt to wound site and topography. Moreover, their high porosity and large specific surface area favor a quick absorption of the wound exudate and control the moisture balance at the wound location. Thanks to their interconnected highly open porosity, it is possible to achieve a balanced transpiration-evaporation equilibrium at the wound site and prevent hypoxia situations [7]. Such outstanding textural properties also enable cellulose aerogel fibers to have a high loading capacity of bioactive agents through supercritical CO₂ techniques. Also, depending on the nature and chemistry of the drugs, the mesoporosity of aerogels (2–50 nm) limits the growth of drug crystals within the aerogel matrix and maintains the drug in the amorphous status [8]. In the drug delivery application, most of the bioactive agents are low water-soluble compounds and such amorphous loading phenomena increase their solubility rate and access to the targeted site [9]. Using hybrid materials, further functionalities can be introduced into the fibrous aerogel structure. For instance, cellulose-chitosan aerogel fibers exhibited antibacterial properties and showed more sustained drug-release profile than pure cellulose aerogel fibers.

Although proof-of-concept and the potential of cellulose aerogel microfibers for wound dressing application have been demonstrated, there is still a long challenging way in their transition from laboratory to clinical application and market. As proven in **chapter 2**, the type of cellulose and its feedstock have a major impact on the performance and manufacturing of cellulose aerogel fibers. Further studies can be devoted to investigating the type of biomass (wood, non-wood, softwood, or hardwood) and pulping technology to identify more parameters that can directly impact the fiber spinning and characteristic of cellulose aerogel microfibers [4]. For instance, nanofibers obtained from bacterial cellulose or tunicate cellulose due to higher purity and crystallinity can be highly relevant for biomedical applications; however, industrial production and the final cost are their current limiting factor [10,11].

Further development and standardization of the analysis methods for aerogels and aerogel fibers (e.g. measurements of pore size distribution, and mechanical properties) could enhance the comparison of the results from various studies. For instance, several characterization methods such as scanning electron microscopy, X-ray microtomography, and N₂ adsorption-desorption were required to achieve a better understanding of the

pore size distribution within the cellulose aerogel fibers as discussed in **chapters 2 and 3**. Therefore, standards and guidelines for such characterizations should be developed by scientists, institutes, and companies active in the field of aerogels [12].

As shown in **chapter 4**, the hybridization of cellulose aerogel fibers provides a wide choice of materials and potential for further development and research as well as obtaining further functionalities including antibacterial properties, and enhanced textural properties. However, understanding and tailoring of hybrid aerogel fibers based on experimental studies and molecular modeling are required to tackle the knowledge gap in this area. Such studies lead to a better comprehension of the structure-functional properties relations between the properties of the individual precursors and the characteristic of the final aerogel. Therefore, hybrid fibrous aerogel materials can be designed and fabricated for specific biomedical applications.

The durability and biodegradability of cellulose based aerogel fibers are other important aspects that should be further discussed. Similar to other biobased and biodegradable products, it is always challenging to balance between product durability and biodegradability. Strong water absorption of cellulose aerogel microfibers is an inherent characteristic of cellulosic material and can facilitate its biodegradability since most organisms and enzymes require moisture to be effective in biodegradation. Such enzymatic reaction and their impact on the performance of the aerogel fibers require further investigation. A significant outlook for research in the field of bioaerogel should be also considered for the preservation of their characteristics during their use [3,5].

A limited number of bioaerogels have entered the clinical phase, and most of them are still in the developmental and laboratory experimental phases [7]. The *in vitro* results of the cellulose aerogel microfibers in **chapters 2, 3, 4, and 5** showed promising biocompatibility of cellulose aerogel fibers. Depending on current clinical needs for wound dressing material, an evaluative discussion on the benefits of bioaerogels for overlapping wound healing stages (hemostasis, inflammation, cell proliferation, and tissue maturation/remodeling) and the principal characteristics of each phase is necessary to be carried out. Apart from the biocompatibility of cellulose aerogel fibers, the correlation between physical properties (density, pore volume, and specific surface area) and bioactivity of aerogels could be also analyzed.

Bioaerogel production on an industrial scale and commercialization remains limited and have not achieved significant market penetration; most commercially available aerogels are based on silica for thermal insulation applications [13]. To enhance the

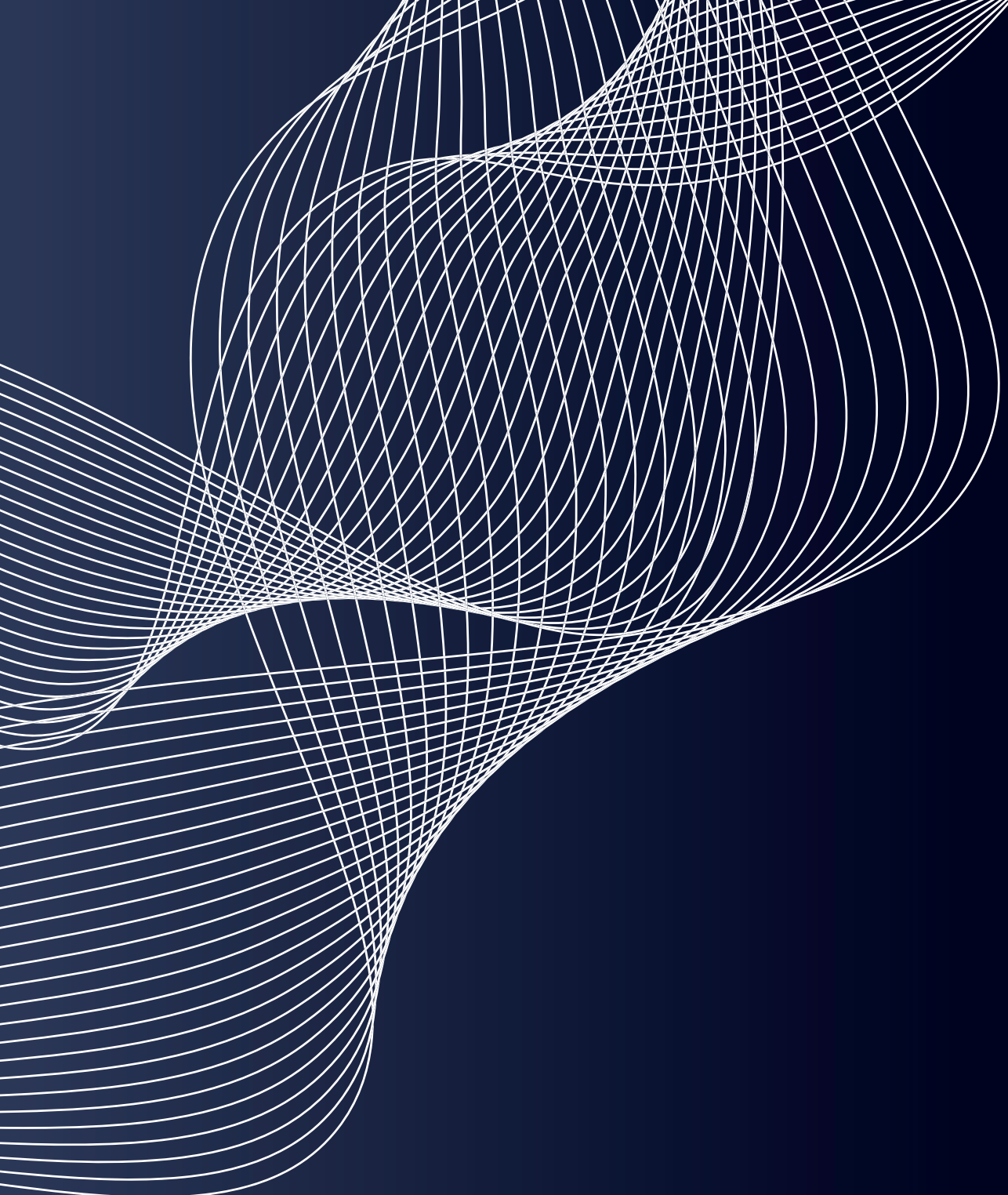
aerogel fabrication process, ambient pressure drying has been widely studied as a possible solution. However, such an approach is based on chemical modifications of aerogels and is typically restricted to silica aerogels [14]. In contrast, supercritical CO₂ drying is a more versatile method for the fabrication of aerogels from a wide variety of precursor materials such as biopolymers. One limiting factor of the supercritical drying of aerogels is that they are processed in batch operations. Therefore, continuous drying of aerogels with supercritical CO₂ is highly favorable for industrial applications. In the case of cellulose aerogel fiber processing, continuous fiber spinning methods are already performed on an industrial scale. Moreover, solvent exchange and drying of fibers are significantly shorter than other geometrical shapes such as monoliths, cylinders, and films due to the micron-size diameter of the fibers. However, further research and investigation on the custom-made supercritical CO₂ drying techniques are required to achieve a fully continuous drying process of the aerogel fibrous structures [12].

Chapter 5 of the thesis, aimed to achieve a more continuous process by dissolving cellulose in ionic liquids and using the novel method of solution blowing spinning. Fabricating nonwoven aerogel fibers by solution blowing spinning eliminates the processing of microfibers into textiles and makes their industrial production more favorable. However, cellulose solvent cost and its sustainability are still limiting demanding factors to scale up such processes. Although the work in developing new solvents for cellulose has been notably empirical, the new directions for identifying sustainable and affordable industrial solutions to dissolve cellulose are vital [15]. In general, it is more challenging to find appropriate inexpensive solvents that can be easily removed from the final product prior to its use for biomedical purposes. Moreover, a product is only truly sustainable when its processing is also sustainable. The assessment of cellulose aerogel microfibers' sustainability requires consideration of both technical economic and life-cycle analyses based on pilot and industrial-scale data.

In the end, it is forecasted that the aerogel field will keep up its rapid evolution in the upcoming years and that the aerogel based products find their way into clinical applications. The important element is the concurrent development of the (bio)material aspects and relevant production process to reduce final aerogel prices and enable practical applications. On other hand, the fabrication of new aerogel types should be based on the target product properties, and regulatory restrictions should be known from the beginning. This goal can be achieved by close collaboration between academic groups, clinicians, and industrial partners, which should be further encouraged.

References

1. Boateng, J.S.; Matthews, K.H.; Stevens, H.N.; Eccleston, G.M. Wound healing dressings and drug delivery systems: a review. *Journal of pharmaceutical sciences* **2008**, *97*, 2892-2923, doi:<https://doi.org/10.1002/jps.21210>.
2. Abdul Khalil, H.P.S.; Adnan, A.S.; Yahya, E.B.; Olaiya, N.G.; Safrida, S.; Hossain, M.S.; Balakrishnan, V.; Gopakumar, D.A.; Abdullah, C.K.; Oyekanmi, A.A., et al. A Review on Plant Cellulose Nanofibre-Based Aerogels for Biomedical Applications. *Polymers* **2020**, *12*, 1759.
3. Maleki, H.; Durães, L.; García-González, C.A.; del Gaudio, P.; Portugal, A.; Mahmoudi, M. Synthesis and biomedical applications of aerogels: Possibilities and challenges. *Advances in Colloid and Interface Science* **2016**, *236*, 1-27, doi:<https://doi.org/10.1016/j.cis.2016.05.011>.
4. Li, T.; Chen, C.; Brozena, A.H.; Zhu, J.Y.; Xu, L.; Driemeier, C.; Dai, J.; Rojas, O.J.; Isogai, A.; Wågberg, L., et al. Developing fibrillated cellulose as a sustainable technological material. *Nature* **2021**, *590*, 47-56, doi:[10.1038/s41586-020-03167-7](https://doi.org/10.1038/s41586-020-03167-7).
5. Budtova, T. Cellulose II aerogels: a review. *Cellulose* **2019**, *26*, 81-121, doi:[10.1007/s10570-018-2189-1](https://doi.org/10.1007/s10570-018-2189-1).
6. Tafreshi, O.A.; Mosanenzadeh, S.G.; Karamikamkar, S.; Saadatnia, Z.; Park, C.B.; Naguib, H.E. A review on multifunctional aerogel fibers: processing, fabrication, functionalization, and applications. *Materials Today Chemistry* **2022**, *23*, 100736, doi:<https://doi.org/10.1016/j.mtchem.2021.100736>.
7. Bernardes, B.G.; Del Gaudio, P.; Alves, P.; Costa, R.; García-González, C.A.; Oliveira, A.L. Bioaerogels: Promising Nanostructured Materials in Fluid Management, Healing and Regeneration of Wounds. *Molecules* **2021**, *26*, 3834.
8. García-González, C.A.; Sosnik, A.; Kalmár, J.; De Marco, I.; Erkey, C.; Concheiro, A.; Alvarez-Lorenzo, C. Aerogels in drug delivery: From design to application. *Journal of Controlled Release* **2021**, *332*, 40-63, doi:<https://doi.org/10.1016/j.jconrel.2021.02.012>.
9. Smirnova, I.; Suttirungwong, S.; Arlt, W. Aerogels: Tailor-made Carriers for Immediate and Prolonged Drug Release. *KONA Powder and Particle Journal* **2005**, *23*, 86-97, doi:[10.14356/kona.2005012](https://doi.org/10.14356/kona.2005012).
10. Lin, W.-C.; Lien, C.-C.; Yeh, H.-J.; Yu, C.-M.; Hsu, S.-h. Bacterial cellulose and bacterial cellulose-chitosan membranes for wound dressing applications. *Carbohydrate Polymers* **2013**, *94*, 603-611, doi:<https://doi.org/10.1016/j.carbpol.2013.01.076>.
11. Apelgren, P.; Sämfors, S.; Säljö, K.; Mölne, J.; Gatenholm, P.; Troedsson, C.; Thompson, E.M.; Kölby, L. Biomaterial and biocompatibility evaluation of tunicate nanocellulose for tissue engineering. *Biomaterials Advances* **2022**, *137*, 212828, doi:<https://doi.org/10.1016/j.bioadv.2022.212828>.
12. Smirnova, I.; Gurikov, P. Aerogel production: Current status, research directions, and future opportunities. *The Journal of Supercritical Fluids* **2018**, *134*, 228-233, doi:<https://doi.org/10.1016/j.supflu.2017.12.037>.
13. Chen, Y.; Zhang, L.; Yang, Y.; Pang, B.; Xu, W.; Duan, G.; Jiang, S.; Zhang, K. Recent Progress on Nanocellulose Aerogels: Preparation, Modification, Composite Fabrication, Applications. *Advanced Materials* **2021**, *33*, 2005569, doi:<https://doi.org/10.1002/adma.202005569>.
14. Smirnova, I.; Gurikov, P. Aerogels in Chemical Engineering: Strategies Toward Tailor-Made Aerogels. *Annual Review of Chemical and Biomolecular Engineering* **2017**, *8*, 307-334, doi:[10.1146/annurev-chembioeng-060816-101458](https://doi.org/10.1146/annurev-chembioeng-060816-101458).
15. Lindman, B.; Karlström, G.; Stigsson, L. On the mechanism of dissolution of cellulose. *Journal of Molecular Liquids* **2010**, *156*, 76-81, doi:<https://doi.org/10.1016/j.molliq.2010.04.016>.



Chapter 7.

Impact paragraph

The prevalence of different kind of wounds especially chronic ones has grown considerably over the past decades. This is mainly due to the rising number of surgeries, escalating worldwide geriatric population, soaring traumatic wounds, and the epidemic of obesity and diabetes as risk factors for the development of chronic wounds [1,2]. Due to the limitations of the existing wound dressing products, a novel biobased wound dressing was developed attempting to address those limitations. As a result, the produced wound dressing from renewable, biocompatible, and biodegradable materials in this work can be applied to and is tunable for a wide range of wound types in order to accelerate and promote the wound healing process.

Aerogels originating from natural polymers, such as cellulose, provide low density, high porosity, large specific surface area, biocompatibility, biodegradability, and the ability to load and locally release bioactive agents [3]. The aforementioned characteristics make bioaerogels promising candidates for biomedical applications such as wound dressing products. Nevertheless, aerogel applications have been widely restricted due to the lack of flexibility, extensibility, and fragile network structures, which are mainly due to the possible configurations of the aerogels such as monoliths, cylinders, and beads [4]. Moreover, commercialization of the aerogels are limited due to the time consuming, expensive, and batchwise processing techniques.

In the current study, however, by producing aerogels in the geometry of microfibers, their mechanical performance, flexibility, and extensibility were improved remarkably. Moreover, benefiting from versatile fiber and textile engineering techniques, bioaerogels can be transformed into micro/nanofibers with different structures including woven, nonwoven, knitted, and braided through shorter and more reproducible processes.

In this study, cellulose-based aerogel microfibers as an emerging class of aerogel materials were explored particularly for biomedical applications of drug delivery and wound dressing. Drug-loaded and non-loaded aerogel microfibers were produced through fiber spinning methods including wet spinning and solution blowing spinning accompanied by supercritical CO₂ drying as a solvent free and green process. Different cellulose-based aerogel microfibers in the form of knitted and nonwoven structures were created for the optimal wound healing and the absorbance of wound exudate. The feasibility of loading various model and actual drugs, such as anti-inflammatory or anti-microbial agents, into the porous structure of the fibers to accelerate wound healing was also positively evaluated.

It should be borne in mind that all the research conducted during this PhD project on cellulose based aerogel microfibers is not providing a “ready-made solution” for biomedical application of drug delivery and wound dressing since this topic is quite “juvenile”. The obtained results present useful instruction and guidelines for future studies.

The result of this study has significant contribution to the scientific and social community. Regarding the scientific aspect, to best of our knowledge, the first indication of aerogel fibers’ existence can be traced back to 2012; however, their potential for wound dressing applications was not investigated prior to the current study. This study can pave the way for other new biomedical applications, such as tissue engineering, where the existence of a highly porous scaffold network in producing human size tissues is essential. Intensive *in vitro* and *in vivo* analysis are required in order to have an in-depth understanding of the cellulose-based aerogel microfibers performance when interacting with living organisms. For example, in the case of wound dressing application, a critical investigation on the advantages of bio-based aerogels for each wound healing stage as well as the exudate control need to be performed.

The current research is also highly beneficial for the social community regarding two main aspects. First, this study is addressing the expanding demand and growing global market of advanced wound dressing products. There is a wide variety of wound dressings commercially available for wound treatment; however, many still lack the ideal characteristics of a wound dressing product. Cellulose-based aerogels microfibers have shown closer behavior to an ideal wound dressing, and this study can be utilized as a road map to enhance a patient’s quality of life. Second, there is an increasing awareness by the public that the impacts of synthetic plastic waste on the environment and our health are global and can be drastic. The development of new, versatile, and multi-functional polymeric materials from renewable resources, such as cellulose, has become a key research focus to meet tomorrow’s engineering applications. Therefore, the integration of environmental sustainability in the fabrication of bio-based materials produced by “greener” processes such as supercritical CO₂ ones is vital in modern technologies to reduce environmental footprints and harmonize polymeric products with our living environment for a better future.

The outcome of the current thesis are relevant and interesting not only for biomedical researchers, clinicians, and patients but also for biomedical corporations. Cellulose-based aerogel fibers can be highly intriguing for biomedical companies that target to expand their biomaterials portfolio for new nanostructured biomaterials. Such

companies can aim for early investment and further investigation in the current research in order to integrate bioaerogel fibers in their health care business. In general, hospitals, clinics, home care facilities, and patients are potential customers of a wound dressing product.

Moreover, the results can be fascinating for not only the researchers in the biomedical field but also those focusing on various technical applications of aerogels such as thermal insulation. Aerogel fibers can be extensively used in technical sectors where the load-bearing and different structure formation in conjunction with the superior thermal insulation performance is vital.

The results of this thesis were published in open access peer reviewed articles making them accessible for researchers and public audience. Through participating in different international conferences, the results were presented to the academic and non-academic attendees. Moreover, promotional contents, such as a video and blog, were created and published on the FibreNet project website. The cellulose-based solution blown aerogel microfibers as fully illustrated in the last section of this thesis was introduced into the public and industrial partners by the doctoral candidate under the name of WoundAeroFiber, which was awarded the Maastricht University Challenge Award.

The current scientific journey that began with the fundamental understanding of the fabrication process of a wound dressing product has been long-lasting and complex. It started with material selection, design, processing as well as multiple improvement actions for better and optimized performance, and ended with a prototype. The cellulose-based aerogel microfibers might face many other challenges before possibly reaching society at the commercial level. However, the contributions made to this field of science through this study are highly self-standing and valuable even if the final goal of advancing society with a new wound dressing product remains elusive.

References

1. Sen, C.K. Human Wounds and Its Burden: An Updated Compendium of Estimates. *Adv Wound Care (New Rochelle)* **2019**, *8*, 39-48, doi:10.1089/wound.2019.0946.
2. Boateng, J.S.; Matthews, K.H.; Stevens, H.N.; Eccleston, G.M. Wound healing dressings and drug delivery systems: a review. *Journal of pharmaceutical sciences* **2008**, *97*, 2892-2923, doi:https://doi.org/10.1002/jps.21210.
3. Maleki, H.; Durães, L.; García-González, C.A.; del Gaudio, P.; Portugal, A.; Mahmoudi, M. Synthesis and biomedical applications of aerogels: Possibilities and challenges. *Advances in Colloid and Interface Science* **2016**, *236*, 1-27, doi:https://doi.org/10.1016/j.cis.2016.05.011.
4. Budtova, T. Cellulose II aerogels: a review. *Cellulose* **2019**, *26*, 81-121, doi:10.1007/s10570-018-2189-

Appendix

The following figures are the supplementary data related to chapter 3.

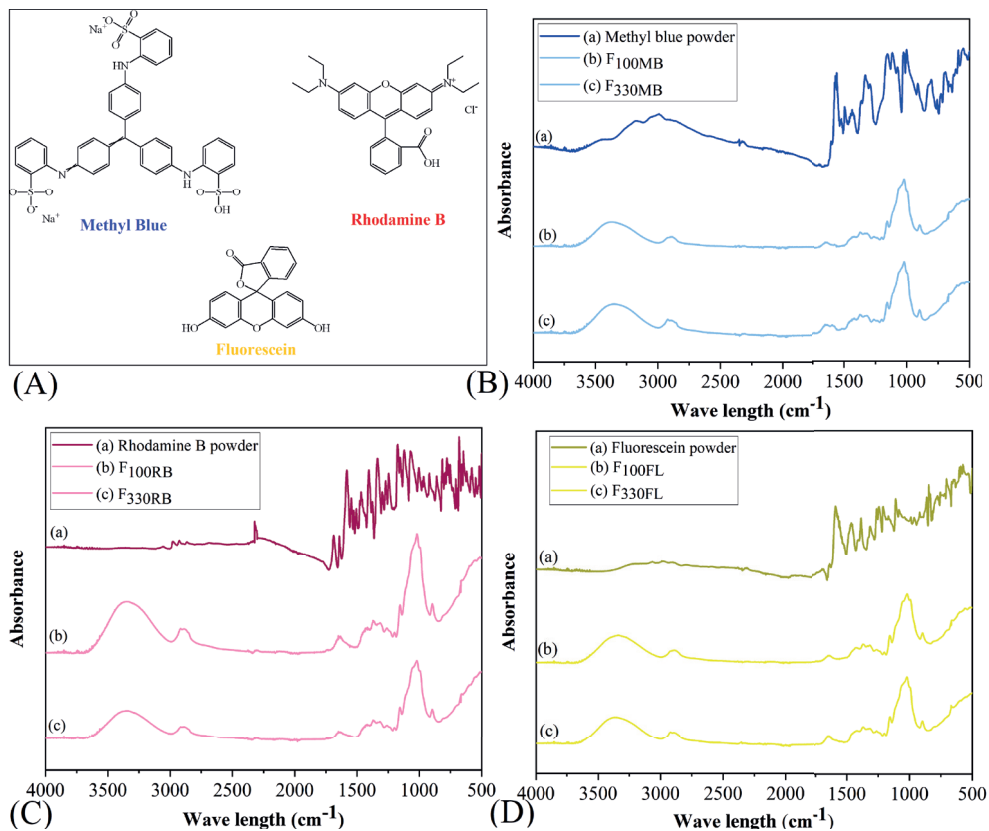


FIGURE APPENDIX 3.1.

(A) Chemical structures of the drug models, methyl blue (MB), rhodamine B (RB), fluorescein (FL). (B) FTIR spectra of the MB powder and the MB solvent exchange loaded CAFs. (C) FTIR spectra of the RB powder and the RB solvent exchange impregnated CAFs. (D) FTIR spectra of the FL powder and the FL solvent exchange impregnated CAFs. Though most of the drugs' bands had overlap with CAFs peaks, moderate loading of fibers with drug models can be observed in the low intensified shoulders; for instance in the wavelength range of 700-1000 cm^{-1} .

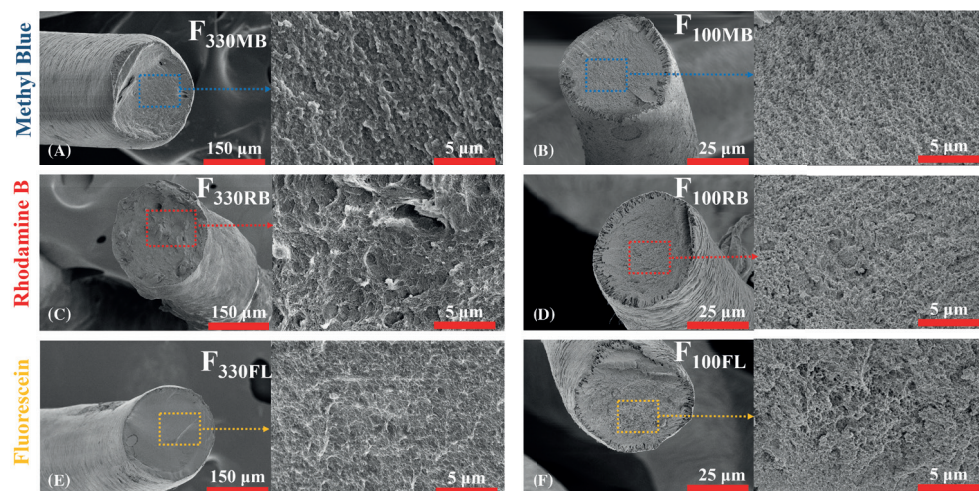


FIGURE APPENDIX 3.2.

Cross-sectional morphology of the mono and multifilament wet spun drug-loaded cellulose fibers exhibiting a macro-porous outer shell with a nano-porous inner core. Loaded fibers with methyl blue, (A) F_{330MB} and (B) F_{100MB} . Impregnated fibers with rhodamine B, (C) F_{330RB} and (D) F_{100RB} . Loaded fibers with Fluorescein, (E) F_{330FL} and (F) F_{100FL} .

Summary

The treatment of wounds, in particular chronic types, is an unresolved challenge due to its complicated healing process, which can adversely impact the patient's quality of life. The design and fabrication of new wound dressing materials with enhanced performance from renewable biobased resources such as cellulose is a continuous demand from healthcare services. Bioaerogels fabricated from biopolymers can simultaneously provide high porosity, low density, large specific surface area, biocompatibility, biodegradability, and the possibility to load and locally release single or multiple drugs and bioactive agents at the wound site. Therefore, they are considered as promising materials to address the limitations of currently existing wound dressings.

In this PhD project, cellulose was used to fabricate aerogel microfibers for biomedical applications of drug delivery and wound dressing. Three main objectives were achieved:

- I. Evaluating the effect of the cellulose properties and the preparation conditions on the internal structure of the aerogel and its physicochemical properties.
- II. Optimizing and designing the fiber processing conditions and textile fabrication techniques for cellulose aerogel microfibers (CAFs) production.
- III. Investigating the feasibility of using cellulose aerogels as advanced biomaterials for the two different applications of drug delivery and wound dressing.

Various cellulose types, dissolving agents, precursor concentration, and the nature of regeneration solvent were indicated to play a vital role in aerogel morphology and properties. Solvent exchange and post-treatment supercritical CO₂ (scCO₂) impregnation were investigated for CAFs drug impregnation. When used as drug delivery matrices, the profile and kinetics of drug release were correlated with the textural properties of cellulose aerogels such as specific surface area and pore volume. CAFs were proven to be a promising material for wound dressing application since they were able to uptake large amounts of moist, water, and wound exudate due to their nanoporous texture. Drug-loaded CAFs can be used to control the release of the encapsulated drug to the wound site while enhancing the healing process. Upon cellulose blending with chitosan, the wound dressing also showed bactericidal properties. Overall, a high potential of CAFs to be used as biomaterials with highly tunable properties and functionalities was demonstrated, which is briefly explained in the following summary of the chapters.

In **chapter 1** an introduction on wound healing, wound dressing, and aerogel fabrication with an emphasis on the bioaerogels and the importance of the production of aerogels in the fibrous format has been provided. Furthermore, the chapter has reviewed advances in drug-eluting medical textiles including different fiber production methods, such as melt-, wet-, and electro-spinning, and textile fabrication techniques, such as knitting and weaving. Various loading processes of bioactive agents to obtain drug-loaded fibrous structures with required physicochemical and morphological properties, drug delivery mechanisms, and drug release kinetics were also discussed. Finally, the current applications of drug-eluting textiles in wound care, tissue engineering, and transdermal drug delivery were highlighted. From this chapter, the technical requirements for fiber production and the ultimate biomedical application were finally derived and further developed into the overall concept of the thesis.

Chapter 2 aimed at evaluating the correlations between the initial cellulose characteristics, aerogel's internal structure, and its prospective biomedical application. Wet-spun cellulose aerogel fibers were obtained by scCO_2 drying from low and high molecular weight microcrystalline cellulose. The CAFs from high molecular weight cellulose ($M_w \sim 565 \text{ kg/mol}$) proved to have a higher surface area ($\sim 197 \text{ m}^2/\text{g}$), denser structure, and finer nanofibrils ($\sim 20 \text{ nm}$) with better thermal stability in comparison with the fibers produced from low molecular weight cellulose ($M_w \sim 163 \text{ kg/mol}$). The fibers were nontoxic, and cell proliferation was observed over time. Both low and high molecular weight CAFs showed promising results to be developed further for biomedical applications such as drug delivery and wound care.

In **chapter 3**, CAFs were explored and evaluated as drug delivery systems using three different drug models of methyl blue, rhodamine B, and fluorescein. It was proven that the solvent exchange scCO_2 impregnation was an effective single-step techniques for drug loading and aerogel formation. Loaded and non-loaded CAFs proved to have a macro-porous outer shell and a nano-porous inner core with interconnected pore structure and a specific area in the range of $100\text{--}180 \text{ m}^2/\text{g}$. The CAFs were able to form knitted mesh and needle punched nonwoven textiles. Humidity and water uptake assessments indicated that the fibrous structures were highly moisture absorbable and non-toxic with immediate drug release profiles due to the highly open interconnected porous structure of the fibers. In conclusion, CAFs are propitious to be further developed for biomedical textile applications such as wound care; however, some drawbacks such as immediate drug release profile and not possessing antibacterial properties require additional modifications of the fibers.

Chapter 4 addresses the potential of chitosan-cellulose aerogel fibers (CHCLAF) for the development of antibacterial wound dressings. Wet spun CHCLAF in two ratios of 1:5 and 1:10 have been produced by scCO_2 drying for wound dressing application. The fibers were also loaded with ibuprofen through post-treatment scCO_2 impregnation. CHCLAF characteristics in terms of morphology, textural properties, thermal stability, mechanical properties, and *in vitro* assessment such as drug release, antibacterial properties, cytotoxicity, and wound exudate uptake were analyzed and compared to pure CAFs. Blended CHCLAF showed a low density ($\sim 0.2 \text{ g/cm}^3$), high porosity ($\sim 85\%$), and large specific surface area ($\sim 300 \text{ m}^2/\text{g}$) with a macro-porous outer shell and a nano-porous inner core. The fibers could be fabricated to braided meshes that were highly water absorbable ($\sim 400 \text{ wt. \%}$) and bactericidal against *escherichia coli* and *staphylococcus aureus*. Furthermore, the fibrous structure was biocompatible with fibroblast cells and was able to release ibuprofen over 48 hours in a sustained manner. The results showed that the CHCLAF have better functionalities compared to the CAFs and thus could be used as a promising antibacterial candidate for wound dressing applications.

In **chapter 5**, solution blowing spinning, an innovative technique for spinning micro-/nano-fibers from polymer solutions, has been combined with scCO_2 drying to develop highly porous cellulose aerogel nonwovens (CANs). In order to tune the hydrophobicity and drug release profile of the CANs, the meshes were surface treated through gas-phase esterification with palmitoyl chloride. The nonwoven aerogels benefited from both inter- and intra-fiber porosity, and the majority of the fiber diameters were between 3-9 μm . The CANs possessed a large specific surface area ($\sim 450 \text{ m}^2/\text{g}$), pore volume ($\sim 3.37 \text{ cm}^3/\text{g}$), and high humidity absorption ($\sim 15 \text{ wt. \%}$). The palmitoyl chloride gas-phase reaction enhanced the contact angle drastically (from 0 to $\sim 130^\circ$) for the surface modified samples and resulted in a more sustained thymol release profile in comparison to the non-modified samples. All samples exhibited cell viability, and the thymol loaded CANs were bactericides against *E. coli* and *S. aureus*. In conclusion, the surface treated CANs loaded with thymol are highly promising materials for wound dressing applications.

Acknowledgments

From the bottom of my heart, I would like to say a big thank you to anyone who directly or indirectly contributed to my doctoral research. I would like to express my sincere gratitude to my supervisors **Prof. Gunnar Seide, Prof. Stefan Jockenhövel, and Associate Prof. Samaneh Ghazanfari** for their recommendations, guidance, and overall insights on this dissertation. Thank you for giving me the chance to be an independent researcher who can confront difficult challenges in a world of uncertainties.

Prof. Lorenzo Moroni, Prof. Pasi Kallio, Prof. Andrij Pich and Prof. Aart Willem Van Vuure thank you for agreeing to assessing my PhD thesis. You have helped me to complete this journey and your feedback certainly enhanced the quality of my dissertation.

These past few years, I have worked in a cross-border European research institute with an international atmosphere and great colleagues. I am amazed how much that has changed me to be stronger than ever and ready to take on completely new challenges! In the Netherlands and Chemelot campus, I had the opportunity to work with my colleagues at Maastricht University and Aachen-Maastricht Institute for Biobased Materials (AMIBM), without whom I would not have been able to complete this research. I would like to thank all the AMIBM team, especially **Ermo Daniels, Achim Besen, Hay Becker, Christian van Slagmaat, Jurrie Noordijk, Nils Leoné, Peter Iijnen, Vahid Ansari, Abdelrahman Abdelgawad, Carlos García Velásquez, Anne Coenen, Naveen Balakrishnan, Stefan Siebert, Christian Schmitz, Yvonne van der Meer, Luisa Bortesi, Pouya Samani, Lara Bitar, Cristina Palacios Mateo, Maike-Eliza Ostheiler, Muhammad Maqsood, Marcelle Grandjean, Monica Jedrzejczyk, Enzo Pichon and Jules Stouten**. **Anne and Naveen**, I appreciate your care during my onboarding process and my first few months of living in the Netherlands. **Christian and Jurrie**, our office was always full of energy because of you, thank you for the positive vibes. **Hay, Stefan and Achim** you kindly helped me to equip and troubleshoot various devices in the biomedical lab, you made the challenges ten times easier with your very presence! **Christian** you are one of the most supportive researchers that I have ever seen, thanks for keeping the biology lab open to everyone. **Ermo**, I wanted to thank you for your extreme support and kindness at those challenging moments when my future was not so clear.

From Germany and RWTH Aachen, I highly appreciate the support of BioTex staff members including **Alicia Fernandez Colino, Julia Wolf, Jacquélien Numan, Saurav Ranjan Mohapatra, and Stavroula Kyriakou**. Furthermore, I would like to thank my

students **Lydia Yates**, **Hana Cvelbar** and **Denée Janssen** for their contribution to my PhD thesis.

Many thanks go out to FibreNet members principally **Prof. Pasi Kallio**, **Mariaana Savia**, and **Soili Pakarinen** for the excellent management of the project. Without any doubt, I learned a lot at FibreNet's offered network-wide training events and they were the most joyful moments of my PhD. **Ali**, thanks a lot for being a great host during my secondment at Tampere university. **Rupert** and **Karin**, what an extraordinary standard of hospitality you uphold during my secondment at TU Graz, thank you! Great FibreNet ESRs, **Farzin Javanshour**, **Royson Dsouza**, **Mengxiao Zhao**, **Vedad Tojaga**, **Mossab Alzweighi**, **Ali Khodayari**, **Alexandros Prapavesis**, **Özkan Yapar**, **Marko Zizek**, **Mónica Gaspar Simões**, **Lucija Jurko** and **Fazilet Güner**, I enjoyed every single moment with you and learned about new aspects of biobased fibers from your research.

I am most grateful to the collaborators for lending me their expertise and intuition to my scientific and technical problems especially **Prof. Pavel Gurikov** and **Dr. Raman Subrahmanyam**; I couldn't be more thankful for your hospitality while I stayed at Hamburg University of Technology.

I cannot forget to thank my family and friends for all their unconditional support in this very intense educational pathway. My friends **Sophie**, **Niko**, **Carlos**, **Marlou**, **Vahid**, **Navid**, **Sina** and **Masoud** thanks for being my second family in Europe; the friendship with you has been amazing and our memories are unforgettable, remaining ever vivid and heartwarming. **Sophie**, your kindness and big smiles are great part of your personality, thanks for always inviting us to your place and surprising us with great meals. You thought me a lot about Austrian culture including Krampus ☺. **Niko** your skills in baking are splendid, you try to approach everything with strategy including the board games that I wasn't good at; happy that we could work together for a while in PhD academy Maastricht! **Carlos**, traveling with you as colleague, project partner and more importantly a great friend has been always full of funny and deep discussions; thank you for introducing me into pineapple world and interesting Colombian culture! **Marlou**, my first Dutch friend, your meal recipes have been always surprising and you go above and beyond as a dutiful and comforting host; Truly, thank you!

Vahid, my supportive, tranquil and musical friend, you always impressed me by your chemistry knowledge and your punctuality during our travels to Chemelot and Maastricht! ☺. **Navid**, 10 years of friendship with you has been amazing and thanks for being a 24/7 online support during my PhD; Also, I am deeply glad to see our

friendship has been transferred from our home country to Europe. **Sina**, I have learned a lot about different aspect of life from you, you always shared relevant and important articles with me, thanks for being a great funny friend! **Masoud**, our friendship formed during difficult time of Covid-19 and we could create a strong bond, you have been always inspirational to me; thanks for encouraging me to achieve my goals.

Cassandra, I am awestruck by your generous heart and kind support. I couldn't be more thankful for your contributions to designing the layout of the thesis. While you had many other things to take care of, you read and designed the layout of my thesis after working hours or during your weekends. You did it with great passion and care, and be aware that it is a gift that last forever and it is very special to me!

Mobin, my younger brother, among the many gifts my family gave me, there was you. An irreplaceable, annoying little brother. So happy to see you have started your academic journey to be medical doctor, who knows maybe one day you use the result of this thesis!

To conclude, I deeply thank my **parents**, for their unconditional trust, timely encouragement, and endless patience. It was their love that raised me up again when I got weary. My **Mom**, my warrior, you knew it would be a long and sometimes bumpy road but you encouraged and supported me along the way from almost 3000 km away. You should know that your support and encouragement were worth more than I can express on paper.

Thank you all, Bedankt allemaal, Danke euch allen, خیلی ممنون , زور سپاس ,

Matin

About the author

Matin Rostamitabar was born in Bayengan (Paveh), Iran on May 25, 1995. He obtained his BSc (2016) in “Polymer Engineering” from Tehran Polytechnic (Iran). His bachelor's thesis was focused on grafting graphene to polyvinyl acetate and investigating the effect of the molecular weight of polyvinyl alcohol on the grafting process.

Afterward, he was awarded a full scholarship from European Education and Culture Executive Agency (EACEA) that allowed him to follow his MSc in an Erasmus Mundus Joint Master Degree program so-called “Functional Advanced Materials & Engineering” (FAME). In October 2016, Matin started his first year of FAME at the University of Augsburg (Germany) and followed his second year at the Université Catholique de Louvain (Belgium), another FAME partner university. The topic of his master thesis was on understanding the flow behavior of end-functionalized model polymers governed by both transient bond dynamics and inter-chain entanglements.

In 2016, Matin started pursuing a joint PhD degree between Maastricht University and RWTH Aachen at Aachen-Maastricht Institute for Biobased Materials (AMIBM). His PhD was within the framework of the “FibreNet” project, an innovative EU-funded H2020-MSCA-ITN project aimed at training PhDs in the field of bio-based fibers. His main research focus was on the fabrication of cellulose based aerogel microfibers for biomedical applications such as drug delivery and wound dressing.

During this period, he had three secondments at the University of Tampere (Finland, 2019), Hamburg University of Technology (Germany, 2020), and Graz University of Technology (Austria, 2021). Moreover, he has written 4 peer reviewed journal articles from the studies described in this thesis and presented his results in 7 FibreNet network-wide training events and 3 international conferences. During his PhD, he achieved couple of honors and awards including, the Nonwovens Innovation Academy Grant (2019), YERUN Research Mobility Award (2019), SWOL Grant (2021), Oral Presentation Award at Brightlands Polymer Days (2021), Maastricht University Challenge Prototype Award (2021).



Furthermore, Matin voluntarily served as chair of PhD academy Maastricht from January 2019 until February 2022. He led a team of PhD volunteers, organized various educative, academic and social activities and collaborated with the PhD Candidates Network of the Netherlands (PNN) as well as Maastricht University council and executive board.

As of March 2022, Matin embarked on a new scientific journey and worked as research and development scientist at Sappi Netherlands Services B.V. He worked on developing biobased packaging materials from natural polymers and fibers such as nanocellulose. Since October 2022, he has joined the "Paints & Coating Product Management" team of Nouryon (the former AkzoNobel Specialty Chemicals) as Product Specialist EHEC and works on cellulose ether products including EHEC (ethyl hydroxyethyl cellulose) and MEHEC (methyl ethyl hydroxyethyl cellulose) which are mainly used as additives in paints & coatings.

List of Publications*Publications included in this dissertation:*

Rostamitabar, M., Abdelgawad, A.M., Jockenhoevel, S., and Ghazanfari, S.: Drug-Eluting Medical Textiles: From Fiber Production and Textile Fabrication to Drug Loading and Delivery; *Macromolecular Bioscience*; 2021, 21, 2100021 (1-31). <https://doi.org/10.1002/mabi.202100021>

Rostamitabar, M., Seide, G., Jockenhoevel, S., and Ghazanfari, S.: Effect of Cellulose Characteristics on the Properties of the Wet-Spun Aerogel Fibers; *Applied Sciences*; 2021, 11, 1525 (1-16). <https://doi.org/10.3390/app11041525>

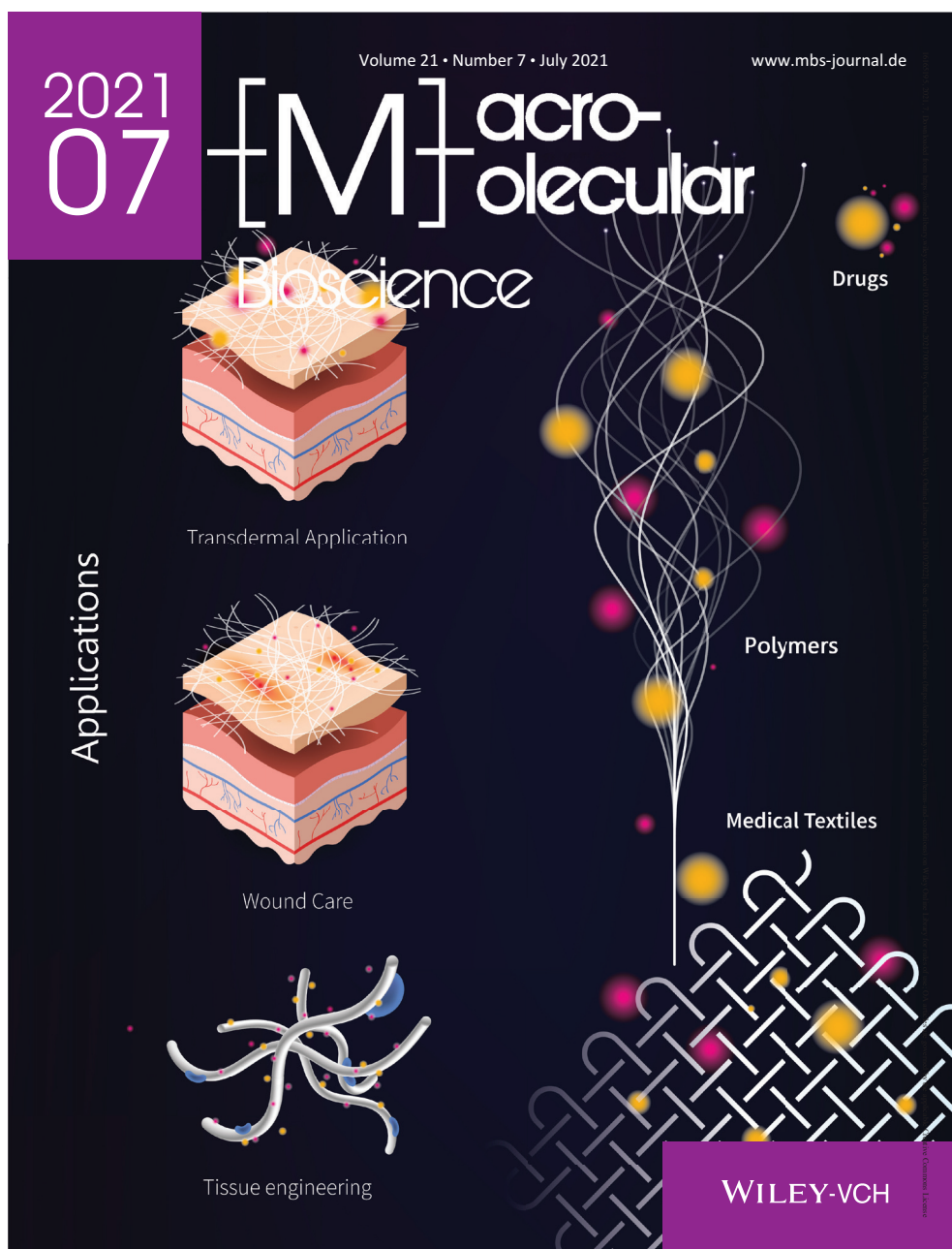
Rostamitabar, M., Subrahmanyam, R., Gurikov, P., Seide, G., Jockenhoevel, S., and Ghazanfari, S.: Cellulose aerogel micro fibers for drug delivery applications; *Materials Science and Engineering: C*; 2021, 127, 112196 (1-14). <https://doi.org/10.1016/j.msec.2021.112196>

Rostamitabar, M., Ghahramani, A., Seide, G., Jockenhoevel, S., and Ghazanfari, S.: Drug Loaded Cellulose-Chitosan Aerogel Microfibers for Wound Dressing Applications; *Cellulose*; 2022, 29, 6261–6281.

Rostamitabar, M., Janssen, D., Ghahramani, A., Kargel, R., Seide, G., Jockenhövel, S., and Ghazanfari, S: Thymol Loaded Cellulose Aerogel Nonwovens for Wound Dressing Application. (To be submitted)

Other publication(s):

Ghiassinejad, S., Mortensen, K., **Rostamitabar, M.**, Malineni, J., Fustin, CA., and van Ruymbeke, E.: Dynamics and Structure of Metallo-supramolecular Polymers Based on Short Telechelic Precursors; *Macromolecules*; 2021, 54, 13, 6400–6416. <https://doi.org/10.1021/acs.macromol.1c00373>

**BACK COVER:****JOURNAL OF MACROMOLECULAR BIOSCIENCE, VOLUME 21, ISSUE 7**

Drug-eluting medical textiles have been extensively used in various biomedical applications recently due to their cost-effectiveness and unique physical and chemical properties. Different fiber production, textile fabrication, and drug loading technologies are used to process the biomaterials to three-dimensional medical textiles that can be used for wound care, tissue engineering, and transdermal drug delivery applications.